Aluminium Resistance Spot Weld Quality Monitoring using Tensors and their Principal Components

Cameron Summerville

December 2020

A thesis submitted for the degree of Doctor of Philosophy of
The Australian National University

I declare that this thesis is my own original work except where due reference is made. All substantive contribution by others to the work presented, including jointly authored publications, are clearly acknowledged.

C. Summerville

Cameron Summerville

December 2020

Acknowledgements

I would like to thank a number of people that have helped me throughout my PhD. First, my supervisory panel, Matthew Doolan, David Adams and Paul Compston, who guided me through my PhD at the ANU. Matt, thanks for all the opportunities throughout my time at the ANU, they were greatly appreciated and I feel fortunate to have had so many great opportunities. Dave, thanks for the numerous conversations where you provided great technical and research advice as well as giving me a sounding board to bounce ideas off. Paul, thanks for your research and career advice throughout my time at the ANU and the opportunities and experience in teaching that you gave me.

I have been extremely fortunate to be able to work closely with the great people at The Ford Motor Company throughout the world during my PhD. Specifically, thank you to Elizabeth Hetrick, Ron Cooper and David Scholl at the Research and Innovation Centre in Dearborn, Detroit. Your advice and enthusiasm for my project has been highly valuable, thank you.

To my colleagues and friends in Engineering, David Tychsen-Smith, Brendan Voss, Vi Kie Soo, Victoria Zinnecker, Chris Stokes-Griffin, Joyce Yeoh, Adam Lilleyman and others. Thanks for all your support and always being available to grab a coffee.

To my Family, thank you for your support and advice throughout my time at the ANU. Mum thanks for all the excellent scientific editing and support. Lauren, thanks for your love and support throughout the entire PhD and helping me work through any challenges along the way.

Finally, thanks to the College of Engineering and Computer Science who supported me throughout my PhD. This research was supported by an Australian Government Research Training Program (RTP) Scholarship.

Abstract

Resistance Spot Welding (RSW) is a sheet metal joining technique used in many manufacturing industries to create high strength joints. RSW uses a high electric current and the resistive-heating caused by the contact resistance between the sheet metal parts to generate sufficient heat to fuse the material together. RSW has been used for decades in the automotive industry to weld steel car body panels together in a quick and efficient manner. More recently, aluminium has been introduced in automotive body manufacturing to reduce the weight of the car while still maintaining high strength.

The crashworthiness of monocoque vehicles created with spot welded sheet metal relies on the quality of the spot welds used to join the panels. Monitoring the quality of welds that leave the production line is therefore critically important to ensure vehicles are safe in the event of a crash. Assessing the quality of spot welds non-destructively is challenging because the spot weld is formed in between the layers of sheet metal which make a part.

One way to achieve real-time, non-destructive quality monitoring of RSW is to monitor the electrical, thermal and mechanical signals throughout the process. Signal-based weld quality monitoring is relatively well understood for steel RSW, however the entire field of aluminium spot weld quality monitoring is particularly sparse in the academic literature.

This thesis addresses the gap in the academic literature of aluminium RSW quality monitoring. A particular focus is placed on understanding the *signal shapes* and the way multiple process signals interact during the process to produce accurate models for aluminium spot weld quality monitoring.

Principal Component Analysis (PCA) was used to represent the major signal shapes that are apparent in a set of steel welding signals. Using this method, training sets were designed in the laboratory to reveal the types of signal shapes that relate to weld quality. From the training data, models for weld quality and fault identification were developed using the signal shapes found with PCA. The models for weld quality were validated in industry using the equipment on an automotive production line. This allowed the technique to be tested and compared to the existing industry weld quality monitoring practices for steel RSW.

To address the challenging problem of aluminium RSW quality monitoring, analysis of the interactions of multiple signals during the process was proposed. To analyse the interactions of multiple signal shapes, a new methodology is developed which involves representing process signal

information as mathematical tensors. The tensors encapsulate the interaction behaviour of multiple signals using the outer-product of tensors. Using Tensor Principal Component Analysis (TPCA) the dominant tensor shapes in the training data could be analysed. Models for aluminium resistance spot weld quality were developed using the tensor principal components to analyse the interactions of the signal shapes from individual signals.

The use of mathematical tensors to represent multiple process signals and their interactions allows for more accurate and robust models for weld quality to be developed in the laboratory. To test the technique in an industrial setting, the tensor based weld quality monitoring method was validated using significant amounts of industrial data. The industrial data, including multiple process faults and thousands of welds, allowed the tensor based weld quality monitoring technique to be thoroughly tested under a number of challenging conditions faced in industry.

The tensor based approach proved to be more robust and accurate in a number of situations than similar models calculated from the information from an individual signal. This showed that the analysis of multiple signals and their interactions simultaneously provided a more robust approach to aluminium RSW quality monitoring than analysis of the information from a single signal.

The implications of these findings are an important contribution to the academic literature in the field of aluminium RSW quality monitoring as little work has been completed previously. The implementation of tensors for signal based weld quality monitoring presents a unique approach to signal based quality monitoring and may prove useful in other manufacturing processes that have complicated interacting process characteristics.

For industry, this research improves the current aluminium RSW quality monitoring capabilities through the analysis of the information from multiple signals and their interactions. In addition, this research provides a new methodology and approach to signal analysis in weld quality monitoring, taking into account the *shape* of the entire signal rather than landmark points selected at different points throughout the process.

List of Publications

- Process Monitoring of Resistance Spot Welding Using the Dynamic Resistance Signature, Summerville C., Adams D., Compston P., Doolan M. (2017). *The Welding Journal, 96 (November),* 403-412.

- Nugget diameter in resistance spot welding: a comparison between a dynamic resistance based approach and ultrasound C-scan, Summerville C., Adams D., Compston P., Doolan M. (2017). *Procedia Engineering, 183,* 257-263.

- Multi-Signal Quality Monitoring of Aluminium Resistance Spot Welding using Principal Component Analysis, Summerville C., Adams D., Compston P., Doolan M. (2017). *9th Australasian Congress on Applied Mechanics (ACAM9), 27 – 29th November 2017.*

- A comparison of resistance spot weld quality assessment techniques, Summerville C., Compston P., Doolan M. (2019). *Procedia Manufacturing, 29,* 305-312.

- Correlating Variations in the Dynamic Resistance Signature to Weld Strength in Resistance Spot Welding Using Principal Component Analysis. Adams D., Summerville C., Voss B., Jeswiet J., Doolan M. (2017). *Journal of Manufacturing Science and Engineering, 139 (April),* 1-4.

Table of Contents

Chapter 1

Introduction

1.1 Background

The global automotive industry currently produces more than 70 million vehicles per year. Modern passenger vehicles are predominantly created with monocoque designs that rely on the car body for structural integrity (as opposed to the ladder frame chassis used in trucks). The sheet metal components in a monocoque are predominantly joined by Resistance Spot Welding (RSW). The resistance spot welds that hold the car body together are critical to the safety and structural integrity of most modern automobiles. Unfortunately accurately assessing the quality of resistance spot welds is particularly challenging.

Resistance spot welds are created between two or more pieces of sheet metal and rely on the electrical resistance at the interface between the sheet metal parts. A voltage is applied to the sheet metal parts using copper electrodes which clamp the metal parts together. With sufficient current flow, the small electrical resistance at the sheet interfaces causes enough resistive heating to melt the base material, welding the sheets together at a localised spot between the welding electrodes.

Knowing the quality of the spot welded joints in cars is important for ensuring the safety of a vehicle in the event of a crash. However, assessing the quality of resistance spot welds non-destructively is difficult and often requires additional steps to be added to the manufacturing process, slowing production and increasing the cost to manufacturers. Destructive testing is common practice in industry to monitor the quality of welds, typically welds are destroyed with a chisel or in a peeling motion so that the weld can be measured.

Some non-destructive testing techniques exist which require the car or parts to be removed from the production line for testing. Methods such as ultrasonic testing, x-rays and infrared thermography aim to provide an image of the spot weld so that its quality can be assessed. However, these methods can be inaccurate, and are often manual and therefore time consuming.

Weld quality monitoring based on analysis of the signals measured during the process (process signals) is a more desirable solution to weld quality monitoring as it can be performed automatically in-line with the manufacturing process. Modern weld timers, which are a computer that controls the welding process, are capable of recording and analysing several signals measured throughout the process. Signal based weld quality monitoring is therefore a better solution to quality assurance in RSW.

In RSW of steel the best weld quality monitoring signal is the resistance across the electrodes, for a number of reasons. For most steels the resistivity of the base material is closely linked to its temperature, this allows inferences to be made about the temperature and amount of heat that is generated in a given spot welding process. The resistance through the joint also changes throughout the process as the interface between the sheet metal parts (the faying surface) melts. Finally, because RSW is an electrically driven process, all modern weld timers record the voltage and current in the process at relatively high sampling frequencies, often automatically calculating the resistance using Ohm's Law.

The automotive industry aims to reduce the weight of passenger vehicles to reduce emissions and increase performance and efficiency, a concept known as 'lightweighting'. Large body panels, traditionally made from steel, are one of the major contributing factors to vehicle body weight and so manufacturers are moving towards lighter alternatives. Aluminium is increasingly used to reduce the weight of components in vehicles due to its lower specific gravity (one third of that of iron). However, aluminium is often particularly challenging to weld due to its unique material properties.

1.2 The Challenge of Aluminium Spot Weld Quality Monitoring

In aluminium RSW the choice of process signal for in-line weld quality monitoring is not as clear as it is in steel. The changes in resistivity of the metal with its temperature is not as pronounced which makes differences in heat generation from weld to weld much more challenging to identify.

Aluminium has a high coefficient of thermal expansion (approximately double that of most steels), which means that the expansion of the joint can be linked to the amount of heat in the process. Unfortunately with sheet metals (typically less than 3mm) used in RSW the thermal expansion from room temperature to melting is minute, and approximately 30 micron for two 1mm thick aluminium sheets. The thermal expansion during RSW pushes back on the electrodes which are being pressed into the sheet metal with a high electrode clamping force. This creates a small amount of electrode displacement or change in the electrode force, depending on how the system is designed. To accurately monitor the differences in the mechanical signals in aluminium RSW (electrode displacement and force), highly accurate sensors are required to operate in harsh environments with significant magnetic noise due to the high currents used in aluminium spot welding (20 to 50kA).

A number of the signals that can be measured during a resistance spot welding process are difficult to implement in a reliable and consistent way that works for different aluminium spot welding systems. The measurement of electrode force relies heavily on the rigidity of the spot welding electrode arms, structure-borne acoustic emissions are very susceptible to noise which can result from the flow of cooling water through the electrodes or environmental noise sources in a production plant. Temperature based measurements can be very challenging to acquire because the spot weld grows from between the sheet metal parts. These challenges (among others) mean that monitoring a single process signal is not sufficient for quality monitoring in aluminium RSW.

It is important that aluminium RSW quality monitoring techniques are improved as more mass production cars are made with aluminium bodies. Improving quality monitoring techniques allows manufacturers to ensure the quality of the resistance spot welds is high which directly affects the crashworthiness of the vehicle.

1.3 Research Topic

The use of aluminium in car bodies has been increasing steadily since the 1970s (Löveborn et al., 2017). Very little academic research has been conducted into the quality monitoring of aluminium resistance spot welds. There has been extensive research into steel spot weld quality monitoring, but the results have not been adaptable to aluminium RSW due to its unique material properties. The lack of published academic research may be linked to the commercial value of such systems. Most of the research that has been conducted into aluminium weld quality monitoring is likely to exist in the weld timer manufacturing and automotive industries, rather than in the academic literature. Modern weld timers are able to monitor aluminium weld quality to a limited extent. However further research is required into the process signals that are available and their relationships to weld quality.

Nearly 25 years ago a paper was published that investigated a number of features from several process signals in aluminium RSW. One of the major conclusions was that none of the individual signals could monitor the quality of aluminium resistance spot welding on their own (M. Hao et al., 1996). Since then, little work has been completed to address this conclusion in the academic literature and so this thesis will focus on the topic of aluminium RSW quality monitoring based on the information collected from multiple process signals.

1.4 Thesis Outline

To develop the research question, a review of the existing literature was completed (Chapter 2). The review focussed on aluminium weld quality monitoring research in the academic literature and patent literature, the factors that affect aluminium spot weld quality, as well as research previously conducted in steel spot weld quality monitoring. In addition to the welding literature the shape analysis literature was reviewed for the techniques that were used in this thesis, Principal Component Analysis (PCA) and Tensor Principal Component Analysis (TPCA).

Using the information in the literature review a methodology was developed to answer the research question (Chapter 3). To develop an approach that analyses the interactions of multiple signals for aluminium weld quality monitoring a number of steps were taken. First an approach was developed that analyses the resistance signal in steel RSW (Chapter 4). The approach was applied to analyse multiple signals in aluminium RSW to investigate which signals are useful for aluminium weld quality monitoring (Chapter 5).

A new representation of welding data, which built on the preliminary work in steel and aluminium, allowed the interactions of multiple signals in aluminium RSW to be analysed for spot weld quality monitoring (Chapter 6). Throughout the thesis the analysis techniques were established using laboratory data created with commonly available alloys. Once the analysis techniques were established, they were tested with industry data. This ensures that the analysis methodologies developed in the laboratory are useful and relevant to industry. With the help of our industry partner, the weld quality monitoring technique that utilises Tensor Principal Component Analysis to analyse the interactions of multiple signals was tested with significant amounts of industry data (Chapter 7).

This research is conducted so that the knowledge can be applied in industry. It is therefore important that the analysis and methodology can: be easily implemented, predict weld quality, be used to solve problems in production, identify faults, determine the cause of poor weld quality, and reveal relationships between weld quality and the measured process signals.

Chapter 2

Literature Review

At the end of Chapter 1 the primary research topic of this thesis was presented. From this literature review the research question was developed based on the academic literature and the challenges associated with aluminium RSW quality monitoring. This literature review will cover the important aspects of the Resistance Spot Welding (RSW) literature as well as the analysis methodologies that are used throughout this thesis.

- This literature review starts by outlining the motivations behind the automotive industry's move towards aluminium in vehicle manufacture in section 2.1.1, followed by a brief summary and justification of RSW for aluminium sheet metal joining which is shown in section 2.1.2.

- Section 2.2 covers the steel RSW quality monitoring literature which has formed the basis of the aluminium weld quality monitoring literature.

- Section 2.3.3 covers the fundamental signal shape analysis technique used, Principal Component Analysis (PCA) which is used heavily in Chapters 4 and 5 and represents the basis of the techniques developed in Chapters 6 and 7.

- Then the factors that affect aluminium spot weld quality and the way that these may be able to be monitored are covered in sections 2.4 and 2.4.2.

2.1 Introduction

Traditionally, mass-production cars have been produced with steel panels. Steel panels have been used for a number of reasons including cost, ease of manufacture, safety and strength. The steel panels that are joined together to make car bodies are predominantly joined using RSW.

2.1.1 Aluminium and the Automotive Industry

Around the year 2000 a number of papers were published analysing the opportunities for replacing steel panels in mass-production cars with aluminium (Barnes et al., 2000; Carle et al., 1999; Kelkar et al., 2001; Miller et al., 2000). The motivations behind the production of aluminium car bodies, include environmental concerns regarding fuel efficiency and recyclability, and mechanical features such as increased passenger safety and performance (Barnes et al., 2000; Miller et al., 2000). The key challenge for the production of aluminium car bodies is their manufacturing cost (Kelkar et al., 2001), specifically, the necessity for joining techniques that can cater for high volume manufacturing, which require significant capital investment for research, development and design (Carle et al., 1999).

2.1.2 Resistance Spot Welding for Aluminium Sheet Metal Joining

RSW has been the sheet-metal joining technology of choice in the automotive industry for decades. Because of this, new joining techniques are often compared to RSW as a benchmark for sheet-metal joining.

The most prominent technology used for sheet-metal joining of steel automotive panels is RSW. However, RSW of aluminium is considered significantly more challenging than steel and the literature includes a number of comparisons of the available joining technologies for aluminium panels in case the challenges in aluminium RSW were insurmountable in mass-production passenger vehicles (Briskham et al., 2006; Han, Thornton, & Shergold, 2010; He et al., 2008).

Many different sheet-metal joining techniques have been researched for aluminium. These include resistance spot welding, self-piercing rivets, friction-stir welding, clinching, blind riveting, laser welding, brazing, shielded-arc welding, adhesive bonding, weld bonding and diffusion bonding.

Comprehensive experimental comparisons have been conducted of three aluminium sheet-metal joining techniques covering RSW, spot friction joining and self-piercing rivets (Briskham et al., 2006). Spot friction joining performed worst in terms of cycle-times, lap-shear and T-peel tests. Self-piercing rivets consistently equalled or outperformed RSW in terms of mechanical strength and energy absorption, with a similarly short cycle-time. However, it was found that the rivets would have to be supplied *'free of charge'* for it to be economically viable. Additionally, self-piercing rivets pose concerns for recyclability due to the mixing of materials, which significantly increases the difficulty of recycling the cars at end-of-life (Han, Thornton, & Shergold, 2010).

RSW was found to be the most economically viable option even with the higher electricity costs and requirements to regularly replace the electrodes to mitigate electrode wear (Briskham et al., 2006). RSW was found to be the most adaptable to the different joints that are required to make a car body. It was concluded that RSW could meet the key criteria for high volume joining technologies once quality control and electrode wear were addressed.

In addition to the advantages and disadvantages highlighted by Briskham et al. (2006) there are some specific challenges that were not discussed in the comparison. Spot friction joining suffers from very poor surface finish on the plunge side of the joint which limits which side of the joint the process can be conducted from. Self-piercing rivets present significant challenges for end-of-life recycling as they embed steel rivets in aluminium sheets. This makes it very challenging to separate the different material streams into ferrous and non-ferrous alloys for recycling. Finally, because RSW has been the predominant joining technology in automotive body shops for joining sheet-metal components for decades, significant infrastructure, knowledge and design standards already exist for RSW as a technique in the automotive industry which makes it a more attractive option.

2.2 Industry RSW Quality Metric: Button Diameter

Button diameter has been employed as the quality metric of choice for automotive manufacturers for decades. The measured button diameter after a destructive test has often been linked to the strength of the weld (Sun et al., 2004). Intuitively, larger button diameters often have higher load bearing capacities. However, various factors such as the HAZ (Heat Affected Zone), cracks, porosity in the weld, expulsion, or even the particular destructive test the weld is subjected to, can affect the final button diameter produced. The button diameter is used as a representative measure of what the spot weld nugget diameter was prior to destructive testing.

Button diameters are often revealed through destructive tests such as a chisel test or roller peel test (which will be covered further in section 3.2 in the methodology chapter). These two methods may not always produce the same outcome for a spot weld given that they load the weld in different ways. The choice of destructive testing technique is often an economical one, with something cost effective, reproducible with low tooling costs being chosen to monitor the quality of spot welds.

Given that the button diameter is a result of the destructive test and not necessarily an exact representation of the weld nugget before it was destroyed it is challenging to model. Resistance spot welds can fail in a number of different ways, and not all produce a measurable button diameter which further complicates the modelling task. Because not all welds produce a measurable button diameter it is not the best measure for weld quality from a quality monitoring perspective.

Spot welds most commonly fail in one of two broad categories; interfacial failure – failure at the interface between the sheets (or faying surface), or by pull-out failure – failure where the spot weld is removed from one of the sheets. However there are 8 different failure mechanisms identified by the AWS between complete button pull-out and complete interfacial failure (American Welding Society, 2013) (Figure 2-1). When a spot weld fails by pull-out, the weld is completely pulled from one side of the sheet metal component producing what is known as a weld 'button', see Fracture Mode 1 (Figure 2-1). When a spot weld fails by interfacial failure, no measurable 'button' is left on either sheet, Fracture Mode 7.

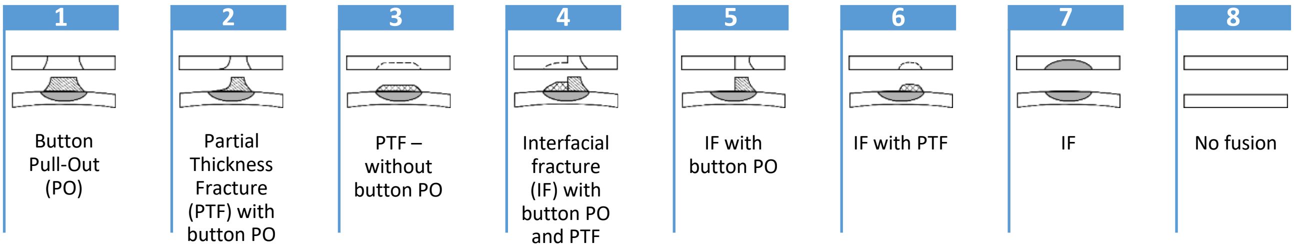

Figure 2-1: The different spot weld fracture modes identified by the AWS (2013)

The diameter of a spot weld, that has failed by pull-out failure is known as the 'button diameter', which is considered a representation of the true diameter of a weld nugget before it is destroyed (Hongyan Zhang et al., 2011). This distinction between the button diameter of a destroyed joint and the nugget diameter of the welded joint (before destructive testing) is used throughout this thesis. The button diameter is quick and easy to measure once a spot weld has been destroyed and is used in industry as the standard quality metric to infer the nugget diameter and subsequently its strength (Hongyan Zhang et al., 2011). However, there are several intermediate fracture modes that produce a measurable button between button pull-out and interfacial failure. Sometimes the joint will fail initially in one region and then progress to brittle fracture or crack propagation in the weld producing different failure mechanisms (Hongqiang Zhang et al., 2014) as seen in fracture modes 2-6 (Figure 2-1).

Spot weld failure is complex given the number of possible failure mechanisms identified by the AWS. The consequences for joint strength and energy absorption of the different failure modes has not been comprehensively studied and it is therefore difficult to compare welds that fail by different mechanisms by the resultant button diameter alone. A weld that fails through complete button pull-out is likely to absorb more energy before failure and achieve a higher shear strength than welds that fail by interfacial failure. However, welds that fail by the mechanisms from 2-6 have not been well documented in the academic literature. Spot welds that fail by failure modes 1, 2, 4, & 5 have buttons that can be measured and perhaps compared, however it is unlikely that the relationships to weld strength or the measured signals are the same for each fracture mode. Welds that fail by failure modes 3, 6, 7 & 8 do not have measurable button diameters and therefore cannot be compared using this metric.

The choice to use button diameter to determine weld quality in industry makes the prediction of weld quality in aluminium particularly challenging. The number of different failure mechanisms experienced by aluminium resistance spot welds means that the scale of weld quality is not continuous compared to the tensile shear load bearing capacity of welds which provides a continuous measure of quality regardless of failure mechanism.

2.3 Steel Spot Weld Quality Monitoring

Many of the factors that affect steel spot weld quality are the same as in aluminium RSW, however the challenges of the oxide layer and low bulk resistivity are not an issue. Broadly, the factors that cause challenges for maintaining steel spot weld quality are the wide range of different grades of automotive steels including Advanced High Strength Steels (AHSS) and Ultra High Strength Steels (UHSS), process faults, electrode wear, different coatings, heterogeneous grade stacks, and stacks with high sheet thickness ratios between the sheets, sealants and lubricants.

2.3.1 Signals

Three review papers have discussed at length the work of researchers that correlate different process signals with aspects of the resistance spot welding process for monitoring or control purposes. The best discussions of the different signals for quality monitoring are in Podrzaj et al. (2008), Ma et al. (2013), and Zhou et al. (2019). An important contribution to the RSW quality monitoring literature is also found in a book; *Resistance Welding – Fundamentals and Applications* (Hongyan Zhang et al., 2011). The book includes dozens of academic papers which cover the different signals used for steel RSW quality monitoring. Broadly these include electrode voltage, current, resistance, electrode displacement, electrode force, acoustic emissions, pneumatic pressure fluctuations (Hongyan Zhang et al., 2011), ultrasound transmission, infrared light emission, thermos electric voltage (Podrzaj et al., 2008), and input impedance (Ma et al., 2013).

Additionally, beyond the academic literature, a patent was filed which uses a number of signals for steel spot weld quality monitoring. It includes an instrumented welding electrode that has sensors to measure electrode voltage, electrode-sheet interface temperature (from a thermocouple inside the electrode), electrode pressure (via a piezoelectric sensor) and the magnetic field strength (indicative of the current, measured by a Hall Effect sensor) (Patent No. US 4,472,620, 1984).

In general, the standard approach to quality monitoring in steel RSW is to take a process signal and extract features from the signal that can be correlated with weld quality. Increasing the understanding of the signals that are correlated with weld quality in different situations has uncovered a number of key signals and attributes that are known to be related to weld quality and nugget growth.

The signal that is most prominent in steel spot weld quality monitoring and control is the resistance signal. A seminal paper by Dickinson et al. (1980) characterised the key aspects of the resistance signal (Figure 2-2). Many aspects of the resistance signal have since been linked to weld quality, nugget growth and process characteristics.

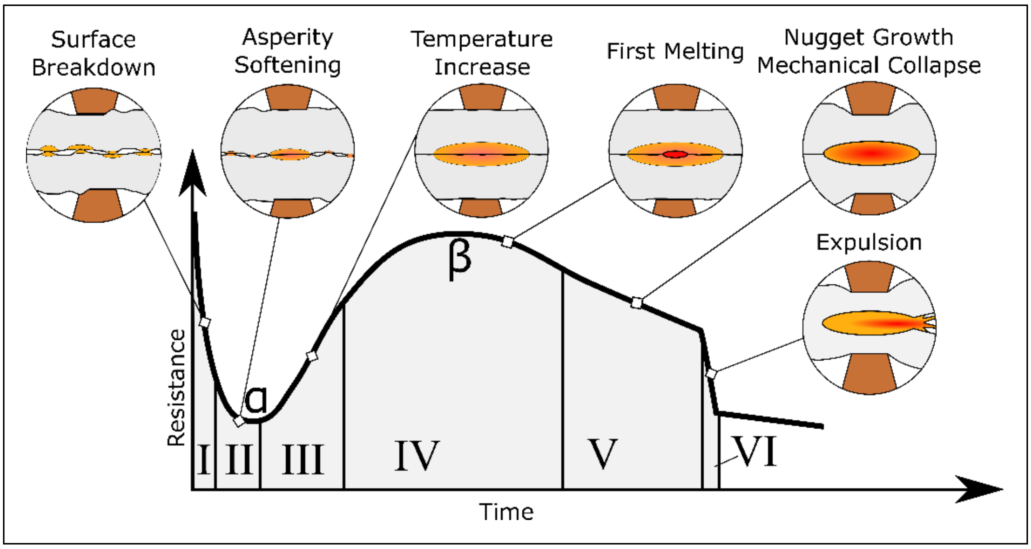

Figure 2-2: Dickinson's theoretical dynamic resistance curve (1980), adapted by Adams et al. (2017)

Cho et al. (2002) found that the β-peak location (in time), the rising rate of the resistance to the β-peak, the maximum resistance minus the minimum resistance in a case where the β-peak is higher than the initial resistance, and the final resistance to all be strongly correlated with the load-bearing capacity and button diameter of welds created with four different welding currents.

As an example which did not use the resistance signal for aluminium quality monitoring, Gong et al. (2011) investigated features of the electrode displacement signal such as the maximum displacement, average velocity of the electrode, variance of electrode velocity, the drop in displacement due to expulsion, and the *'residual height of the weld'*. They found that the maximum displacement and the average velocity of the electrode was most important for weld quality monitoring.

2.3.2 Approaches

Many different approaches to signal-based weld quality monitoring have been taken in steel including multilayer artificial neural network (Cho et al., 2002), learning vector quantization (Park et al., 2004), moving range charts (H. Wang et al., 2009), genetic K-means cluster analysis (Hongjie Zhang, 2011), Bayesian belief network (Gong et al., 2011), multi-objective Taguchi method (Muhammad et al., 2013), Hopfield associative memory neural network (Hongjie Zhang et al., 2017), recurrent neural network (X. Wang et al., 2017), back propagation neural network (Wan et al., 2018), radial basis function neural network (Hongjie Zhang et al., 2018), wavelet analysis (Wu et al., 2018), and random forests (Xing et al., 2018).

Additionally, the patent for steel weld quality monitoring in the Bosch weld timers shows an example of the commercial research that has been undertaken in the steel resistance spot weld quality monitoring field (Patent No. US 9,839,972, 2017). The Bosch system monitors a few key points of the resistance signal and uses statistical process monitoring techniques to show the process stability and provides a measure of difference from a *'reference weld signal'*.

Typically the literature achieves a level of correlational analysis of signal features with weld quality, and given the number of new materials (with unique challenges) and feature extraction methods, not much of the research gets beyond finding correlations. Due to the number of new materials, the different spot welder designs and different process faults, signal-based weld quality correlations are rarely validated with additional data. Validation of models with new data can be extremely challenging and the results can often be affected by small changes in the process. Because of this, it is important that the mechanics of the model can be understood and scrutinised so that problems can be solved when new conditions arise.

2.3.3 The Approach used in this Thesis – Principal Component Analysis

The work in this thesis takes the approach of feature extraction of welding signals that can be correlated with weld quality. The features are extracted using a technique called Principal Component Analysis which will be discussed in the next section. Some recent work by a research group in China has taken a similar approach to quality and process monitoring in a similar field they call *'Small-Scale Resistance Spot Welding'* (Wan et al., 2016b, 2016a, 2016c, 2018; Zhao et al., 2014). Small-scale resistance spot welding concerns spot welding of very thin gauge sheets (less than 0.5mm) for applications such as electronics and medical devices (Shinji Fukumoto et al., 2008).

Small scale resistance spot welding has its own unique challenges as the contact resistance is a larger portion of the total resistance of the joint which creates issues for joint quality and electrode wear. This is very similar to the challenges faced in aluminium RSW due to the high resistance oxide layer and low bulk resistivity of the aluminium. The group has looked at using PCA, Neural Networks, Grey Relational Analysis and a genetic algorithm to monitor the quality of small-scale resistance spot welds achieving good prediction results.

The analysis of manufacturing process signals for weld quality monitoring presented in this Thesis builds on the work of Doolan et al. (2003) and Voss et al. (2014; 2017). These researchers used PCA of signals for process monitoring of sheet-metal stamping.

PCA calculates eigenvectors for a signal set which represents the signal data using a more convenient basis that is aligned with the dataset's variation. The first principal component is aligned with the direction of highest variation in the dataset and each subsequent principal component is orthogonal and ordered in terms of the amount of variation that it represents in the dataset.

For process monitoring this is a particularly useful technique for representing complicated signal information with fewer variables and minimal information loss. Additionally, because the principal components are aligned with the major signal variation in the dataset, PCA allows the researcher to design the variation in their dataset to encapsulate particular aspects of the process. If parameters that relate to weld quality are varied, the resultant signal information that is picked up in the principal components is most likely to be strongly related to weld quality.

Unlike neural networks, the decomposition of signal data into its principal components (the shapes of the signals) is completely reversible which allows any model constructed from principal components to be scrutinised. This also allows for the features of the data (signal shapes) to be visualised. Analysis of the signal shapes that are strongly related to weld quality or a specific fault allows for a better understanding of the mechanisms in the process that govern weld quality.

Originally, Cootes et al. (1992, 1995) developed the Point Distribution Models (PDM) technique which uses PCA to create a trainable method for shape variation representation. The method was demonstrated with a set of worms of different size and shape, each represented by a vector of measured boundary points. The principal components calculated from the dataset of vectors represents the shape variation in the dataset of objects. The first two principal components were used in the example to show the two major modes of shape variation in the worms, which corresponded to length and curvature Figure 2-3.

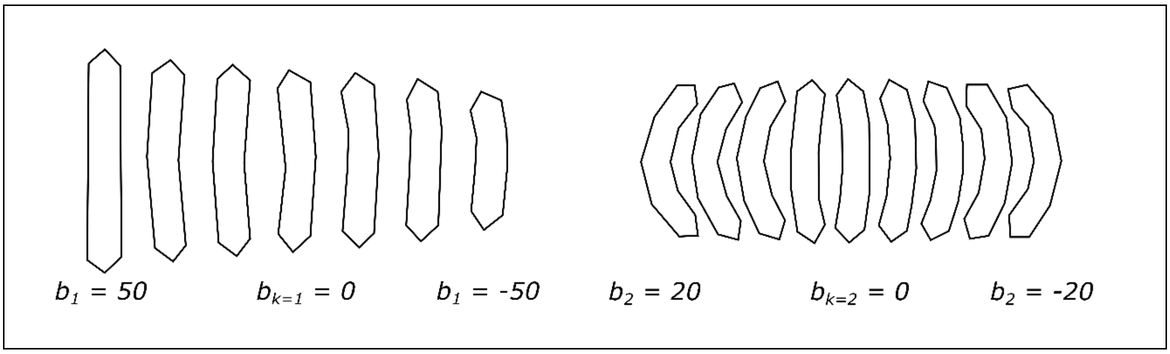

Figure 2-3: Shape variation of the first two principal components, adapted from (Cootes et al., 1992)

Doolan et al. (2003) applied this technique to sheet-metal stamping force signals to classify misaligned, fractured and good parts using two principal component scores from each stamping force signal. The motivation behind using the PDM and PCA was to move away from monitoring systems that only assessed whether each force measurement (at a distinct point in time) throughout the process was within set bounds, which ignored the overall shape of the stamping force curve. It was thought that identification of the force signal shapes would increase the understanding of the process and improve fault classification. Voss et al. then used the methodology to identify specific process changes to characterise die wear (2014) and lubrication types on individual parts (2017).

PCA has also been used for monitoring changes more broadly in remote sensing data to monitor tropical forest clearing (Hayes et al., 2001), process control in an autobody assembly process (Ferrer, 2007), respiratory monitoring (Jin et al., 2009), facial recognition for driver drowsiness monitoring (Benrachou et al., 2013) and long-time structural health monitoring of a sports stadium (Datteo et al., 2017). This shows the versatility and broad application of PCA as a shape analysis technique.

In this Thesis, PCA and the PDM concept are used to monitor the resistance spot welding process including prediction of load bearing capacity, button diameters from chisel and peel tests, and identification of faults in the process. Chapter 4 will explain how the PDM and PCA are used with individual welding signals for process monitoring, Chapter 5 will apply this to multiple signals in aluminium RSW, and Chapter 6 will extend the feature extraction technique to analyse the interactions of multiple signals in aluminium RSW. This will be done by representing multiple welding signals as mathematical tensors and using the concepts of PDM. The feature extraction achieved by principal component analysis for welding signals will be generalised beyond signal *vectors* to *welding tensors* using a technique known as Tensor Principal Component Analysis (TPCA) which will be covered in detail in Chapter 6. This addresses the challenge identified in the literature that no individual signal is sufficient for complete process monitoring of aluminium RSW as the resistance signal is in steel RSW.

2.4 Factors that Affect Aluminium Spot Weld Quality

Much of the literature in aluminium RSW has focussed on addressing the challenges associated with quality consistency and the differences from the well understood process of steel RSW. Aluminium presents a number of unique challenges as well as exacerbating existing process issues due to its material properties. Some of the challenges associated with aluminium RSW are electrode wear, quality consistency, cracking and porosity in the weld (Rashid et al., 2011; Turnage et al., 2018), the aluminium-oxide layer (Crinon et al., 1998), and the low bulk resistance. All of these factors cause weld quality inconsistency.

One of the major contributing factors to all these issues is the high resistivity of the aluminium oxide layer. The oxide layer increases the contact resistances at all interfaces which increases the local resistive heating significantly. This makes it a key factor for maintaining quality consistency (Han, Thornton, Boomer, et al., 2010). Usually the oxide layer is burnt early in the process which causes high heat initially at the electrode-sheet interface which accelerates electrode wear.

The magnitude of the contact resistance in aluminium RSW can be affected by a number of factors with many studies finding varying results. The factors (sorted by the interfaces they affect) include:

Interfaces	**Factors**
Electrode-sheet interface only	• Electrode tip design • Electrode-sheet alignment • Electrode wear
Faying surface only	• Adhesives or sealants
Electrode-sheet and faying surface	• Electrode clamping force • Sheet surface condition

These factors and their consequences for weld quality consistency, mean that contact resistance has received significant attention in the literature.

Section 2.4.1 will cover factors such as sheet surface conditions that affect both the electrode-sheet and faying surface resistance equally. Section 2.4.2 will cover the factors that predominantly affect the electrode-sheet interface which are also the factors that affect electrode wear. A lot of the literature that is focused on the electrode-sheet interface covers how these factors can be mitigated to reduce electrode wear and increase electrode life.

2.4.1 Aluminium Sheet Contact Resistance

The contact resistances in welding at the electrode-sheet and faying surfaces have been studied with different temperatures, pressures and metal properties (Song et al., 2005). The interaction with temperature is complicated, with an increase in temperature not always decreasing contact resistance, while the relationship to electrode force or pressure is simpler. Song's study confirmed the findings of Thornton et al. (1996) regarding the relationship between clamping pressure and contact resistance, showing that the contact resistance is inversely related to electrode clamping pressure (Song et al., 2005).

Due to the undesirable consequences caused by high contact resistance in aluminium RSW, a number of strategies have been trialled in the literature and some inventions have been patented. Pre-heating cycles in the weld schedule have been investigated to reduce the variation in contact resistance (caused by the oxide layer) prior to welding to ensure a more consistent result (Z. Luo et al., 2015). The pre-heating cycle burnt away the oxide layer which resulted in better contact resistance at both the electrode-sheet and faying surfaces. The use of a pre-heating cycle was found to be significantly better at producing consistent contact resistances than increasing the clamping force. The pre-heating cycle resulted in an increase in button diameter and strength of welds of 33%, as well as improving the quality consistency (Z. Luo et al., 2015).

Contact resistance of the base material is also known to be highly dependent on the surface finish of the sheet metal for a number of different aluminium alloys (Thornton et al., 1996). When the aluminium sheet surface is mechanically disturbed this gives a lower contact resistance as the oxide layer resistance is reduced. Rashid (2011) showed that the contact resistance is highest when the sheet is in its *'as-received'* form (rolled), followed by a *'smooth'* surface (using 600 Grade grinding paper), and lowest with a *'rough'* surface (using 180 Grade grinding paper). This trend is attributable to the disturbance of the oxide layer which causes a drop in contact resistance between the electrode-sheet and sheet-sheet interfaces.

Contact resistances caused by thin oxide layers can also be broken down by minute sliding at the electrode-sheet or faying surface. Crinon et al. (1998) estimated that as little as 10 μm was sufficient for the shear stresses to break down a thin oxide layer which has the potential to completely change the contact resistance and outcome of the process. James et al. (1997) used asymmetric electrodes to show that different shear stresses induced at the interfaces can change the contact resistance at the faying surfaces by one or two orders of magnitude from conventional domed electrodes (commonly used for aluminium RSW). Given that electrodes can change shape as they wear, this may provide a possible explanation for some of the poor quality consistency in aluminium RSW.

Another mechanism in RSW that may replicate this behaviour is the phenomenon of electrode sliding. Electrode sliding is caused by poor alignment or wear in the electrode arms of a spot welder. Small displacements of 10 μm or more are possible in a worn resistance spot welding machine. Small displacements like this are known to drastically change the contact resistances and the heat generated for RSW as shown by (Crinon et al., 1998).

These strategies for reducing the contact resistances at the electrode-sheet and faying surfaces all contribute to reducing large variation in the total resistance which helps to improve weld quality consistency in aluminium RSW. The other major concern for weld quality consistency is the accelerated electrode wear that is caused by the high resistance (due to the oxide layer) at the electrode-sheet interface.

2.4.2 Electrode Wear Mitigation and Electrode-Sheet Resistance

Electrode wear is a significant issue in RSW and so much of the literature is focussed on addressing this challenge. Electrode wear mitigation is not central to the goals of this thesis, but useful insights can be drawn from the work completed to understand the behaviour of the electrode-sheet interface, which can be a cause for poor quality welds.

Aluminium naturally forms an oxide layer when exposed to air. The oxide layer of aluminium has significantly higher resistivity than the aluminium base material, which causes the electrodes in aluminium RSW to wear quickly. The high electrode wear is due to the additional heat that is produced at the electrode-sheet interface.

Electrode life in aluminium RSW has been found to be extremely variable due to electrode pitting and aluminium-copper alloying at the electrode sheet interface (S. Fukumoto et al., 2003). Three different electrode-life tests produced results ranging from 400 to 900 welds, showing the vulnerability of the process to different forms of electrode wear (S. Fukumoto et al., 2003). The wide variation in electrode life shows that the process can be vulnerable to small changes.

The effects of different sheet surface conditions on electrode life have been investigated by several authors. Li et al. (2007) compared the effects on electrode life of sheets that were in *'as-received'* condition, *'electric-arc cleaned'* (using an arc welding machine to burn off impurities), '*degreased'* and *'chemically cleaned'* finding that cleaning the sheets improved the electrode life by factors of between 8.5 and 11.5 over the *'as-received'* condition. The effects of the sheet surface condition on the tensile-shear load-bearing capacity was also recorded showing the following:

- Chemically cleaned sheets produced the strongest and most consistent welds,

- degreased sheets produced strong welds with minor variation,
- electric arc-cleaning of the sheets produced the most variation in weld strength,
- and as-received sheets performed worst out of the surface conditions studied.

Naimi et al. (2015) compared the contact resistance of as-received sheets, NaOH-pickled sheets and sheets that had been glass-blasted, showing that chemical and abrasive cleaning of the sheets reduced the contact resistance by disturbing the oxide layer on the sheets. The reduction in contact resistance also improved weld quality and consistency.

Patrick et al. (1984) suggested how the aluminium oxide layer thickness could induce different electrode wear mechanisms (Figure 2-4). Patrick proposed that the high resistance oxide layer could constrict current flow and cause significant heat at the electrode-sheet interface when it is welded which could accelerate electrode wear (Patrick et al., 1984). It is known that the electrode sheet interface generates more heat in aluminium (Z. Li et al., 2007), however the figure from (Patrick et al., 1984) is most likely exaggerated to show the mechanism.

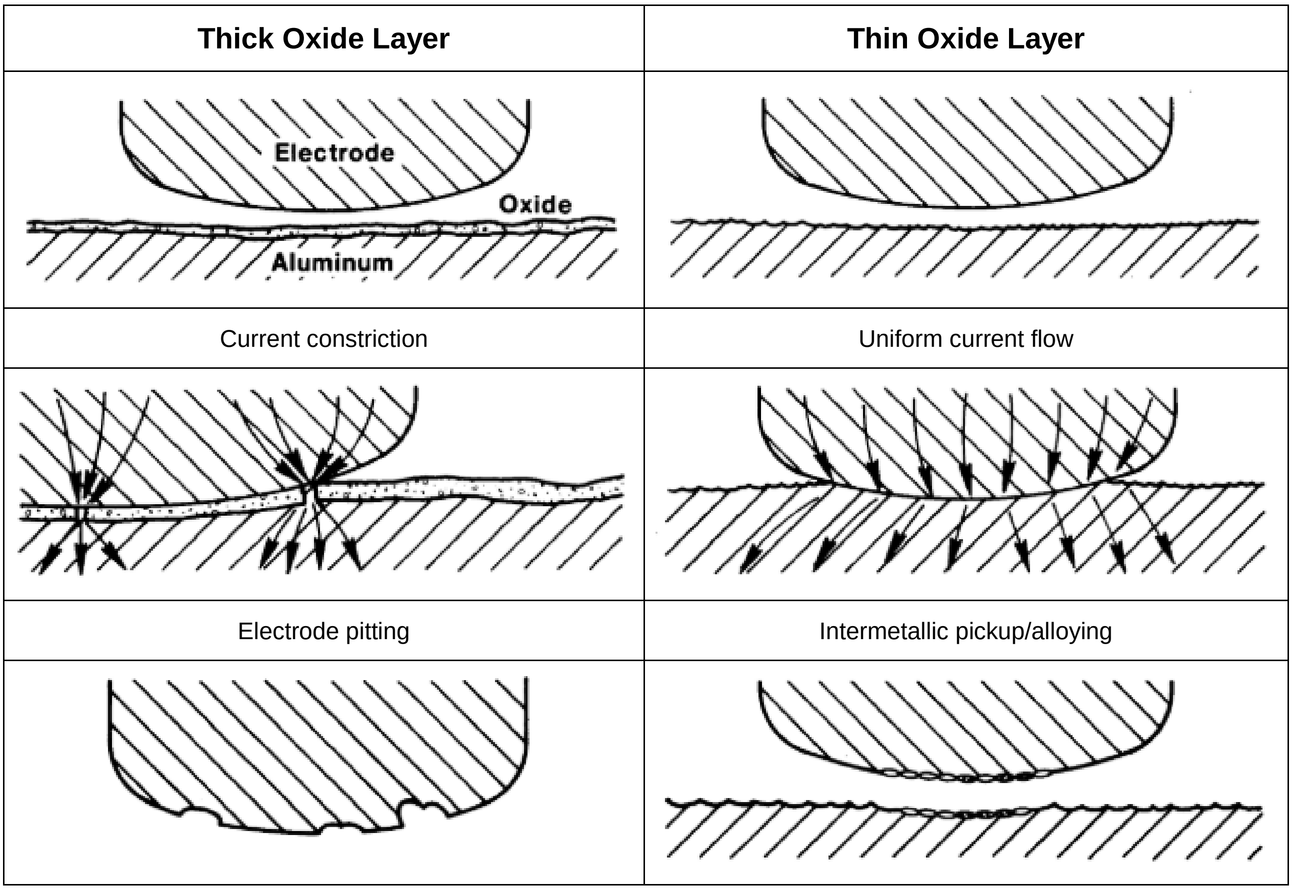

Figure 2-4: Effects of aluminium oxide layer thickness on electrode wear mechanisms (adapted from (Patrick et al., 1984))

Electrode-sheet alloying (Figure 2-4) has been investigated with Scanning Electrode Microscopy (SEM) by some of the same authors (Lum et al., 2004). They showed that regularly ‘cleaning’ the alloyed material from the electrode tip with an abrasive pad (polypropylene and aluminium oxide wool) significantly increased electrode life without requiring the electrode to be re-dressed.

A number of techniques can reduce the effects of electrode wear on weld quality in aluminium RSW. Reducing the electrode-sheet interface resistance reduces alloying and electrode pitting by minimising the heat at the interface (Patil et al., 2011). The electrode-sheet contact resistance can be reduced in a number of different ways.

The use of lubricants to improve electrode life has been researched with varying results. One lubricant was found to almost double the electrode life in an aluminium RSW process (Rashid et al., 2007). However, a slight drop in joint strength and nugget diameter was also observed and attributed to lower resistive heating caused by the drop in total resistance. Another lubricant trialled in the same study was found to reduce electrode life and weld quality which suggested the chemical composition and properties of the lubricant are very important. Another study found that wax lubricants from deep drawing increased contact resistances (rather than reducing them), this effect had to be mitigated by using a pre-heating current to displace the lubricant from the faying surface (Han, Thornton, Boomer, et al., 2010).

A technique similar to the application of a lubricant was the application of an electrically conductive carbon paste to the electrode/sheet interface (Patil et al., 2011). With this technique electrode life almost doubled before the quality of the welds dropped below a predetermined limit. The carbon paste was chosen because it was chemically inert to both the copper electrode and aluminium sheet which reduces the chance for electrode sheet alloying.

In a recent review article focussing on electrode life in aluminium RSW (W. J. Zhang et al., 2017), electrode surface coatings were discussed suggesting that the ideal surface coating would: reduce electrical resistance at the electrode/sheet interface, strengthen the electrode to protect from deformation in wear and reduce the propensity of the electrodes to adhere to the aluminium work piece. However, these effects have not been achieved without negatively effecting weld quality.

Electrode tip surface texture is a popular area of research in aluminium RSW which reduces the electrode/sheet interface resistance to improve quality consistency and electrode life (Deng et al., 2018). Lower electrode-sheet contact resistance and longer electrode life are correlated with a higher surface roughness on the electrode faces because the surface roughness helps to breakdown the electrode sheet interface resistance under the electrode clamping force (Thornton et al., 1997).

Several electrode tip surface modification techniques have been patented showing the perceived commercial value of such solutions to aluminium electrode wear. Some of the patents include a defined surface roughness (Patent No. US 7,249,482, 2007; Patent No. European 0 291 277, 1990; Patent No. US 6,861,609, 2005), or *'multiple extrusion rings'* (Figure 2-5 a) designed to break through the oxide layer on the surface and reduce the electrode/sheet interface resistance (Patent No. US 4,591,687, 1986). General Motors produced a similar design (Figure 2-5 b) with concentric rings cut into the electrode face with a specific electrode-tip dresser (Patent No. US 8,436,269, 2013). By reducing the electrode-sheet interface resistance, the bulk of the heat generation occurs at the faying surface which helps to mitigate electrode wear and generates the heat at the interface that is to be welded.

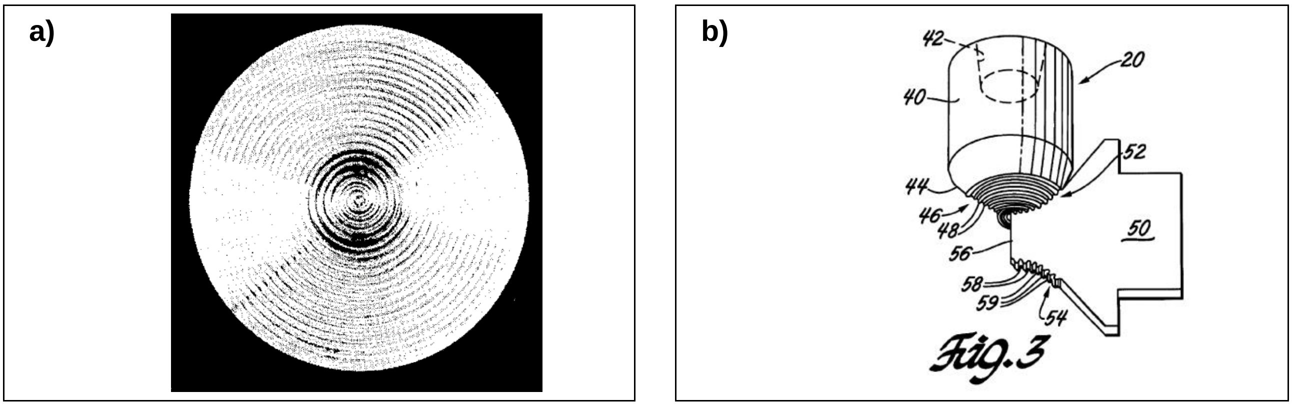

Figure 2-5 a) Extruded concentric rings electrode design (Patent No. US 4,591,687, 1986), b) GM electrode with concentric rings (Patent No. US 8,436,269, 2013)

2.5 Aluminium Quality Monitoring

Real-time quality monitoring of spot welds has been a focus of RSW research for a number of years, however the majority of the efforts have been focussed on steel and, more recently, advanced high strength steels. Quality monitoring research aims to reduce the need for costly destructive and non-destructive testing methods for ensuring quality consistency in passenger vehicles. To reduce the need for destructive and non-destructive testing, a number of methods have been proposed that model weld quality using measurable signals during welding. In steel resistance spot welding, a number of different signals have been successfully used to monitor quality including: electrode displacement and force (Gong et al., 2011; Podrzaj et al., 2014; Simoncic et al., 2014; P. Zhang et al., 2007; Y. S. Zhang et al., 2007), dynamic resistance & acoustic emissions (Podrzaj et al., 2005; Polajnar et al., 2008; Yi et al., 2016).

Quality monitoring in aluminium RSW is more difficult due to the different temperature-resistivity relationship and the propensity for the material to oxidise. However the electrode dynamics have been linked to weld button size, exploiting aluminium's high coefficient of thermal expansion to infer nugget growth (C. T. Ji et al., 2004). Acoustic emission counts measured from the electrodes directly have also been correlated with nugget nucleation in a preliminary study which found relationships to button diameter and strength (Yi Luo et al., 2013). Although promising, further work is required in acoustic emissions quality monitoring to address the issues of production environment noise in RSW.

Aluminium resistance spot weld quality is vulnerable to several factors that are difficult to control in production and so effective monitoring of weld quality is very important to ensure vehicle safety. Unfortunately, prediction of aluminium weld quality represents a large omission in the aluminium RSW literature with only two papers found that quantitatively predict the quality of aluminium resistance spot welds. The first is by Hao et al. (1996) and the other is shown in the work in Chapter 5 of this Thesis.

Hao et al. (1996) progressed aluminium resistance spot weld quality monitoring significantly by measuring several process signals and using linear and multiple linear regression to predict the load-bearing capacity of aluminium spot welds. It was found that none of the individual signals measured could be used alone to infer many aspects of the process as resistance can in steel RSW. It was concluded that a monitoring and control strategy could not be achieved using a single process signal. This finding means that the approach to aluminium resistance spot weld quality monitoring must be fundamentally different to the techniques that have been successful in steel RSW.

Weld quality monitoring studies, such as Hao's (1996), often try to find correlations with manually selected, simple features of the different signals. Hao selected a number of landmark points from different signals: initial values, final values, maximum values, mean values, difference between the minimum and maximum, slopes, and the integral of the curve. Figure 2-6 provides a visual representation of what the MFDC features mentioned in Hao's table '*Primary Extracted Features Used for the Analysis*' might look like, to show how the signal information is characterised.

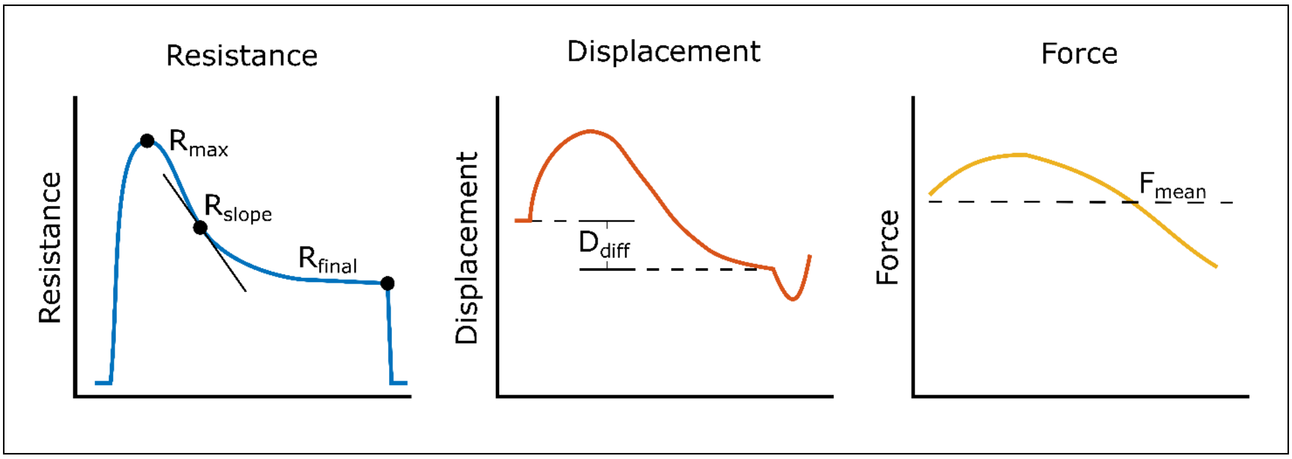

Figure 2-6: Graphical representation of the estimated features from the table: 'Primary extracted features used for the analysis' Hao et al. (1996)

Manually selected landmark points or simple features of a signal, such as its slope, are limited by the ability of the researcher to select the correct points for modelling. This type of feature extraction relies on the researcher's knowledge of the process and materials (which are frequently updated in industry).

The use of landmark points is effective for reducing the dimensionality of welding signals but it may over simplify the overall shape of those signals. It is not difficult to find two welds with similar resistance signals for example, that result in the same values for all of these metrics in an aluminium welding process (Figure 2-7). It is in these cases that the shape of the signal is more important than landmark points on the signal. Section 2.3.3 will cover principal component analysis and point distribution models which analyse the shape of signals.

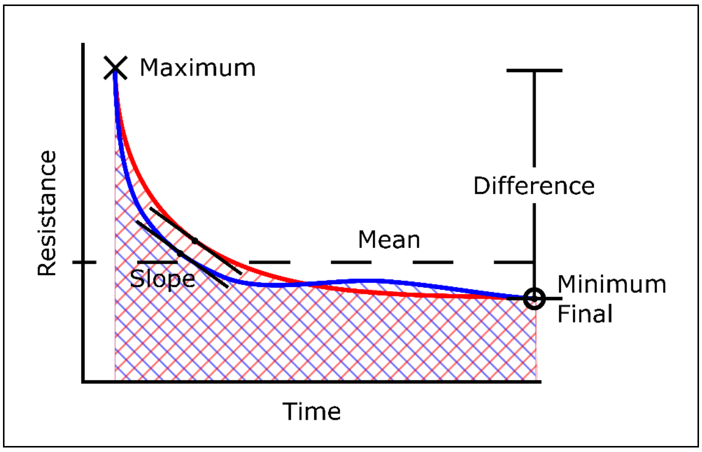

Figure 2-7: An example of hypothetical aluminium resistance signals that cannot be effectively identified from one another with a landmark point comparison

A short conference paper presented a *qualitative* weld quality monitoring technique that collected four different signals in an aluminium welding process (voltage, current, electrode displacement and force) and visually classified welds into three different categories (Pan et al., 2008). This paper is of interest because it uses PCA, one of the primary analysis techniques used in this thesis. Unfortunately, due to the brevity of the conference paper it was not clear how PCA was used, but most likely it was used to extract features from the signals for visual classification of the different process conditions. The welds were represented by principal component scores and visually separated into three different categories; good, bad and expulsion. Unfortunately this work has not been continued with no further publications in the academic literature. This thesis uses principal components (and tensor principal components) to create quantitative models for button diameter and tensile load bearing capacity as well as fault identification and separation in aluminium RSW.

An analysis technique called *kernel ridge regression* was used to predict the strength of welds based on the chosen input parameters such as: welding current, welding time and clamping force (Maalouf et al., 2017). This means that the method cannot be used for weld quality monitoring because it does not measure in-process information.

Little research in quality monitoring of aluminium RSW has been completed to date with few signals showing promise. The rest of this section summarises the literature that focusses on research that has linked signals in aluminium RSW to aspects of the process and as well as the small section of the literature which has made suggestions for adaptive control techniques.

2.5.1 Electrical Signals

In steel RSW, the resistance signal provides a good representation of the weld nugget growth using the resistivity-temperature relationship of iron in steels (Adams et al., 2017; Cho et al., 2002; Dickinson et al., 1980; Livshits, 1997; Yi Luo et al., 2016a, 2016b). The aim in steel RSW quality monitoring is to look for evidence of nugget growth and mechanical collapse of the material to show that the heat input has melted the material, fusing it together. This is a good strategy that works in a normal operating window in steel. However in aluminium RSW the resistance signal is not as useful.

Aluminium resistance signals do not exhibit a *'beta-peak'* as in Dickinson's (1980) theoretical resistance signal for steel RSW. The *beta-peak* in steel RSW resistance signals represents the increase in resistivity with temperature of the nugget. Analysis of the *beta-peak* can show if the spot weld's temperature is sufficient to produce a good spot weld. Unfortunately, the relationship between aluminium's temperature and its resistivity is not as strong as it is in steel, so aluminium resistance signals are not as useful for quality monitoring, showing very limited temperature related information. Example electrical signals are shown in Figure 2-8. The secondary peak in the resistance signal is likely to be due to the inductance in the process when the current changes from the low pre-heating current to the high welding current.

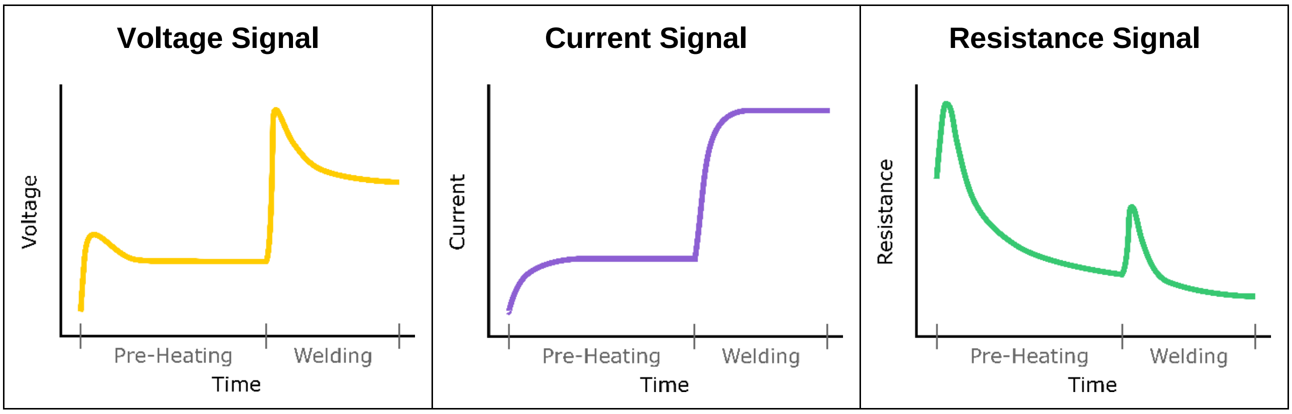

Figure 2-8: Example aluminium RSW electrical signals

In aluminium RSW the electrode-sheet interfaces have been found to be the same order of magnitude as the resistance at the faying surface. The electrode-sheet and faying surfaces also change throughout welding in the same way, which means the information at the faying surface is masked by the electrode-sheet interfaces and is not as useful for monitoring spot weld growth (Thornton et al., 1996).

A study that was focussed on a new approach for mitigating the effects of electrode wear in aluminium, also applied a neural network to predict the button diameters of the welds based on the electrical signals measured by the weld timer at the very end (Boomer et al., 2003). The study only varied welding current to generate variation in button diameter which unfortunately does not show that the technique would be useful for weld quality monitoring in a production environment where the factors affecting weld quality will not be changing weld schedules. Modelling weld quality was not the primary focus of this study so the details relating to the neural network model were not extensive.

Weak correlations between button diameter and manually extracted landmark points from the resistance signal were found in Aluminium RSW in Hao's study (1996), including the mean resistance value and final resistance value of a weld. However, limited work has been completed to date using the electrical signals for weld quality monitoring.

2.5.2 Mechanical Signals

Of the signals that have been investigated for correlations to aluminium spot weld quality, mechanical signals are by far the most popular and potentially useful. In general, the electrode force or electrode displacement signals are measured. Example signals are shown in Figure 2-9 for context.

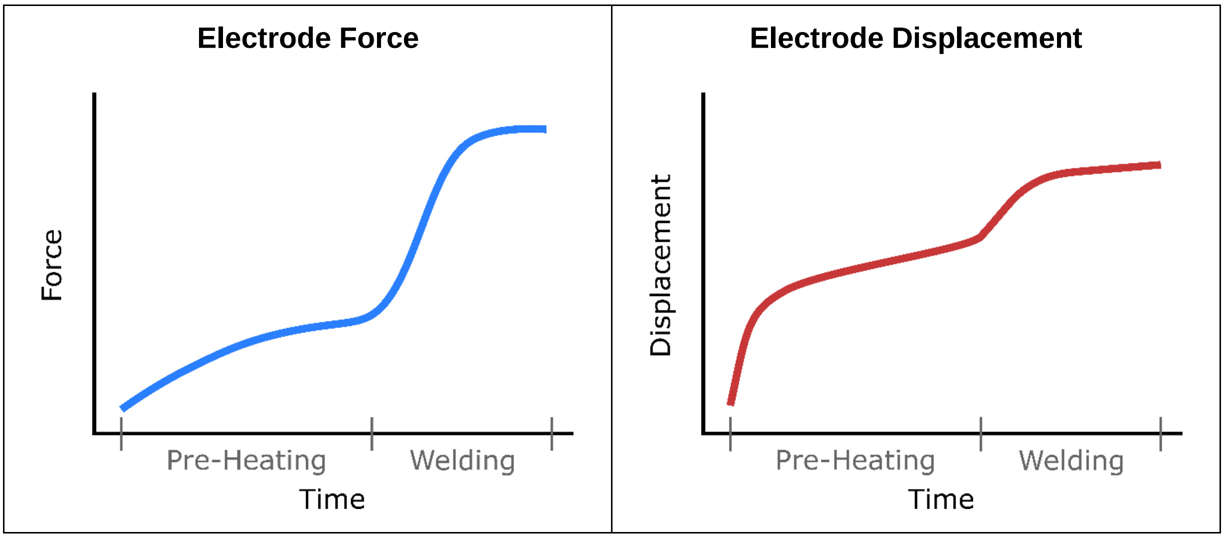

Figure 2-9: Example RSW mechanical signals

Aluminium has a high coefficient of thermal expansion, approximately double that of most steels. This means that the amount of thermal expansion or the increase in force on the electrodes throughout the process can be linked to the amount of heat in the process. Both these signals provide a one-dimensional representation of the amount of thermal expansion of the spot weld. This is used to infer the radial growth of the spot weld at the faying surface. Unfortunately the mechanics of the particular spot welder design play a significant role in the behaviour of these signals. For instance, pneumatically controlled spot welders provide a constant force to the sheet-metal which means that arguably only the electrode displacement is relevant for quality monitoring (as the force should stay constant). More modern spot welder designs often use servo driven electrodes to allow for more control during the process, and the servo-driven design often lends itself to monitoring changes in the electrode force which are typically minute in comparison to the electrode clamping force required to weld aluminium. The rigidity and stiffness of the welder have a large effect on the force signals.

Total or differential electrode expansion has been linked to weld quality in a number of studies with varying results. The differential electrode expansion is the difference between the peak of the displacement curve and the trough during the forging cycle. Hao et al. (1996) found that the differential electrode displacement was correlated with the button diameter for 2mm sheets but not for 1mm sheets of the same material, as shown in Figure 2-10 (M. Hao et al., 1996). Later, total electrode displacement for thinner sheets (1mm and 1.5mm) was found to be correlated with button diameter (C. T. Ji et al., 2004). Further work by the same group found the maximum electrode displacement of thinner sheets 1mm and 1.5mm was correlated with button diameters over a small range (C. Ji et al., 2010). For the rest of the data outside the narrow range, the maximum electrode displacement values corresponded to a wide range of button diameters (0 – 4mm).

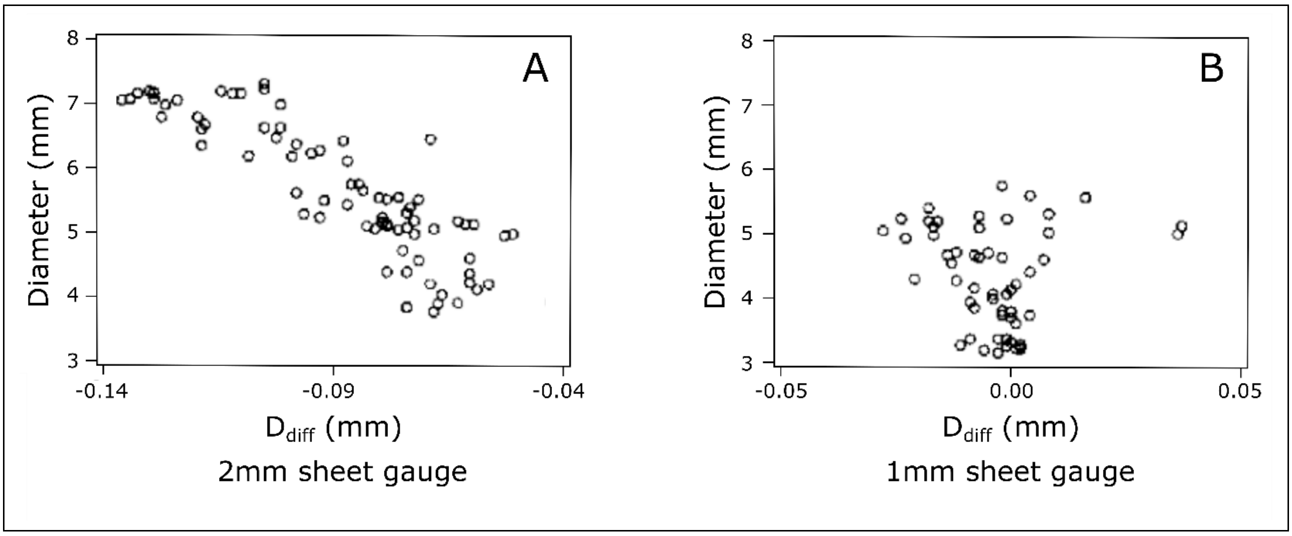

Figure 2-10: Button diameter vs. differential electrode displacement, (A) 2mm sheet, (B) 1mm sheet (M. Hao et al., 1996)

Further work is required to understand the relationships between the electrode displacement curves and weld quality. From the current literature it does not appear that electrode displacement can be used to monitor weld quality on its own.

Changes in electrode force can be measured from the minute growth and collapse of the aluminium spot welds in modern weld timers. Accurate load cells are required to measure these changes which can be particularly sensitive to magnetic noise. Load cell location and technology is dependent on the electrode arm design and is not always measured from the same place.

Little work has been reported in the academic literature linking electrode force measurement signals to weld quality. However, a few small contributions have been published. Variation in the electrode force in an pneumatic clamping system was linked to weld strength, based on the assumption that when there is more intense heating in a RSW process, the electrode force will fluctuate more (Simončič et al., 2014). However, pneumatic clamping is used less and less in modern automotive spot welders with technologies that provide greater control favoured over the constant force of a pneumatic system.

Welds were categorised into three different button diameter ranges by plotting welds using features of their electrode force signals (Chien et al., 2002). Their *'peak force gain over applied force'*, a ratio between the peak force and the force set by the weld schedule, and the *'peak force time to current cut'* which was a representation of the lag in the mechanical system that causes the force to peak after the welding current had stopped where used to categorise welds. This complicated representation allowed welds to be visually separated with a low level of accuracy.

Despite a lack of reported success in the academic literature, major automotive spot weld timer manufacturers, ARO (ARO, 2019), Bosch (Haeufgloeckner, 2017), WTC (Welding Technology Corp, 2019) and Matuschek (Matuschek, 2018) all use electrode force or displacement measurements for quality monitoring in their aluminium RSW systems. This shows that there is significant proprietary research into the correlations between weld quality and the electrode force or displacement which is not reflected in the published academic literature.

2.5.3 Acoustics Signals

The use of acoustic emissions from the electrodes has been suggested in the literature and trialled in steel RSW and briefly in aluminium RSW but faces challenges in implementation in production. The acoustic emissions from steel spot welding are thought to be related to the progression of nugget growth as the material melts and changes phase (Polajnar et al., 2009), and expulsion (Charde et al., 2016), although the links to weld quality are yet to be shown consistently in the literature.

Acoustic emissions measured from the electrodes during RSW steel have not been found to be sufficient for determining weld quality alone, although some useful information related to quality has been uncovered. Difficulties with noise have been cited, including the electrode cooling water noise, environmental noise, electrical noise and electrode knock, all of which cannot be related to quality and are more likely to be present in production (Polajnar et al., 2008).

Acoustic emissions have been linked to aspects of the process of nugget growth and collapse in aluminium RSW. Luo et al. (2013) identified expulsion, and cracking caused by thermal contraction during the forging cycle from acoustic emission signals. Some preliminary correlations to button diameter and tensile-shear load bearing capacity were made using the *'acoustic emission count'*. The acoustic emission count represents the number of peaks in the signal and was correlated with button diameter with a very small sample size of only eight welds (Figure 2-11 a) (Yi Luo et al., 2013) and tensile shear load bearing capacity (Figure 2-11 b). The tensile-shear load-bearing capacity of welds was said to have a logarithmic relationship with the acoustic emission count, however this means that the full range of load values (~1.5kN to ~6kN) is represented by any acoustic emission count between 300 to 500, while the strongest welds had acoustic emission counts between 300 to 1000 (also, the full range of measurements). This shows that much more work is required before acoustic emissions could be used as a signal for quality monitoring in aluminium RSW.

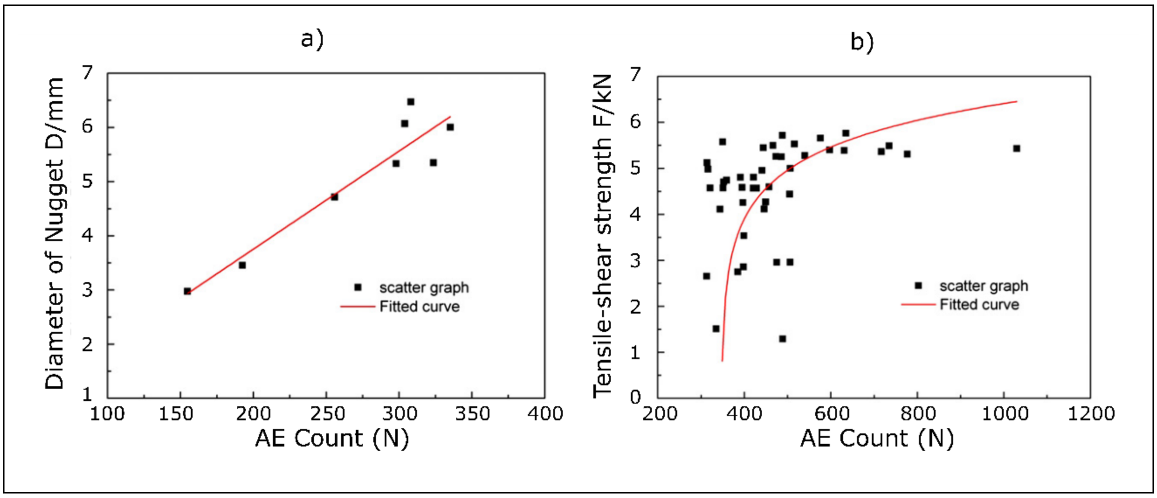

Figure 2-11 a) Button diameter vs. acoustic emission count (Yi Luo et al., 2013), b) Tensile strength vs. acoustic emission count (Yi Luo et al., 2013)

These are the only two instances of the use of acoustic emissions for weld quality monitoring in the literature, apart from an almost identical paper by Luo which uses the same data and has very similar results (Y. Luo et al., 2013). There are no known commercial systems that use acoustic emissions for weld quality monitoring, which is most likely due to the significant challenges associated with noise and implementation.

2.5.4 Adaptive Control

Adaptive control in steel RSW is most commonly achieved by increasing the welding current or time mid-process to increase the heat input into a spot weld that has been determined not to be generating enough heat. This decision is usually made by monitoring the resistance signal, which is not as closely linked to the heat input in aluminium RSW.

One of the motivations behind developing effective weld quality monitoring in aluminium RSW is to be able to adaptively control the process so that changes can be made mid-process to rectify issues as they arise. Clearly a better understanding of the factors that affect the process and the resultant weld quality is required. A handful of articles that have discussed adaptive control in aluminium RSW are discussed below.

Unfortunately, in aluminium RSW, further heat input into a spot weld is not as effective as it is in steel due to the high thermal conductivity of aluminium which often also causes warping in the panel. Panel warpage produces problems for closure gaps and part quality further down the production line. Adaptive control techniques such as this are likely to render the information in most quality monitoring techniques redundant, as the operating window has changed and would require further analysis and modelling to understand the effects of each intervention.

Little work in adaptive control of Aluminium RSW has been reported in the literature, however similar techniques to that used in steel RSW have been proposed. Most methods monitor an output signal such as electrode displacement or force, and use current modulation in an attempt to achieve an idealised rate of change or final value which is experimentally determined. Ji et al. (2004) suggested a specific rate of electrode displacement of 4.3mm/s or a rate of force of 16,000N/s for a given material stack, however this is not a universally applicable solution. It has also been proposed that welding could be stopped when the rate of change of electrode displacement becomes zero, signalling that the spot weld is no longer growing (C. T. Ji et al., 2004). This may be a more applicable technique for a general approach to adaptive control but may also be highly dependent on the welding current that is chosen. All these conclusions are most likely specific to the welding setup, welding machine and material only.

A neuro-fuzzy algorithm was developed to deal with part fit-up issues. The method changed the current during welding to achieve an electrode displacement curve similar to an experimentally derived, idealised curve (Y. S. Zhang et al., 2005). Interestingly it was found that the current only had to be altered by as much as ±200 amps during welding to achieve something very close to the idealised displacement curve. This is promising work and requires further development and testing for implementation in industry.

The same approach was applied to electrode wear by the same group of researchers, compensating for electrode wear based on electrode displacement signals (Y. S. Zhang et al., 2007). However, there are other parameters beyond electrode wear and part fit-up that affect weld quality in aluminium RSW, namely surface condition, material type and a wide range of other faults. These studies show promise for complete adaptive control of aluminium RSW, but more work is required in the areas identified as well as different faults beyond the brief study that looked at an unidentified part fit-up issue.

Methods for adaptive control of the welding process have been patented, such as adaptive control of the electrode displacement curve (Patent No. US 4,861,960, 1989). This patent does not specify the material that the invention is intended for, but mentions that the invention adapts for surface oxide variations which implies it is for aluminium RSW. Given the importance of thermal expansion as a monitoring tool in aluminium adaptive control, this invention would have clear benefits for adaptive control of aluminium spot weld quality. The authors of another patent claimed that through monitoring the electrode displacement they could produce a model for measured strength of spot welds (Figure 2-12).

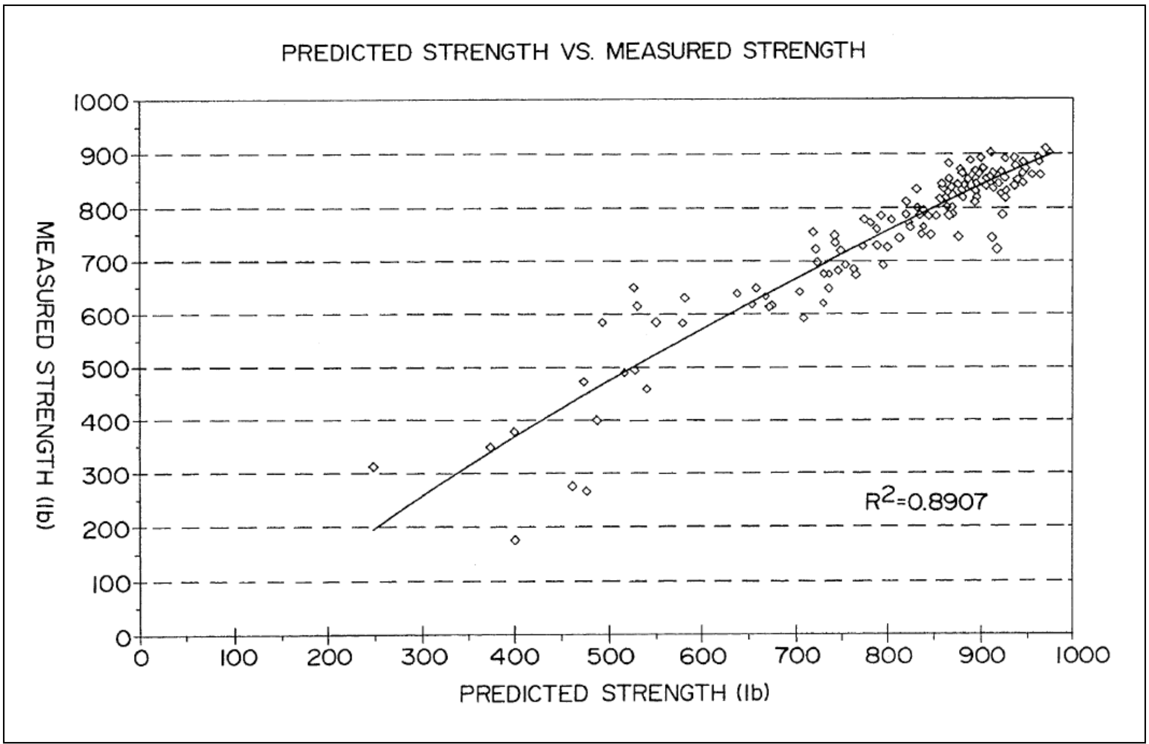

Figure 2-12: Weld quality model (Patent No. US 5,558,785, 1996)

This represents one of very few weld quality model attempts in aluminium RSW (Patent No. US 5,558,785, 1996). Unfortunately, there is insufficient detail in the patent documentation to understand what was done to achieve this or to further the understanding of modelling the aluminium RSW process for the purpose of this literature review.

For clarity, both axes of Figure 2-12 range from 0 to ~4.5kN with measured weld strength (or load bearing capacity) ranging from ~0.9 to ~4.25kN. The error in the prediction appears to increase as the welds get weaker which is most likely due to the different failure mechanisms that are prevalent with smaller and poorly formed spot welds.

2.6 Conclusion

It has been established that there are significant challenges associated with maintaining high quality in aluminium spot welding that are not as prevalent in steel RSW. The challenges result in significant quality inconsistency and electrode wear which has the potential to cause issues for vehicle safety in the automotive industry. Unfortunately, due to the volatility of the process to small changes and the consequences for weld quality that are caused by aluminium's unique properties, one process signal is not sufficient for weld quality monitoring.

To address this, a methodology using PDM (Point Distribution Models) and PCA (Principal Component Analysis) for weld quality monitoring has been developed in this thesis in steel RSW (Chapter 4). This will be applied to the analysis of multiple signals in aluminium RSW (Chapter 5) and extended to complete analysis of the process signals and their interactions using TPCA (Chapters 6 and 7).

The aluminium RSW literature has focussed on the mitigation and monitoring of electrode wear as well as techniques for improving quality consistency and monitoring. However, quality monitoring of aluminium RSW still remains a significant gap in the literature, and a challenge in industry as automotive manufacturers have begun to mass produce car bodies from aluminium. To achieve consistent quality monitoring of aluminium RSW the correlations to weld quality of the various measurable signals and the way that the interactions of these signals correlate with weld quality needs to be further investigated to improve aluminium weld quality monitoring. This forms the research question of this Thesis.

Can the interacting behaviour of multiple process signals measured during aluminium RSW be used to monitor weld quality? Can they provide useful insights into the process and final quality of aluminium resistance spot welds?

The concept of manufacturing process monitoring based on PDM signal shape analysis was introduced in the context of sheet-metal stamping. This technique was applied to steel weld quality monitoring in Chapter 4 which shows that the features extracted from the resistance signal in steel RSW are very useful for weld quality monitoring. To address the more challenging process of aluminium RSW and to answer the research question of this Thesis, a Tensor Principal Component Analysis based technique was developed to analyse multiple signals and their interactions in aluminium RSW which improves upon the results that can be achieved with a single signal.

Chapter 3

Methodology

Aluminium weld quality monitoring is a challenging task as has been highlighted in the Literature Review and Introduction. Weld quality is typically measured as the weld's strength or the size of the weld measured after a destructive test. To develop a novel approach to aluminium spot weld quality monitoring and address the primary research question of this thesis, some preliminary work was completed in steel spot weld quality monitoring. Developing a weld quality monitoring technique for steel RSW allowed for a number of challenges to be addressed before moving to the more challenging problem of aluminium weld quality monitoring.

The approach taken to developing weld quality models in this thesis is two-fold. Initially, models and analysis techniques were developed with laboratory data which is easy to collect and allows uncontrolled variables to be kept to a minimum. Once the techniques are refined, the models and analysis methodology were tested in industry with industrial welding data. Prediction of weld quality on a production line to improve vehicle safety and reduce costs to production is the broader goal of this research and so the research was tested in the environment in which it is intended for.

To create a weld quality model process signals are measured during each weld. Welds are then destructively tested to determine their quality. Once the quality of welds has been measured, analysis of the signals recorded during welding is conducted to find the features of the signal that are related to weld quality. Using the measured weld quality and the signal features that relate to the quality, a model is calculated.

The purpose of a signal-based weld quality model is to predict the quality of welds in production without the requirement of intermittent destructive or non-destructive testing. The features of the signals found during training are extracted from the production weld signals and passed through the model. This means that the quality of the weld can be predicted on the production line. For industry this represents significant cost saving as it reduces the need for time consuming and costly non-destructive testing of welds in production.

This chapter covers the common methods used in this thesis, the samples, destructive testing, signal collection, equipment and how weld quality models are created.

3.1 Methodology to Address the Research Question

At the end of the literature review the research question was posed.

> *Can the interacting behaviour of multiple process signals measured during aluminium RSW be used to monitor weld quality? Can they provide useful insights into the process and final quality of aluminium resistance spot welds?*

To address this research question first a method for monitoring weld quality in steel resistance spot welding was developed. This was completed first because steel RSW and the factors that relate to weld quality are better understood than in aluminium RSW. In steel RSW the resistance signal is known to have a strong relationship with the quality of the weld. This allowed for a signal based weld quality method to be developed which only requires the analysis of a single signal. From this exercise a signal shape feature extraction technique that predicts the result of a destructive test was used to model weld quality.

The signal shape analysis technique was extended to analyse five signals in a simple aluminium RSW study that included process variation in the form of electrode wear only. This allowed for the investigation of the usefulness of different process signals for aluminium weld quality monitoring in a relatively simple preliminary study.

To investigate the efficacy of analysing the interactions of multiple signals for aluminium weld quality monitoring, a new signal representation had to be employed. This made the analysis more complicated and required significant work to develop a model for weld quality. Initially this technique was developed with data in the laboratory with variation in the process limited to differences in machine settings and prolonged electrode wear.

Finally, the aluminium weld quality technique that analyses the interactions of multiple signals was tested with significant industrial aluminium RSW data. This allowed for the technique to be tested with a wide range of process faults and conditions and tested the theory that the interactions of process signals would create successful weld quality monitoring models.

3.2 Destructive Testing and Measurement Methods

The quality of resistance spot welds can be measured in a number of different ways. The decision of which method to use depends on the material, situation and purposes of the test. From the perspective of safety and design, the strength of the joint should be the primary measurement of weld quality. However, the automotive industry has adopted the button diameter of spot welds as their primary measure of quality as it is easy to obtain and can be measured for any joint configuration. The button diameter is used as a proxy for the strength of the spot weld. A standard sample size of 25mm by 100mm was used for all weld trials in different configurations for different destructive tests (Figure 3-1).

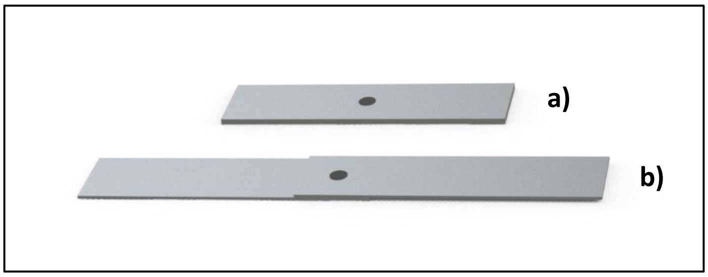

Figure 3-1: Weld samples, a) chisel sample, two or more sheets stacked directly on top of one another, b) tensile-shear sample, two partially overlapping sheets with a weld in the middle, allowing each sheet to be held individually for tensile shear testing.

In this thesis a number of studies use the tensile-shear load bearing capacity of spot welds as the primary measure of weld quality. The tensile-shear load bearing capacity is used due to its repeatability, direct relation to the strength of the joint, and to mitigate some of the effects of different failure mechanisms on weld quality models. The tensile-shear load bearing capacity was used in the preliminary studies for modelling aluminium laboratory data instead of the measured button diameter so that a continuous measure of quality could be used. Using the tensile-shear load bearing capacity somewhat mitigates the complexity of different failure mechanisms and the different types of buttons they produce.

There are a number of factors that can affect to the strength of a spot weld which may not be represented by the measured button diameter from a destructive test. Some of these include: expulsion, the Heat Affected Zone (HAZ), porosity in the nugget, cracking, circularity of the nugget and different fracture mechanisms. These are some of the reasons why the tensile-shear load bearing capacity was used in the preliminary studies for aluminium weld quality monitoring.

A number of different measurements of strength are commonplace in resistance spot welding including: tensile-shear strength, peel strength, cross-tension strength, impact and fatigue strength. Information on these tests can be found in standards documents such as the AWS D8.7M Standard: *Recommended Practices for Automotive Weld Quality – Resistance Spot Welding* (AWS, 2005). Most commonly, the tensile-shear strength or tensile-shear load bearing capacity is measured due to its ease of measurement and repeatability.

3.2.1 Tensile-Shear Testing Protocols and Equipment

The tensile-shear test provides a number of metrics for assessing weld quality. Primarily, the test is used to determine the maximum tensile-shear load bearing capacity of the weld before failure, often called the tensile-shear strength or just weld strength. A tensile-shear test can also be used to determine the energy absorbed up to the load bearing capacity and often results in a button pull-out. After the test the button diameter can often be measured, however it is usually stretched during the test and is not the primary purpose of the tensile-shear test.

The tensile testing machine used for all tensile tests was an Instron 5500R with a testing rate of 10mm/min for all welds (Figure 3-2). This provides a quasi-static load to the joint until failure and results in the tensile-shear load bearing capacity in Newtons.

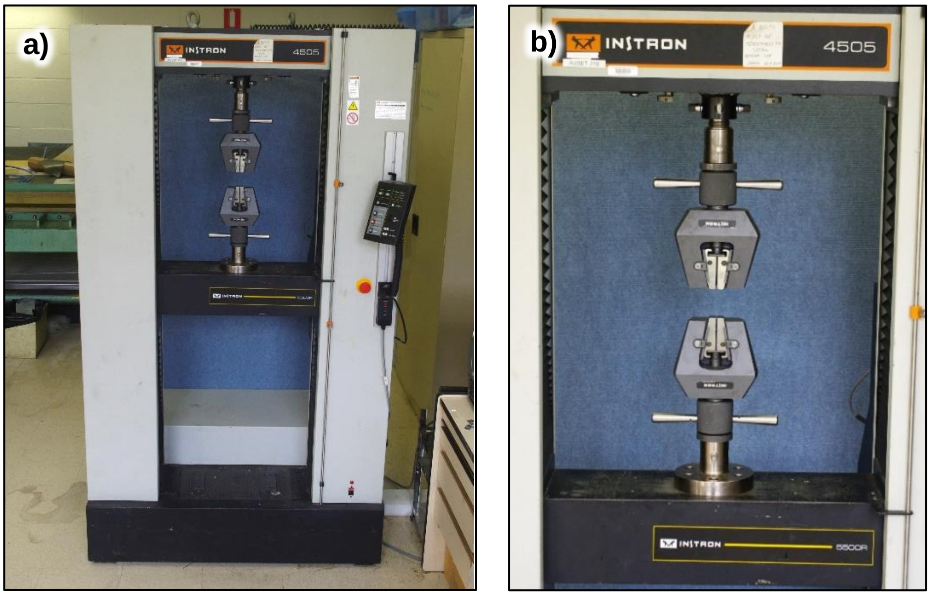

Figure 3-2: a) Instron 5500R universal testing machine, b) sample grips

All samples for the tensile-shear tests were overlapped by 25mm with the spot weld created in the middle of the overlap (Figure 3-1 b). To remove the moment placed on samples, shims were used in each grip of the Instron to centralise the location of the nugget in between the jaws. The same

100kN load cell was used for most welds as the next smallest load cell is 5kN. This load cell has a linearity of 0.15% of the range of the load cell (100kN).

3.2.2 Button Diameter Measurement Process

Button diameter measurements can often be taken after a destructive test. The button diameter is calculated as the average of the smallest and largest diameters of the weld button, measured with Vernier callipers (Figure 3-3 a) (American Welding Society, 2012). This technique works well in steel resistance spot welding because the failure mechanism is often complete button pull-out or complete interfacial shear failure rather than partial thickness fractures. Unfortunately this is not always the case for aluminium spot welding which is more susceptible to a range of different failure mechanisms. This topic will be discussed further in Chapter 7, in the industrial case study. The weld samples that were to be assessed by their button diameter were completely overlapped with the spot weld created in the middle of the sheet (Figure 3-1a).

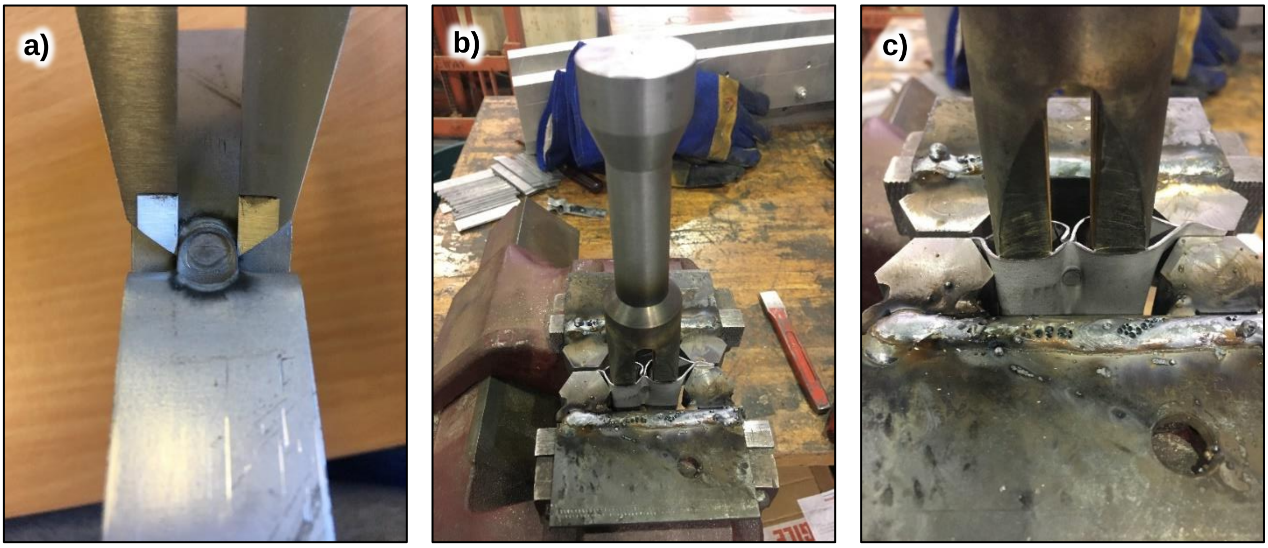

Figure 3-3: a) Spot weld chisel tool and fixture, b) destroying a spot weld, c) button diameter measurement

A specially designed chisel tool was made (Figure 3-3 b) to destroy spot welds for button diameter measurements (Figure 3-3 c). The chisel applies a load with a wedge either side of the spot weld and is designed to be used with a hammer. Conducting the test manually reduces the chances of striking the nugget with the blade of the chisel. It also allows for consistent loading of the spot welds on each side of the spot weld at the same time, rather than loading one side then the other with a conventional air chisel. The chisel method loads the spot weld in a different direction to the tensile-shear test and commonly produces a button pull-out failure. Additionally, the chisel method applies a percussive load rather than a quasi-static like the tensile-shear tests.

3.3 Welding Signal Collection and Processing

The main signals collected during the welding processes in this thesis included the: electrical signals (current, voltage and resistance), electrode displacement and electrode force. The resistance signals were calculated using Ohm's law ($R = V/I$). For AC welding the resistance was calculated using the peaks of the current and voltage signals. While in Medium Frequency Direct Current (MFDC) welding the resistance were calculated directly from the regular measurements of current and voltage.

Displacement signals were measured during welding using a laser triangulation sensor (Figure 3-4). Two different lasers displacement sensors were used. The measurement window of the sensor used in Chapter 5 was 5mm with a repeatability of 9μm (Micro-Epsilon optoNCDT1402). The sensor was mounted to the upper electrode and referenced using a plate mounted on the lower electrode. The relative difference from the starting value was used to track the change in displacement during welding. The same approach was taken to measure the electrode displacement in Chapter 6, however a newer, more accurate laser (Micro-Epsilon optoNCDT 1750). The measurement window of this laser displacement sensor was 2mm with a repeatability of 1.6μm.

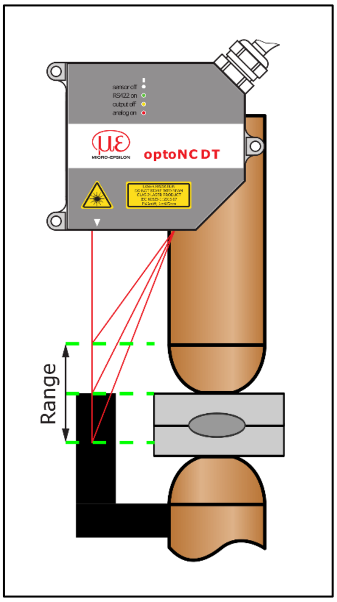

Figure 3-4: Electrode displacement measurement setup, laser adapted from (Micro-Epsilon, 2017)

The electrode force in Chapter 5 was measured using a 5kN load cell mounted under the lower electrode.

3.4 Principal Component Analysis

This thesis will show that to create a model for weld quality it is important to extract relevant features from the measured signals. The features used for weld quality monitoring should encapsulate information from the entire process. It is important to analyse information from the entire signal because different phenomena can affect the measured signals at different points in the process. The best way to encapsulate this information is to look at the entire shape of the signal.

The analysis of signal shapes is possible through the use of PCA. PCA calculates a new set of orthogonal axes which are aligned with the directions of highest variance in the data (Figure 3-5). This means that the data can be represented as their position along the new axes and because they are orthogonal and aligned with the dataset's variance the later principal components often describe minute amounts of variation in the data. This allows for the information to be represented more efficiently only using the first few principal components with minimal information loss.

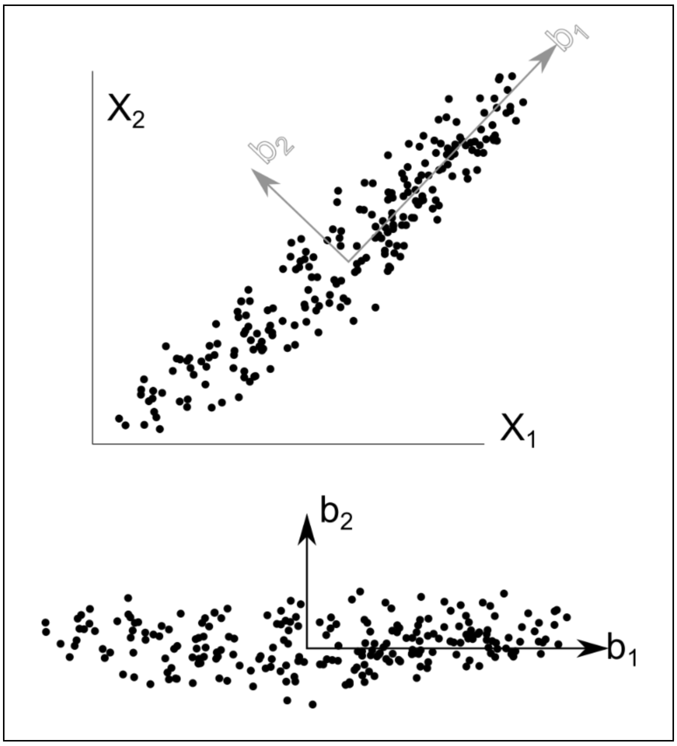

Figure 3-5: A visual representation of PCA in two-dimensions (David Adams, 2016). The data from the original axes (X_1, X_2) can be more efficiently represented by the principal components of the data (b_1, b_2)

The example in Figure 3-5 is of signals that have two measurements in them (x_1 and x_2). Each point represents a signal using its x_1 and x_2 values as coordinates on the X_1 and X_2 axes. Normally these signals would be represented in the time domain with the measurement x_1 at $t = 1$ and x_2 at $t = 2$. The principal components (new axes) can also be represented in the time domain which shows the major signal shapes in the data based on the variance in the dataset.

The process of calculating the principal components of a dataset will be shown with an example signal set (X). X consists of n vectors stored in an $n \times m$ matrix with each column representing a weld's signal. Each row (m) of the matrix corresponds to the point in time that the measurement was taken.

$$X = \begin{bmatrix} x_{1,1} & \cdots & x_{1,n} \\ \vdots & \ddots & \vdots \\ x_{m,1} & \cdots & x_{m,n} \end{bmatrix}$$

First, the mean signal ($\bar{x}$) from X is subtracted from each signal to make the dataset zero-mean. In the context of weld quality monitoring this is done so that the changes from the mean signal can be analysed.

Then the covariance matrix (C) of all vectors in X is calculated using the covariance equation between two vectors.

$$C = cov(a, b) = \frac{1}{N-1}\sum_{i=1}^{N}(a_i - \mu_a) * (b_i - \mu_b)$$

The eigenvalue equation for the covariance matrix (C) of X is:

$$Cv = \lambda v$$

PCA calculates the eigenvalues (λ) for the signal set (X) by computing the *characteristic equation*.

$$(C - \lambda I)v = 0$$

$$\det(C - \lambda I) = 0$$

The unique solutions to the characteristic equation represent the eigenvalues (λ). A brief example:

$$C = \begin{bmatrix} 3 & 1 \\ 1 & 3 \end{bmatrix}$$

$$C = \begin{vmatrix} 3-\lambda & 1 \\ 1 & 3-\lambda \end{vmatrix} = (ad - bc) = (3-\lambda)^2 - 1 = 0$$

$$\lambda^2 - 6\lambda + 8 = 0$$

$$\lambda_1 = 4, \qquad \lambda_2 = 2$$

Using the eigenvalues, the eigenvalue equation can be solved for the eigenvectors.

$$X - 4I = 0 = \begin{bmatrix} -1 & 1 \\ 1 & -1 \end{bmatrix} \quad \rightarrow \quad v_1 = \begin{bmatrix} 1 \\ 1 \end{bmatrix}$$

$$X - 2I = 0 = \begin{bmatrix} 1 & 1 \\ 1 & 1 \end{bmatrix} \quad \rightarrow \quad v_2 = \begin{bmatrix} -1 \\ 1 \end{bmatrix}$$

The ordered eigenvectors of the covariance matrix of the data are called the *Principal Component Matrix*. Each eigenvector has a corresponding eigenvalue. The eigenvalues represent the spread of the data along the eigenvector. In Figure 3-5 the range of the data is greater along principal component b_1 than principal component b_2 which means that the eigenvalue for b_1 is greater than the eigenvalue associated with b_2.

The percentage of the variation in the data that is described by a particular eigenvector (or principal component) can be calculated as it eigenvalue divided by the sum of all eigenvalues. This shows the amount of variation (or range) in the point cloud along each principal component. For instance the explained variance of the principal components in Figure 3-5 might be 90% and 10% respectively.

The explained variance is used to determine the importance of the principal components for describing the data. In Figure 3-5 the majority of the variance in the data is along the new principal axis b_1. If the data was only represented by its position on the axis b_1 then 10% of the datasets variance would be lost. Often in welding data, the first four principal components describe the vast majority of the total variation in the data (greater than 95%).

3.5 Modelling Weld Quality

Throughout this thesis the same approach was taken to weld quality monitoring. To train a model, welding data was collected (called a training set or training data) which aimed to generate a broad range of weld quality in the data. Training welds were destroyed to determine their quality. Features were extracted from the welding signals and their correlation with weld quality was assessed. Signal features that were correlated with weld quality were used to create a model from the signal information.

Once a weld quality model was developed, its accuracy was tested (where possible) on new data to show that it could predict the quality of new welds not included in the training data. Validation data in this thesis ranges from normal operating conditions (only electrode wear variation), to extreme process faults and electrode wear that would cause an issue if they were to occur on a production line in industry.

3.5.1 Weld Quality Model Rules

A process for creating weld quality models from principal components was developed for this thesis. The process was used throughout for consistency and comparative purposes. The rules that have been determined for selecting principal components for weld quality monitoring are as follows:

1. A Pearson’s correlation coefficient (R-value) is calculated between a set of principal component scores and the measure of weld quality. At the same time a hypothesis test is calculated for each correlation resulting in a p-value. Statistical precedence suggests that the significance of a correlation can often sufficiently be determined if the p-value is less than 0.05, which has been found to be appropriate for weld quality monitoring.

2. Once the set of principal components with statistically significant correlations to weld quality has be determined the amount of variance that the principal component explains in the training data is assessed. Again, an empirical threshold value has been chosen of greater than 1% to avoid using signal variation that can often be considered as noise. This has been found to be a good threshold for welding signal data throughout this thesis.

3. Once principal components are selected, the principal component scores are used to calculate a model of weld quality for the training data. In all cases a simple linear regression with no interaction terms has been used.

Using a standardised set of rules for weld quality models created using signal features allows for comparison of the different feature extraction techniques that will be used in Chapters 4, 5, 6 and 7.

3.5.2 Process Faults used to Test the Weld Quality Models

Throughout this thesis a number of spot welding process faults were used test the weld quality models created and to induce variation in the output quality, shown in Figure 3-6.

The baseline condition refers to welds created with an appropriate set of welding settings (known as a weld schedule) without any uncontrolled variance. Electrode cap offset changes the electrode sheet contact area and was created by sliding one of the electrode arms further into the machine to produce the offset. Electrode tilt or electrode-sheet misalignment was created either by fixing the sheet metal sample in an angled fixture or by adjusting the angle of the welder when a robot mounted welder was used.

For the adhesive condition Teroson MS 9220 automotive adhesive was applied to the faying surface of welds prior to welding. Electrode clamping force variation was changed by adjusting the force setting by set percentages from the baseline condition. Electrode wear was induced by not redressing the electrode tips during prolonged welding trials. Material changes were used to create process variation by applying the baseline weld schedule to a material stack that had one of the sheets replaced with a different grade of the base material. The no equaliser fault is a process condition unique to servo driven, robot mounted spot welders (the most common type in industry). The spot welder has an equalisation process to ensure that the workpiece is directly in between the upper and lower electrodes when they close. If this function is turned off, inaccuracies in the robot programming result in the sample being slightly above or below the intended interface between the electrodes when they close. This causes the sheet metal to bend up or down to lie in the middle of the upper and lower electrodes as it yields to the large electrode clamping force.

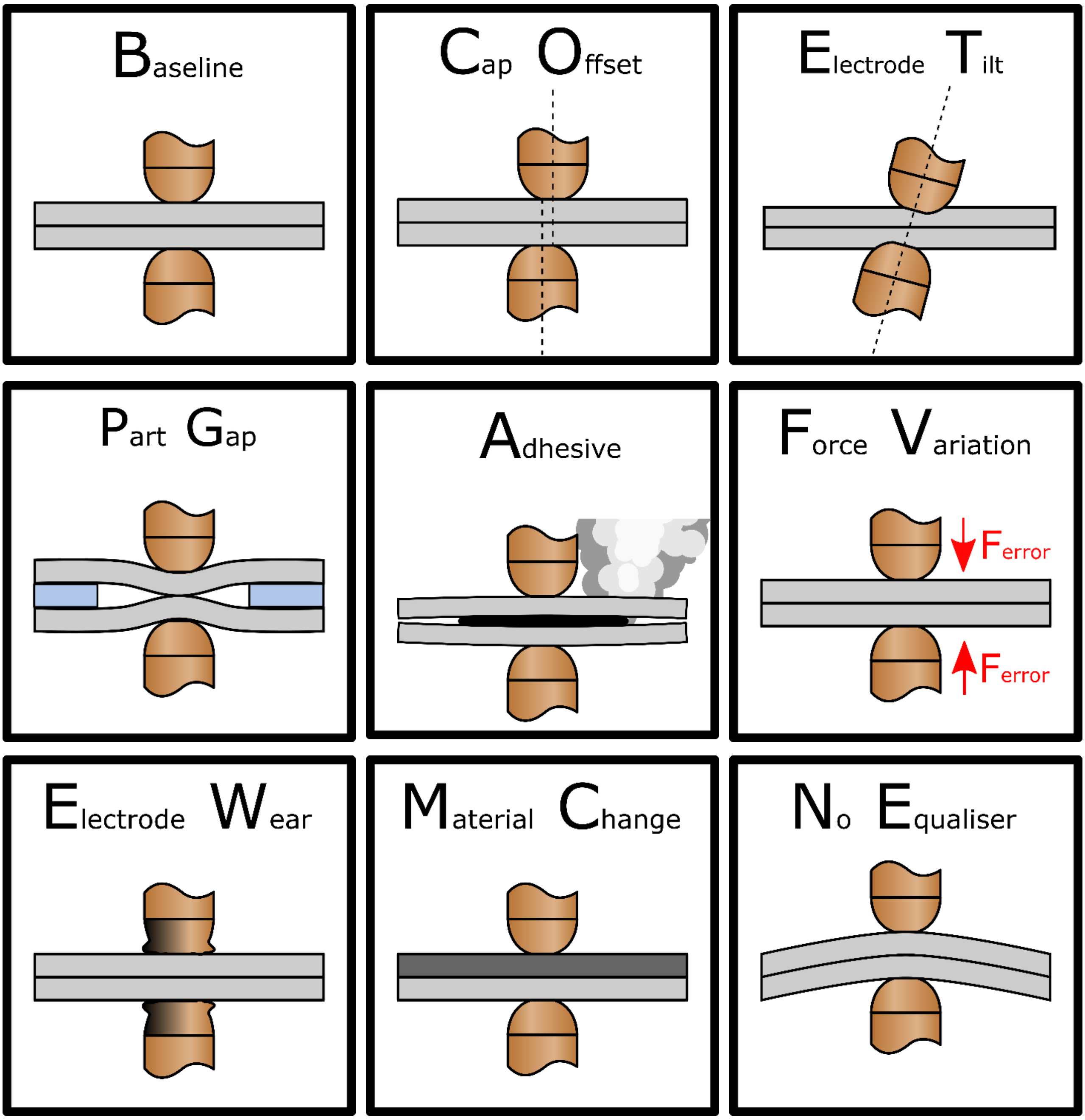

Figure 3-6: Resistance spot welding fault conditions

The part gap fault was induced using acrylic or insulated steel strips with semicircles cut into them (Figure 3-7). A pair of part gap strips were placed on the faying surface, separating the sheets by 3mm and constraining them with a circle of diameter 19mm.

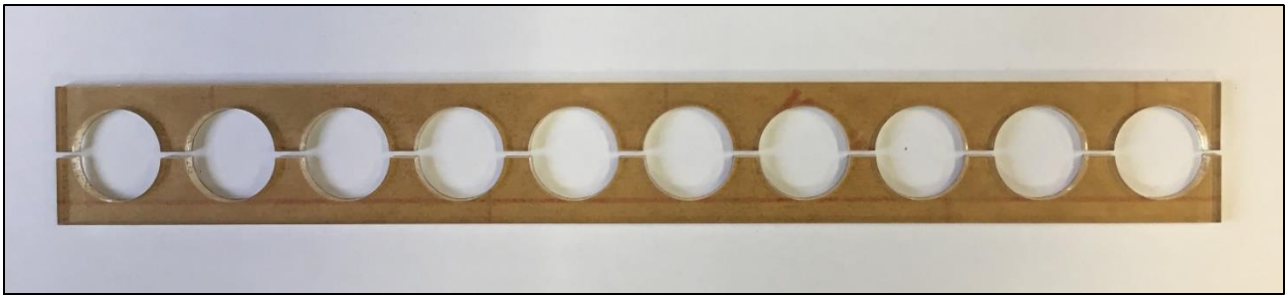

Figure 3-7: Acrylic part gap fixture for the robotic spot welder

3.6 Welders

A number of different welders were used to collect data throughout this thesis. This allowed for simpler equipment to be used in the preliminary phases to develop the approach to weld quality monitoring for steel. Once a basic technique was established, the gauge of the material was increased to a thickness more relevant to the automotive industry which required a larger welder. The larger welder then allowed for preliminary work in aluminium spot quality monitoring to be completed. To further the work in aluminium RSW and to ensure that the techniques developed were relevant to industry an industrial robot welding system in the laboratory was used with thin gauge aluminium. Finally a new aluminium spot welding system in industry was used to test weld quality monitoring methods with material stacks and process faults relevant to industry.

3.6.1 CIG Portable AC Spot Welder

The first welder that was used was a small portable spot welder known as a *CIG Porta-Spot*. This welder was used in the initial data collection phase of this thesis due to its simplicity. It allowed for a proof of concept weld quality model to be developed with process monitoring capabilities. This is presented in Chapter 4. The CIG welder has a 4-bar clamping mechanism to provide the electrode clamping force (Figure 3-8 a). The lower electrode is fixed and the upper electrode moves on an arc rotating around a fixed point, otherwise known as an X-type gun. The CIG is an AC spot welder with controllable weld time via a control box. This welder has a simple control methodology which applies a full sine wave alternating welding current to workpieces for a set time. The simplicity of this machine allowed for weld quality monitoring techniques in steel RSW to be developed without having to deal with more complicated control algorithms.

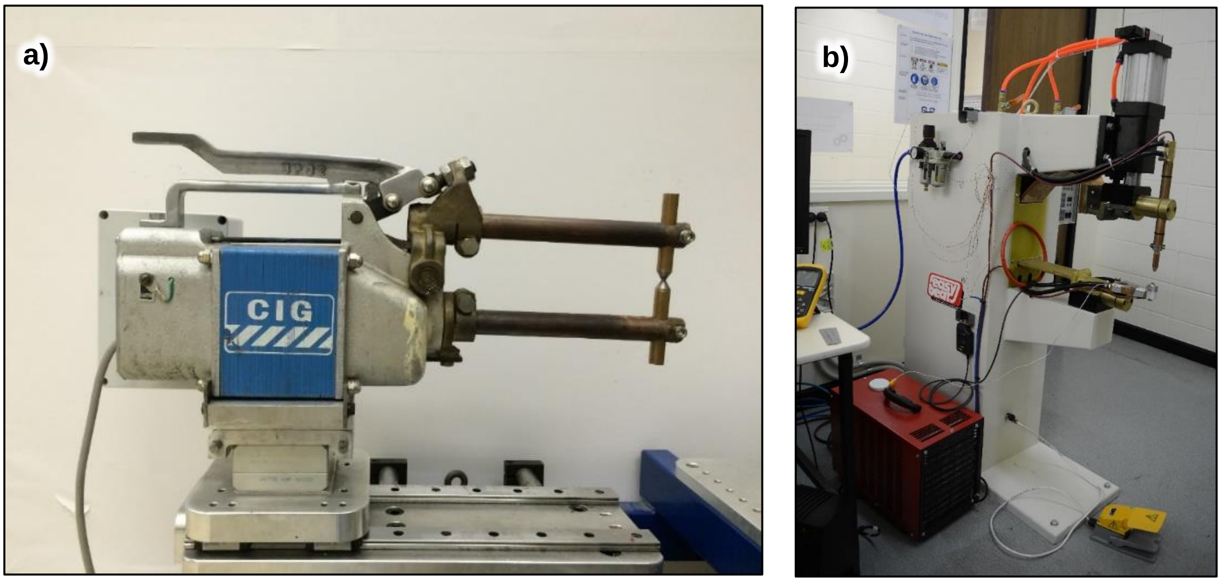

Figure 3-8: a) CIG portable spot welder at the ANU, b) DN-50K AC pedestal spot welder at the ANU

3.6.2 AC Pedestal Welder

The second welder that was used extensively is an AC pedestal spot welder which targets constant power delivery to the spot weld (Figure 3-8 b). This welder has internal control that moderates the input voltage to the spot weld to achieve constant heat. The clamping force is provided by a pneumatic cylinder which is attached to the upper electrode, while the lower electrode stays stationary. The upper electrode moves axially which is known as a C-type gun. The AC pedestal spot welder has significantly more electrical capacity than the CIG portable spot welder. This welder was used to collect preliminary data in aluminium to investigate the signals that may be useful for aluminium quality monitoring in Chapter 5. To weld aluminium with this machine the full power output was used meaning that the voltage and current signals were simple sine waves. This maintained the simplicity of the analysis of the electrical signals that was achievable with the smaller CIG Porta-Spot with steel RSW.

3.6.3 MFDC Industrial Robotic Spot Welder

A Medium Frequency Direct Current (MFDC) spot welder mounted to an automotive manufacturing robot was used to collect both steel and aluminium data to test the weld quality monitoring models (Figure 3-9a). MFDC is the industry standard providing high frequency control of the process.

The MFDC spot welder has more electrical capacity than the AC pedestal welder and CIG Porta-Spot. The clamping force is provided by a pneumatic cylinder controlled by the robot lower electrode of the welder is fixed and the upper electrode moves on an arc powered by a large pneumatic cylinder controlled by the robot and weld timer. The weld timer controls the voltage to maintain a constant current on the secondary side of the welder.

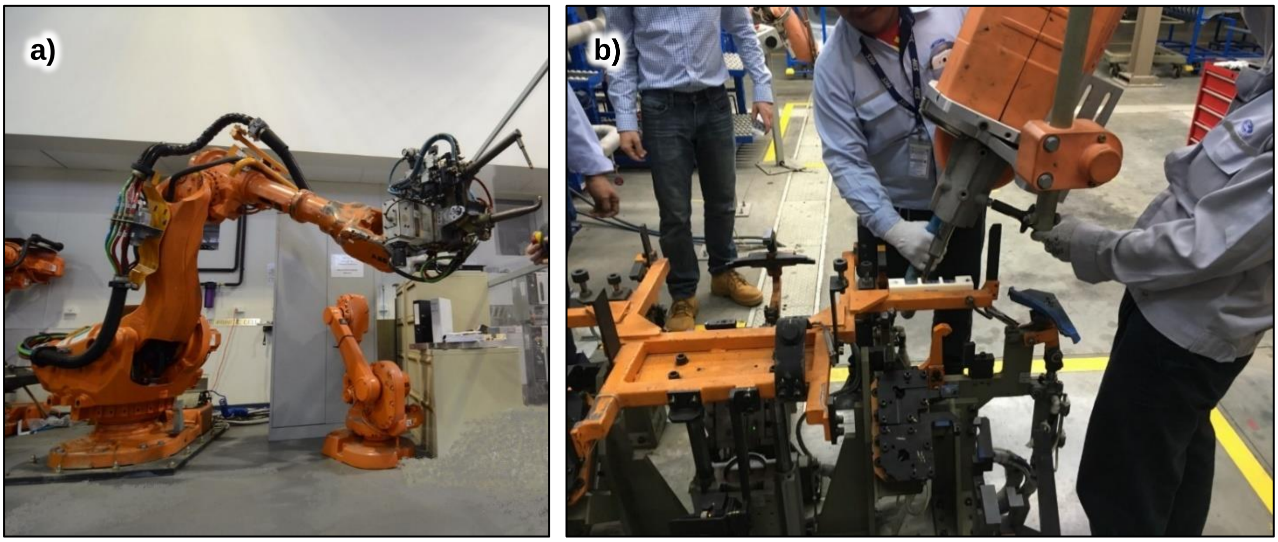

Figure 3-9: a) MFDC robot spot welder at the ANU, b) Thailand automotive manufacturing plant spot welder

3.6.4 Industry Spot Welders (Thailand and Dearborn)

Two other spot welding systems were used to collect the data during this thesis. First an industrial trial of the quality monitoring method was conducted in an automotive manufacturing plant in Thailand. The spot welder used in this facility was a pneumatic C-type MFDC spot welder that was manually operated by a trained welding technician (Figure 3-9b).

Finally, a state of the art industrial spot welding system, designed to weld aluminium, at an automotive manufacturer's research facility was used to collect the data presented in Chapter 7. This welder is an MFDC X-type gun with servo-driven clamping force and was mounted to a modern automotive manufacturing robot. This allowed the methodology to be tested with industry standard equipment with a wide range of faults that are relevant to industry. The MFDC welder targets a constant welding current.

3.7 Materials

A number of automotive grade sheet metal materials are used in this thesis (Table 3-1).

Table 3-1: Material properties and chemical composition

Material		Zinc-annealed Mild Steel	Dual-Phase Steel	Boron Steel	AA5052-H32
Trade Name		BlueScope Zincanneal G2S	DP600	Usibor® 1500	-
Chemical Composition	C	0.035-0.07	0.15	0.25	-
	P	0-0.025	0.05	0.03	-
	Mn	0.2-0.3	2.5	1.4	0.1
	Si	0-0.02	0.8	0.4	0.25
	S	0-0.02	0.01	0.01	-
	Al	0.02-0.07	0.01-1.5	0.01-0.1	-
	N	0-0.008	-	-	-
	Cu	-	0.2	-	0.1
	B	-	0.005	0.005	-
	Ti + Nb	-	0.15	0.12	-
	Cr + Mo	-	1.4	1	-
	Fe	-	-	-	0.4
	Mg	-	-	-	2.2-2.8
	Cr	-	-	-	0.15-0.35
	Zn	-	-	-	0.1
Coating		ZF100	-	Al-Si	-
Tensile Strength (MPa)		≥350	590-700	≥1400	215-265
Reference		(BlueScope Steel, 2003)	(ArcelorMittal, 2019a)	(ArcelorMittal, 2019b)	(Atlas Steels, 2013)

The zinc-anneal mild steel is a standard mild steel with a zinc-coating to prevent corrosion. The Dual-Phase steel is an Advanced High Strength Steel (AHSS) used in production where higher strength is required. The Usibor steel is classed as an Ultra High Strength Steel (UHSS) and is used in production where high strength and passenger safety is concerned. The 5052 aluminium alloy was used in the laboratory, and was restricted by aluminium sheet availability in Australia. Three proprietary production grade 5xxx and 6xxx aluminium alloys were used in Chapter 7. The grades are similar to 5182 5754, 6022 and 6111 however they have tighter tolerances on specific alloying elements to closely control the properties of the materials. The specific sheet thicknesses used in each study are outlined in each of the results chapters.

3.8 Notation

Throughout this thesis a common mathematical notation will be used. Scalars will be represented by lowercase letters (x), vectors will be represented by boldface lowercase letters ($\boldsymbol{x}$), matrices will be represented by boldface uppercase letters ($\boldsymbol{X}$), and later on, tensors will be represented as boldface, script, uppercase letters ($\boldsymbol{\mathcal{X}}$). Some of the common variables used throughout the thesis and their meaning are shown in Table 3-2.

Table 3-2: Mathematical notation

Variable			Explanation
$\boldsymbol{X}$	$\rightarrow$	$\boldsymbol{X} \in \mathbb{R}^{\boldsymbol{m \times n}}$	Matrix of n welding signals that are m-dimensional vectors.
$\boldsymbol{x_i}$	$\rightarrow$	$\boldsymbol{x_i} \in \boldsymbol{X}$	Single welding signal (vector) for weld i.
$\overline{\boldsymbol{x}}$	$\rightarrow$	$\overline{\boldsymbol{x}} \in \boldsymbol{X}$	Mean signal (vector) from the set of signals in $\boldsymbol{X}$.
$\boldsymbol{P}$	$\rightarrow$	$\boldsymbol{P} \in \mathbb{R}^{\boldsymbol{m \times m}}$	Matrix of m principal components that are m-dimensional.
$\boldsymbol{P}^{+}$	$\rightarrow$	$\boldsymbol{P}^{+}$	The pseudo-inverse of the principal component matrix $\boldsymbol{P}$.
$\boldsymbol{P_m}$	$\rightarrow$	$\boldsymbol{P_m} \in \boldsymbol{P}$	Principal component vector m.
$\boldsymbol{B}$	$\rightarrow$	$\boldsymbol{B} \in \mathbb{R}^{\boldsymbol{m \times n}}$	Principal component score matrix for m principal components and n welds.
$\boldsymbol{b_i}$	$\rightarrow$	$\boldsymbol{b_i} \in \boldsymbol{B}$	Principal component score vector for weld i.
b_{ij}	$\rightarrow$	$b_{ij} \in \boldsymbol{b_i}$	Principal component j score for weld i.

3.9 Conclusion

This chapter has outlined the key aspects of the common methodologies used in this Thesis. The approach to the research question continues in the next four results chapters. Chapter 4 shows the development and testing of the PCA weld quality monitoring approach developed in steel RSW. Chapter 5 extends this approach to investigate various signals in aluminium weld quality monitoring. Chapter 6 presents the development of a new representation of welding signal information to encapsulate signal shape interactions and how this is used for weld quality monitoring. Chapter 7 applies this new technique to industrial data that allows the new methodology that analyses the interactions of multiple signals to be tested with challenging industry data.

Chapter 4

Quality Monitoring of Steel Resistance Spot Welding using Principal Component Analysis

The key concepts in this chapter were developed in the papers:

- *Correlating variations in the dynamic resistance signature to weld strength in resistance spot welding using Principal Component Analysis, Adams, D., Summerville, C., Voss, B., Jeswiet, J., Doolan, M., Journal of Manufacturing Science and Engineering, 2017.*

- *Process monitoring of resistance spot welding using the dynamic resistance signature, Summerville, C., Adams, D., Compston, P., Doolan, M., The Welding Journal, AWS, 2017.*

- *Nugget diameter in resistance spot welding: a comparison between a dynamic resistance based approach and ultrasound C-scan, Summerville, C., Adams, D., Compston, P., Doolan, M., Procedia Engineering, 2017.*

This chapter presents the preliminary work in steel spot weld quality monitoring.

- In Section 4.1 a simple example is shown to introduce the reader to the concepts of modelling resistance spot weld quality using the principal components of a set of resistance signals.

- Section 4.2 tests the weld quality monitoring technique in a more challenging situation with five different material stacks that are relevant to the automotive industry.

- To show that the different process faults could be addressed individually with models trained on that fault data, section 4.4 shows how the process faults can be identified using the principal components of the training data and quadratic discriminant analysis.

4.1 Correlating the Principal Components of Resistance Signals with Weld Quality

This section will introduce the reader to the concept of modelling spot weld quality with a simple example using five welds. The process of calculating principal components for the set of resistance signals is shown, followed by the calculation of principal component scores and how these are used to calculate a model for resistance spot weld quality.

In RSW there are many different process conditions that can affect the final quality of the weld and the measured signals differently. Feature extraction from welding signals is key to identify the quality information in the signal. To achieve this, the signal features must be relatable to the physics of the process so that they are applicable to the wide range of process conditions apparent in an industrial welding line.

In steel RSW the resistance measured through the material during welding is known to be linked to the quality of the weld through the resistivity-temperature relationship of the base material (Dickinson et al., 1980). Some example resistance signals from steel welds created with different welding currents are show in Figure 4-1.

The electrical resistance drops once the weld nugget is formed due to the direct current path that is achieved by the welded material. The relationship between the electrical resistance and the quality of the weld becomes complex when different grades of steel, surface coatings, process faults and weld schedules are considered all of which can affect the resistance signal and weld quality differently.

To monitor the weld quality of the range of different materials and process faults in RSW the information in the resistance signal related to weld quality needs to be extracted. Some of the differences between the signals (Figure 4-1) are fairly easy to identify. The higher welding currents appear to result in a lower final resistance for instance. However, the effect of varying weld currents on the resistance signal from 0-75ms is difficult to characterise.

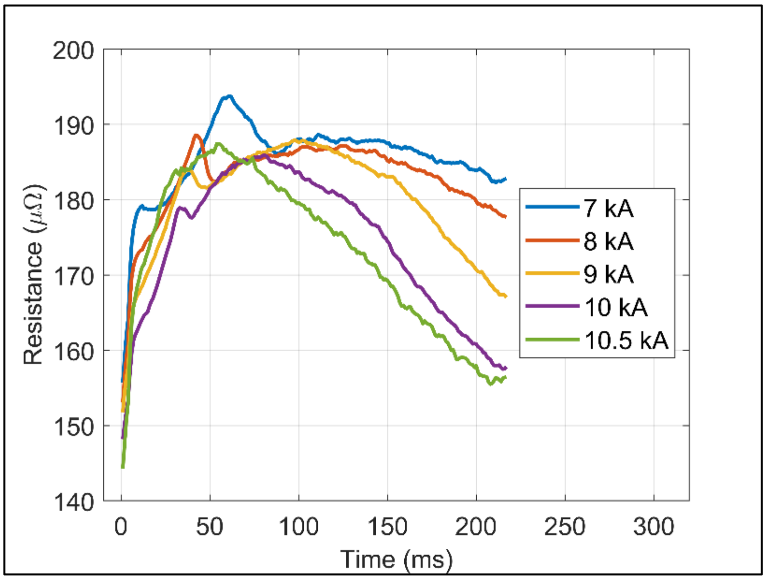

Figure 4-1: Resistance signals of steel welds created with different welding currents

It is important to use signal information throughout the entire process to accurately model weld quality. During a RSW process the resistance measured across the electrodes is dominated by different sources of electrical resistance (S. C. Wang et al., 2001). It is therefore important to use information throughout the entire process to understand all the contributing factors to the final quality of the weld. The beginning of the process is dominated by the electrode-workpiece and faying surface resistances, which then transfers to the bulk resistance as the material heats and the contact resistances reduce or disappear. To use information from the entire resistance curve for weld quality monitoring, the shapes of the signals can be analysed.

Principal Component Analysis (PCA) is a technique that can be used to analyse the shapes of signals. PCA calculates a new set of orthogonal axes for a set of signals (vectors) that are aligned with the variance of the dataset. The principal components can be sorted such that those that describe the majority of the signal set variation are first. The first few principal components can be used to analyse the dominant signal shapes in the dataset.

PCA has been used to analyse the shapes of signals for process monitoring purposes (Cootes et al., 1992; Doolan et al., 2001; Rolfe et al., 2001; B. Voss et al., 2017). The principal components of the data can be represented as signals, or, more specifically the variance from the mean signal that is associated with the principal component.

Once the principal components have been calculated for a training set, the principal component scores can be calculated for welds (shown in Eq. 4-1 and Figure 4-2b). Principal component scores ($\boldsymbol{b_i}$) can also be calculated for subsequent welds that have the same signal and it is of equal length, which is key for modelling production welds (Eq. 4-1).

$$b_i = P^+(x_i - \bar{x}) \qquad \textbf{Eq. 4-1}$$

The principal component scores of signals represent the distance along the new principal axes or the coordinates of the weld on the principal axes. Figure 4-2 shows the original signals and their first principal component scores (note that the principal component scores are centred on zero). As the welding current used increases the principal component 1 scores decrease. A lower principal component 1 score results in a curve that looks more like the 'Lowest' (green) curve shown in Figure 4-2a which refers to the lowest score, a higher score results in a curve that looks more like the 'Highest' blue curve. While a mean score (zero) results in the dashed red line 'Mean' which is the mean signal in the original signal set.

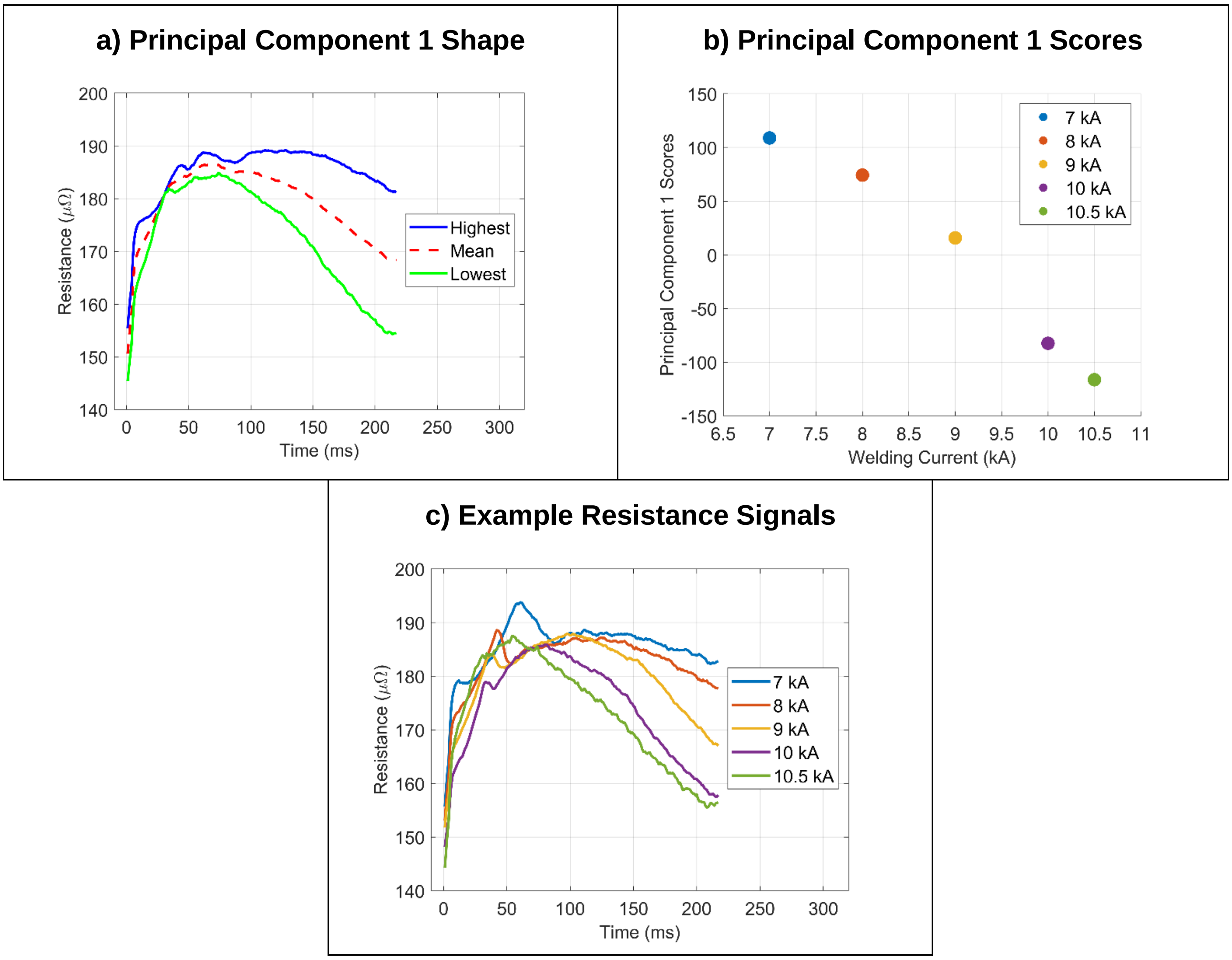

Figure 4-2: a) Principal component 1 shape, b) principal component 1 scores and c) the example resistance signals

Representing welding signals in terms of principal component scores allows the signal shapes represented by principal components to be used for modelling purposes. The relationship between the principal components ($\boldsymbol{P}$), the mean signal ($\bar{\boldsymbol{x}}$), the original signal ($\boldsymbol{x}_i$), and its principal component scores ($\boldsymbol{b}_i$) is shown in Eq. 4-2.

$$x_i = Pb_i + \bar{x} \qquad \textbf{Eq. 4-2}$$

The effects of an individual principal component can be visualised (as shown in Figure 4-3 and Figure 4-2a) by substituting the highest ($\boldsymbol{max}\ (\boldsymbol{b_m})$) and lowest principal component scores ($\boldsymbol{min}\ (\boldsymbol{b_m})$) into the equation for a given principal component, m, and comparing them to the mean signal.

$$x_+ = P_m\left(max\ (b_m)\right) + \bar{x} \qquad \textbf{Eq. 4-3}$$

$$\bar{x} = P\bar{b} + \bar{x} \qquad where\ \bar{b} = 0 \qquad \textbf{Eq. 4-4}$$

$$x_- = P_m\left(min\ (b_m)\right) + \bar{x} \qquad \textbf{Eq. 4-5}$$

These principal component shapes (Figure 4-3) represent the unique (orthogonal) signal shapes of the signal set and can be used in weld quality monitoring. The equations for the lines in Figure 4-3 are in Eq. 4-3, Eq. 4-4 and Eq. 4-5.

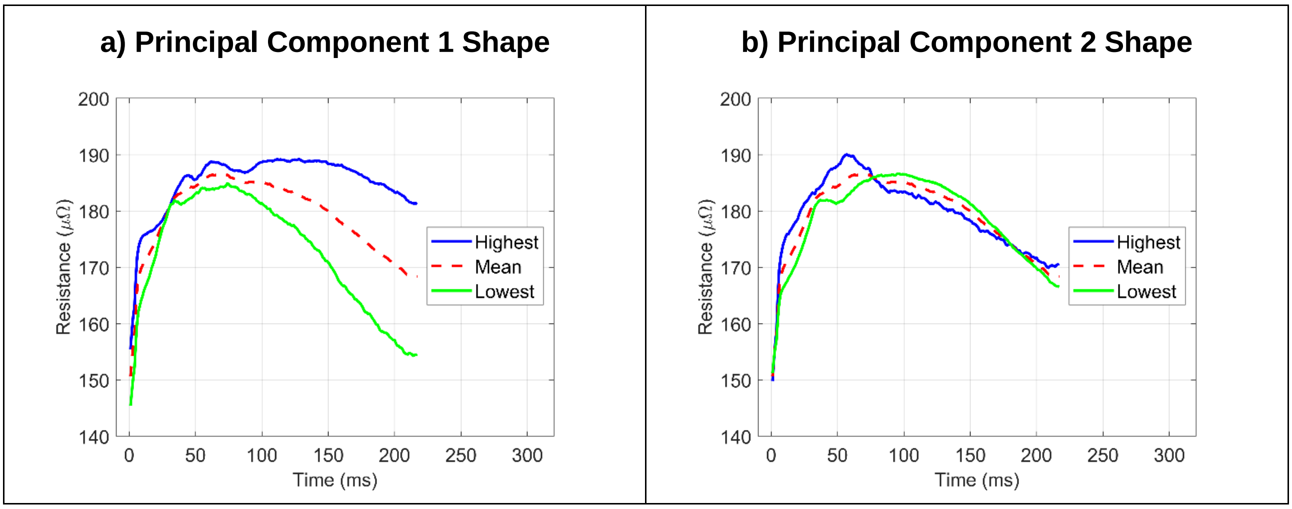

Figure 4-3: First two principal component shapes of the signals shown in Figure 4-1

The principal component scores (of training data) in this thesis are all zero-mean, meaning that they range from negative to positive values with a principal component score of zero representing the mean of that principal component. This is because the mean signal of the training set is first subtracted as in (Adams et al., 2017).

Figure 4-3 provides two examples of Eq. 4-3, Eq. 4-4 and Eq. 4-5 showing the range of the training set signals along the principal component. This represents the total span along the principal component using the minimum and maximum principal component scores in the time domain. Throughout this thesis this representation will be referred to as a *principal component shape*.

A principal component shape shows a mode of variation of the training set signals and when this relates to weld quality, conclusions about the physics of the process can be inferred based on the shape of the principal component. The shape of the resistance signal in steel RSW was shown to be important in the seminal paper by Dickinson et al. (1980) in which different parts of the signal were linked to the physical phenomena in the welding process.

4.1.1 Modelling Weld Quality with Principal Component Scores

The weld quality metric measured for the welds in Figure 4-1 was the button diameter shown in Figure 4-4 plotted against the welding current for each weld. As can be seen for this data the button diameter increases with the welding current to a point. After 10kA the welds with the steel that was used for this example begin to experience significant expulsion and this slightly reduced the measured button diameter.

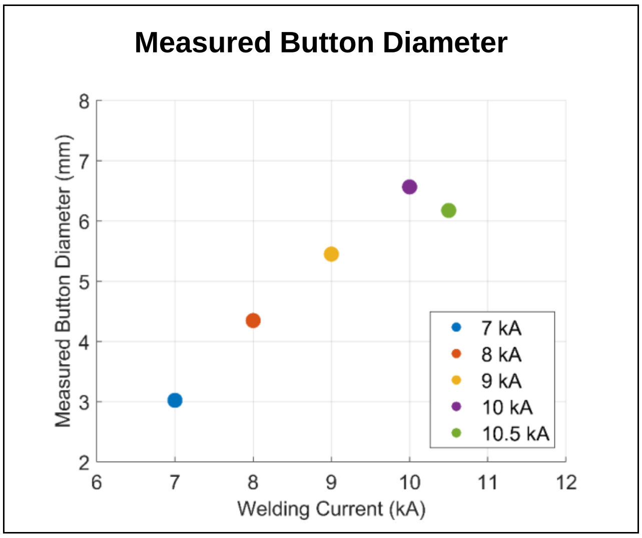

Figure 4-4: Measured button diameter for the example welds

The principal component scores, which represent the signal information in terms of the principal components, can be used to calculate models for weld quality. This is done by assessing the correlation between the principal component scores and the quality of the weld (Figure 4-5). The strength of the correlation is shown by the Pearson's Correlation Coefficient (R or R^2) and the likelihood of the correlation is assessed using the p-value. A lower p-value represents a significant correlation, while a higher R^2 relates to a stronger correlation between the variables. As can be seen the correlation between the first principal component scores and the button diameter is significantly better than the correlation between the second principal component scores and the button diameter.

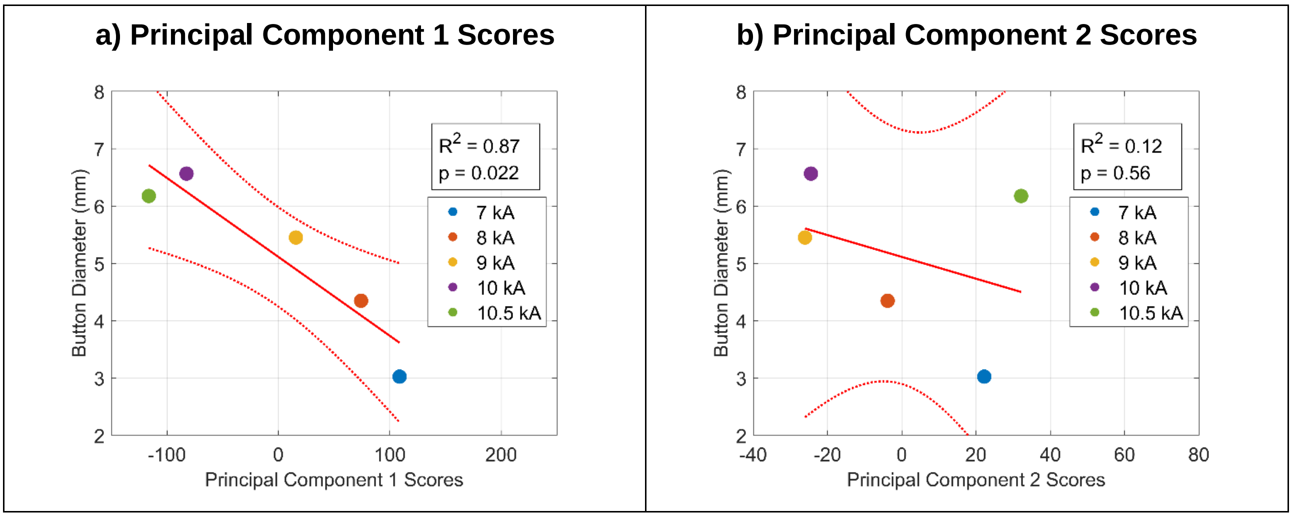

Figure 4-5: Correlations between the first (a) and second (b) principal component scores and the measured button diameter from a destructive test

In this simple example the negative correlation between the first principal component scores and the button diameter can be used to make a good model for weld quality. Figure 4-6 shows the result of a simple linear regression between the first principal component scores and the button diameter of the welds. The equation for this model is shown in Eq. 4-6.

$$D_i = -0.0138(b_{1,i}) + 5.11 \qquad \textbf{Eq. 4-6}$$

In complicated datasets more principal component scores are required to model a weld's quality.

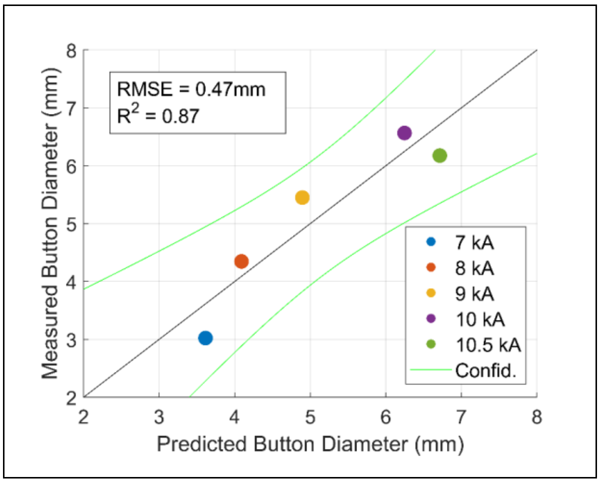

Figure 4-6: Weld quality model calculated from principal component scores

In this example the signal shape shown in Figure 4-3a was used to calculate a model for weld quality. Using this signal shape instead of manually chosen points on the signal requires no prior knowledge about what aspects of the resistance signal for this material is correlated with weld quality. The use of principal components calculated from welding signals clearly represents a useful technique for weld quality monitoring. Signal information throughout the entire process is used to model weld quality through the principal component scores of each weld.

This model can be applied to new welds. The principal component scores can be calculated for new resistance signals of the same length for welds using Eq. 4-1. The principal component scores that are calculated for the new signal can be put into Eq. 4-6 which results in a predicted button diameter. This allows for non-destructive evaluation of welds on a production line through analysis of their signals.

The rest of this chapter will present this technique with data from a range of automotive steel stacks to show the benefits and limitations of weld quality monitoring using PCA of the resistance signal in steel RSW.

4.2 Modelling Steel Weld Quality Using Principal Component Analysis

To test the PCA based weld quality monitoring technique five different, challenging steel material stacks were selected that are relevant to automotive manufacture.

In Section 4.2 weld quality models will be calculated using training datasets for each material stack that vary the welding current used to create the weld. This caused significant variation in the button diameters of the welds which made the data useful for calculating weld quality models. The models were then applied to new validation data which was created with a number of different process faults which were designed to produce poor quality welds and simulate issues that could occur in an industrial welding process.

The models calculated for the training data showed strong correlations between predicted and measured button diameters of the welds. Predicting the button diameters of the welds with challenging process faults in the validation data proved challenging with the high strength steel data. However in Section 4.4 it is shown that the different faults can be successfully classified using the principal components of the training data with high accuracy.

4.2.1 Methodology

The data collected to test the PCA based weld quality monitoring technique for resistance signals in a range of different automotive steels investigated the following material stacks (Table 4-1).

Table 4-1: Steel spot weld stacks

Stack 1	Stack 2	Stack 3	Stack 4	Stack 5
1.1mm Mild Steel	1.4mm Dual Phase	1.4mm Dual Phase – 1.1mm Mild Steel	1.2mm Usibor	0.6mm Mild Steel – 1.0mm Usibor – 1.2mm Usibor

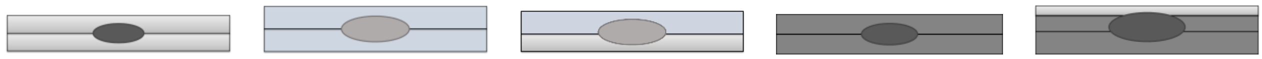

These stacks vary in grade and gauge to test the weld quality monitoring technique. For each new stack a training set was produced by varying the welding current around the base weld schedule current. For each of the material stacks data was collected for a number of induced faults to test the weld quality monitoring models with process faults. The fault data also allows for fault separation using the principal components. The process faults were as follows: electrode tilt (electrode-sheet misalignment), electrode offset (2mm axial misalignment of the upper and lower electrodes), part gap (3mm spacers between the sheet), adhesive/sealant on the faying surface (TEROSON MS 9220), dross on the sheet surfaces from laser cutting and electrode clamping force variation. Each of these faults are shown in Figure 4-7.

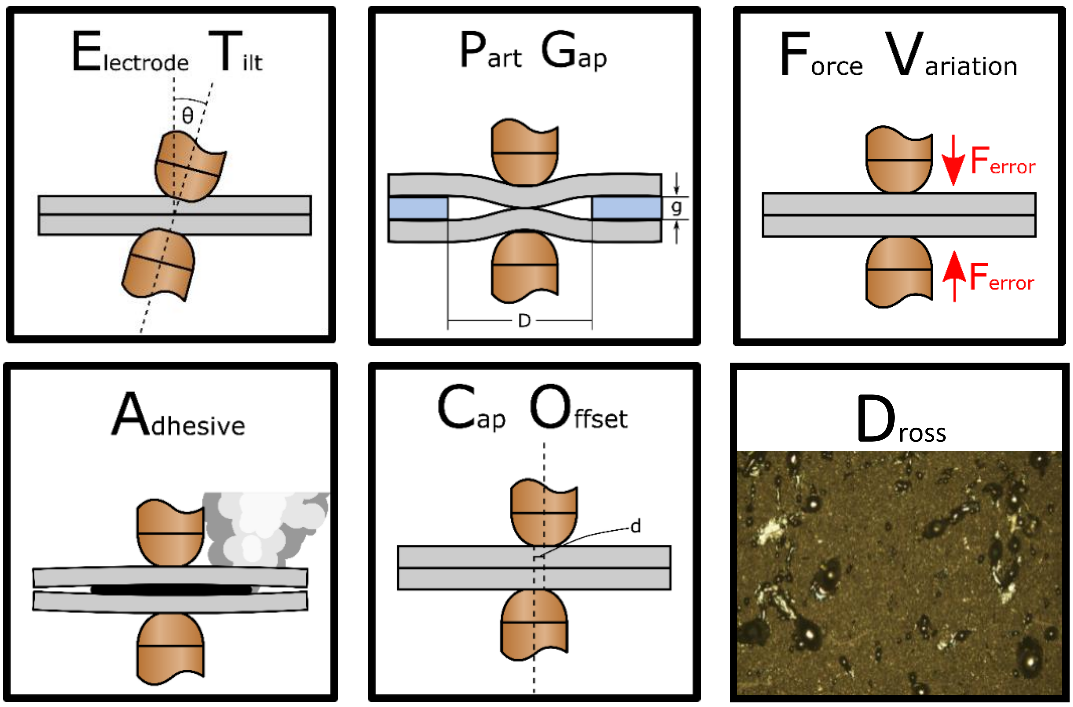

Figure 4-7: Fault conditions

The chemical composition of the different steels used in this chapter and the material properties are shown in the appendix. The number of welds for each fault condition are summarised for each material in Table 4-2.

Table 4-2: Fault conditions for each material's validation datasets (number of welds in brackets)

	Mild-Mild		DP-DP		DP-Mild		Usibor-Usibor		Usibor-Usibor-Mild	
Faults	Control	(93)	Control	(25)	Control	(25)	Control	(29)	Tilt 10°	(23)
	Tilt 5°	(20)	Force-40%	(5)	Force-40%	(5)	Tilt 10°	(25)	Force-50%	(29)
	Force -15%	(15)	Force-20%	(12)	Force-20%	(12)	Force-50%	(25)	Adhesive	(29)
	Force+15%	(15)	Force+20%	(13)	Force+20%	(13)	Adhesive	(24)	Part Gap	(30)
			Force+40%	(5)	Force+40%	(5)	Cap Offset	(25)	Cap Offset	(30)
			Tilt 5°	(22)	Tilt 5°	(22)	Dross (1 side)	(27)		
			Tilt 10°	(8)	Tilt 10°	(8)	Dross (2 sides)	(27)		
			Part Gap	(30)	Part Gap	(30)				

The steels used include a mild steel, an Advanced High Strength Steel (AHSS) – DP600, and an Ultra High Strength Steel (UHSS) – Usibor, spanning ~300 to ~1500MPa tensile strengths. There are also two different surface coatings in the materials, the mild steel has a Zinc-anneal coating while the Usibor when die-quenched forms an Al-Si coating.

The settings of the welder that are chosen to produce a weld are known collectively as the *'weld schedule'*. A weld schedule includes the time, current and electrode force that is used to create a weld. First, base weld schedules for each material were determined (Table 4-3).

Table 4-3: Base weld schedule for each material

Material	Weld Time (ms)	Weld Current (kA)	Clamping Force (kN)
Mild-Mild	217	10	3.5
Dual Phase	217	8.5	3.8
DP-Mild	217	8.5	3.8
Usibor-Usibor	520	7	3
Usibor-Usibor-Mild	520	7	3

To create training datasets for each stack, the base weld schedule was determined and then the welding current was varied above and below the base welding current (shown in Table 4-4). A longer welding time and lower welding current was used for the Usibor stacks to avoid expulsion during welding which can affect both the resistance signals and weld quality.

Table 4-4: Parameters varied for training datasets

Material	Training Current Values (kA)						Clamping Force (kN)	Welding Time (ms)
Mild-Mild	6.5	7	8	9	10	10.5	3.5	217
Dual Phase	6.5	7	8	9	10	10.5	3.5	217
DP-Mild	7	7.5	8	9	10	10.5	3.8	217
Usibor-Usibor	5.5	6	6.5	7.25	7.5		3	520
Usibor-Usibor-Mild	4	5	6	8	9	10	3	520

Varying the current for each material created variation in the weld quality by generating different amounts of heat in the welding process for fusing the sheets together. This is similar to the process of collecting a ‘weld lobe’ which is a specific type of industrial study in which the input parameter space is mapped to find the settings that produce acceptable weld quality for production. This is commonly conducted in industry to determine the base weld schedule when new materials or stacks are introduced into production.

Each weld was subjected to a destructive chisel test to break the spot weld so that the button diameter could be measured. For each weld the major and minor button diameters were measured and the average was taken as the measure of the spot weld’s quality following the American Welding Society’s (AWS, 2005).

Resistance signals for each weld were recorded on the Bosch Weld Timer (PSI6300.630 L1) which measures the welding current on the secondary side of the welder using a Rogowski Coil and voltage probes fixed to the electrode arms. The welder was an Obara MFDC X-type spot welder with a pneumatic cylinder to provide the clamping force for welding. The electrodes were water-cooled and used 16mm ISO style caps with a 6mm flat face. The welder was mounted to an ABB 6600 Robot with an IRC5 Controller. This information is outlined in more detail in Section 3.6.3.

The Mild-Mild and DP-DP stacks both had training data that had to be removed due to the presence of expulsion or no measureable button diameter, which lowered the number of welds available for training (Table 4-5). However, the covariance matrices were checked and found to be non-singular. The models for weld quality for these stacks performed as well for the training data as the other material stacks which shows that the number of training welds does not have to be large.

Table 4-5: Number of welds per dataset

	Mild-Mild	Dual-Phase	DP-Mild	Usibor-Usibor	Usibor-Usibor-Mild
Training	20	25	30	35	46
Validation	203	120	120	182	141

4.2.2 Results Summaries

The destructive testing results for some of the training datasets are shown in Figure 4-8 and Figure 4-9. The spread of button diameters caused by changing the welding current for the two DP material stacks (Appendix Figure 1) were very similar to the mild steel stack shown in Figure 4-8a. The same variance in button diameter could not be achieved with the Usibor-Usibor stack which was found to be very susceptible to process parameter changes (Figure 4-8b). This caused significant expulsion at welding currents above 7.5kA, which affected the maximum button diameter that was achievable. A larger range in button diameters was achieved for the three sheet Usibor-Usibor-Mild stack (Figure 4-9) although it was not as large as the range of the Mild, DP and DP-Mild stacks.

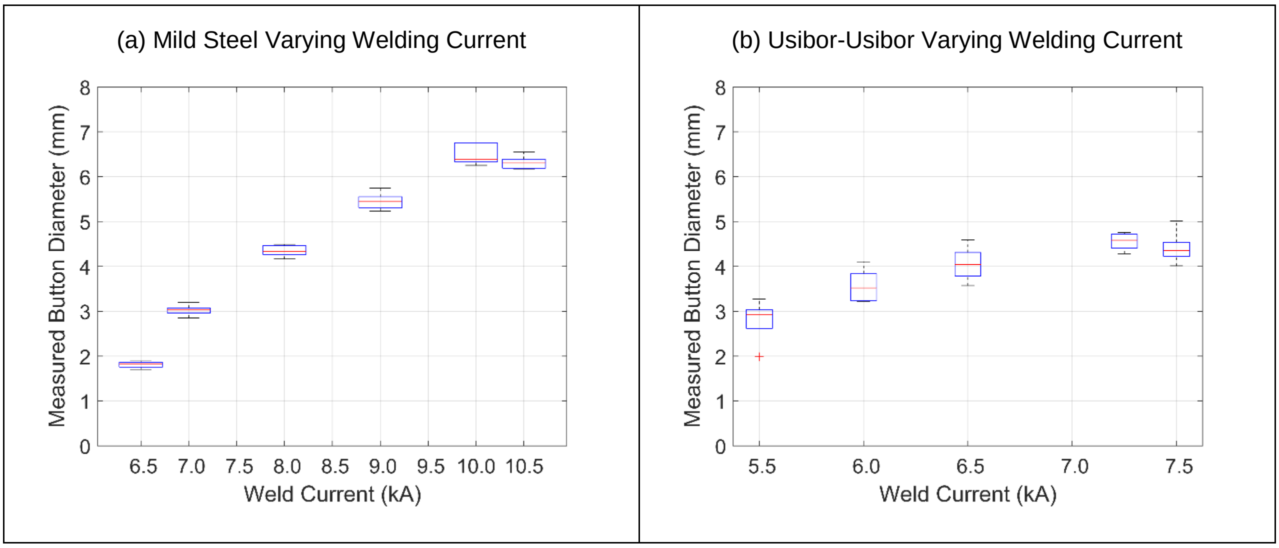

Figure 4-8: Mild steel and Usibor-Usibor training set destructive testing data summary

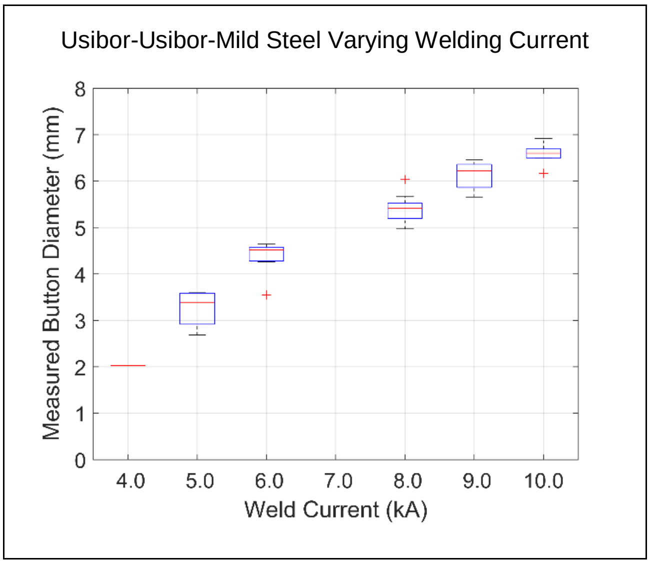

Figure 4-9: Usibor-Usibor-Mild training set destructive testing data summaries

In Figure 4-10 and Figure 4-11 the destructive testing results for some of the fault condition datasets are shown. The variance in weld quality caused by the induced process faults was significantly less than that caused by varying the input current. The variance in button diameter caused by the faults for the DP-Mild (Figure 4-10a), Usibor-Usibor (Figure 4-10b) and Usibor-Usibor-Mild (Figure 4-11) stacks were particularly small. The Mild Steel and DP-DP material stack results are shown in Appendix Figure 2.

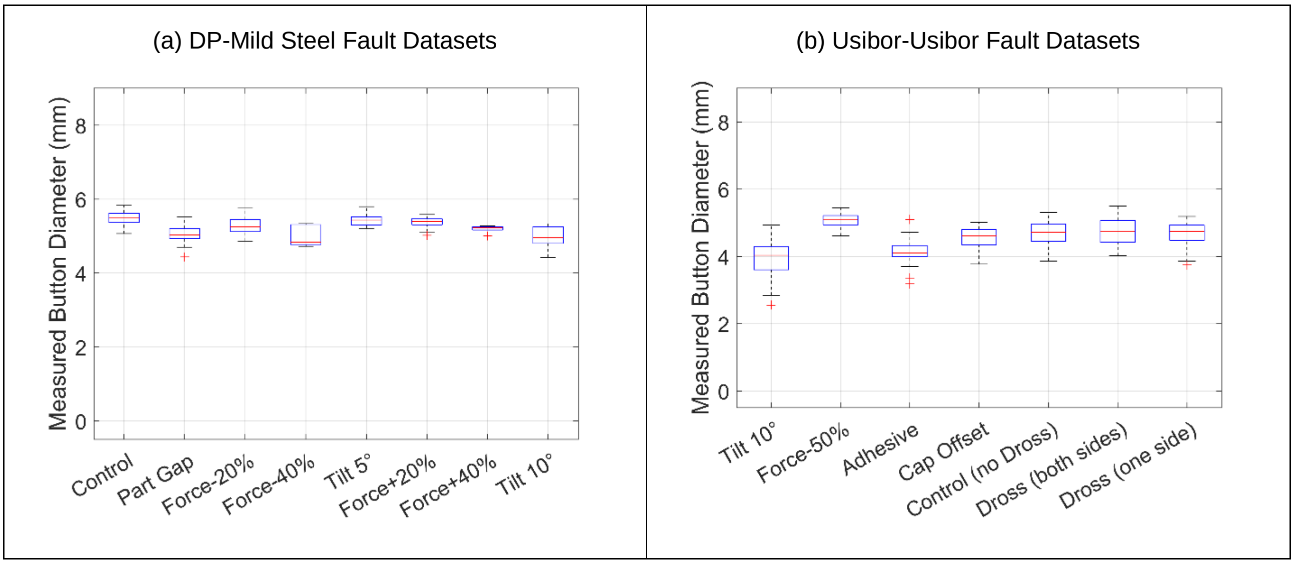

Figure 4-10: DP-Mild and Usibor-Usibor fault dataset destructive testing summaries

Figure 4-11: Usibor-Usibor-Mild fault dataset destructive testing summaries

Figure 4-12, Figure 4-13 and Figure 4-14 show the mean resistance curves of the different welding currents that were used for each of the training datasets. Note that the Usibor stacks (Figure 4-13b & Figure 4-14) have a longer welding time. The material stacks that include DP or Mild Steel (Figure 4-12 and Figure 4-13a) have similar shaped resistance curves that show increasing resistance with temperature, while the Usibor material stacks do not. This is most likely due to the unique properties and surface coating of this material.

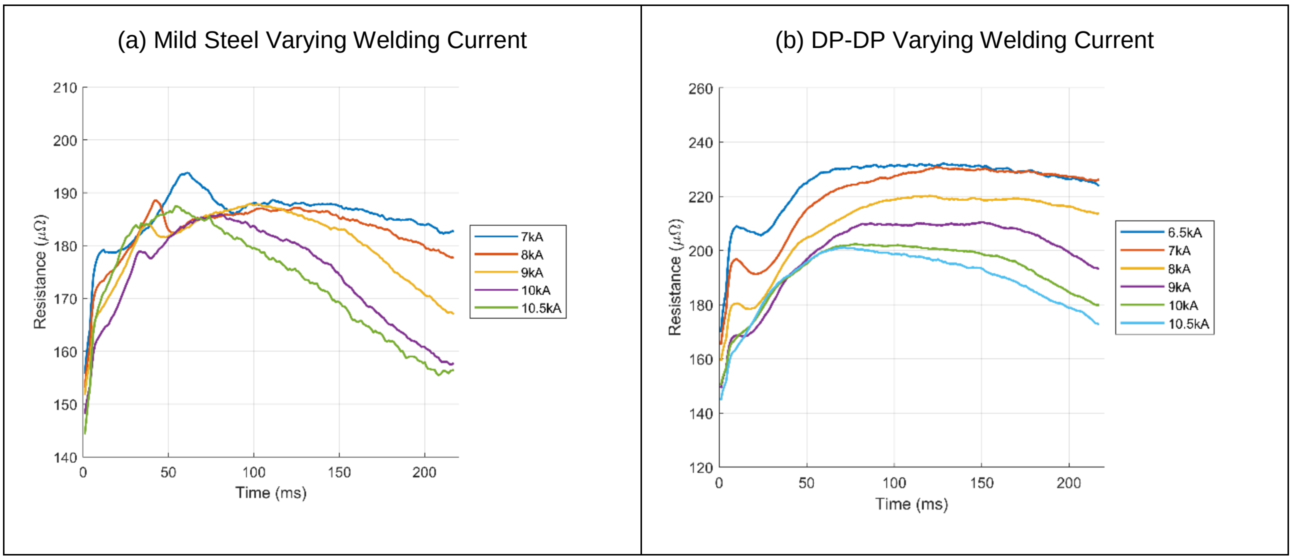

Figure 4-12: Mild steel and DP-DP, varying welding current mean resistance signals

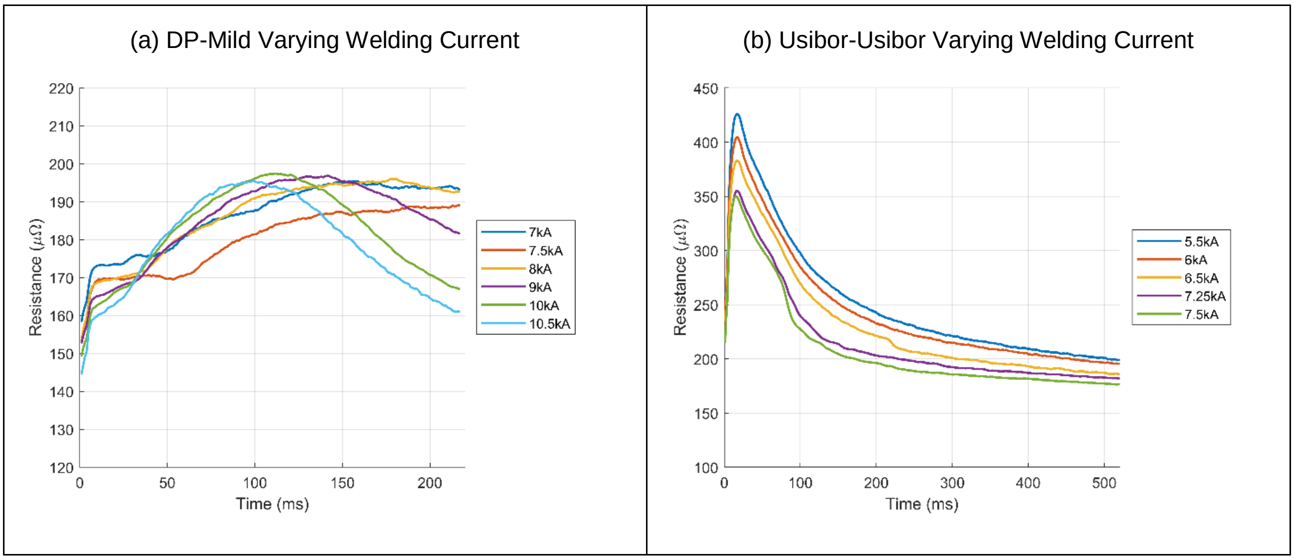

Figure 4-13: DP-Mild and Usibor-Usibor, varying welding current mean resistance signals

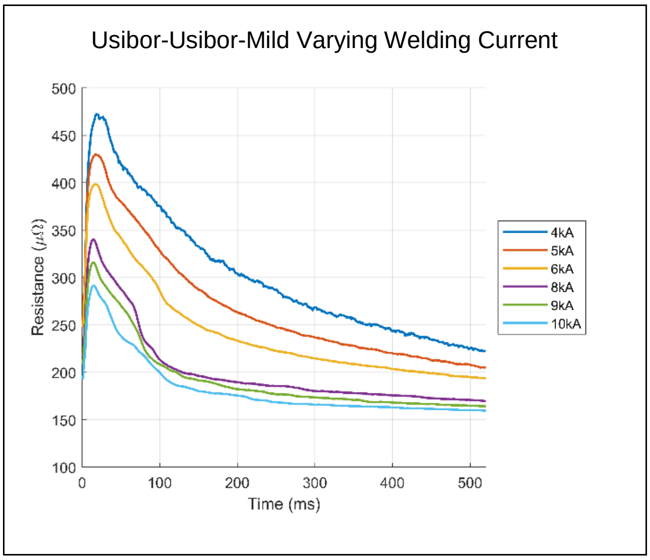

Figure 4-14: Usibor-Usibor-Mild, varying welding current mean resistance signals

Figure 4-16 and Figure 4-16 show the mean resistance signals for each fault of the 5 different stacks that were investigated. There is significant variance in the mean resistance signals caused by the faults, comparable to the variance seen when the welding current was varied in the training data for each stack, except in the Usibor-Usibor-Mild fault data (Figure 4-16b). The resultant resistance curves for the DP-DP and DP-Mild (Appendix Figure 3) material stacks were very similar.

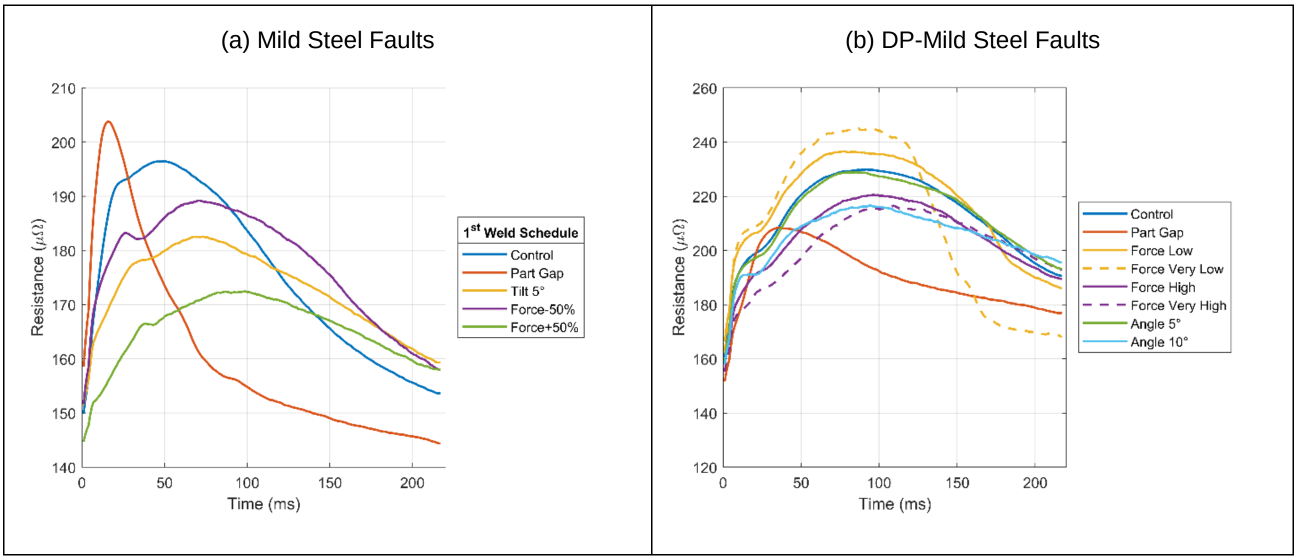

Figure 4-15: Mild steel and DP-Mild fault mean resistance signals

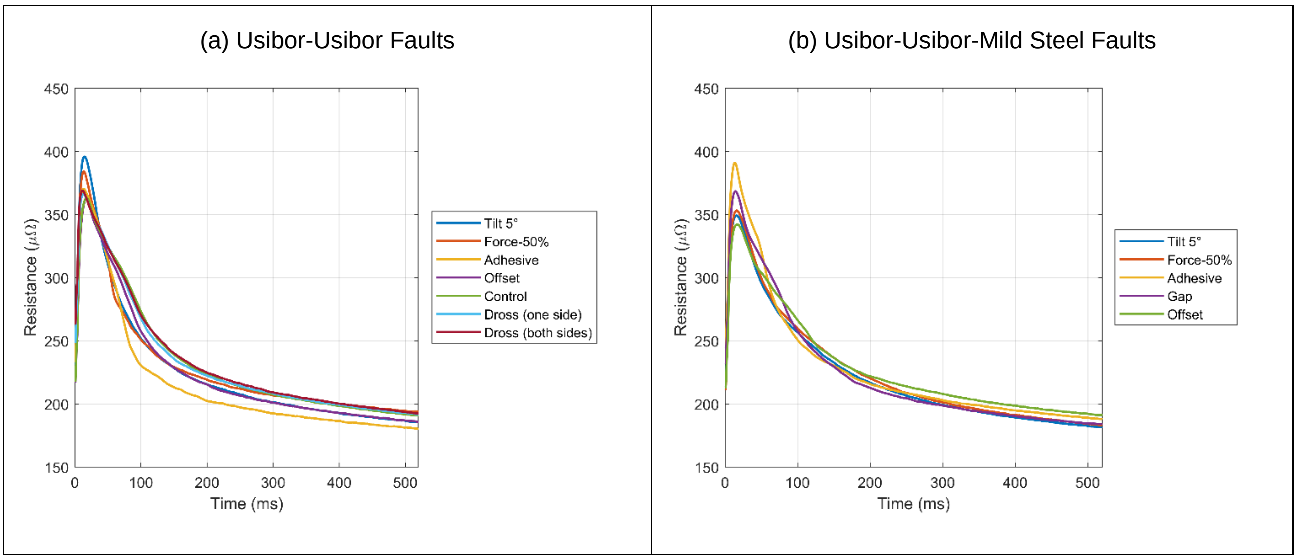

Figure 4-16: Usibor-Usibor and Usibor-Usibor-Mild fault mean resistance signals

4.2.3 Modelling Weld Quality

Models for button diameter were calculated from the training dataset principal component scores for each material. Principal components that explained more than 1% of training set variance and were correlated with button diameter (p-value < 0.05) were used in the button diameter models. The linear regression equations for button diameter (which include the selected PCs) for each material stack and the correlation between the predicted and measured button diameters are shown in Table 4-6.

Table 4-6: Button diameter model equations and prediction accuracies

Material Stack	Button Diameter Equation	R^2	RMSE (mm)
Mild	$4.83 - (16.0\boldsymbol{PC1}) \times 10^{-3}$	0.89	0.43
DP-DP	$4.68 - (7.14\boldsymbol{PC1}) \times 10^{-3}$	0.84	0.61
DP-Mild	$4.95 + (-17.4\boldsymbol{PC1} - 35.4\boldsymbol{PC3}) \times 10^{-3}$	0.85	0.65
Usibor-Usibor	$4.05 - (1.38\boldsymbol{PC1}) \times 10^{-3}$	0.64	0.41
Usibor-Usibor-Mild	$4.66 - (1.46\boldsymbol{PC1}) \times 10^{-3}$	0.89	0.40

Notably, for all of the material stacks the 1st Principal Component was strongly correlated with the button diameter of the welds shown by the R^2 and RMSE of the models which are presented in Figure 4-17. For four out of five of the stacks the first principal component encapsulated enough information to accurately model the quality of all welds and was found to be the only principal component that met the selection criteria. The specific correlations of the principal components to button diameters are outlined in Table 4-7 and will be discussed further in Section 4.2.4. The fact that the first principal component for every material stack is correlated with button diameter shows that PCA is very effective at extracting the critical information from a training set for weld quality monitoring.

Figure 4-17 shows the models created for button diameter using the varying welding current datasets for each material stack with predicted button diameter against the measured button diameters from destructive testing. The Usibor-Usibor-Mild button diameters shown are the average button diameters of the 1.2mm Usibor to 1.0mm Usibor interface, which is the thicker pair of sheets. The modelling results for the thinner side of the stack between the 1.0mm Usibor to the 0.6mm Mild steel were comparable in performance.

The green error bars on the weld quality models in this thesis indicate the uncertainty in the prediction and diverge the further from the mean of the training data the model is applied.

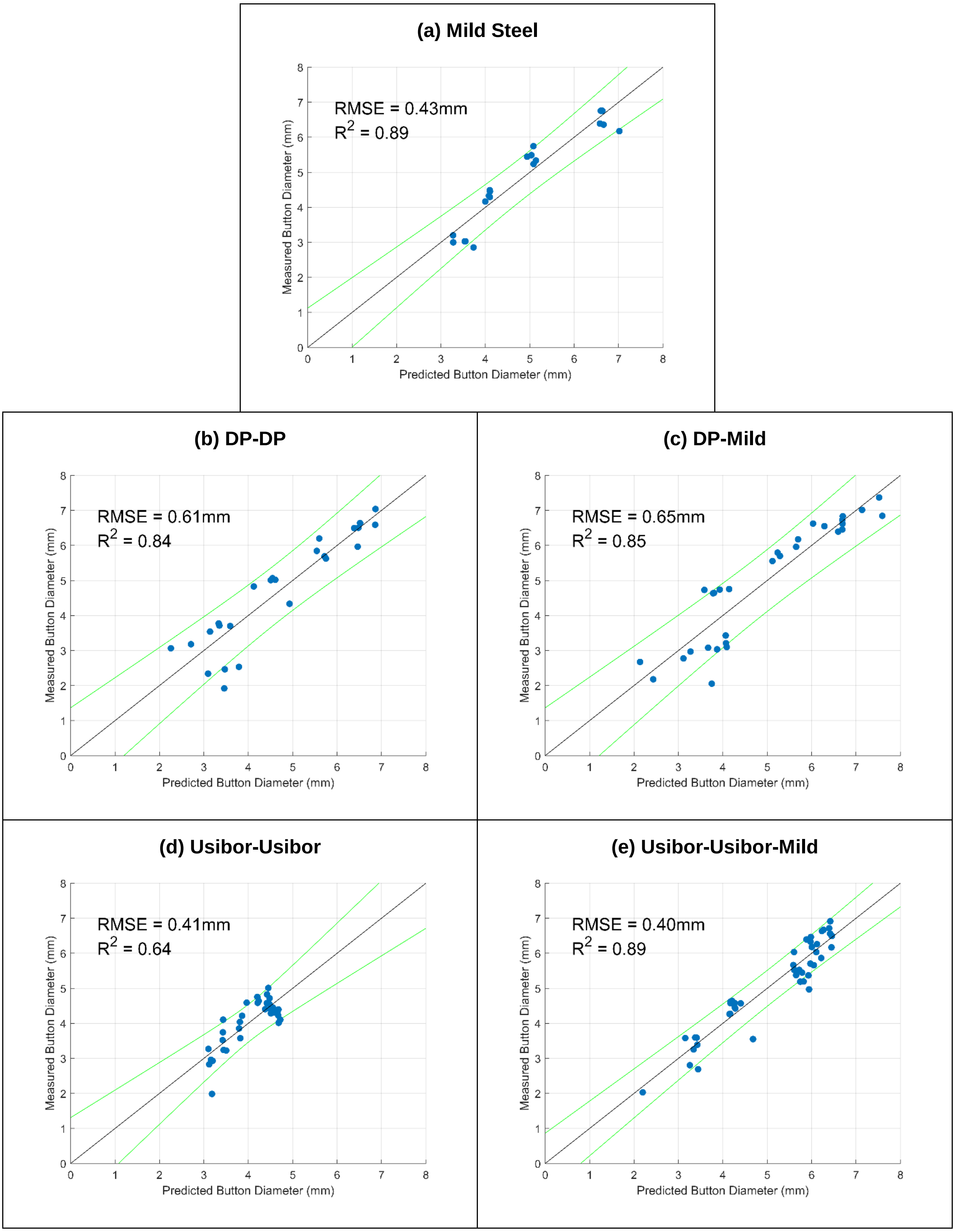

Figure 4-17: Button diameter models

For each material stack, the quality of the welds was modelled using one or two of the principal components. The R^2 values for the Mild-Mild, DP-DP, DP-Mild and Usibor-Usibor-Mild were all above

0.84 and the RMSE values were ~10% of the range of the datasets. The models and statistics show that PCA efficiently extracts critical information for weld quality monitoring from the resistance signals.

The range of the Usibor-Usibor button diameter data is smaller than the other materials and this was due to the small welding lobe of the material. The surface coating and processing of the Usibor material means that it produces a lot of expulsion when welded. This was not acceptable for training data for this study and so welds with expulsion were removed. Material availability was an issue and this limited the amount of samples available for weld lobe determination and training. The limitation on training data and the small weld lobe meant that only a small range of button diameters could be collected and this negatively affected the R^2 of the Usibor-Usibor model.

The RMSE of the two material stacks with Dual Phase steel (DP-DP and DP-Mild) were slightly higher than the others, and this appears to be more pronounced at the lower button diameters which is likely to be due to larger variation in the destructive testing results at low welding currents (Appendix Figure 1).

4.2.4 Comparison of the Principal Component Shapes

Each of the training sets was created by varying the welding current around the base weld schedule to create variance in the button diameters of the training data. Analysis of the major principal components which were found to be correlated with button diameter provides insight into the signal shapes that are varying with weld quality. For the different stacks there are notably different resistance signal shapes caused by the different material properties in the stacks.

For each of the material stacks the first principal component was found to be statistically significantly correlated with the button diameter of the welds in training. This shows that PCA is effective for finding the major signal variation induced by varying the weld current which was also demonstrated to affect the button diameters from destructive testing in Figure 4-8, Figure 4-9 and Appendix Figure 1.

The principal component shapes that were selected for weld quality monitoring are shown in Figure 4-18, interestingly as shown in Figure 4-18 (c) the third principal component for the DP-Mild material stack was also found to be correlated with button diameter while only the first principal component of every other stack was correlated with button diameter.

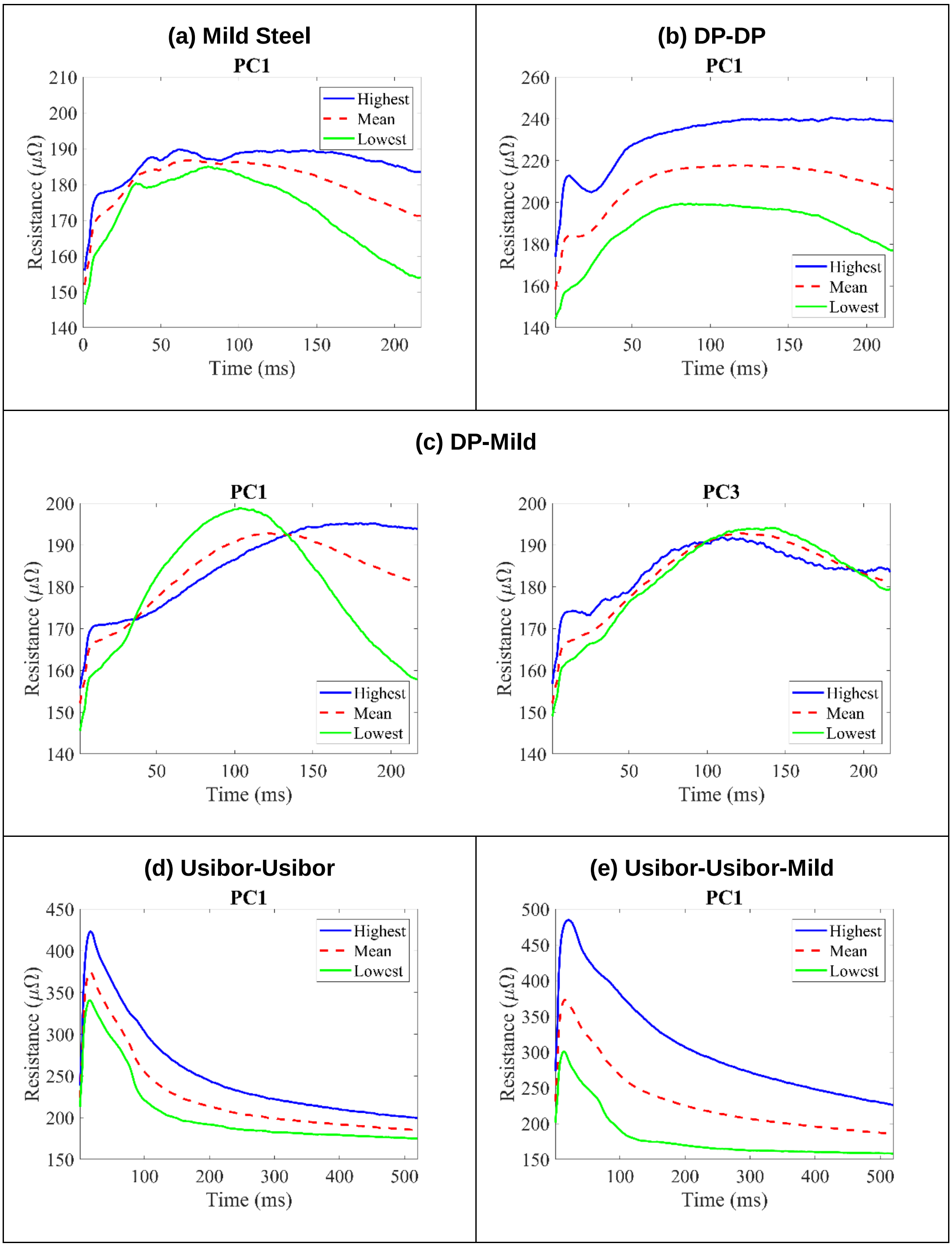

Figure 4-18: Principal components selected for weld quality monitoring for each material stack

The mean resistance signals in Figure 4-13, Figure 4-14 and Appendix Figure 3 show that the major signal variation in the DP-DP, Usibor-Usibor and Usibor-Usibor-Mild stacks is predominantly in the height of the signals and this is represented in the first principal component of each of these datasets (Figure 4-18). The correlation between the first principal components and button diameter show a clear link between the heat input into the weld and the size of the button diameter from destructive testing.

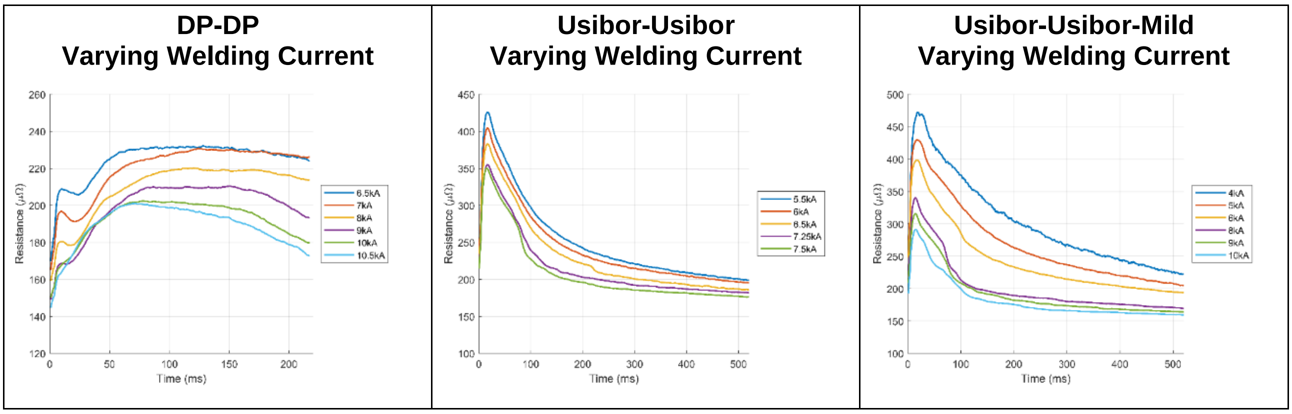

For reference, from section 4.2.2

In all cases except for the DP-Mild stack, the first principal component was related to the overall height of the resistance signal and this was found to be correlated with the button diameter of welds with different welding currents. The first principal component shape of the heterogeneous DP-Mild stack is different to the first principal component shapes of the homogenous material stacks.

Observation of the mean signals in Figure 4-13 for the DP-Mild stack shows that there are two different types of signal shapes in the dataset. The higher welding currents (9, 10 and 10.5kA) show the presence of a β-peak and look more like the Mild-Mild steel high current mean signals. The β-peak is the result of the increase in resistance caused by rapid heating of the material. This is followed by a decrease in resistance as the weld nugget grows and goes through mechanical collapse, thereby improving the electrical connection of the joint by fusion of the two pieces of sheet metal.

The lower current mean signals of the DP-Mild stack look like the low current DP-DP mean signals with no prominent collapse after the β-peak. The β-peak is in the fourth stage of Dickinson's explanation of the progression of resistance signals in steel welds (Dickinson et al., 1980), shown in Figure 4-19.

A low score for the first principal component of the DP-Mild material stack is indicative of a high β-peak and this was found to be correlated with button diameter for this material stack. The first stage of Dickinson's theoretical resistance signal for steel welds is not present in any of the steel weld stacks collected on the particular weld used, which is likely to be due to the current and voltage measurements recorded by the Bosch weld timer.

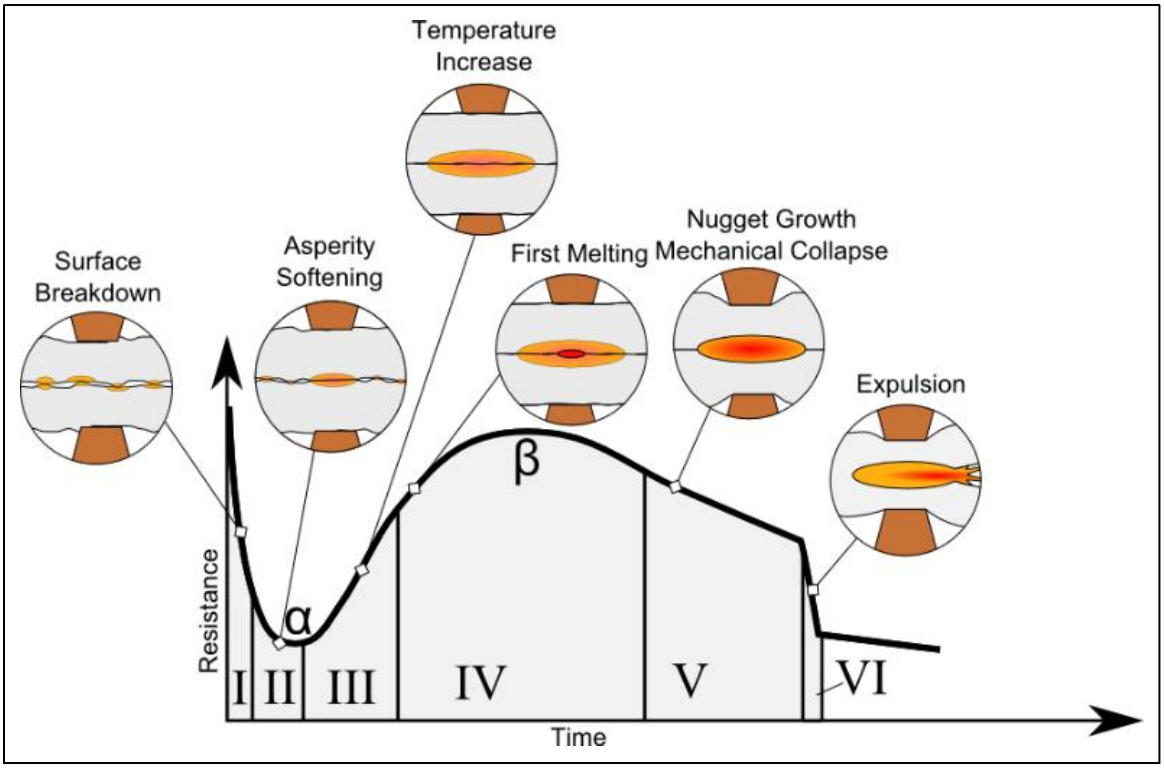

Figure 4-19: Adaptation of Dickinson's (1980) theoretical dynamic resistance signal for steel welds (Adams et al., 2017)

Principal Component Analysis has been demonstrated to effectively identify signal shapes that are correlated with weld quality for training sets, shown by the strength of the correlation with button diameter of each of the first principal components. The goal of PCA is to find a new set of orthogonal axes that aligns with the variation in the dataset to represent the signals more efficiently. This means that each subsequent principal component describes signal variation independent from the first principal component with decreasing explained variance.

The variation in the training datasets was induced by varying one factor, the welding current, so the major signal variation is captured in the first principal component and correlated with button diameter. The second principal component for each stack was not found to be correlated with the button diameter.

Table 4-8 shows the explained variance of each of the principal components with the second principal components responsible for between 0.6 – 19.6% of the variation. This is due to design of the training data and that the variation caused by varying welding current, while everything else is kept constant, can be explained by one principal component. If the training data had more factors affecting the process, more principal components would have been likely to have been correlated with weld quality.

Table 4-7: The correlations of the principal components selected for modelling button diameter

	Principal Components, R^2 to Measured Button Diameter		
Material	1	2	3
Mild	0.89		
DP-DP	0.84		
DP-Mild	0.72		0.13
Usibor-Usibor	0.64		
Usibor-Usibor-Mild	0.89		

Table 4-8: The explained variance of the first five principal components

	Principal Component Explained Variance (%)				
Material	1	2	3	4	5
Mild	85.9	6.0	3.4	2.6	0.5
	Cumulative % explained variance	*91.9*	*95.3*	*97.9*	*98.4*
DP-DP	88.3	9.3	1.2	0.5	0.2
	Cumulative %	*97.6*	*98.8*	*99.3*	*99.5*
DP-Mild	74.2	19.6	3.2	1.1	0.6
	Cumulative %	*93.8*	*97.0*	*98.1*	*98.7*
Usibor-Usibor	93.7	2.2	1.6	0.9	0.5
	Cumulative %	*95.9*	*97.5*	*98.4*	*98.9*
Usibor-Usibor-Mild	98.5	0.6	0.3	0.2	0.1
	Cumulative %	*99.1*	*99.4*	*99.6*	*99.7*

4.2.5 Validating Weld Quality Models with Fault Datasets

This section presents the extrapolation of the weld quality models to fault data. The purpose of this is to assess the applicability of the underlying signal shape variation found in the training data to conditions that could affect button diameter by other means that are likely to occur in production. It is a challenging task for the models to stretch from interpolation to extrapolation by predicting the button diameters of welds with faults, but this will help to inform training set design for maximum applicability in the future.

The part gap welds were removed from this analysis as the signal shapes produced from the extreme part gap fault condition were very different to all other welds. These welds will be analysed later in Section 4.4 which shows that these signals can be easily identified using their principal components and discriminant analysis as welds outside normal operating windows.

First, the models that were calculated for the weld lobe training data that had varying current were applied directly to the fault data to see if the trends in the training data models could be applied to the fault datasets. To do this principal component scores were calculated for the fault data from the training set principal components and mean signals using Eq. 4-1. The results of the predictions are summarised in Table 4-9.

Table 4-9: Modelling faults with training set model

	Predicted and Measured Button Diameter Statistics		
Material Stack	R	R^2	RMSE
Mild Steel	-0.58	0.33	1.98mm
DP-DP	-0.52	0.26	1.4mm
DP-Mild	-0.14	0.02	5.7mm
Usibor-Usibor	-0.43	0.19	0.87mm
Usibor-Usibor-Mild	0.11	0.01	0.54mm

As can be seen from the R-values of the correlation (Pearson's correlation coefficient, Pearson 1900) the model coefficients from the training set models do not predict the button diameters of the fault data shown by the high RMSE and low R^2 values for each material stack. The R values for the first four stacks show that the correlation between the predicted and measured button diameters is actually weakly inversely correlated, showing that the model coefficients do not apply to the different faults included in each stack.

This shows that a weld quality model made from a single principal component is not robust to process changes. This can be addressed by including different sources of variation in the training data such as process faults or varying other input parameters.

The predicted button diameters for the DP-Mild fault data had an extremely high RMSE (Table 4-9) which was due to the difference in signal height. This can be found by comparing Figure 4-13 (a) and Figure 4-15 (b), there is an ~30μΩ difference in peak resistance between the fault datasets and the training weld signals. The magnitude of the resistance signal may have been affected by differences in the electrode caps used for example which resulted in a higher RMSE than the other models.

Given that the models calculated for the training data were not directly applicable to the fault datasets, the models were retrained using the principal component scores using a small sample of the fault welds. For the Mild Steel, DP-DP and DP-Mild stacks a sample of control welds and electrode tilt data was used and for the Usibor stacks a mix of the electrode tilt and force-50%. These fault pairings were selected as they showed a statistically significant correlation with button diameter.

Each of the models improved in performance when retrained with a sample of the fault welds (including re-calculating the principal components and weld quality models), reducing the RMSE and improving the R^2 between predicted and actual values (Figure 4-22, Figure 4-21 and Figure 4-22). The welds that were used to retrain the models were excluded from the figure and statistics so as not to bias the results.

The model that performed best for the validation data was the Mild Steel model showing good correlation with button diameter for the force variation and control data (Figure 4-22). The Force+15% welds in general were slightly under-predicted while the Force-15% welds slightly over-predicted. This shows that the principal components created by varying the welding current do not have the same strong correlation with the button diameter of welds that have varying clamping force.

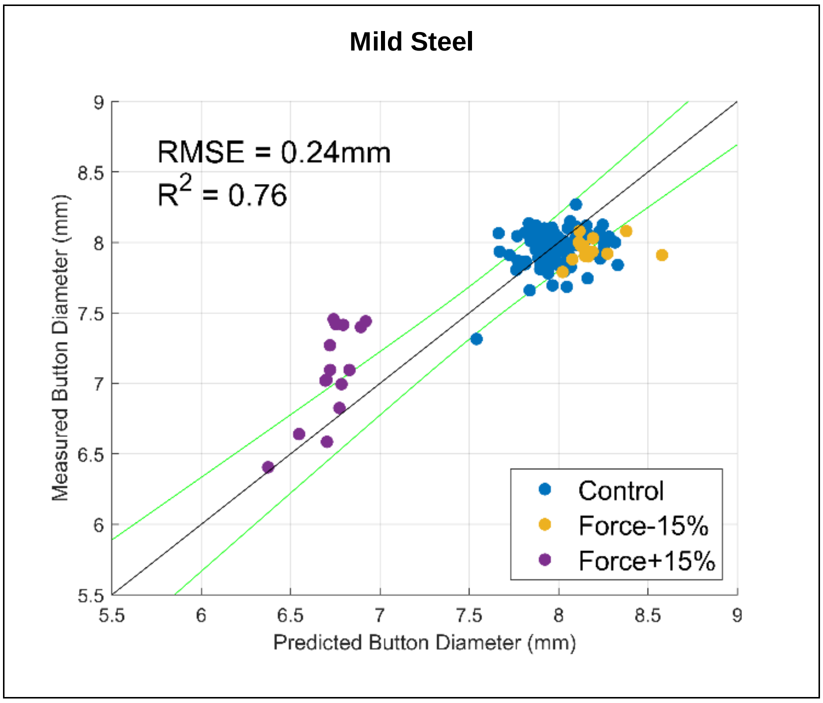

Figure 4-20: Mild steel, predicting the button diameter of fault welds

The DP-DP model (Figure 4-21a) performed moderately well with an RMSE of 0.38mm while the RMSE of the DP-Mild (Figure 4-21b) was significantly reduced due to the adjustment of the model using the principal component scores of the electrode tilt and control welds from the validation data. The error in the DP-Mild model was most likely reduced due to the correction in the height of the signals when the fault data was added into the PCA and model calculation. The force reduction welds are similarly over-predicted, as with the Mild Steel model.

The Usibor-Usibor (Figure 4-22a) and Usibor-Usibor-Mild steel (Figure 4-22b) models could not be successfully retrained using the validation data due to the signal variation available for modelling.

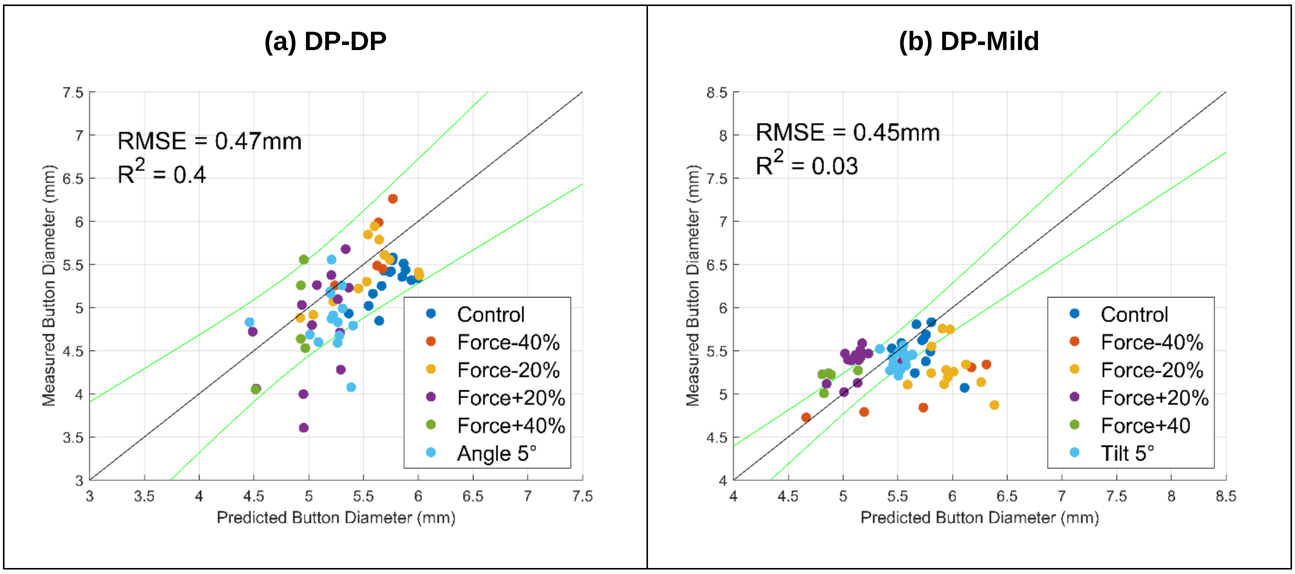

Figure 4-21: DP-DP and DP-Mild, predicting the button diameter of welds

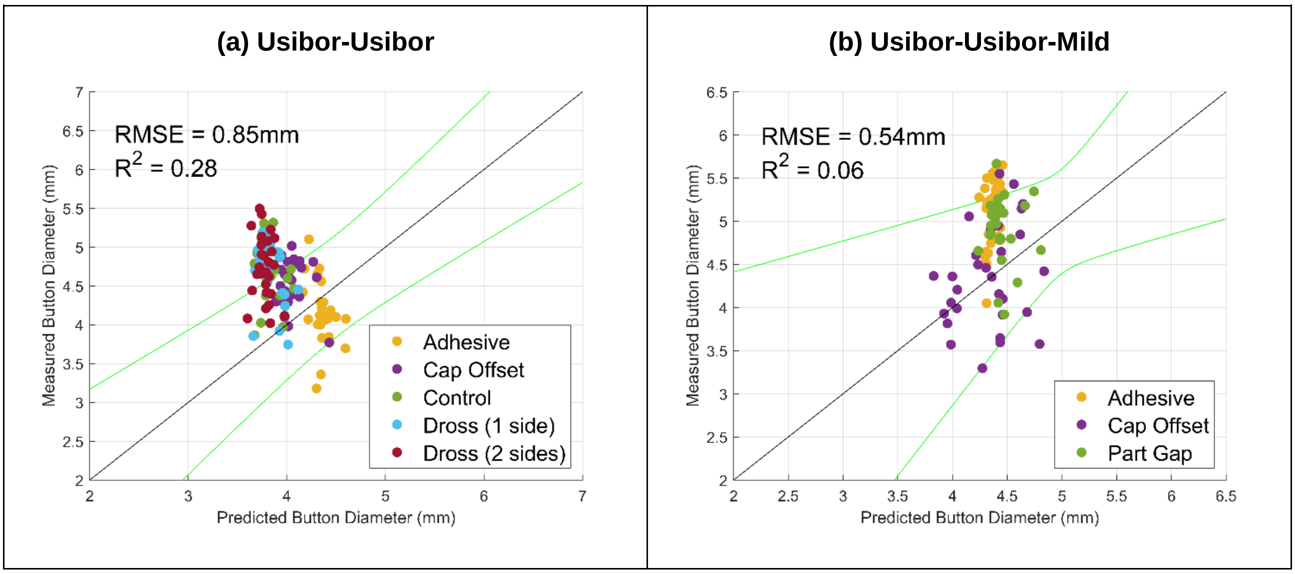

Figure 4-22: Usibor-Usibor and Usibor-Usibor-Mild, predicting the button diameter of fault welds

4.2.6 Different Types of Signal Shapes

Figure 4-23 shows the mean signals for the Mild Steel data. Figure 4-23 (a) shows the mean signals from the varied welding current in the weld lobe data set. The mean signals from the weld lobe set show significant variance throughout the welding signals, with the majority in the second half of the process.

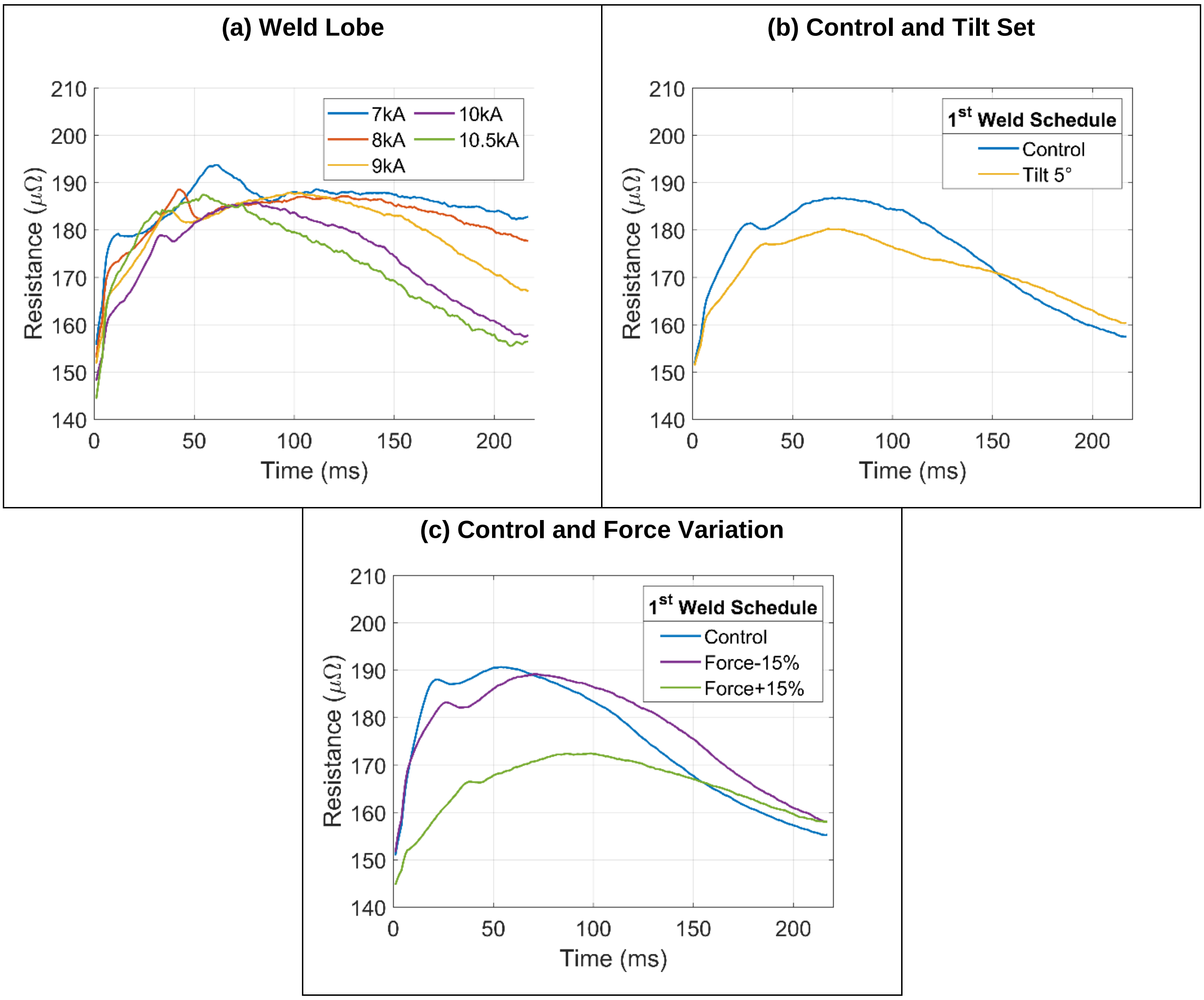

Figure 4-23: Mild steel mean signals

The variation caused by the faults, Figure 4-23 (b) and (c), which are all created with a welding current of 10kA, is seen at the start of the welding signal. The tilt data was collected in a randomised fashion with two thirds of the welds created with a 5° tilt and the other third created with 0° tilt (Control welds). The difference between the tilt and control weld signals shows variation at the start of welding. This was found to produce a good model for weld quality for the mild steel using the principal components calculated from the weld lobe dataset and performs better than a model that has principal components calculated from the tilt dataset. The mean control signals are slightly different as the control mean signal shown with the tilt 5° data is only calculated from the welds that are interspersed with the tilt welds, not an actual control dataset.

This shows that for weld quality monitoring, principal components should be calculated from data with a wide range of weld quality and the model should be trained with welds similar to the validation data.

For the Usibor stacks, the fault welds could not be successfully modelled. This is due to the difference in signal shape variation seen in the training data and the welds with induced process faults shown in Figure 4-13 and Figure 4-16. Additionally, the induced faults in the Usibor stacks did not affect the measured signals or weld quality significantly. This may be caused by the lower welding current and longer weld time that was required to weld the Usibor material. A lower welding current and longer welding time could reduce the effects of the faults on the measured signals by generating the heat over a longer period.

Extrapolation of the weld quality monitoring models had limited success, with promise shown in the Mild Steel and the DP-DP stacks, however the heterogeneous stack with the DP-Mild and the Usibor stacks were not well-predicted. From Figure 4-17, it was shown that button diameter can be modelled effectively for a given type of variation (varying welding current) but this did not apply in the same way to the variation caused by process faults. To better model the weld quality of the different faults for the Advanced High Strength Steels, more work is needed to understand the resistance signals and the effects of the surface coating and weld schedules required to weld the challenging material.

4.2.7 Discussion

As shown in Table 4-8 the vast majority of the variance in the signals is representable along a few principal components. Because the variation in the training data is caused by varying the welding current (which is known to effect weld size), PCA can be used to effectively extract important signal information for weld quality monitoring.

If this process was targeted at each fault individually the modelling approach of different conditions is likely to be more successful. However, for fault-specific models to be a viable option, it must be shown that the fault in the process can be identified using the signals. Creating models for every fault in RSW is beyond the scope of this work, however section 4.4 shows that the faults in the different material stacks can be successfully separated using the principal components of the training data. With this knowledge, signals could be analysed by more specific models that are trained with fault information included in the model increasing the accuracy of the prediction.

From this study, it can be seen that there is sufficient information in the resistance signal of steels to characterise the variation of weld quality when welding current is varied (Figure 4-17) and that PCA is an efficient method for extracting these features (Table 4-8).

Principal components that explain less than 1% of the variance were deemed to be insignificant and likely to be noise for modelling purposes. This limits the number of factors that can be correlated with button diameter and shows the complexity of the variance in the training set data.

If only one principal component explains more than 1% of the training set variance it shows that there is really only one contributing factor to the training set variation. This means that the model can only use that factor to predict weld quality of future welds. Generally, a model with more parameters will be more robust to changes in the process and this comes down to training set design. In the Usibor-Usibor-Mild, the model which performed the worst at predicting outside its training bounds, 98.5% of the variance in the training set was explained by the first principal component.

In this study the PCA based weld quality modelling technique was tested with very challenging welding conditions. After this rigorous testing, the modelling technique was implemented in industry to test it in the conditions that it is designed for. Implementing it in an industrial manufacturing facility allowed it to be benchmarked against the industry alternatives for weld quality monitoring.

4.3 Application to Industry

In the previous section the principal components of the resistance signal were used to model button diameter in challenging circumstances in the lab. The methodology developed was applied to data which was collected in an automotive manufacturing plant. Two conditions were investigated, electrode tilt (or electrode misalignment) and normal operating conditions. The prediction of weld button diameters using models calculated from the principal components of the resistance signals was compared to the industry standard non-destructive testing technique, ultrasonic C-scans.

Resistance signals were measured for every weld, welds were then tested with an ultrasonic c-scan and subsequently destroyed to measure their actual button diameters. The signal based weld quality prediction method was found to significantly outperform ultrasound for inferring the button diameters of welds in production (Figure 4-24).

The model for button diameter in this study outperformed the ultrasonic C-scans for inferring button diameter in an industrial manufacturing plant shown in Figure 4-24. The ultrasonic C-scan was found to be particularly susceptible to electrode misalignment which can occur when welds are created by welding technicians as was done in the manufacturing plant. The ultrasonic C-scans tended to over-predict the button diameter when welds were created with tilted electrodes (Figure 4-24a) while the button diameters of these welds were more accurately predicted using PCA and the resistance signal. This study was published in Procedia Engineering (Summerville et al., 2017a).

The electrode-tilt fault condition significantly reduced the button diameters measured from destructive testing (Figure 4-24). Clearly it would be useful to be able to identify the presence of process faults such as electrode tilt, so that substandard welds can be identified from their signal shapes. The next section presents the analysis required to identify and cluster welding process faults using the common signal shapes found from PCA.

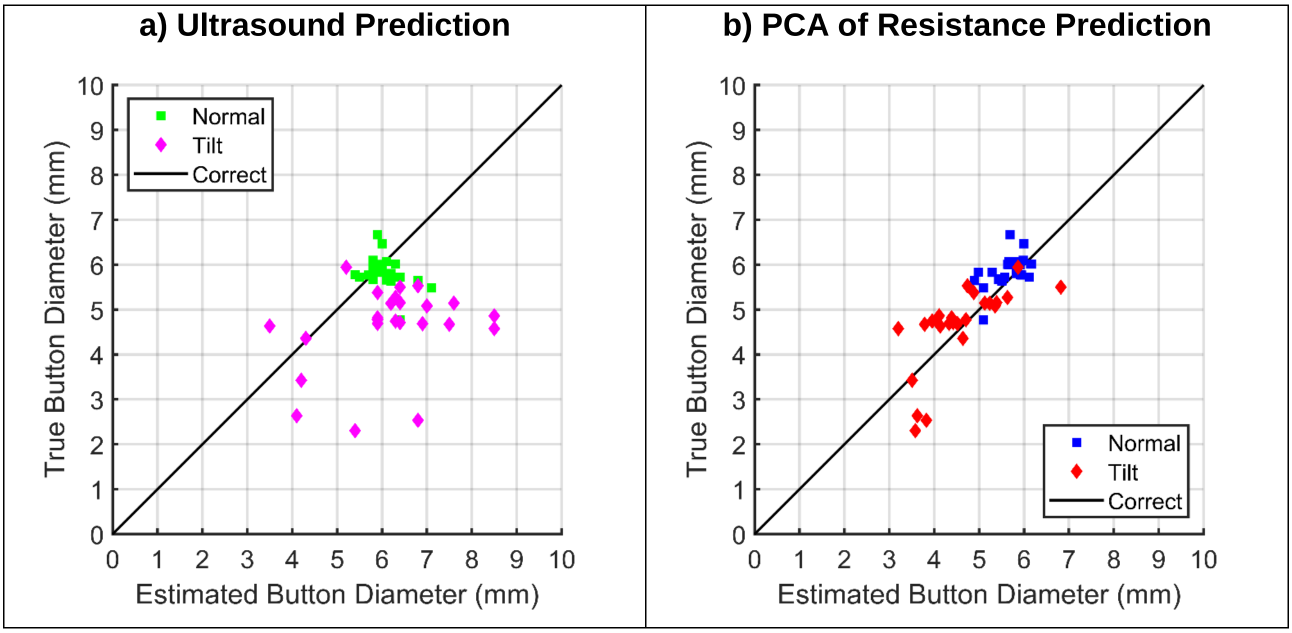

Figure 4-24: Comparison of (a) ultrasonic C-scans and (b) PCA based weld quality modelling for inferring button diameter in industry

4.4 Fault Type Identification & Analysis

The results shown in Figure 4-22 show that welds with different process conditions (such as faults) can be challenging to model with normal training data such as variation in weld settings and electrode wear. This suggests that the relationships between the signal features and weld quality are different to those in the training data. It has been demonstrated that accurate models for weld quality can be made for a range of different conditions in Figure 4-6 and Figure 4-17a, b, c, d and e. To model the multitude of fault conditions a wide range of models could be produced, however this is beyond the scope of this thesis. Instead, it can be shown that the wide range of process faults that can occur in RSW can be identified and separated using principal components.

To be able to analyse welds with different process conditions using different models, it must be shown that they can be effectively identified and separated from other welds, such as those created under normal operating conditions. To achieve this, this section will demonstrate how the principal component scores of new welds can be used to effectively identify and separate welds into different process conditions. This is a required step for fault-specific models to be applied to different welding conditions.

Many of the induced process faults in the previous section did not have a significant impact on the quality of the welds. Faults such as the electrode force reduction, electrode tilt, electrode cap offset, and dross on the electrode sheet interface are likely to accelerate electrode wear, which can reduce the heat that is delivered to the weld, reducing weld quality over time. The other faults such as part gap, increased electrode force and adhesives are more likely to have an immediate effect on each weld's quality, producing different types of weld quality variation. These process faults are all likely to result in process instability with detrimental effects to weld quality and so it is beneficial to be able to identify these in process to reduce the chance of low quality welds being formed in production.

Principal Component Analysis was used in the previous section to extract major modes of signal variation from welds with varying current for weld quality prediction. This had limited success for predicting the button diameters of the extreme process faults that were investigated in the fault datasets.

Fortunately, the principal components of welding data are useful for outlier detection (Figure 4-25). In another study, the first principal components calculated from a steel welding process were monitored using a moving range chart methodology, which represent welds as their difference from the welds around them (the *'moving range'* like a *'moving average'*). It showed that welds with electrode misalignment resulted in principal component score one values significantly beyond the three sigma (standard deviations) limit imposed by standard moving range chart methodology. All welds with electrode misalignment were clearly identifiable using this methodology.

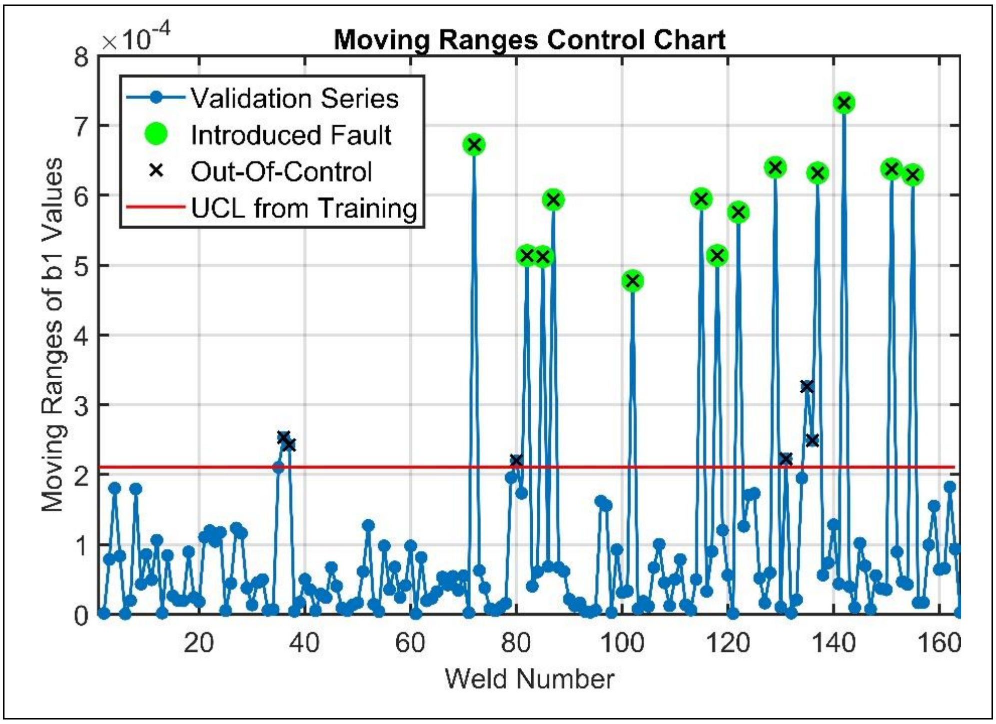

Figure 4-25: Using PCs for outlier detection in steel welding process (Summerville et al., 2017)

When new signal shape variation is introduced in the form of a fault (that the PCA was not trained with), the principal component scores required to describe the new signal appear as outliers. Using this property of the analysis technique, a range of different faults can be separated efficiently and effectively in an automated fashion using only a few principal component scores. To demonstrate this, the principal component scores (calculated from the training data PCA) were used to represent the signal variation in the fault datasets to determine whether they could be separated based on their different signal shapes.

The identification of faults in a RSW process from signal information would enable preventative maintenance procedures on a welding line which would improve confidence in weld quality and reduce costs in production. Fault identification from welding signals is not currently available on any commercial weld timers and is of great interest to industry and limited examples of fault identification in the literature exist (Brown et al., 2000; W. Li, 2007; Y. S. Zhang et al., 2005).

4.4.1 Background

PCA creates a new set of axes to represent a dataset with fewer dimensions by aligning the new axes with the highest variance in the data. The principal component scores of new welds can be used to represent how much a principal component is present in a weld’s signal. Using the first few principal component scores, the signal shape of a weld can be characterised based on the major modes of variation and this allows for separation of welds into different fault classes based on their signal shape. To investigate whether the faults can be identified from one another, the welds are clustered using their principal component scores.

Discriminant Analysis (Fisher, 1936) is a clustering technique that calculates decision functions for each group of welds that separate them from every other group in the dataset. The decision function is based on the density and shape of the cluster and results in a 0 or 1 dependent on the principal component scores of the weld. Discriminant Analysis was chosen instead of other clustering techniques such as k-means clustering as the faults that occur in a welding process drift and deteriorate and this results in changes in their signal shapes. The changes in their signal shapes produces a range of different principal component scores with different means and distributions for each fault. Quadratic discriminant analysis was chosen for this study as it allows for different distributions in each group.

Figure 4-26 shows an example of a quadratic discriminant rule that separates one group of points from another. Each point on the figure represents a weld with the x and y axes plotting two of the welds’ principal component scores. The interface between the yellow and purple areas represents the discriminant function of Class 1 which separates it from Class 2.

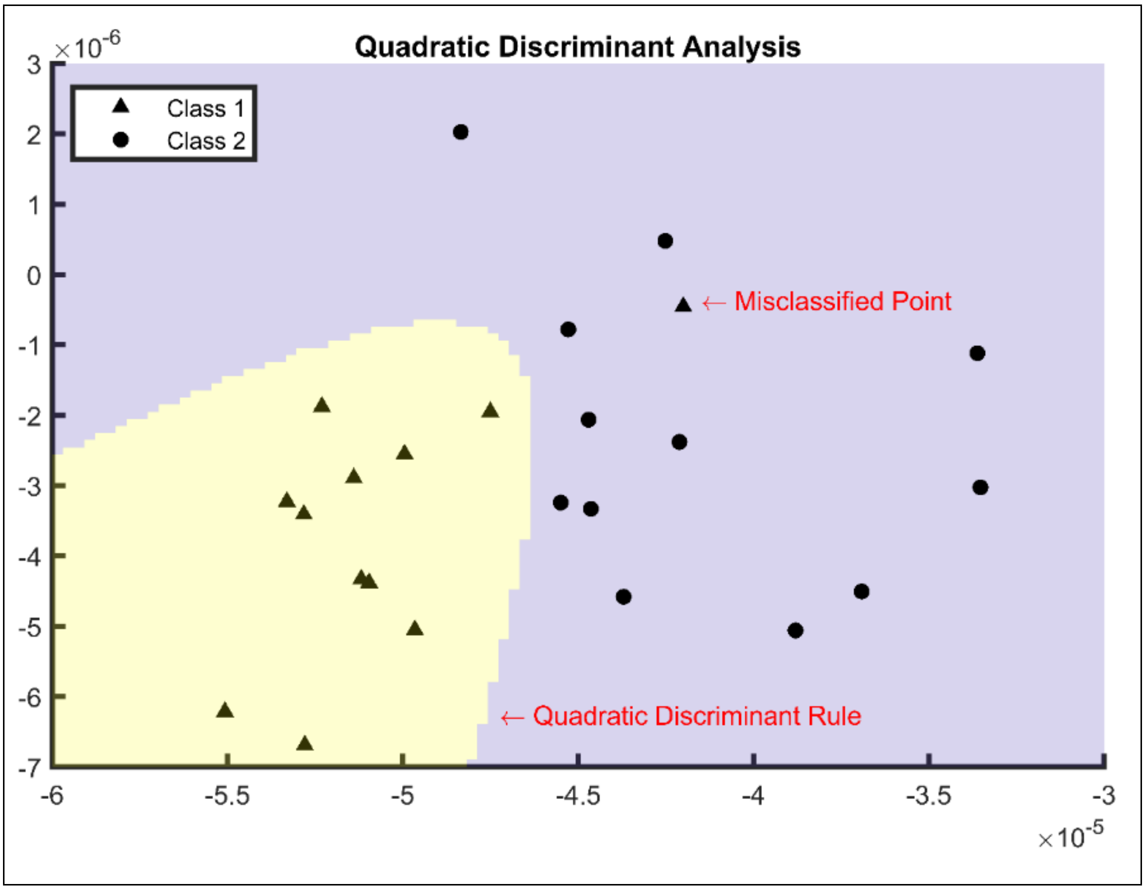

Figure 4-26: Quadratic discriminant analysis example

In Discriminant Analysis a set of discriminant functions is calculated for each class of welds which forms a binary rule that separates it from another class. The particular rule in the example below is a quadratic rule, allowing for quadratic terms to be used in the equation. The Discriminant Analysis rules are challenging to represent in this study as more than two principal components were used to separate the welds, and so the rules are four dimensional and difficult to plot.

The principal component scores of the fault datasets, calculated from the training data (which varied welding current only) were used to calculate quadratic discriminative rules for each different fault class using all of the welds. This provides insight into the amount of useful signal information characterised by the principal components of the training data for identifying induced process faults and represents the maximum separation that can be achieved with this data.

When principal components are calculated for welds with different process conditions than the training data, the signals tend to result in outlier principal component scores. This can exaggerate the difference of the new welds from the training data which present as statistical outliers and can be useful for fault identification as in shown in Figure 4-25.

Another alternative to fault identification and classification is to collect significant training data with all the faults of interest, so principal components can be calculated that represent major signal shapes of the faults. The difference between these two methods is in the certainty of which fault class a weld belongs to. If significant fault training data is collected and discriminant rules for particular faults are known beforehand a weld can be identified as a particular fault. In (Summerville et al., 2017b) the approach taken was fault identification with no prior knowledge of the fault. It was found that even without prior knowledge of the fault, analysis of the signal shapes used allowed for the type of fault to be inferred.

The fault data in this study was limited due to time and material availability, and so the fault identification methodology using principal components from the training data with no prior knowledge of any faults was chosen. This solution is more likely to be implementable in industry given it doesn't require all possible process faults to be investigated prior to starting production.

This section will use four principal components for each material stack to calculate discriminative rules that separate all the different faults, from which an overall classification accuracy can be calculated.

4.4.2 Methodology

To calculate discriminative rules to identify faults from their different signal shapes the first four principal component scores were used. The principal component scores of the fault dataset were calculated from the training data which only varied the welding current. The principal components used for this analysis are therefore not the major modes of variation of the fault data. Separation of the faults can still be achieved using principal components of the training set and reduces the magnitude of training data required to complete fault identification on the plant floor.

For each fault group a set of quadratic discriminant rules are calculated that separate it from the other groups. Unfortunately, because four principal component scores are used to create the discriminant rules, they can't be visualised. Figure 4-27 shows a visual representation of a discriminant rule calculated from three principal component scores for reference and the generic form of the equation is shown in Eq. 4-7.

$$R = C + aP_1 + bP_2 + cP_3 + dP_1^2 + eP_2^2 + fP_3^2 + g(P_1 \cdot P_2) + h(P_1 \cdot P_3) + i(P_2 \cdot P_3) \quad \textbf{Eq. 4-7}$$

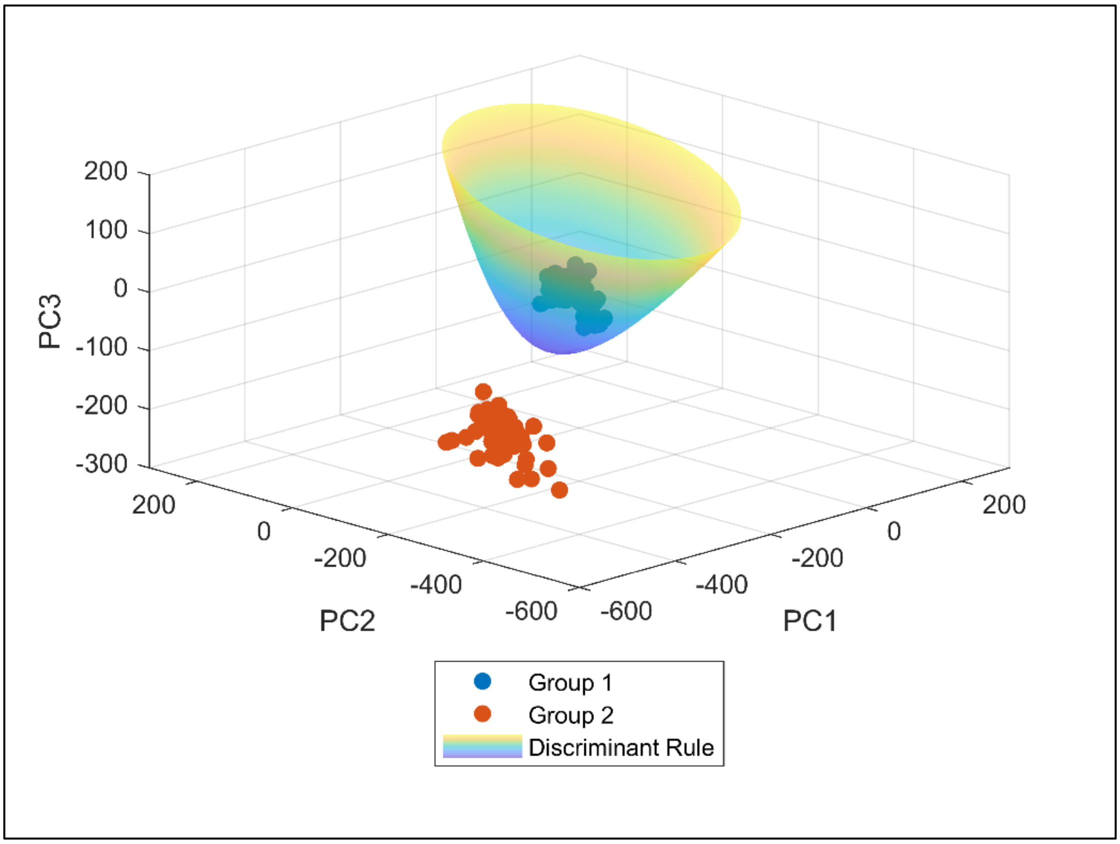

Figure 4-27: Three dimensional quadratic discriminant rule

The discriminant rules were calculated using all fault welds to determine the maximum separability of the fault data from the signal shapes found in the training data.

4.4.3 Results Summaries

Table 4-10 and Table 4-11 summarise the mild steel classification accuracy for the fault separation using quadratic discriminant analysis and the principal components from the training data. Using the first four principal component scores for each weld, 99% of all welds could be successfully categorised into their given fault classes. This shows that for mild steel there is sufficient information to identify faults from principal component scores calculated from a training set that only varies welding current.

Table 4-10: Mild steel fault identification accuracy

Welding Condition	Control	Part Gap	Force-15%	Force+15%	Tilt 5°	Total
% of Welds Correctly Classified	98	100	100	100	100	**99%**

Table 4-11: Mild steel fault identification confusion matrix

Mild Steel		Classified As				
		C	PG	F-15%	F+15%	T5°
Fault Group	C	98%	0	2%	0	0
	PG	0	100%	0	0	0
	F-15%	0	0	100%	0	0
	F+15%	0	0	0	100%	0
	T5°	0	0	0	0	100%

Figure 4-28 shows the separation of the mild steel welding faults in two dimensions using the first and second principal component scores of the welds. The Part Gap, Force+15% and the remaining fault classes are spread in groups along the first principal component, while the control, force variation and Tilt 5° welds are somewhat spread out across the second principal component.

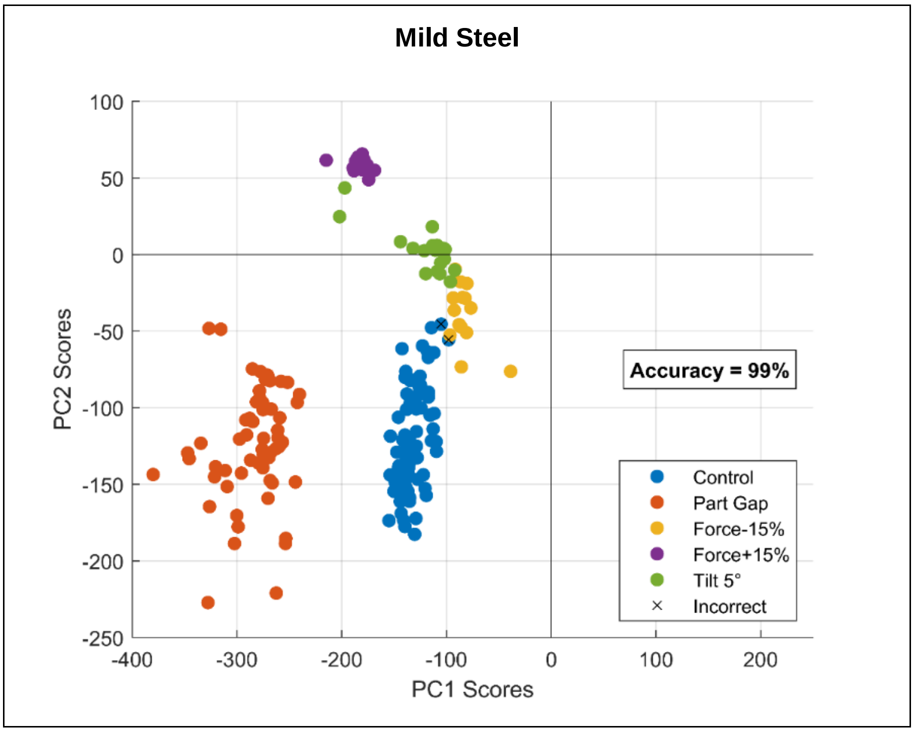

Figure 4-28: Mild steel weld fault separation using PCA and QDA

The first four principal component shapes of the mild steel welds are shown in Figure 4-29 with the first corresponding to variation in the overall height and the second corresponding to a change in resistance in the first half of the process. The third principal component shape characterises variation in resistance predominantly in the middle of the process while the fourth principal component represents a difference in the time that the peak occurs from ~40ms to ~60ms.

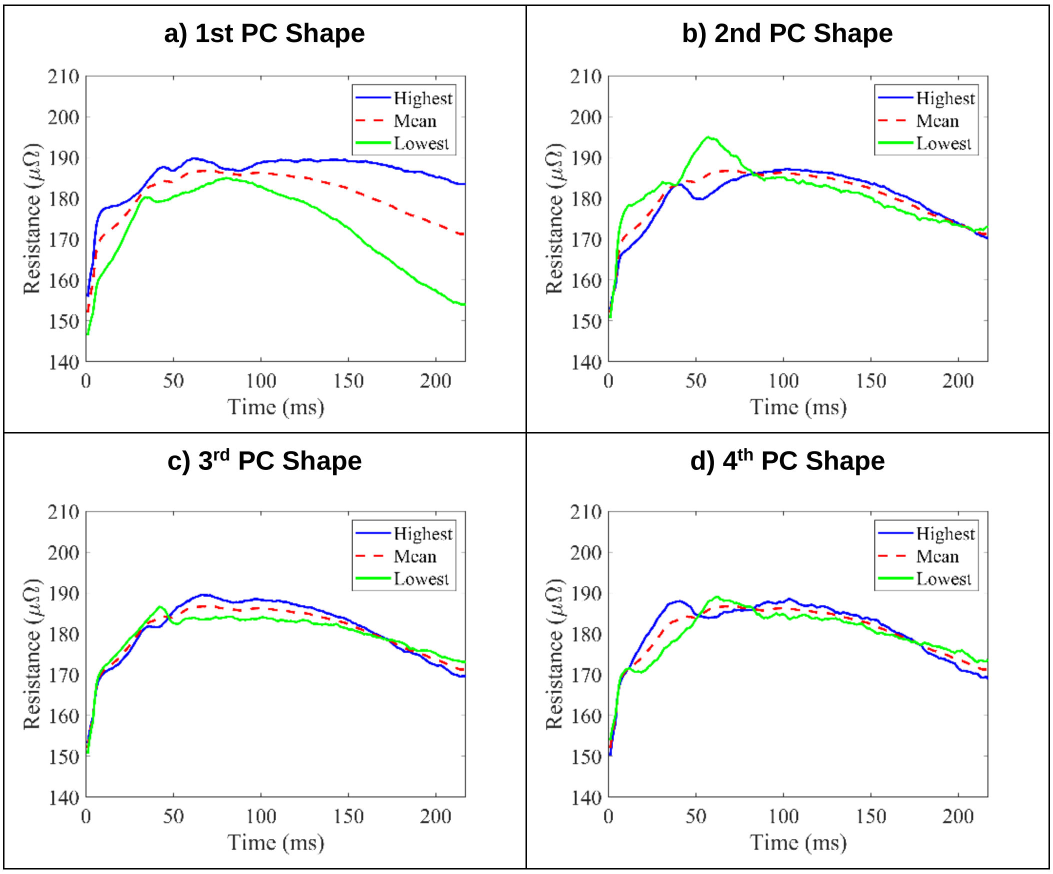

Figure 4-29: First four principal component shapes of the mild steel training data

The classification accuracy of the faults was 99% using quadratic discriminant analysis and the first four principal component scores for the mild steel (Table 4-10). The confusion matrix shows that 2% of the control welds were incorrectly classified as Force-15% welds. Figure 4-28 shows that the different faults do not form tight clusters when represented as their principal component scores. This figure plots the welds using the first two principal component scores for each weld.

The same process was conducted for the DP-DP and DP-Mild stacks with similar success. Table 4-12 shows the classification accuracy summary and Table 4-13 confusion matrices for the two material stacks. 91% of the welds with induced faults in the DP-DP stack were correctly classified.

Table 4-12: DP-DP and DP-Mild fault identification accuracy

Welding Condition		Control	Force -40%	Force -20%	Force +20%	Force +40%	Tilt 5°	Tilt 10°	Total
% of Welds Correctly Classified	DP-DP	100	100	100	92	100	68	100	**91%**
	DP-Mild	52	100	83	100	100	91	100	**82%**

Table 4-13: DP-DP and DP-Mild fault identification confusion matrices

DP-DP

Classified As

Fault Group	NF	F -40%	F -20%	F +20%	F +40%	A5°	A10°
NF	100%	0	0	0	0	0	0
F-40%	0	100%	0	0	0	0	0
F-20%	0	0	100%	0	0	0	0
F+20%	0	0	0	92%	0	8%	0
F+40%	0	0	0	0	100%	0	0
A5°	14%	0	5%	14%	0	68%	0
A10°	0	0	0	0	0	0	100%

DP-Mild

Classified As

Fault Group	NF	F -40%	F -20%	F +20%	F +40%	A5°	A10°
NF	52%	0	4%	0	0	40%	4%
F-40%	0	80%	20%	0	0	0	0
F-20%	17%	17%	58%	0	0	8%	0
F+20%	8%	0	0	31%	8%	0	54%
F+40%	0	0	0	20%	80%	0	0
A5°	41%	0	0	0	0	59%	0
A10°	0	0	0	0	0	0	100%

The welds that weren't correctly classified were from the Force+20% and 5° tilt fault classes. The first confusion matrix in Table 4-12 (DP-DP) shows that the Force+20% welds were incorrectly classified as 5° Tilt welds and the 5° Tilt welds were incorrectly classified as 14% control welds, 5% Force-20% and 14% Force+20% (reading the rows of the matrix). This suggests that these fault types show similar signal shape behaviour for this material. This is shown with the first two principal component scores in Figure 4-30. From the plot of PC1 scores vs. PC2 Scores in Figure 4-30 it is challenging to understand how all the welds have been correctly classified using quadratic discriminant analysis. One Tilt 5° weld is highlighted that is surrounded by Tilt 10° welds when they are plotted by their PC1 and PC2 scores. However, the graph of PC2 scores vs. PC3 scores shows that the Tilt 10° fault class is separated along the 3rd principal component from the rest of the experimental conditions. The discriminant analysis in this section uses the first four principal component scores to separate the faults which sometimes makes it challenging to see how all the welds are successfully clustered.

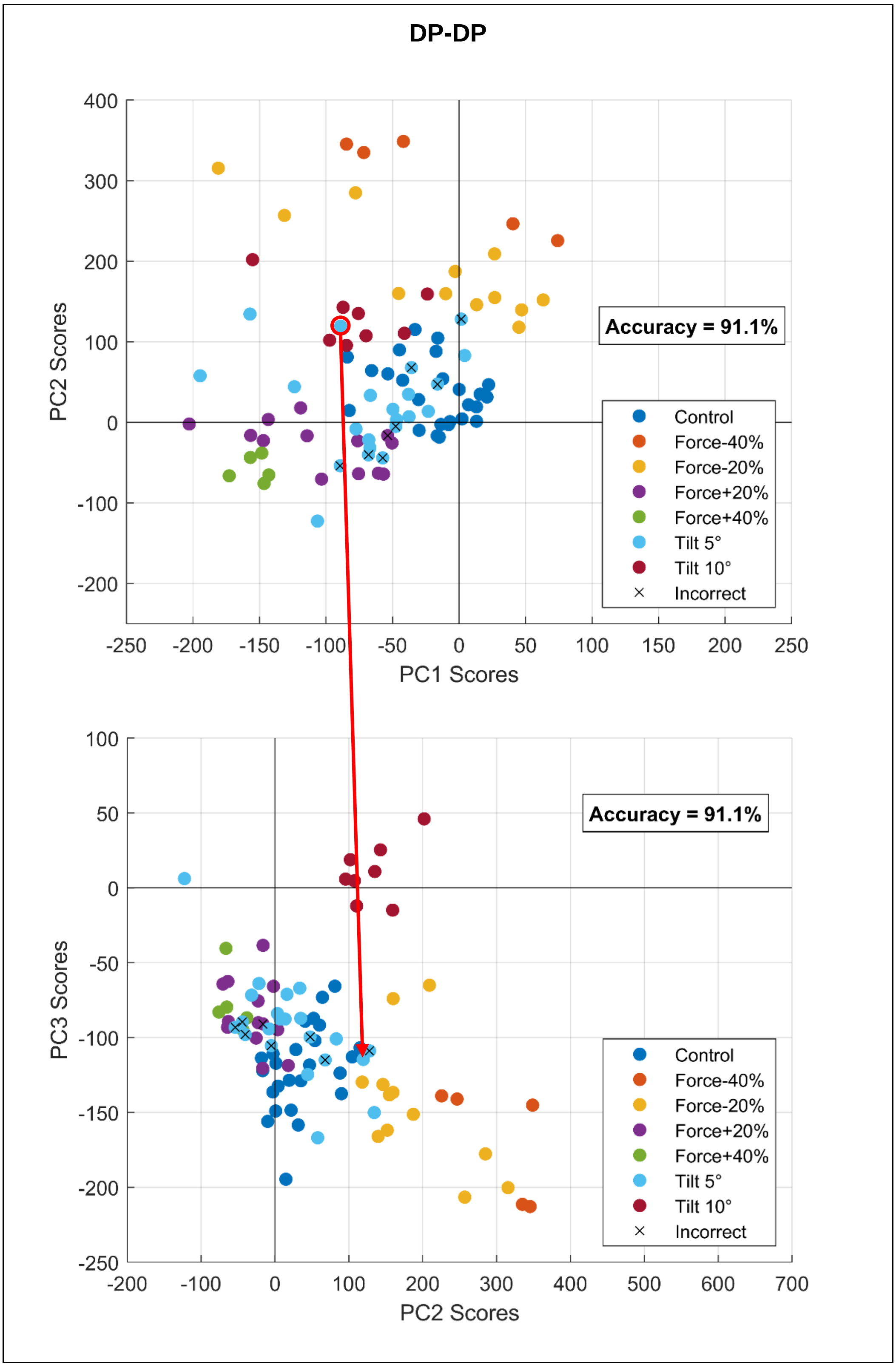

Figure 4-30: DP-DP fault classification in two dimensions

The DP-Mild welds were correctly classified with an overall accuracy of 82%. The welds that were incorrectly classified are from the Control, Force-20% and Tilt 5° fault categories. Reading the rows of the second confusion matrix in Table 4-12 shows that the Control welds were predominantly incorrectly classified as a 5° tilt with some welds classified as Force-20% and a 10° tilt. The Force - 20% and Force-40% faults were incorrectly classified as each other while some of the Force-20% were classified as control and 5° tilt. Some of the Force+20% and Force+40% were incorrectly classified as each other while most of the Force+20% welds were incorrectly classified as the 10° tilt. Almost half of the DP-Mild 5° tilt welds were incorrectly classified as control welds showing that fault separation is more challenging for the heterogeneous DP-Mild stack.

Figure 4-31 shows that the different fault classes are not well spread across the first principal component of the DP-Mild varying welding current dataset, and this was the only training set where the height of the signal was not shown in the first principal component shape. This was represented somewhat in its second principal component shape and this seems to separate the DP-Mild fault classes more effectively. In section 4.2.5 it was discussed that there was a difference in the magnitude of the resistance signals of the DP-Mild training and fault datasets (~30μΩ) which explains the high positive second principal component scores.

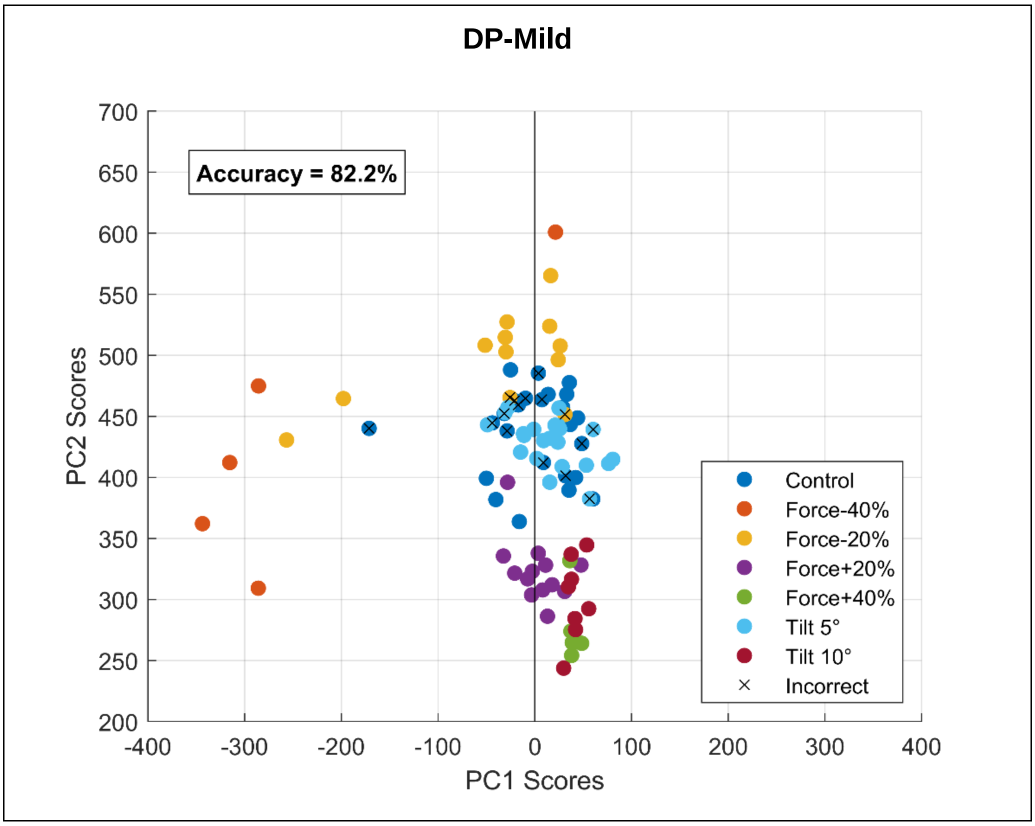

Figure 4-31: DP-Mild fault separation in two dimensions

The Usibor-Usibor material stack faults were successfully separated using the training set principal components and QDA (Table 4-14 and Figure 4-32). Notably, the welds with Dross on one side were mostly incorrectly classified as welds with Dross on both sides. The analysis was conducted again considering Dross as one fault which significantly increased the overall classification accuracy to

86%. The 10° tilt fault was not particularly well classified with a number of welds classified incorrectly as several of the other faults. The same trend was seen in the 10° tilt fault for the Usibor-Usibor-Mild as well with a number of the welds classified as several of the other faults in the dataset. The Force-50% was not well classified with 43% of the welds classified as 10° tilt. Figure 4-32 shows large signal shape variation within the sets making it challenging to distinguish the faults from one another.

Table 4-14: Usibor-Usibor and Usibor-Usibor-Mild fault classification accuracy and confusion matrix

Welding Condition	Tilt 10°	Force -50%	Adh.	Part Gap	Cap Offset	Cont.	Dross (1 side)	Dross (2 sides)	Total
Usibor-Usibor	72	96	87		88	90	78	30	**77%**
Usibor-Usibor (Combined Dross)	72	96	87		88	86	85		**86%**
Usibor-Usibor-Mild	70	38		100	83	87			**76%**

Usibor-Usibor

Classified As (columns); Fault Group (rows)

	T10°	F-50%	ADH	2CO	C	D1	D2
T10°	72%	8%	4%	8%	0	0	8%
F-50%	4%	96%	0	0	0	0	0
ADH	9%	0	87%	4%	0	0	0
2CO	0	0	8%	88%	4%	0	0
C	0	0	0	3%	90%	7%	0
D1	0	0	0	0	15%	78%	7%
D2	4%	4%	0	4%	7%	52%	30%

Usibor-Usibor: Dross as 1 Fault

Classified As (columns); Fault Group (rows)

	T10°	F-50%	ADH	2CO	C	D
T10°	72%	8%	4%	8%	0	8%
F-50%	4%	96%	0	0	0	0
ADH	9%	0	87%	4%	0	0
2CO	0	0	8%	88%	4%	0
C	0	0	0	3%	86%	10%
D	0	2%	0	2%	11%	85%

Usibor-Usibor-Mild

Classified As (columns); Fault Group (rows)

	T10°	F-50%	ADH	3PG	2CO
T10°	70%	14%	0	7%	3%
F-50%	43%	38%	0	20%	7%
ADH	0	0	100%	0	0
3PG	0	10%	0	83%	7%
2CO	4%	3%	0	7%	87%

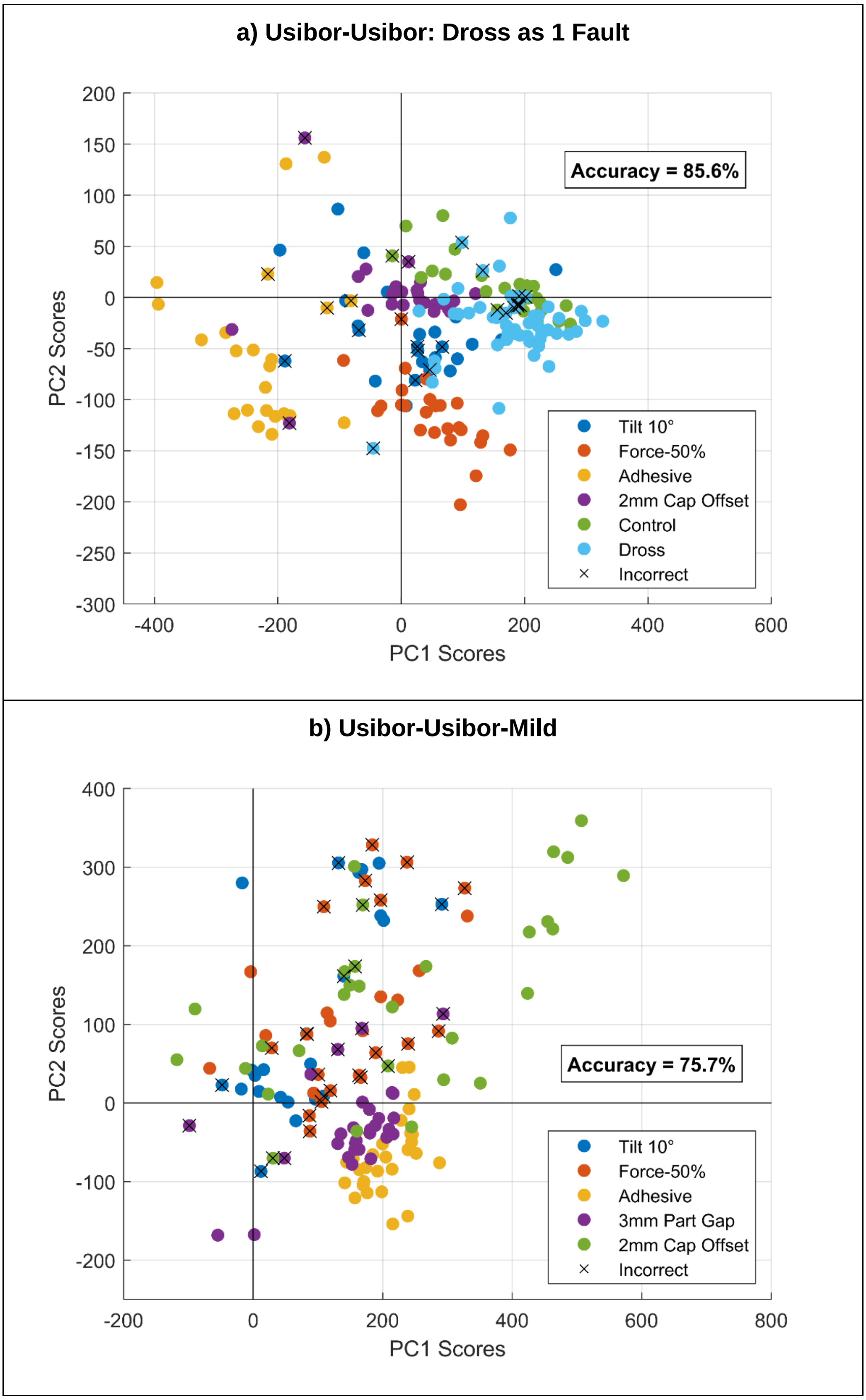

Figure 4-32: Usibor-Usibor and Usibor-Usibor-Mild fault separation in two dimensions

4.4.4 Analysis

The signals of the high strength steels did not change as much as the mild steel when process faults were introduced. This may be due to the material properties of the Dual-Phase and Usibor materials and means they are more challenging to predict the quality of and separate into different fault classes.

In all of the material stacks except the Mild Steel stack, the electrode tilt fault was found to be challenging to cluster. The electrode tilt welds were collected with randomly interspersed control welds (at a rate of 2:1) to try to maintain the random nature of the fault and to avoid the electrodes conforming to the electrode tilt after a few welds. However, the fixture used to hold the welding samples allowed for compliance in the plane of the electrode tilt and was observed to rotate when the electrodes clamped shut. This reduced the effect of the induced electrode angle. In these material stacks the Tilt faults were often incorrectly classified as the control welds and vice-versa suggesting that the effects of the electrode tilt were minimised by the compliance of the fixture.

4.5 Discussion & Limitations

This chapter has presented PCA as a feature extraction method for weld quality monitoring using resistance signals measured during welding. The methodology developed allows for signal shapes to be extracted from training data in the form of principal components. The principal components can be correlated with the output quality of the welds using the principal component scores. The principal component scores were also found to be useful for separating different process faults in a welding process. This efficient use of the welding signal information presents a structured and effective approach to weld quality monitoring.

The use of PCA means that the major signal shapes can be extracted from a dataset and these can be correlated with the quality. Conducting feature selection in this way means that the success of the models is not reliant on manual feature extraction determined by empirical knowledge. In this regard, extensive knowledge is not needed about each specific material stack, which is particularly useful for the automotive industry which requires many different joints to be welded with frequent introduction of new materials to increase the strength and reduce the weight of cars.

The PCA-based methodology presented is appropriate for analysis of one signal per weld. It was shown to be sufficient to model five steel stacks of different grade and gauge and number of sheets. The application of these models to extreme process faults was not as successful, but those process faults could be successfully separated using the principal components of training data allowing for preventative maintenance in the process to rectify the issue causing the fault.

Throughout this study, welds with expulsion were removed from the analysis due to the extreme effects of expulsion on the resistance signal. Given the success of the fault type separation, it is likely that expulsion welds could be easily identified using PCA, however this was not investigated.

Currently the PCA-based weld quality monitoring method cannot analyse signals of different length, an option that is often available on modern weld timers which adaptively control the weld schedule during welding. There are a few ways that this could be addressed. The extension of welding signals could be ignored and the information inside the base weld schedule could be relied on to predict the quality with the knowledge that adaptive control has been implemented on a weld. Alternatively, properties of the adaptive intervention such as the amount welding current is increased or signal length could be appended to signals as another feature of the welding process like each resistance measurement, however models would have to be specifically trained for this. Another alternative to dealing with signals of different length would be to take a fixed number of samples from each welding signal, essentially forcing the signals to be the same length through signal scaling/resampling. This omits the information regarding the additional heat input, but may work within reasonable adaptive control limits (as long as the time isn’t able to extend too far beyond the base schedule).

A particular training and validation methodology for button diameter prediction was chosen for this study. This involved creating a training set with one kind of variation in it (welding current) and validating on welds that had different contributing factors to signal shape and weld quality which was not found to be very successful. It would be particularly advantageous to be able to characterise the differences in the signal datasets to better understand the types of models that are successful and where their predictive limits lie.

One possible solution to this problem is to understand how much of the variance of a new signal can be explained using the principal components of the training data, selected for modelling weld quality. This would allow for the amount of required variance in a training set to be optimised and how many factors should be varied to create an appropriate model for weld quality. At this stage it isn’t clear how much of the variance in the validation data the training set principal components should describe but it would be useful to be able to quantify why a model is or isn’t successful at predicting the output quality or separating different faults.

The accuracy of the weld quality models could be improved by including a few more varied factors into the training data. Analysis of the mean signal shapes in the Mild Steel shows that varying the welding current has most effect on the end of the resistance signal whereas the start of the signal had the most variation when the clamping force was changed. The first principal component of the training data consequently showed the most variance at the end of the signal and this was the principal component most strongly correlated with button diameter for the training data. This resulted in an over and under-prediction of the force variation welds because the relevant signal information was not extracted in the first principal component of the training set.

The variation in button diameter of the control datasets in the Usibor-Usibor, DP-DP, and DP-Mild (not collected for the Usibor-Usibor-Mild stack) is comparable to the variation in button diameter of many of the faults. Given that the control welds were collected under controlled conditions with no induced faults or variance other than unavoidable electrode degradation, these datasets represent the amount of quality variation in each material. The Mild Steel control welds had significantly less variation in button diameter than the other material types.

4.6 Conclusion

This chapter presented a methodology for weld quality monitoring of a range of automotive steels. Principal Component Analysis was used to extract features in the form of signal shapes from the resistance signal of resistance spot welds. The button diameter of spot welds that were created with different weld currents was successfully modelled from the principal components of the resistance signal for five different material stacks that varied in gauge, grade and number of sheets. These models were directly applied to welds with induced process faults and then retrained using a sample of the fault welds to improve their accuracy. The induced process faults were successfully separated using the principal components of a training set with no fault data using discriminant analysis.

The weld quality monitoring model and fault separation capability will allow for reduced destructive testing in production through increased confidence in the quality of welds produced. This will save time, increase efficiency and reduce the costs incurred in production. Investigation of the prediction of weld quality and the separation of process faults using signal shape analysis has also provided insights into the challenges associated with different advanced high strength steels.

Chapter 5

The Extension of PCA-based Weld Quality Monitoring to Multiple Signals in Aluminium

The key concepts and results of this chapter are presented in:

- *Multi-Signal Quality Monitoring of Aluminium Resistance Spot Welding using Principal Component Analysis, Summerville C., Adams D., Compston P., Doolan M., 2017, 9th Australasian Congress on Applied Mechanics (ACAM9), 27-29 November 2017.*

In Chapter 4 Principal Component Analysis (PCA) was used to analyse signal shapes in steel RSW. The principal components of the resistance signal were used to calculate models for weld quality, relating the signal information of a weld to its button diameter. The principal components of the resistance signal were also used to separate faults in a welding process for comprehensive weld quality monitoring using a single process signal.

The primary research question of this thesis is focussed on improving weld quality monitoring capabilities in aluminium RSW. In this chapter, the preliminary work completed in steel RSW will be progressed to develop a new quality monitoring methodology focussed on the challenges presented by aluminium RSW.

The PCA based approach to signal shape analysis was employed to analyse five different signals in aluminium RSW; current, voltage, resistance, electrode displacement and change in electrode force.

A model for the tensile-shear load bearing capacity of welds was calculated from each signal using its principal components. This allowed for a comparison of the amount of useful information in each signal for aluminium weld quality monitoring (section 5.4.1). Interestingly, the voltage and resistance signals produced the best models for weld quality.

In section 5.4.2, a multi-signal model for weld quality was calculated using selected principal components from each of the five signals. The combined model had an R^2 value of 0.769 between the measured and predicted tensile-shear load bearing capacities with an RMSE (Root-Mean-Squared-Error) of 114N. The low RMSE showed the success of the model and was approximately 5% of the mean tensile-shear load bearing capacity of the welds. This outperformed the only previous attempt in the literature which achieved an RMSE of between 12-15% of the mean strength of the welds. This work represents a significant contribution to the literature, due its reduction in predictive error when compared to the only other attempt, and that it adds to the small number of papers that calculate a model for aluminium spot weld quality. The success of this model shows the benefits of analysing the information from multiple signals with signal shape analysis.

5.1 Introduction

Due to the high welding currents and short welding times required to weld aluminium, the process is particularly vulnerable to uncontrolled variation and accelerated electrode wear. The lower electrical resistivity of aluminium requires higher welding currents to generate the required heat compared to steel. The high heat transfer rate of aluminium also requires that the heat is delivered over a shorter period of time to reduce excess heat input into the panel. This makes the challenge of producing high weld quality consistently more difficult and so accurate in-line quality monitoring is even more important than in steel RSW.

The methodology developed in Chapter 4 uses the resistivity-temperature relationship of the material to infer the progression of weld nugget growth. Unfortunately, in aluminium the strength of this relationship is not as pronounced. The lower resistivity of aluminium and the smaller increase in its resistivity with temperature (Figure 5-1) means that it is harder to find useful information in the resistance signal measured during welding. To apply the PCA based method to the more challenging task of aluminium weld quality monitoring, the method will be adapted to monitor more than one signal as the information in the resistance signal is not sufficient alone (M. Hao et al., 1996).

In this chapter the single signal approach from Chapter 4 is applied to multiple process signals for aluminium weld quality monitoring. To do this PCA will be calculated for each process signal to investigate the usefulness of the different signals for weld quality monitoring. The information in the principal component shapes of each signal can be used to calculate a model for the strength of the welds (using the principal component scores of welds). This process will determine which signals are useful for monitoring weld quality in aluminium.

The hypothesis of this chapter is that signal shape analysis of multiple process signals will improve aluminium weld quality monitoring beyond what is possible with a single signal. Analysing the information from multiple signals for each weld should allow for better weld quality models to be produced that are more robust to the challenges associated with aluminium RSW.

In this chapter a brief literature review will show that there are limited previous attempts in the field to create aluminium weld quality models. Then the exact methodology of the analysis technique and data collection will be shown. Subsequently, models for weld quality will be calculated from the individual signals and then a model will be created using a combination of the different signals. This will allow for a comparison of multi-signal models and single signal models created in the same way. Finally, a discussion of the relevant importance and usefulness of the signals investigated will be presented followed by the conclusion of this study and the next steps.

5.2 Background

The temperature coefficient of resistivity for aluminium is smaller than in steel which is shown by the slopes of the curves in Figure 5-1a. This means variation in the resistance signals of aluminium spot welds are subtle. There is a distinct change in the electrical resistivity of aluminium at the phase transition between solid and liquid, which explains the drop in resistance that is seen in the measured signals during aluminium RSW (shown in section 5.4 Results of this chapter in Figure 5-3e).

The coefficient of thermal expansion of aluminium is twice that of most steels (Figure 5-1b) which makes it useful for tracking weld nugget growth in RSW. The thermal expansion of the material during welding exerts a force on the electrodes and this can be monitored to make inferences about the progression of weld nugget growth for weld quality monitoring.

The electrode displacement caused by thermal expansion of a spot weld has not been used extensively in steel RSW monitoring. This is partly due to the successes in resistance signal based weld quality monitoring which is easier to measure and is strongly related to the temperature of the joint. The electrode displacement or electrode force increase caused by the thermal expansion of the spot weld is more commonly used in aluminium spot weld quality monitoring due to the subtle changes in resistivity with temperature.

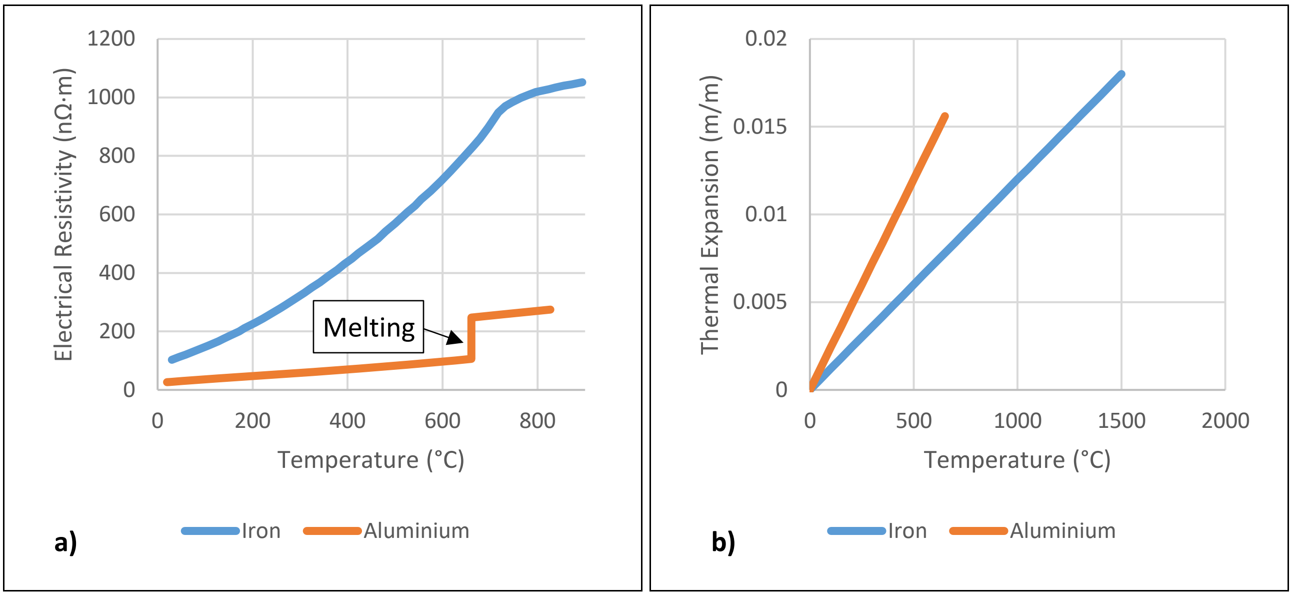

Figure 5-1: a) Resistivity-temperature relationship of iron & aluminium (Desai et al., 1984; Weiner et al., 1952), b) thermal expansion of iron & aluminium from ambient to melting

There are a number of process signals that can be measured during RSW for aluminium weld quality monitoring including but not limited to: electrical measurements (current, voltage, resistance, inductance), mechanical signals (electrode force, electrode displacement), acoustic or vibrational signals (structure-borne acoustic emissions, sonic emissions, ultrasound transmission), and thermal responses (such as infrared light emission).

Attempts to model the quality of aluminium resistance spot welds are not common in the literature with one notable contribution prior to the work presented in this chapter. Hao et al. (1996) modelled the weld quality of aluminium welds using features, manually selected, from a number of signals measured during welding (as discussed in Section 2.5 of the Literature Review). Features such as maximum values, minimum values, slopes and mean values were used to calculate a multiple linear regression model for weld strength achieving RMSE (Root-Mean-Square Error) of between 400-500N. One of the primary conclusions was that one signal was not sufficient to provide a 'universal' quality predictor for the varied input parameters in aluminium RSW.

To improve upon the methodology of Hao et al., the use of PCA is proposed to allow for whole signal shapes to be represented by principal component scores for correlation (as in Chapter 4). Using whole signal shapes in analysis is likely to be more robust to changes in welding conditions that can render selected values such as maximum resistance irrelevant when changing setup.

One of the key findings of the work of Hao et al. was that no one signal could adequately predict the strength of an aluminium weld, acknowledging that further work was required in this space. A multi-signal weld quality monitoring method is proposed in this chapter that uses unique signal shapes extracted from the current, voltage, dynamic resistance, electrode displacement and force signals measured during welding.

This thesis will focus on the electrical and mechanical signals in aluminium RSW to monitor the process, and other measurements such as acoustics and thermal measurements will be investigated in future work. Some preliminary work with infrared signals for weld quality monitoring was completed but had to be relegated to future work due to time constraints, while investigation of acoustic signals for aluminium weld quality monitoring is starting in another PhD project in the manufacturing research group at ANU.

5.3 Method

Five signals were collected during an aluminium RSW process with the only uncontrolled variation from electrode wear and natural variation of the material. Time series signals for voltage, current, resistance, electrode displacement and electrode force were recorded for all 133 welds during welding. The important information from the time series signals was extracted using PCA which was used to produce the multi-signal weld quality monitoring model for aluminium RSW.

5.3.1 Materials and Equipment

Welds were created between two 1mm thick sheets of AA5052-H32 (Section 3.7) using a 50kVA AC pedestal welder with pneumatic clamping (Section 3.6.2). The current used was ~18kA RMS and the electrode clamping force during welding was 2kN with a welding time of 0.14s (7 x 50Hz cycles). The electrodes were made from pure copper using a domed electrode design with a 4mm flat face cut into the end.

5.3.2 Data Collection

For each weld a number of signals were measured at a rate of 5kHz (to ensure no aliasing occurred). The signals measured were the welding current using a Rogowski coil, voltage drop across the electrodes, electrode force using a 5kN load cell and electrode displacement using a laser triangulation sensor (section 3.3). The electrical signals were reduced to the peak values at each half cycle, comprising 14 data points for each weld. From the peak voltage and current values, dynamic resistance was calculated at each half cycle using Ohm's law (ignoring the machine inductance). The electrode displacement and electrode force signals were also reduced to one measurement at each half cycle for comparison to the electrical signals. The tensile strength of all welds was measured in an Instron 5500R universal testing machine (section 3.2.1) as the measure of quality for the multi-signal weld quality monitoring model.

5.3.3 Weld Strength Model Methodology

To calculate a model for weld strength from the five signals collected during welding, each signal set was decomposed separately using PCA. As outlined in section 3.5.1 in the Methodology, all principal components from each signal set that accounted for less than 1% of the explained variance were removed from further analysis. The principal component's correlation with weld strength was assessed using its principal component scores and a Pearson correlation coefficient, with correlations containing a p-value of < 0.05 deemed to be significant (section 3.5.1). This test was used to determine which principal components were to be included in the weld quality monitoring model. Once the principal components significantly correlated with weld strength were determined, a simple linear regression model was calculated.

5.4 Results

The tensile shear loads from the destructive testing are shown in Figure 5-2. The prevalence of interfacial shear failure shows the vulnerability of the process to the extreme process conditions of aluminium RSW.

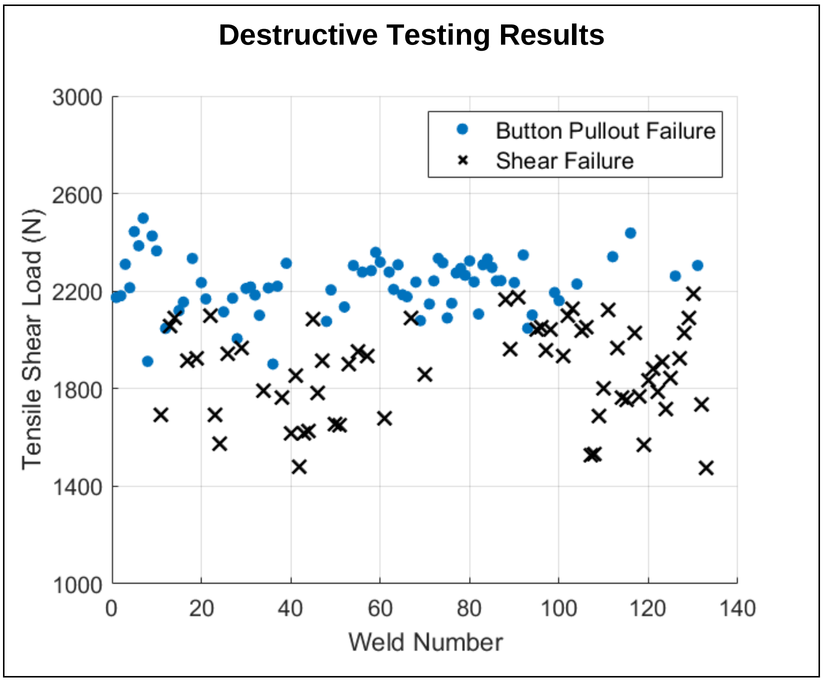

Figure 5-2: Tensile-shear load of aluminium welds

The five sets of processed signals for all 133 welds are shown in Figure 5-3, noting the small variation in electrical signals and larger variation in electrode displacement and force. Electrode force and displacement are represented as changes from the initial value when welding began (represented as zero in each figure). PCA was calculated for each signal set producing the set of principal components for each signal.

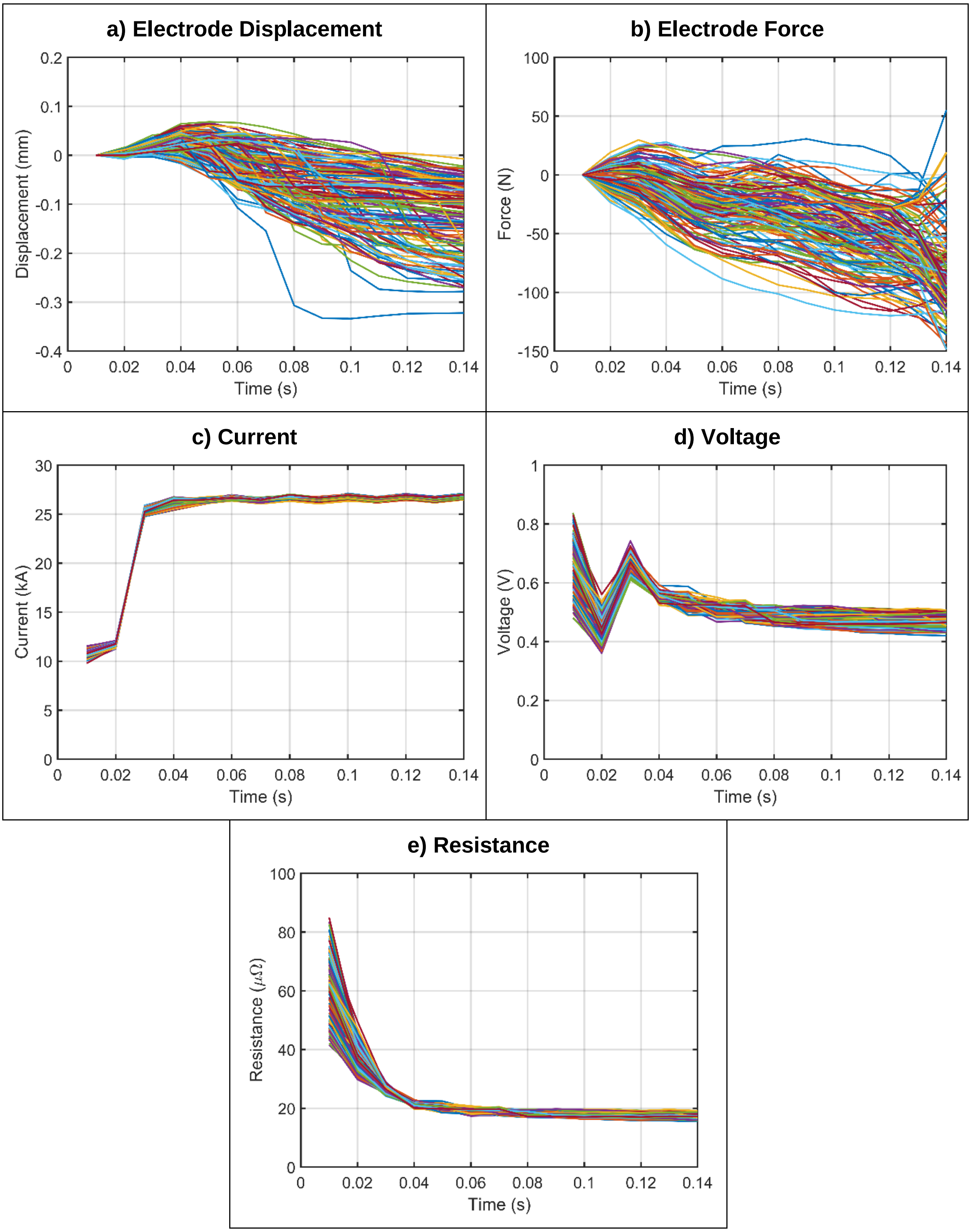

Figure 5-3: Processed mechanical and electrical signals measured during aluminium RSW

The principal components with an explained variance greater than 1% were assessed to see if they had a correlation with weld strength using Pearson correlations (Pearson, 1900). To determine which signal shapes would be used in the model a p-value < 0.05 for the correlation was used, consistent with statistical conventions. The p-value represents the likelihood that a similar correlation could be found by chance.

The principal components with a significant correlation to tensile-shear strength, their coefficients of determination with weld strength (R^2) and the associated explained variance of their signal set are shown in Table 5-1. The R^2 represents the strength of the correlation between the measured and predicted values being tested.

Table 5-1: Principal components significantly correlated with weld strength (p-value < 0.05)

Signal	Principal Component	Name	Explained Variance (%)	R^2
Current	1	C1	53.3	0.04
	3	C3	4.8	0.29
	5	C5	1.5	0.05
Voltage	1	V1	75.1	0.12
	2	V2	9.9	0.48
	3	V3	4.4	0.04
	4	V4	3.8	0.06
Resistance	1*	R1	92.3	0.11
	3*	R3	1.5	0.48
Displacement	3*	D3	4.2	0.17
Force	1*	F1	70.8	0.37

*Principal component shape shown in Figure 5-4

The individual correlations with weld strength presented in Table 5-1 are all relatively low ($R^2 < 0.5$) showing that none of the principal components are highly correlated with weld strength when considered individually. Additionally, the major variation (first principal component) in all signals was found to be correlated with weld strength, except in the electrode displacement signal. A selection of principal component signal shapes from Table 5-1 is shown in Figure 5-4 which shows the subtle variation in the resistance signal and the different variation in the mechanical signals.

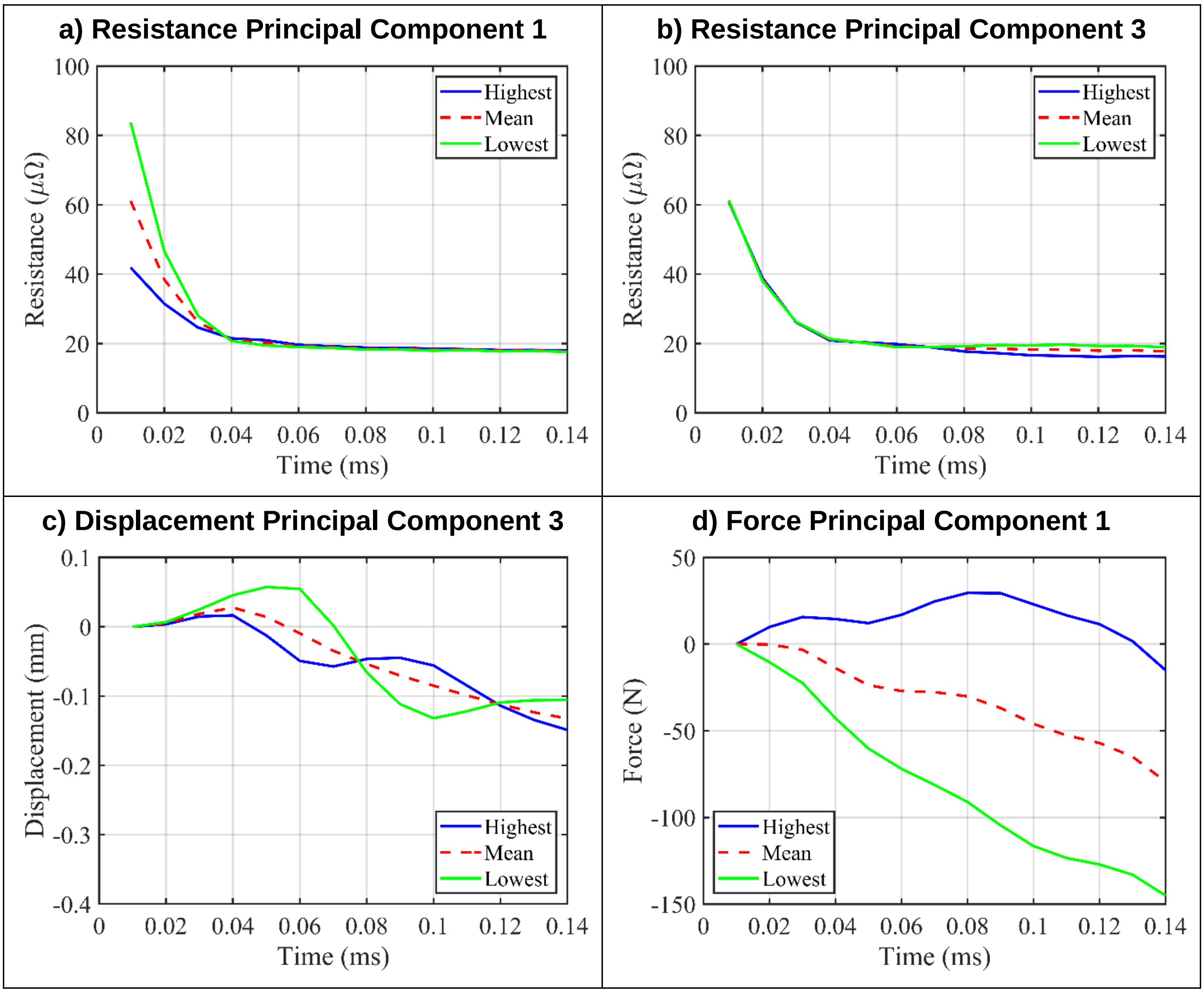

Figure 5-4: Principal component shapes of the signals highlighted in Table 5-1.

5.4.1 Individual Signal PCA Weld Quality Models

First, the principal components of individual signals were used to calculate models for weld quality in isolation to understand the amount of useful information in each process signal. This is the same methodology as followed in Chapter 4 and shows the challenges associated with using one process signal to monitor the quality of aluminium RSW as highlighted by (M. Hao et al., 1996). Using the same criteria as in Chapter 4, principal components from each process signal were selected for weld quality monitoring. The principal components used to create each of the models in Figure 5-5 are those shown in Table 5-1.The voltage signal produced the best model for weld quality resulting in the highest R^2 to tensile load and lowest RMSE. Individually the mechanical signals could not produce an adequate model for weld quality with the electrical signals performing better individually. Given the susceptibility of the aluminium RSW process to poor quality consistency, the performance of a multi-signal model will be assessed next to understand the potential improvements that can be made by using more signal information to monitor weld quality.

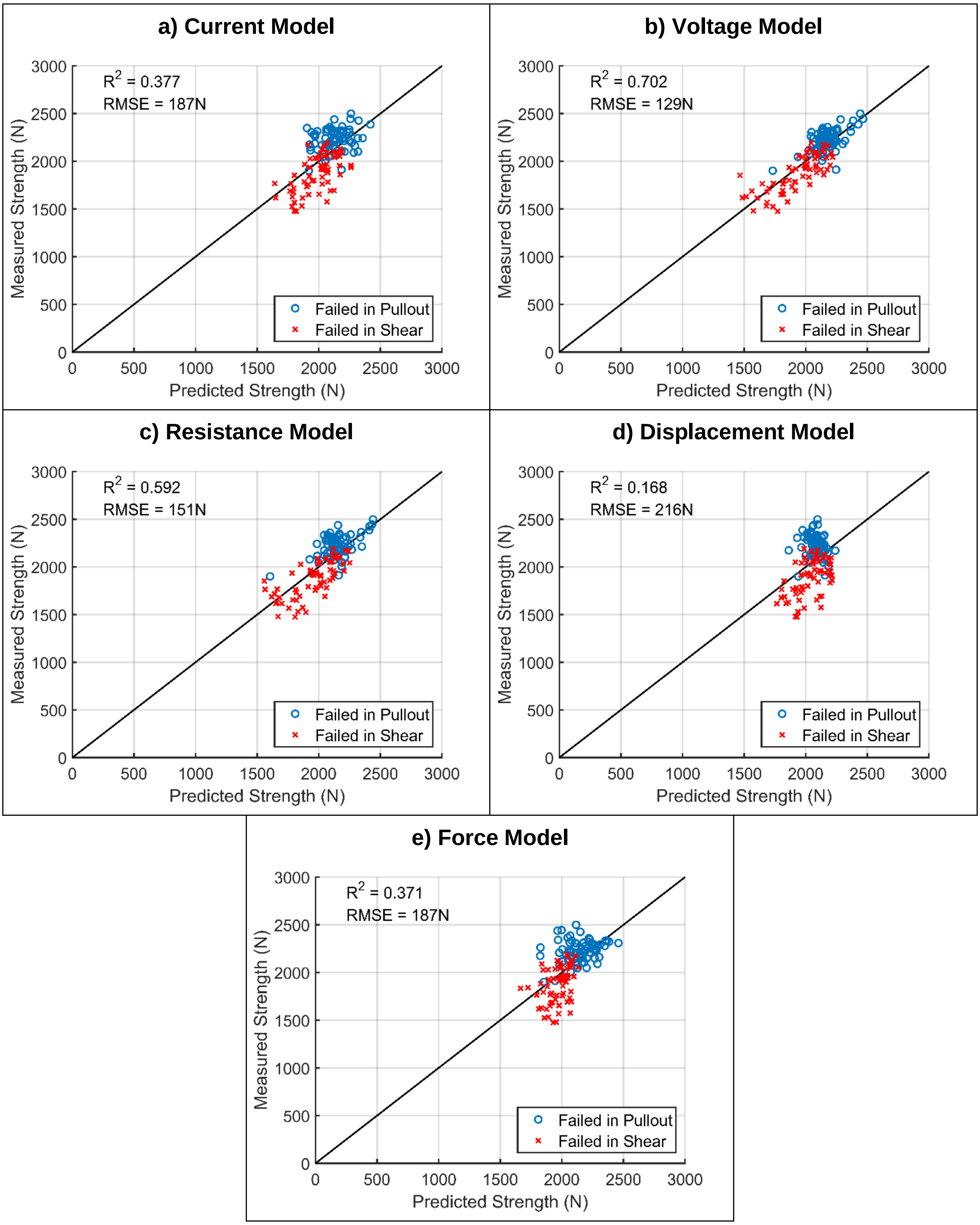

Figure 5-5: Single signal PCA weld quality models

5.4.2 Multi-signal PCA Based Weld Quality Model

Once the principal components for each signal set with a significant correlation to weld quality had been determined, a multi-signal weld quality monitoring model could be produced. A linear regression model was calculated between the principal components in Table 5-1 and weld strength, shown in Eq. 5-1.

Table 5-2 shows the linear regression coefficients for the principal components used in Eq. 5-1. The magnitude of the coefficients does not indicate the relative importance of the coefficient for the model, it is merely to scale the different units which are used for the different signals.

Table 5-2: Linear regression coefficients

Name	Linear Regression Coefficient	Value	Signal Units	Magnitude
C1	a	-2.1	A	$\times 10^{-2}$
C3	b	-3.1		
C5	c	-25		
V1	d	0.91	V	$\times 10^{3}$
V2	e	-6.98		
V3	f	-3.53		
V4	g	2.74		
R1	h	-0.32	mΩ	$\times 10^{7}$
R3	i	7.30		
D3	j	-8.24	mm	$\times 10^{2}$
F1	k	-3.63	N	$\times 10^{2}$

$$Y = (\mathrm{a}C_1 + \mathrm{b}C_3 + \mathrm{c}C_5) + (\mathrm{d}V_1 + \mathrm{e}V_2 + \mathrm{f}V_3 + \mathrm{g}V_4) + (\mathrm{h}R_1 + \mathrm{i}R_3) + (\mathrm{j}D_3 + \mathrm{k}F_1) + 2060 \qquad \textbf{Eq. 5-1}$$

The confidence intervals and accuracy of the multi-signal weld strength model is shown in Figure 5-6. The model has an R^2 value of 0.769 between the predicted and measured values and a Root-Mean-Square Error (RMSE) of 114N. It is interesting to note that the model is capable of predicting the tensile-shear load of welds that failed through both button pull-out and interfacial shear failure which are two completely different failure mechanisms.

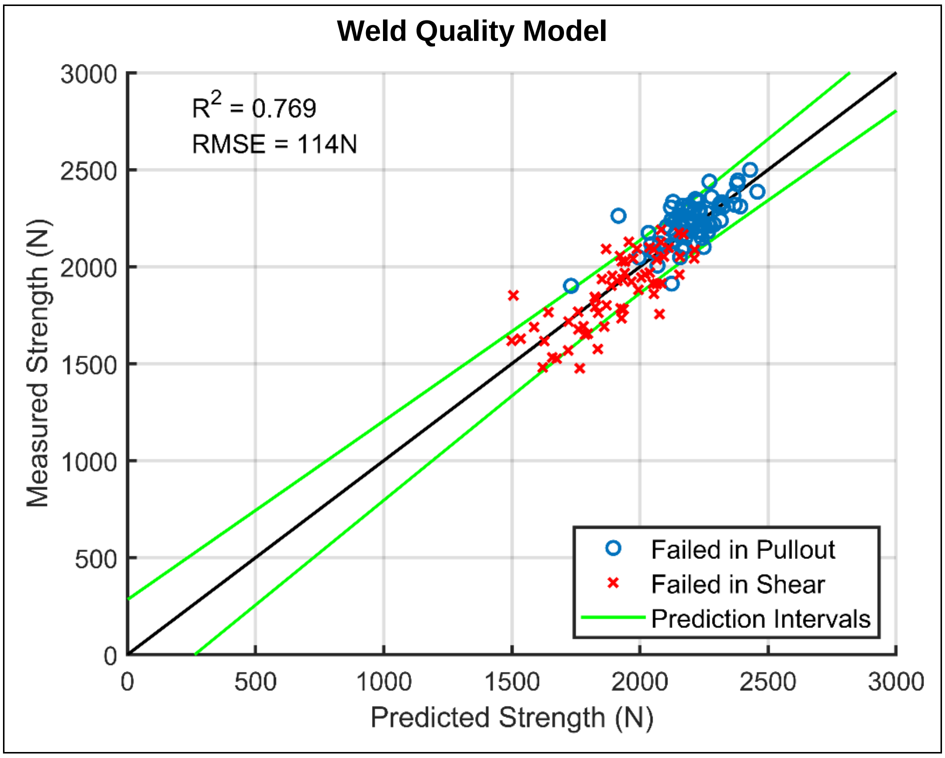

Figure 5-6: Multi-signal weld quality monitoring model

5.5 Discussion

Most of the variation in the voltage signals was found to be correlated with weld strength, shown by the first four principal components of the voltage signals in Table 5-1. The variance between signals was more pronounced in the electrode voltage than the current signals which is due to the constant power algorithm of the welder. The variation in the voltage signal is also seen in the resistance signals which are calculated from current and voltage.

The first and third principal component scores of the resistance signal, R1 and R3, were found to be significantly correlated with weld strength, with variation at the start and end of the signal, shown in Figure 5-4 a) and b) respectively. Variance at the end of the resistance signals, shown in the third principal component shape, was more strongly correlated with weld strength (R^2 = 0.48, R3) than variance at the beginning (R^2 = 0.11, R1). A lower resistance towards the end of the signal, as seen in R3 (Figure 5-4b), was found to be correlated with a low weld strength. This is thought to be a consequence of expulsion at the faying surface, causing material loss from the weld nugget, explaining the reduction in overall weld strength. This is supported by the shape of the resistance signals in Figure 5-7 a) which are examples of signals with high and low third principal component scores. The signals with high, positive third principal component scores show a distinct drop in resistance after ~0.07 seconds (blue line in Figure 5-7b). The same signal variation was found to be caused by expulsion in another study focussing on expulsion detection in aluminium RSW by Hao et al. (1996). The signals with high, positive third principal component scores belonged to welds with low weld strengths that were more likely to fail in shear (shown in Figure 5-8), while the opposite was found of those signals with low, negative scores which were more likely to fail in button pull-out. The signal shapes represented in the principal components are not only useful for modelling weld quality, here they are also useful for understanding the potential causes for poor quality welds.

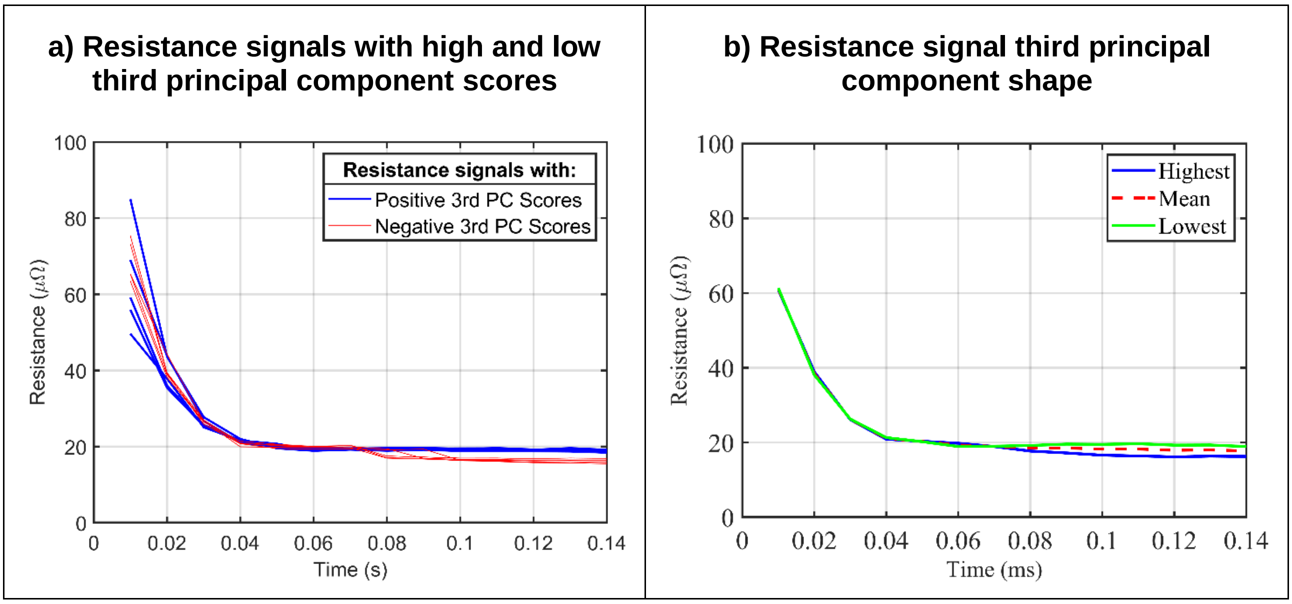

Figure 5-7: The effect of the R3 scores on the resistance signals

5.5.1 Multi-signal Weld Quality Model

The weld quality model (Figure 5-6) uses multiple signals measured during a RSW process to address concerns in the literature by Hao et al. (1996) that one signal alone is not sufficient to monitor the quality of welds in aluminium RSW. The multi-signal weld quality monitoring model achieved an RMSE of 114N, which is approximately ±5% of the mean strength of the welds. This result is a significant improvement on the RMSE achieved by Hao (1996), which ranged from 410-540N (~12-15% of the mean strength). Hao used similar multiple linear regression with automatically selected features from the signals such as maximum, minimum, mean and slope values. The improvement in prediction error shows the inherent value in using PCA to represent complete signal shape variation over the alternative of selected landmark points and features as using similar linear regression with principal components yields a tighter confidence interval.

It is interesting to note that the resistance signal was found to be more useful for weld quality monitoring than previously thought. The literature and the information presented in Figure 5-1, coupled with the minute variation in the resistance signals across the dataset suggested that the resistance signal would not hold much useful information for monitoring weld nugget growth. The magnitude of the resistance signal in the second half of the process had an $R^2 = 0.48$ with the tensile-shear load of the welds. This may be due to the clear distinction between the resistivity of solid and liquid aluminium in Figure 5-1. When the aluminium goes through its phase transition there is a clear increase in its resistivity. The third principal component of the resistance signals was found to be inversely correlated with the tensile strength of the weld. A high third principal component score corresponded to a resistance signal with a higher tail and higher strength and chance of failing in button pull-out suggesting material has completely melted. Conversely, a lower third principal component score corresponds to a resistance signal with a lower tail and strength and higher chance of failing through interfacial shear, suggesting that complete melting of the nugget has not occurred (Figure 5-8).

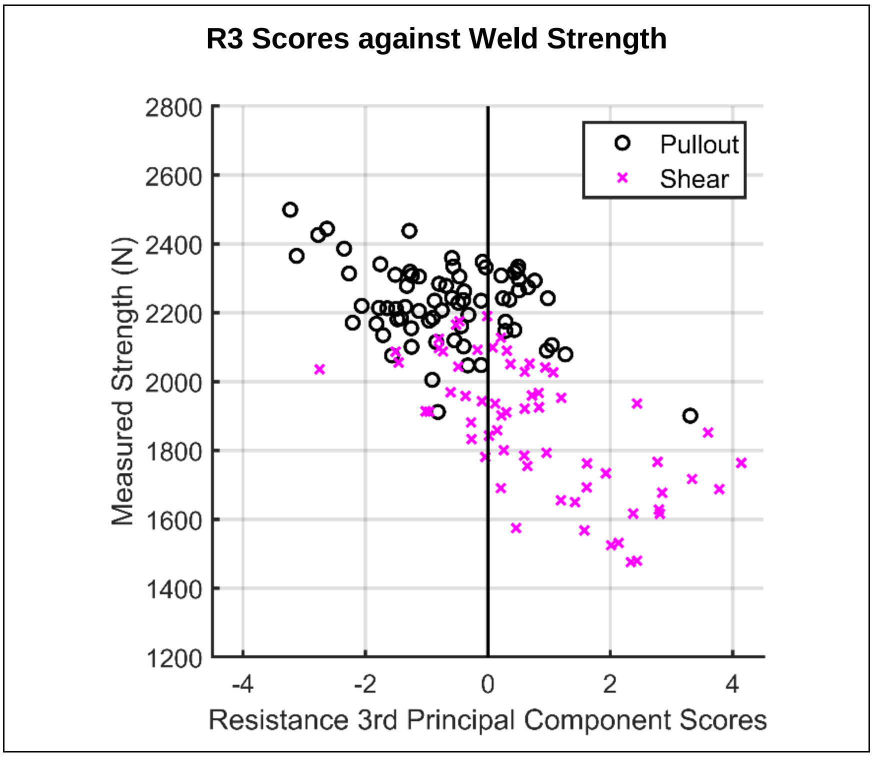

Figure 5-8: Principal component R3 scores against weld strength

5.6 Conclusion

The multi-signal weld quality monitoring model was created for aluminium RSW using the voltage across the electrodes, current through the work-piece, dynamic resistance, electrode displacement and electrode clamping force during welding. The major variation in these signal sets was extracted using PCA. Using a number of selected principal components, a model was calculated resulting in an RMSE of 114N between the predicted and measured strength of the welds found through destructive testing. This was an improvement on models made from information from one process signal alone.

Further work is required for a system that is ready to implement in a production environment. None of the principal components, when considered individually, were found to be strongly correlated with weld strength in this study (all $R^2 < 0.5$). This shows that the principal components of highest variance of the aluminium welding signals are not necessarily highly correlated with weld strength. Investigation into alternate methods is therefore required to obtain better predictive results for aluminium RSW. The key limitations of the signal analysis completed in this chapter are:

1. Signal features are orthogonal and based on level of variance. This sometimes means that signal quality information is spread across a number of principal components (as with voltage for example).

2. That the signal shape interactions between the different signals is not considered.

To address the first limitation, methods which draw out different features of the data such as different approaches to PCA and Kernel PCA can be considered. To address the second limitation, much more work is required to develop analysis techniques that account for the covariance of multiple signals in aluminium weld quality monitoring. Consideration of the interactions and covariance between the different signals is likely to improve the accuracy of the model which attempts to simplify the complex interactions between the electrical, thermal and mechanical aspects of the process that governs the quality of aluminium resistance spot welds.

Chapter 6

Analysing the Interactions of Multiple Signals in Aluminium Resistance Spot Welding

In Chapter 4 it was shown that the quality of steel resistance spot welds can be monitored using PCA to extract features from the resistance signal alone. In Chapter 5 this technique was used to analyse information from additional signals to build a model for weld quality for the more challenging task of aluminium resistance spot welding (RSW). PCA was calculated for multiple process signals and the principal component scores were used to create a model for weld quality monitoring. This produced a model that was better than any individual signal as suggested in the literature, however the feature extraction stage of the technique did not encapsulate the interactions of the signals in the process.

In this chapter a new feature extraction technique will be presented that represents welding signal information as tensors. This allows the correlating behaviour of multiple signals to be analysed for weld quality monitoring. This chapter shows that the quality of welds can be predicted using tensor principal components calculated from two welding signals under several different welding conditions. Information about the welding process was analysed using the tensor principal component shapes which provided insight into how the signal shapes interact and their relationships to weld quality.

To develop the Tensor Principal Component Analysis (TPCA) weld quality monitoring methodology:

- Section 6.1 covers the relevant background of tensors and their principal components when calculated from two signals.

- Section 6.3 introduces some further tensor concepts and the tensor principal component analysis decomposition method.

- Section 6.4 explains how models can be calculated for monitoring weld quality with tensor principal components and highlights a number of considerations associated with calculating the tensors from welding signal data.

- Section 6.5 presents a case study that monitors the quality of resistance spot welds collected in the laboratory using TPCA.

At the outset, it should be noted that the mathematical tensors used throughout this thesis must not be confused with the tensors commonly used in engineering and physics to describe fields, such as stress tensors. The ‘weld tensors’ that are calculated in this chapter can be thought of as an object or property of the welding data that can be calculated as the outer product of any number of process signals (vectors) and are similar to multi-dimensional arrays (Kolda et al., 2009).

6.1 Context

As highlighted in Chapter 5, aluminium resistance spot welds are more susceptible to variation in quality due to the material properties and welder settings that must be used to weld aluminium sheets. The short weld times reduce the amount of available information in the signals and means that the data available for quality monitoring is relatively sparse. To make the most of the limited data in aluminium RSW this chapter presents a process that analyses the interacting behaviour of multiple signals to address this.

Analysis of the interacting behaviour of multiple signals in aluminium RSW is proposed for quality monitoring to account for the complex relationships between the electrical and mechanical signals. Analysis of multiple signals in this way should help to identify situations that appear superficially similar but have different outcomes for weld quality. This will provide a more robust quality monitoring technique for the complex process of aluminium RSW, which is of particular interest to the automotive industry. This technique will be tested on two datasets in the laboratory that include a range of process faults and electrode wear in the case study in Section 6.5.

In signal based modelling applications the interaction terms are important to consider when the relationship between one signal and the result is dependent on the value of another. In RSW the size of the weld depends on the interacting variables of heat, resistance, thermal expansion and pressure.

The quality of aluminium spot welds is the result of a complicated process with several interacting properties that can drastically affect the strength or button diameter of the weld. Characteristics such as aluminium's high resistance oxide layer, its high thermal conductivity, low resistance and high coefficient of thermal expansion make quality monitoring of aluminium RSW particularly challenging. Issues such as porosity and cracking are more common in aluminium RSW due to: the oxide layer (which is burnt off), and the high thermal expansion and contraction when the material is heated and cooled (Rashid et al., 2011; Turnage et al., 2018). The mechanical, electrical and thermal properties of aluminium have complex interactions that govern the quality of the spot weld. It is challenging to model aluminium RSW effectively by monitoring only one aspect of the process such as the electrical or mechanical signals. To analyse multiple aspects of the process and their interactions, welding signals tensors will be analysed.

The electrical and mechanical signals in aluminium RSW have been shown to contain useful information for weld quality monitoring (Hao et al., 1996). However, the interactions of these properties in aluminium RSW have not been considered in weld quality monitoring. The use of tensors in this chapter includes the interactions of two signals into weld quality monitoring.

Given that the relationships between the measured signals and weld quality can be dependent on other signals it is important to consider interaction between the signals. In statistical modelling, if the effects of the independent variables on the dependent variable are influenced by each other, interactions terms are included in the model. In a simple model with three variables the interaction term is the multiplication of the two independent variables (Eq. 6-1).

$$y = ax_1 + bx_2 + cx_1\, x_2 \qquad \textbf{Eq. 6-1}$$

To analyse the interaction behaviour of two signals using a shape based feature extraction technique, like PCA, the interactions of the signal shapes must be calculated before the feature extraction stage. To analyse the signal shape interactions between multiple signals in RSW a new data representation will be employed in this chapter, mathematical tensors. Mathematical tensors will represent the interacting behaviour between two signals before feature extraction is conducted.

6.2 Introduction to Tensors

Mathematical tensors are calculated as the outer product of two or more vectors (Kolda et al., 2009). The outer product of two vectors produces a matrix, otherwise known as a rank-one, second order tensor (shown below).

$$\begin{bmatrix} r_1 \\ \vdots \\ r_n \end{bmatrix} \begin{bmatrix} d_1 & \cdots & d_m \end{bmatrix} = \begin{bmatrix} r_1 d_1 & \cdots & r_1 d_m \\ \vdots & \ddots & \vdots \\ r_n d_1 & \cdots & r_n d_m \end{bmatrix}$$

The outer product of two vectors, R_n and D_m multiplies each entry of the vectors by every entry in the other, producing an $(n \times m)$ tensor. The entries of the tensor are considered the interactions of the two signals at two given points in the signals. The use of the outer product means that the interactions of any two points in the signals can be analysed.

In welding with two measured time-varying signals, the tensor for each weld looks like a matrix, and the dataset of all weld tensors is a 3-dimensional array of the weld tensors stacked along the third dimension. Figure 6-1 shows an example of a welding tensor in three different ways, a) the matrix representation, b) a 2D colour-map plot and c) the 3D representation. ‘Mode 1’ and ‘Mode 2’ correspond to the rows and columns of the tensor.

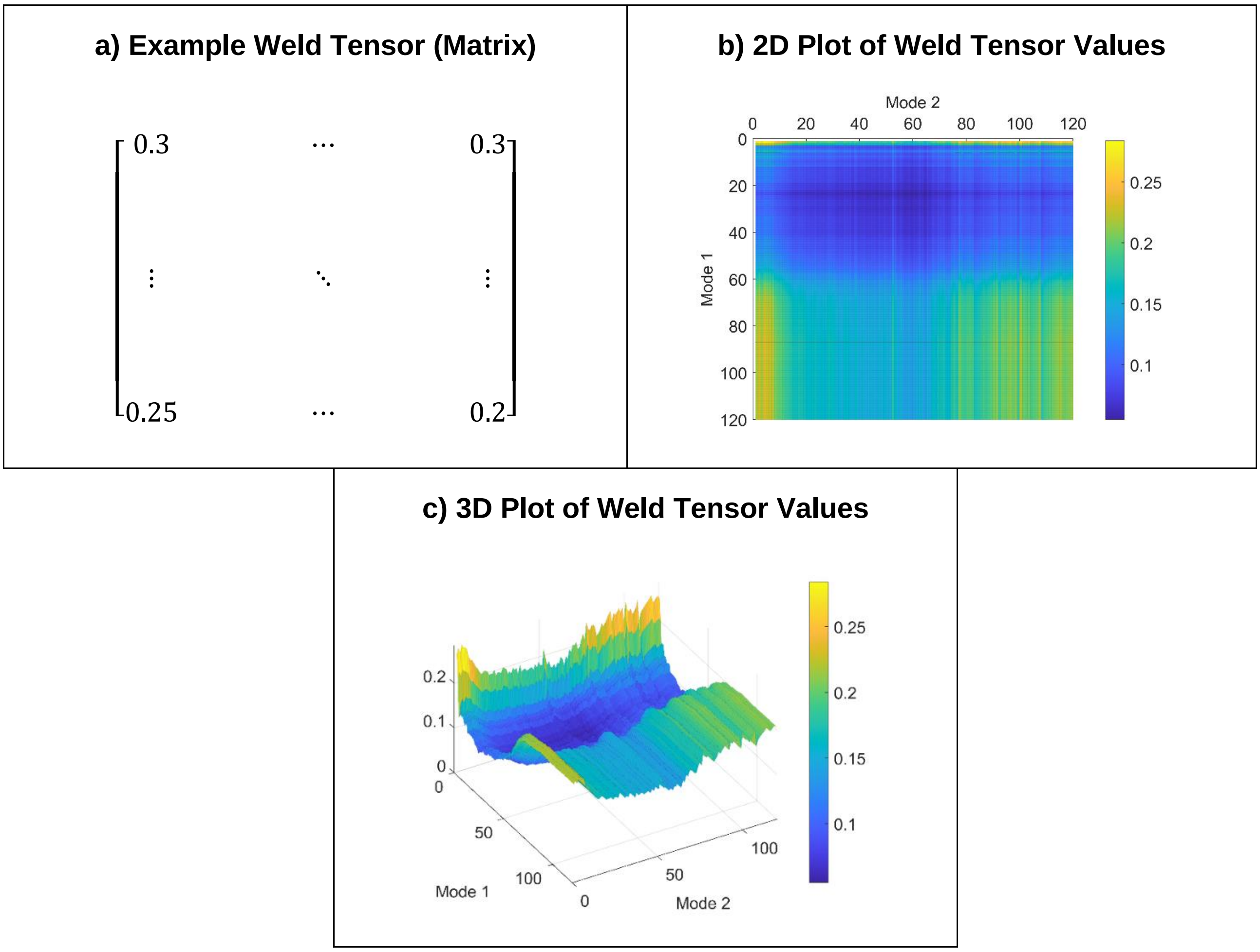

Figure 6-1: Welding tensor, a) matrix representation, b) 2D colour-map plot, c) 3D representation

In the two signal case presented in Figure 6-1 a) and b) the main diagonal of the matrix represents the multiplication of the two signals at the same points in time ($R_1D_1 \dots R_nD_n$). Column 1 of the matrix is the first value of the first signal multiplied by every value in the second signal ($R_1(D_1 \dots D_n)$). Row 1 corresponds to the first value of the second signal multiplied by every value in the first signal ($D_1(R_1 \dots R_n)$). This is relevant for welding as it can show when the values at a particular point of one signal are strongly correlated with the values in another signal, this is referred to as the *interacting behaviour* of the signals.

The regions of the tensor that are off the main diagonal (most easily seen in the matrix or 2D graph in Figure 6-1 b) correspond to the correlations between the two signals at different points in time. This is important as this is information that the tensor principal component analysis offers that is not captured by the methods presented in Chapter 4 and Chapter 5. In weld quality monitoring, this is an important concept as aspects of the process such as the temperature of the weld nugget can lag behind the changes in resistance. Understanding how these interactions at different points in time relate to weld quality may be very useful for successful weld quality monitoring.

The first row ($D_1(R_1 \dots R_n)$) shows the interactions between the start of the first signal and the entire second signal. We can see that the first row of the example tensor in Figure 6-1 b) shows some of the highest values on the tensor (shown in yellow). This is because both signals are high above the mean signals here. This can be useful for understanding effects which cause changes later in the process in the electrical and mechanical signals of the process. If we were to complete only the point-wise multiplication of the two signals ($R_1D_1 \dots R_nD_n$, the main diagonal) or calculate PCA for either of the signals in isolation, any potential interaction between the two signals at different times in the process would be missed and this is why the outer-product and TPCA is used in this chapter.

The tensors are calculated to find interactions between the two signals at different stages in the process. If we divide the tensor into four quadrants (Figure 6-2), we can think of quadrant one and four as points where the two signals are interacting in the first or second half of the process.

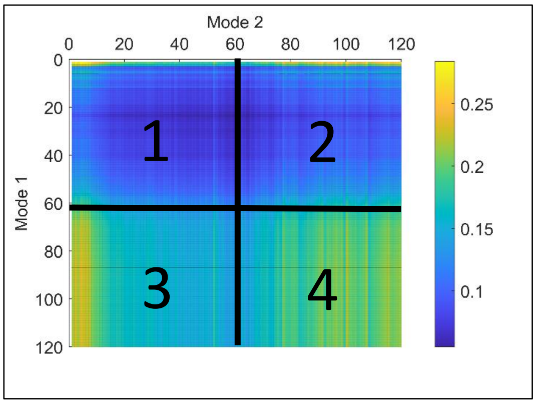

Figure 6-2: Weld tensor split into quadrants for analysis

Quadrants two and three show the correlation between the first half of one signal and the second half of the other. Correlation in quadrants two or three may show that the behaviour of one signal regularly effects the behaviour of the other later in the process. Analysing this behaviour with TPCA allows for these interactions in the process signals to be linked to weld quality. This provides additional useful information for the challenging task of aluminium weld quality monitoring.

Following on from Chapter 4 and Chapter 5, the *shape* of the weld tensors will be analysed using a higher order form of PCA known as the Tucker Decomposition (Kolda et al., 2009). TPCA will allow for analysis of the shape of the tensors which will indicate the major *shapes* of the correlating signals in a welding dataset so that this information can be linked to weld quality. The major Tensor Principal Components (TPCs) that are linked to weld quality will represent different process behaviours of the thermal, mechanical and electrical aspects of the process. This will improve aluminium weld quality models by accounting for the interlinked aspects of the process through signal shape analysis.

6.3 Tensor Analysis

This section briefly introduces some key concepts of tensors and their analysis before covering the Tucker Decomposition. Tensor algebra requires additional steps to manipulate the matrix equations which is required for TPCA. Due to the multi-dimensional structure of the tensors, the algebra and therefore the notation is more complicated. Some initial concepts and notation conventions are introduced in Table 6-1, and further concepts will be introduced later as they become relevant.

Table 6-1: List of concepts and their notation

Concept	Explanation	Notation
Vectors	Lowercase letters	x, y, z
Matrices	Boldface uppercase letters	$\boldsymbol{X}, \boldsymbol{Y}, \boldsymbol{Z}$
Tensors	Boldface script letters	$\boldsymbol{\mathcal{X}}, \boldsymbol{\mathcal{Y}}, \boldsymbol{\mathcal{Z}}$
Tensor indexing notation	Indices are often used to show the order of the tensor	$\boldsymbol{\mathcal{X}}_{\boldsymbol{abc}}$
Order of a tensor	Number of dimensions in the n-dimensional array	$order(\boldsymbol{\mathcal{X}}) = 3$
Outer product of two vectors	Produces a tensor	$x \otimes y$

To analyse the shapes of tensors, tensors need to be multiplied by matrices. To multiply a tensor by a matrix the tensor is 'unfolded' into a matrix so that conventional matrix by matrix multiplication can be used. Tensor unfolding (or *matricising*) involves 'unfolding' a tensor along a given dimension and stacking the slices of the tensor next to each other to form a matrix (a concept that is covered in (Kolda et al., 2009)). These concepts and their notation are described in Table 6-2 and a visual representation is shown in Figure 6-3.

Table 6-2: Tensor algebra concepts

Concept	Notation	Explanation
Mode-n unfolding (matricising) of a tensor	$\boldsymbol{\mathcal{X}}_{(\boldsymbol{n})}$	Subscript mode in parentheses
Tensor times a matrix mode-n multiplication	$\boldsymbol{\mathcal{X}} \times_n \boldsymbol{Y}$	Times sign with subscript mode

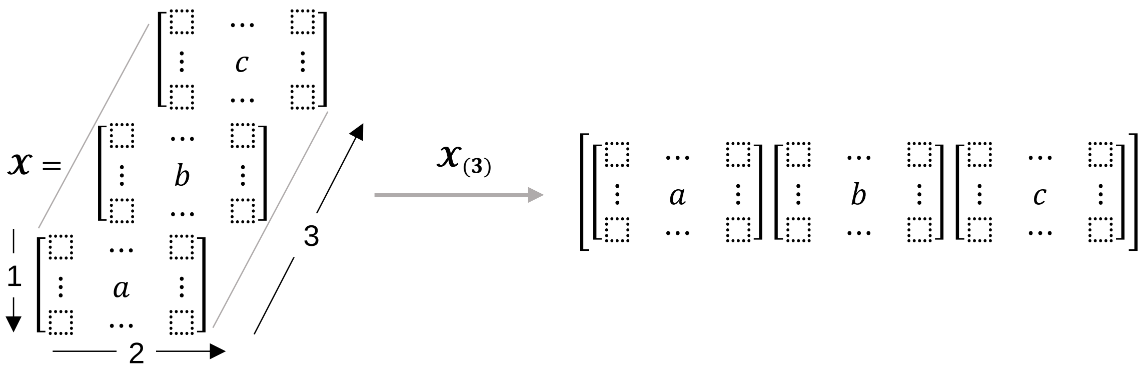

Figure 6-3: Mode-3 tensor unfolding

6.3.1 The Tucker Decomposition

Similar to the motivations behind the original work which used PCA to represent shape variations in a trainable way (Cootes et al., 1992), Tensor Principal Component Analysis (TPCA) is used in this chapter to analyse the spot welding process using the information from multiple process signals.

The algorithm that was used for calculating TPCA is the *Tucker Decomposition* which was developed by Tucker in the mathematical literature (1963). The value of the Tucker decomposition has since been realised in a number of applications that require the analysis of higher dimensional data such as in hyperspectral images (Karami et al., 2012) and video analysis (Sandeep et al., 2016).

The Tucker Decomposition was chosen to decompose welding tensors because it is a higher order version of PCA (Kolda et al., 2009). The Tucker decomposition allows for the concepts developed in Chapter 4 to be applied to tensors of aluminium signal data to analyse the interactions of multiple signals. The Tucker algorithm (Tucker, 1963) decomposes a tensor into a ‘tensor core’ ($\boldsymbol{\mathcal{G}}$) and a number of factor matrices which describe the amount of variation between signals ($\mathbf{A}, \mathbf{B}, \mathbf{C}$), the same as principal components in PCA. The decomposition equation for a dataset of 2-signal tensors from a welding process ($\boldsymbol{\mathcal{X}}$) is shown in Eq. 6-2. The same equation is represented in an elementwise form in Eq. 6-3. The subscript letters represent the number of rows and columns in the matrices and tensors.

$$\boldsymbol{\mathcal{X}}_{ijk} \approx \boldsymbol{\mathcal{G}}_{pqr}\boldsymbol{A}_{ip}\boldsymbol{B}_{jq}\boldsymbol{C}_{kr} \qquad \textbf{Eq. 6-2}$$

$$\boldsymbol{x}_{ijk} \approx \sum_{p=1}^{P}\sum_{q=1}^{Q}\sum_{r=1}^{R} \boldsymbol{g}_{pqr}\,\boldsymbol{a}_{ip}\,\boldsymbol{b}_{jq}\,\boldsymbol{c}_{kr} \qquad \textbf{Eq. 6-3}$$

Here, i corresponds to the number of points in the first signal, j corresponds to the number of points in the second signal and k is the number of welds in the training dataset which are combined in the multidimensional array of tensors ($\boldsymbol{\mathcal{X}}_{ijk}$). The other indices p, q and r (from the tensor core $\boldsymbol{\mathcal{G}}_{pqr}$) are the number of principal components that the data is decomposed into in each dimension of the tensor array. In many cases i and j will be the same number when all signals are the same length and measured at the same frequency, this results in a square tensor. In the case that i and j are different each weld tensor will not be square and this could occur if more data is collected outside the electrical phase of a welding process for a mechanical or vibrational signal for example. In welding the mechanical signals such as electrode displacement or force may continue to change after current flow has stopped, however the resistance through the joint cannot be measured without the flow of current.

Eq. 6-2 shows the core tensor $\boldsymbol{\mathcal{G}}$ with 3 indices (a 3-dimensional array of weld tensors), and the factor matrices $\boldsymbol{A}, \boldsymbol{B}, \boldsymbol{C}$ which are 2-dimensional arrays. To multiply the core tensor by the matrices the tensor is unfolded using mode-n unfolding so that it can be multiplied by the factor matrices. If the 3-dimensional tensor $\boldsymbol{\mathcal{G}}$ is unfolded along its 3rd dimension the result is a $(pq \times r)$ matrix $\boldsymbol{G}$, which can be multiplied by the $k \times r$ matrix $\mathbf{C}'$ using conventional matrix multiplication.

The algorithm used in this thesis is the *TuckerALS* (Alternating-Least-Squares) algorithm by Kroonenberg et al. (1980) from the *Tensor Toolbox* for MATLAB by Bader et al. (2015). As the name suggests, it uses an Alternating-Least-Squares approach to find the decomposition of the welding tensor data. First the algorithm initialises the factor matrices $\boldsymbol{B}$ and $\boldsymbol{C}$ with random numbers so that it can solve for A with respect to the tensor $\boldsymbol{\mathcal{X}}$ (which encapsulates the welding data). The algorithm continues solving for $\boldsymbol{B}$ and $\boldsymbol{C}$ using $\boldsymbol{A}$ until it converges so that the core tensor can be calculated. The change in the difference of the norms of the core tensor and original data tensor is assessed as the convergence criterion. This process is documented in Appendix Table 3. Once the tensor decomposition for the welding data is calculated, the tensor principal components for the weld tensors are in the tensor calculated from $\boldsymbol{\mathcal{G}} \times_1 \boldsymbol{A} \times_2 \boldsymbol{B}$ and the tensor principal component scores for the training data are in $\boldsymbol{C}$.

6.4 Tensor Decompositions for Weld Quality Monitoring

Representing welding signals as tensors allows for additional information about the interaction of multiple signals to be included before the feature extraction stage of the analysis process. This is of particular interest in aluminium RSW due to the complex relationship between the electrical, mechanical and thermal aspects of the process.

6.4.1 Signal Normalisation for Weld Quality Monitoring

To represent welding signal information as a tensor it is important that the signals are normalised so that the magnitude of the variation is comparable between different signals. Unfortunately, no clear solution has be found to date to this challenging task, and so a number of possibilities were tested before selecting the solution used in this thesis. This was done to ensure that the important information in the signals was not removed during the normalisation process. This section outlines some of the challenges with the signal normalisation problem, the solutions that were considered and the method that was chosen for the TPCA modelling.

When the outer product (tensor product) of the signals is taken, each of the signal entries are multiplied by all entries in the other signals. If the signals have significantly different magnitudes, the variation of one signal will be lost when it is multiplied by another with a greater magnitude. Similarly if the standard deviations of the points in a signal are significantly different, those with smaller standard deviations could be diminished (Figure 6-4).

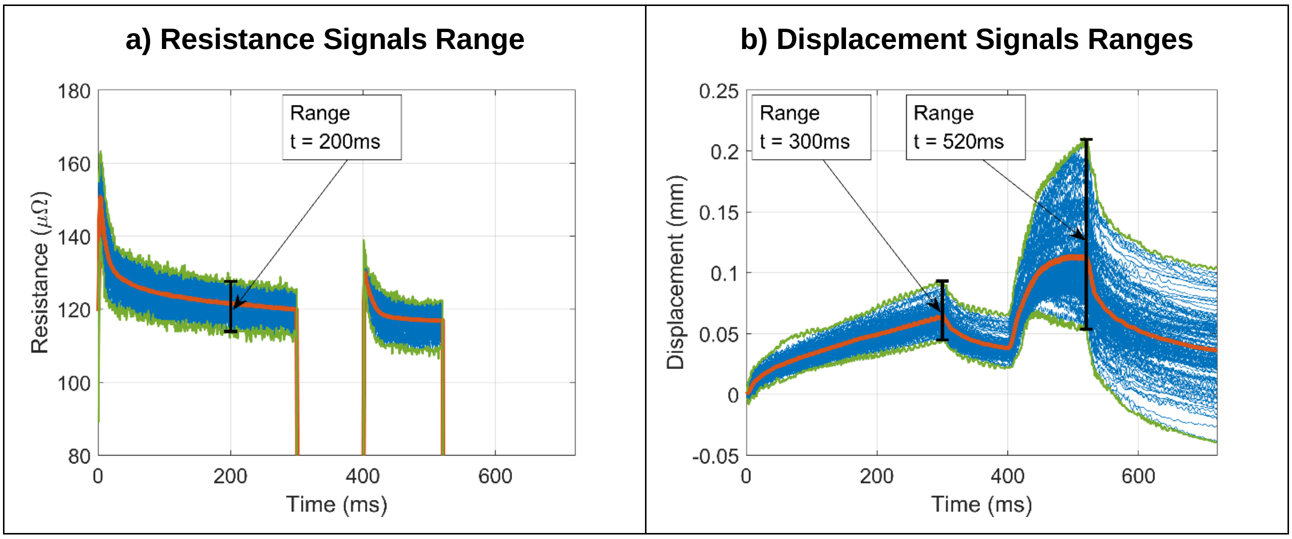

Figure 6-4: Comparison of mean signal range and signal set range, the maximum and minimum values at each time point are shown in green and the mean signal is represented in orange.

One solution that was considered was subtracting the mean signal from each signal set and scaling the signals so that their range was between -1 and 1. However this means the tensors focus on the polarity of the signals with respect to their mean (above or below). For example, when both signals of a weld are below the mean (their scaled signals are negative) the result of the outer product is a positive tensor. This is indistinguishable from the situation where both signals where above the mean. This possible solution highlights whether *both* scaled signals are above (or below) the mean, *or*, one signal is above and the other is below. This is not thought to be the important information for calculating a model for weld quality and was therefore abandoned.

Another similar approach to linear scaling was considered which scaled the signals to between 0 and 1 so that positive and negative signals were not an issue. However the differences in the standard deviation of each point in each signal dominated the resultant tensors. This was due to very different signal set ranges across the signal. An example of this can be seen in Figure 6-4b where the range at 300ms is significantly smaller than at 520ms. This meant that variation at this point in time was heavily exaggerated in the final tensor, reducing the impact of information at other points in time in the analysis.

The signal scaling solution that was chosen was to use a z-score calculation at each point in time in the signals. This reduced the effects of the different standard deviations of the signal datasets by normalising them across the signals. This is similar to the technique recommended by Leznik (2005) for normalising different variables in PCA using variable standardisation. When these signals were used to calculate the tensor all variation from the mean signal could be considered in the analysis.

To calculate the z-scores, the signals were divided by the standard deviation at each point in time so that the standard deviation at each point is equal to one. This meant that each point in a signal dataset had a mean of zero and standard deviation of one which reduced the effects of the different magnitudes of each signal for calculating the tensor.

Finally, before the outer product of the signals was taken, the signals were scaled to between zero and one so they were not centred on zero, minimising the chance of signal information being lost when it was multiplied by zero. The only foreseen downside here was that two signal points that were close to zero would be minimised in the calculation of the tensor and the information would be slightly non-linearly scaled by the multiplication. The signal normalisation is shown in Figure 6-5. Only two welds' signals are shown (x and y) so that the effect of the normalisation on individual signals can be seen.

Unfortunately, if there was significant error in the measurements, it could be exaggerated in the signal scaling process and multiplication. This is likely to present as a significant outlier in the process through the tensor principal component scores as was seen in the fault identification in section 4.4.

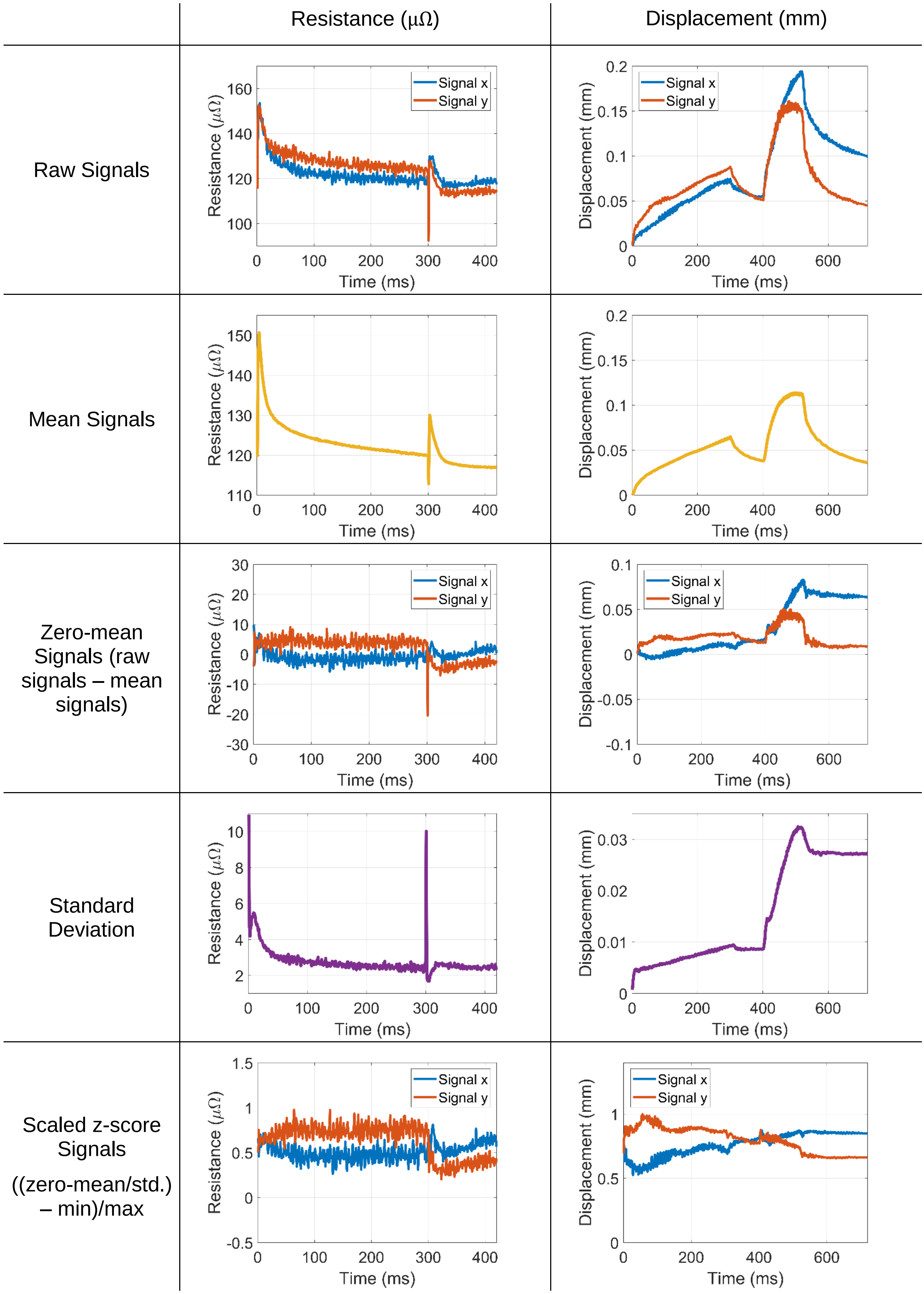

Figure 6-5: Signal normalisation of resistance and displacement signals with two example welds.

The signal shape analysis was focused on the indicative signal shapes, and so the magnitude of the original signal was not important and was only measured as variance from the mean of the training data. The normalising equations (Eq. 6-4 and Eq. 6-5) are shown below where $r \in \mathbb{R}^{a \times c}$, $d \in \mathbb{R}^{d \times c}$, the resultant $range(\check{r}) = [0,1]$, $range(\check{d}) = [0,1]$ and the range of the tensors is $range(\boldsymbol{\mathcal{U}}) = \sim[0,1]$. Finally, the mean tensor was subtracted from the welding tensors to make them zero-mean. This is an important step in TPCA, as it is in PCA, because otherwise the principal components must describe the distance of the tensors from origin as well as the variation in the dataset (Figure 6-6).

$$\check{r} = \frac{((r - \bar{r})/std(r)) - \min r}{\max(r)} \quad \textbf{Eq. 6-4}$$

$$\check{d} = \frac{\left((d - \bar{d})/std(d)\right) - \min(d)}{\max(d)} \quad \textbf{Eq. 6-5}$$

$$\boldsymbol{\mathcal{U}} = \check{r} \otimes \check{d} \quad \textbf{Eq. 6-6}$$

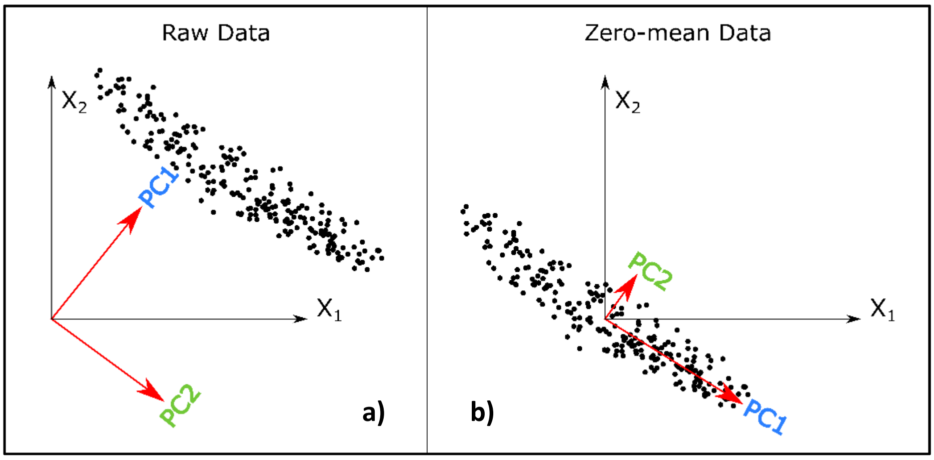

Figure 6-6: Importance of mean subtraction in PCA and TPCA. a) First PC describes distance of cluster from the origin instead of dataset variance. b) First PC describes major variation in the data.

The mean tensors were found to be almost completely flat in practice (small range across the tensor). This is due to the fact that the mean tensor is the mean of the product of two sets of signals that are both zero-mean with standard deviations of one. The calculation of the mean tensor and subtraction of the mean tensor from new data is shown in Eq. 6-7 and Eq. 6-8 respectively.

$$\bar{\boldsymbol{\mathcal{U}}}_{xy} = \frac{1}{z}\sum_{i=1}^{z} \boldsymbol{\mathcal{U}}_{xyi} \quad \textbf{Eq. 6-7}$$

$$\boldsymbol{\mathcal{U}}_{xyz} = \boldsymbol{\mathcal{U}}_{xyz} - \bar{\boldsymbol{\mathcal{U}}}_{xy} \quad \textbf{Eq. 6-8}$$

The result of Eq. 6-7 and Eq. 6-8 is shown in Figure 6-7.

Weld Tensors

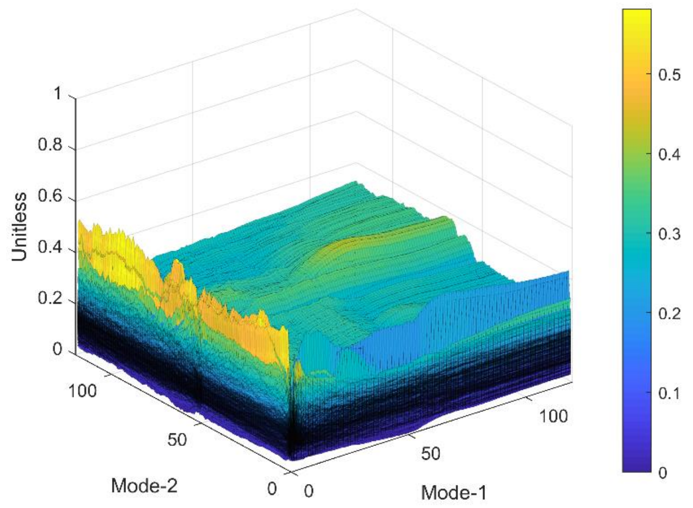

Mean Tensor

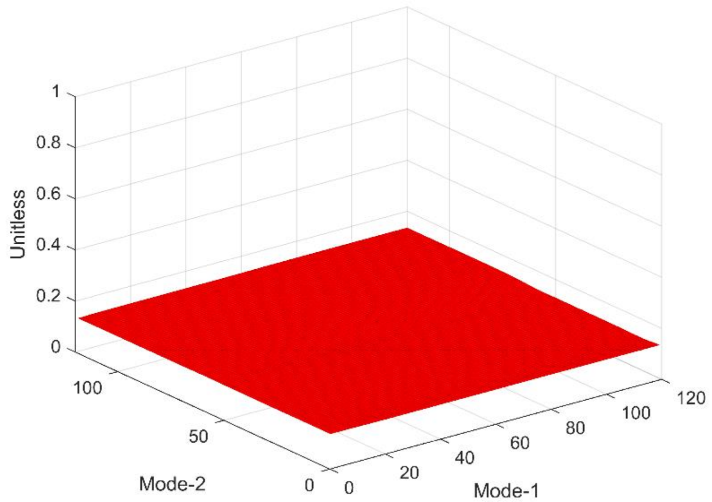

Zero-mean Tensors
(tensor – mean tensor)

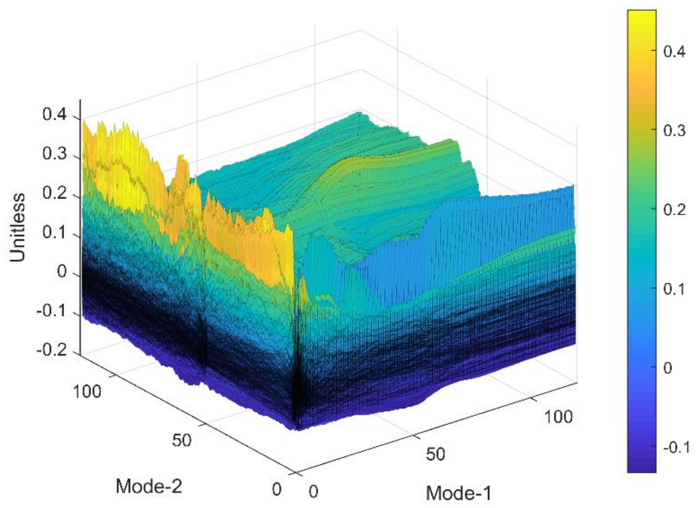

Figure 6-7: Subtracting the mean tensor from all welding tensors

6.4.2 Calculating Tensor Principal Component Scores

The concept of calculating principal component scores for new data from the principal components of a training set was used in Chapter 4 extensively to validate the weld quality models developed. This concept can be generalised to tensors so that models created with TPCA can be validated with new data. The concept of tensor unfolding or matricising, covered in section 6.3 is key to understanding how a TPCA weld quality model can be validated with new data.

To calculate tensor principal component scores ($\boldsymbol{C}$) for new welding data ($\boldsymbol{\mathcal{Y}}$) that has dimensions $i \times j \times w$ the process is as follows. First the decomposition of the training data in $\mathcal{X}$ with dimension $(i \times j \times k)$ must be simplified. By calculating the tensor $\boldsymbol{\mathcal{M}}$ with dimensions $(i \times j \times r)$ from $\boldsymbol{\mathcal{G}}, \boldsymbol{A}$ and $\boldsymbol{B}$, the tensor principal components of the individual weld tensors can be represented (Eq. 6-9). Substituting Eq. 6-9 into Eq. 6-2 produces Eq. 6-10 which shows the original welding data tensor $\boldsymbol{\mathcal{X}}$ is approximately equal to the principal components of the individual weld tensors in $\boldsymbol{\mathcal{M}}$ multiplied by the principal component scores in $\boldsymbol{C}$.

$$\boldsymbol{\mathcal{M}} = \boldsymbol{\mathcal{G}} \times_1 \boldsymbol{A} \times_2 \boldsymbol{B} \qquad \textbf{Eq. 6-9}$$

Substituting into Eq. 6-2 results in,

$$\boldsymbol{\mathcal{X}} \approx \boldsymbol{\mathcal{M}} \times_3 \boldsymbol{C} \qquad \textbf{Eq. 6-10}$$

To calculate principal component scores ($\boldsymbol{R}$) for new data ($\boldsymbol{\mathcal{Y}}$) with dimensions $i \times j \times w$, the process is as follows. $\boldsymbol{R}$ has dimensions $w \times r$, which are w welds and r principal components.

$$\boldsymbol{\mathcal{Y}} \approx \boldsymbol{\mathcal{M}} \times_3 \boldsymbol{R} \qquad \textbf{Eq. 6-11}$$

$\boldsymbol{\mathcal{M}}$ has dimensions (i, j, r)

$\boldsymbol{\mathcal{Y}}$ has dimensions (i, j, w)

Mode-3 Unfolding of $\boldsymbol{\mathcal{M}}_{(\mathbf{3})} \rightarrow (i \times j, r)$

Mode-3 Unfolding of $\boldsymbol{\mathcal{Y}}_{(\mathbf{3})} \rightarrow (i \times j, w)$

$$\boldsymbol{R} \approx \boldsymbol{M}_{(\mathbf{3})}^{+} \boldsymbol{Y}_{(\mathbf{3})} \qquad \textbf{Eq. 6-12}$$

To solve Eq. 6-11 for $\boldsymbol{R}$, both tensors $\boldsymbol{\mathcal{Y}}$ and $\boldsymbol{\mathcal{M}}$ must be unfolded in the same manner so that the locations of the indices are maintained. In this case, both tensors are unfolded along the third dimension of the array resulting in an $(ij \times w)$ matrix, $\boldsymbol{Y}$, and an $(ij \times r)$ matrix, $\boldsymbol{M}$. This allows the equation to be rearranged to solve for $\boldsymbol{R}$ (Eq. 6-12).

6.4.3 Tensor Principal Component Shape Analysis

To show the shape variation that a tensor principal component contributes to a welding tensor, a similar technique was used to that in Chapter 4 – *principal component shapes*. To produce a tensor principal component shape, the underlying methodology is the same but the principal components are tensors rather than vectors. The process is shown graphically in Figure 6-8 and involves multiplying the r^{th} tensor principal component by the maximum and minimum of the associated tensor principal component scores in $\boldsymbol{C}_{\boldsymbol{kr}}$ (i.e. $\min(\boldsymbol{C}_{\boldsymbol{k}})$ and $\max(\boldsymbol{C}_{\boldsymbol{k}})$) and adding the mean tensor ($\bar{\boldsymbol{\mathcal{X}}}_{\boldsymbol{ij}}$), which was removed in the tensor principal component analysis phase.

Explanation | **Graphical Representation**

Tensor Principal Component

$$\boldsymbol{\mathcal{M}}_{\boldsymbol{ijr}}$$

$$i = 1, \dots, I, \quad j = 1, \dots, J, \quad r = 1$$

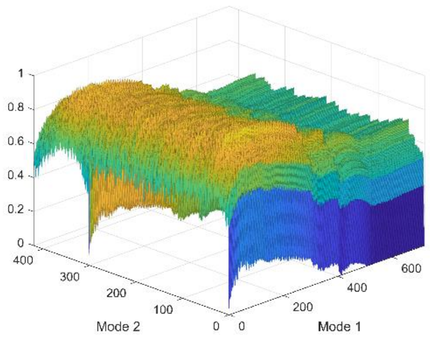

Maximum and Minimum Tensor Principal Component Score Shapes

$$\boldsymbol{\mathcal{M}}_{\boldsymbol{ijr}} \cdot \max(\boldsymbol{C}_{\boldsymbol{kr}}) + \bar{\boldsymbol{\mathcal{X}}}_{\boldsymbol{ij}}$$

$$\bar{\boldsymbol{\mathcal{X}}}_{\boldsymbol{ij}}$$

$$\boldsymbol{\mathcal{M}}_{\boldsymbol{ijr}} \cdot \min(\boldsymbol{C}_{\boldsymbol{kr}}) + \bar{\boldsymbol{\mathcal{X}}}_{\boldsymbol{ij}}$$

$$i = 1, \dots, I, \quad j = 1, \dots, J,$$
$$k = 1, \dots, K, \quad r = 1$$

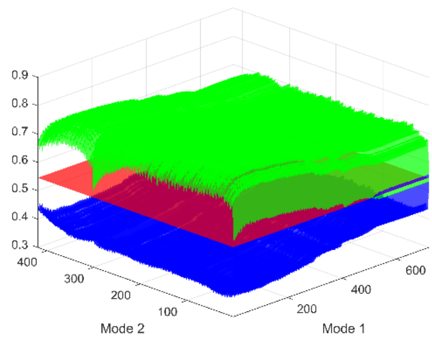

Figure 6-8: Tensor principal component shape calculation and explanation

To visualise a tensor principal component's *shape* for welding data, a tensor is reconstructed by multiplying the tensor principal components in $\boldsymbol{\mathcal{M}}_{\boldsymbol{ijr}}$ by one tensor principal component score from the factor matrix $\boldsymbol{C}_{\boldsymbol{kr}}$ (the same methodology as used in Chapter 4). The maximum (positive) and minimum (negative) tensor principal component scores are used to show the magnitude of the shape as shown in Figure 6-8.

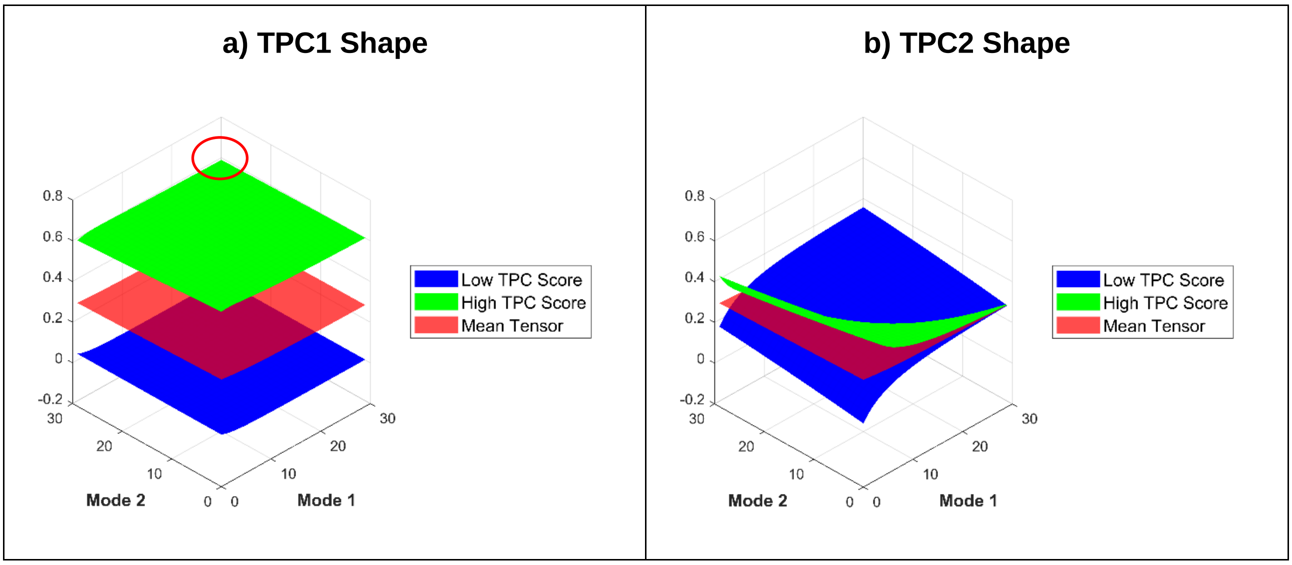

Figure 6-9: Simplified hypothetical tensor principal component shapes

To show how the Tensor Principal Component (TPC) shapes can be analysed, we will analyse two hypothetical TPC shapes. The tensors that these principal components are calculated from the outer product of two signals. Because the two signals were multiplied, the information captured in the tensor principal component shapes tells us about the relationships between the two signals in the process at all points in time. The multiplication of two values from the signals (which are a single point on the tensor) provides information about the way that the two signals were co-varying.

The final point of each signal, which is circled in red in Figure 6-9a, shows that multiplying the first tensor principal component by the largest first tensor principal component score produces a high value at that point. Working backwards, to produce a value equal to the circled point, both normalised signals had to be large at that point in time. Conversely, to produce the value of the lowest tensor principal component score at the same position on the tensor, both signals had to be small at that point in time (refer to section 6.2 to revisit tensor calculation).

The tensor variation described by the first tensor principal component relates to the interacting behaviour between the two signals ranging from two large signals to two small signals. This tensor principal component describes direct correlation between the two signals at all points in time because the tensor principal component is flat. This relates to co-variation of two signals that are consistently above the mean, or two signals that are consistently below the mean.

6.4.4 Limitations of the Tensors

As was highlighted in section 6.4.1, the challenge of extracting the relevant information for weld quality monitoring from the original signals is complicated by the multiplication required to calculate the weld tensors. However this was required to understand the interacting behaviour of the two signals for signal shape analysis.

Calculating the outer product of the two signals means that the specific values of the individual signals is lost. If the weld tensor $\boldsymbol{\mathcal{A}}$ is below the mean, it could be the result of either signal, r or d being far below the mean. This is represented with simple signals below using brackets to show which signal is below its mean. It is possible for $\boldsymbol{\mathcal{A}}$ to be the same in both cases if the other signal is above its mean. This shows that the analysis does not rely on which signal was below the mean. However this is an oversimplification of what happens in practice and the shapes of the signals are inevitably shown in the final weld tensors.

$$\boldsymbol{\mathcal{A}} = r \times \left(d \ll \bar{d}\right)$$
$$\boldsymbol{\mathcal{A}} = (r \ll \bar{r}) \times d$$

Additionally, the tensors show when the signals are positively correlated because a tensor that is high in magnitude is caused by two high signals and a lower in magnitude tensor is caused by two low signals. To assess negative correlations between two signals, a zero-mean signal set can be multiplied by minus one prior to taking the outer product with other signals. This was investigated and found to produce very similar results and did not significantly improve modelling results.

To achieve a methodology that incorporates both information about the interactions and the specific values of the signals a hybrid approach with PCA of the signals and TPCA of the tensors could be used. This would look similar to Eq. 6-1 which drew the analogy to a linear model with interactions.

$$y = PCA(x_1) + PCA(x_2) + TPCA(x_1 \otimes x_2)$$

In practice this is not required and the information encapsulated by the tensors is sufficient to model weld quality and this will be shown later in the case study in section 6.5.

The necessary scaling of the signals for calculating the weld tensors required some trade-offs to ensure that the relevant information was retained for the analysis. One particular aspect that the signal scaling highlighted was that each choice of signal scaling methodology focussed more on one aspect of the signals' shapes and position within the dataset. This may require further work to investigate which aspects of the signals within their own datasets is most important for weld quality monitoring, however further work on this falls beyond the scope of this thesis.

6.4.5 Generalising to Three or More Signals

The technique developed for aluminium weld quality monitoring can be generalised to more than two signals, although this is beyond the scope of the work in this thesis. The process involves taking the outer product of multiple vectors and then following the same process to calculate the Tucker Decomposition. An example with more than two signals can be made from the data in Chapter 5 where five process signals were analysed. The resultant tensor decomposition would be as follows.

$$\boldsymbol{\mathcal{X}}_{cvrdfw} \approx \boldsymbol{\mathcal{G}}_{pqstux}\boldsymbol{A}_{cp}\boldsymbol{B}_{vq}\boldsymbol{C}_{rs}\boldsymbol{D}_{dt}\boldsymbol{E}_{fu}\boldsymbol{F}_{wx} \qquad \textbf{Eq. 6-13}$$

$$\boldsymbol{\mathcal{X}}_{xvrdfw} \in \mathbb{R}^{14\times14\times14\times14\times14\times133}$$

With the important information encapsulated in the matrix $\boldsymbol{F}_{wx}$ which is the tensor principal component scores for the interactions of all five signals. The matrix $\boldsymbol{F}_{wx}$ contains the principal component scores of the fifth order weld tensors. Visualising this tensor is more challenging than the two signal case, however the problem can be broken down into interactions between pairs of signals. For welding signal data the number of dimensions can be high which in turn creates large tensors. In this example which uses AC welding data which is limited to one measurement per half cycle of a 50Hz signal, the size of the tensor for each weld is still very large, $14^5 = 537824$.

6.5 Case Study: Quality Monitoring using the Interactions of Multiple Signals

This sections presents a proof-of-concept for the TPCA feature extraction and weld quality monitoring technique developed for aluminium RSW. To do this, welding data was collected under a number of different experimental conditions. The different experimental conditions provided variation in the signal information and quality of the welds.

6.5.1 Introduction

This study was conducted to test the TPCA weld quality monitoring technique. Some of the data collected was in the form of a weld lobe study, which varied welding current and clamping force to generate variation in weld quality. Weld lobe studies are often conducted in industry to setup new materials or different stack-ups before they are implemented in production. The primary measure of quality collected was the tensile load at failure, however for some of the welding data destructive chisel tests were conducted to allow for preliminary modelling of the measured button diameter which is the metric most commonly used in industry.

6.5.2 Analysis Methodology

The data collection for this study was conducted in the lab and as such the amount of data that could be collected was limited by various resources. A leave-one-out analysis methodology was adopted to maximise the training data available for computing weld quality models. A leave-one-out strategy involves removing one weld from the dataset, using the remaining data to compute a model for weld quality and then using that model to predict the quality of the weld that was removed. This process is repeated by removing each weld individually for the entire dataset. The analysis methodology is outlined in the steps below:

1. Training data signals are normalised to reduce the effects of different signal magnitudes before multiplication.

2. Tensors are calculated from the scaled training weld signals.

3. The tensor principal components are calculated from the training weld tensors.

4. Tensor principal components that describe less than 1% of the training set variation are removed from the analysis.

5. The correlation between tensor principal component scores of the training data and weld quality are assessed.

6. A weld quality model is calculated from the tensor principal components of the training data that are significantly correlated with weld quality (p-value < 0.05) using linear regression.

7. To predict the quality of new welds, the signals of validation welds are scaled using the same scaling as the training set.

8. Tensors are calculated from the scaled validation signals.

9. Tensor principal component scores for the validation welds are calculated.

10. The tensor principal component scores of the validation welds are put into the linear regression, resulting in a predicted weld quality for each weld.

11. The RMSE and R^2 values are calculated between the predicted and actual strength of the welds to assess the accuracy of the TPCA weld quality model.

6.5.3 Datasets and Experimental Setup

The weld lobe dataset comprised 159 welds, approximately half of which were tested in a tensile shear test while the other half were subjected to a chisel test, allowing for both tensile load and button diameter to be modelled (Table 6-3). A second dataset was collected with uncontrolled electrode wear, meaning that the tips were not re-dressed throughout the experiment and the same weld schedule was maintained for all welds.

Table 6-3: Dataset destructive testing summaries

Dataset Name	Number of Welds	Number of Tensile Tests	Number of Chisel Tests
Weld Lobe Set	159	78	81
Electrode Wear Set	300	270	30

The electrode wear set was completed by creating 300 welds without re-dressing, adjusting or removing the electrodes. The base weld schedule (Table 6-4) was used and welds were collected in consecutive runs of 30 welds. The second weld in each set of 10 was subjected to a chisel test so the effects of electrode wear on button diameter could be tracked at 10 weld intervals. The weld schedule times for all data were fixed with the same preheating, cooling, welding and forging cycle so that welds could be analysed using the same tensor decompositions (Table 6-4). The forging cycle refers to the part of the cycle where the electrodes are closed but no current is flowing through the weld, this helps to compress the weld as it cools (shown at the end of Figure 6-10b).

Table 6-4: Base weld schedule summary

	Squeeze	Preheating	Cooling	Weld	Forge
Time (ms)	200	300	100	120	250
Current (kA)		10		20	
Electrode Force (kN)			3		

Two signals were collected to monitor the process, electrical resistance through the joint and the electrode displacement due to thermal expansion and contraction of the joint. These two signals measure the electrical and mechanical aspects of the process which will be used to calculate tensors and predict weld quality. Representative welding signals are shown in Figure 6-10 with the information used in analysis highlighted. There is no welding current from 300-400ms or 520-720ms of the original signals as these are the cooling and forging cycles of the weld schedule (Tang et al., 2002). The values of the resistance signal during the cooling & forge times were removed from the analysis as the resistance cannot be calculated without the flow of current through the joint. However, the information from the displacement curve during this period is included in the analysis as this may have useful information about the progression of the welding process between the preheating and welding phases (Figure 6-10b).

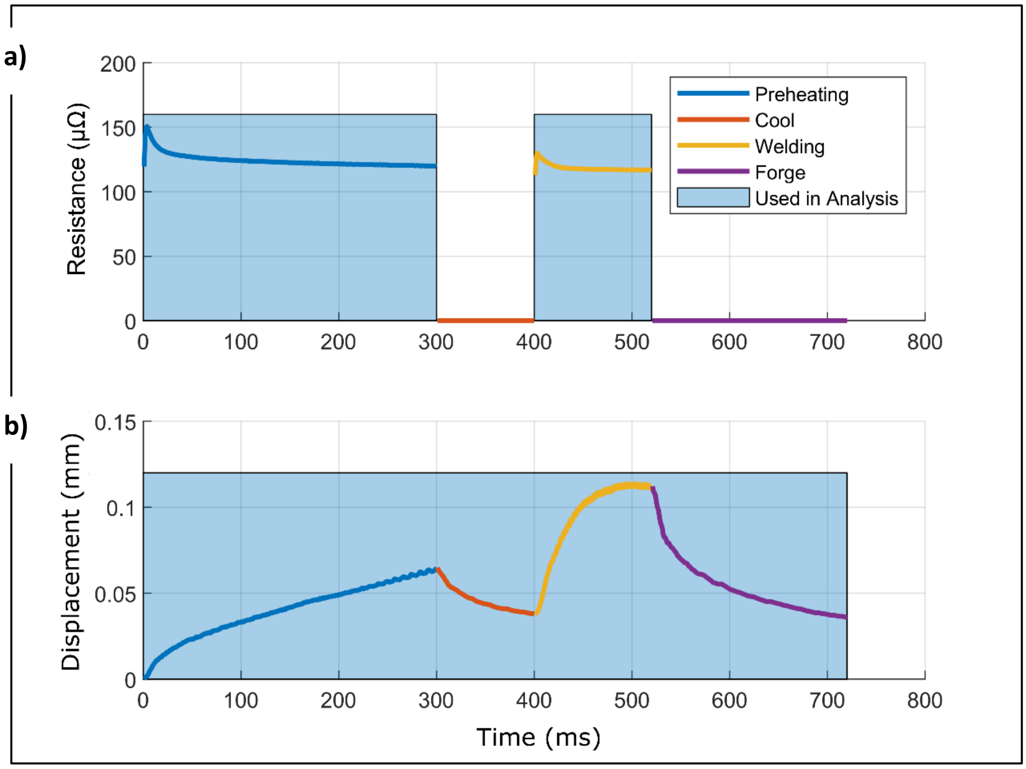

Figure 6-10: Welding signal examples. The parts of the signals used in the analysis are shown with blue shading. Resistance signal (a) and the displacement signal (b).

The lengths of the signals are shown in Table 6-5 which determine the numbers of rows and columns in the weld tensors. Note, the resistance signal is shorter than the displacement signal due to the removed cooling and forging cycle information.

Table 6-5: Dataset tensor indices summaries

Index	Dimension	Training Set	Electrode Wear Set
i	Length of Resistance Signal	420	420
j	Length of Displacement Signal	720	720

The experimental conditions for the weld lobe dataset are shown in Table 6-6. Current during the welding phase and the electrode force were varied independently across a range of settings that produced welds that failed through button pull out during a destructive chisel test.

Table 6-6: Weld lobe dataset experimental conditions

Experimental Condition	1	2	3	4	5	6	7	8	9	10	11	12	13	14	15	16
Welding Current (kA)	20	20	20	20	20	20	22	22	22	14	15	16	17	18	18	18
Electrode Force (kN)	2	2.5	3	3.5	4	4.5	2	2.5	3	3	3	3	3	3	3.5	4

The MFDC robotic spot welder was used for this study with aluminium specification electrode caps, RWMA – Class 2, chromium-zirconium copper (Resistance Welder Manufacturers' Alliance, 2009). The caps were a dome type cap with a 6mm flat face for welding. The material that was welded was 1mm AA5052, all welds were conducted on two sheets with sample dimensions of 100mm by 24mm and no additional surface preparation. Due to the long welding trials, some welds within the same set where collected on different days under slightly different ambient conditions.

6.5.4 Results

The mean displacement and resistance signals collected during the welding processes for each of the different experimental conditions in the weld lobe dataset are shown in Figure 6-11 and Figure 6-12. The variation caused by the different experimental conditions is not as pronounced in the resistance signals as it is in the displacement signals which is common in aluminium RSW. The lower clamping force results in higher thermal expansion during the welding phase of the process as shown in Figure 6-12. The variation in the resistance signals is much greater from start to finish than any of the variation caused by the different experimental conditions. Insets in the resistance signal plots show the minute variation in the resistance signals caused by the different experimental conditions.

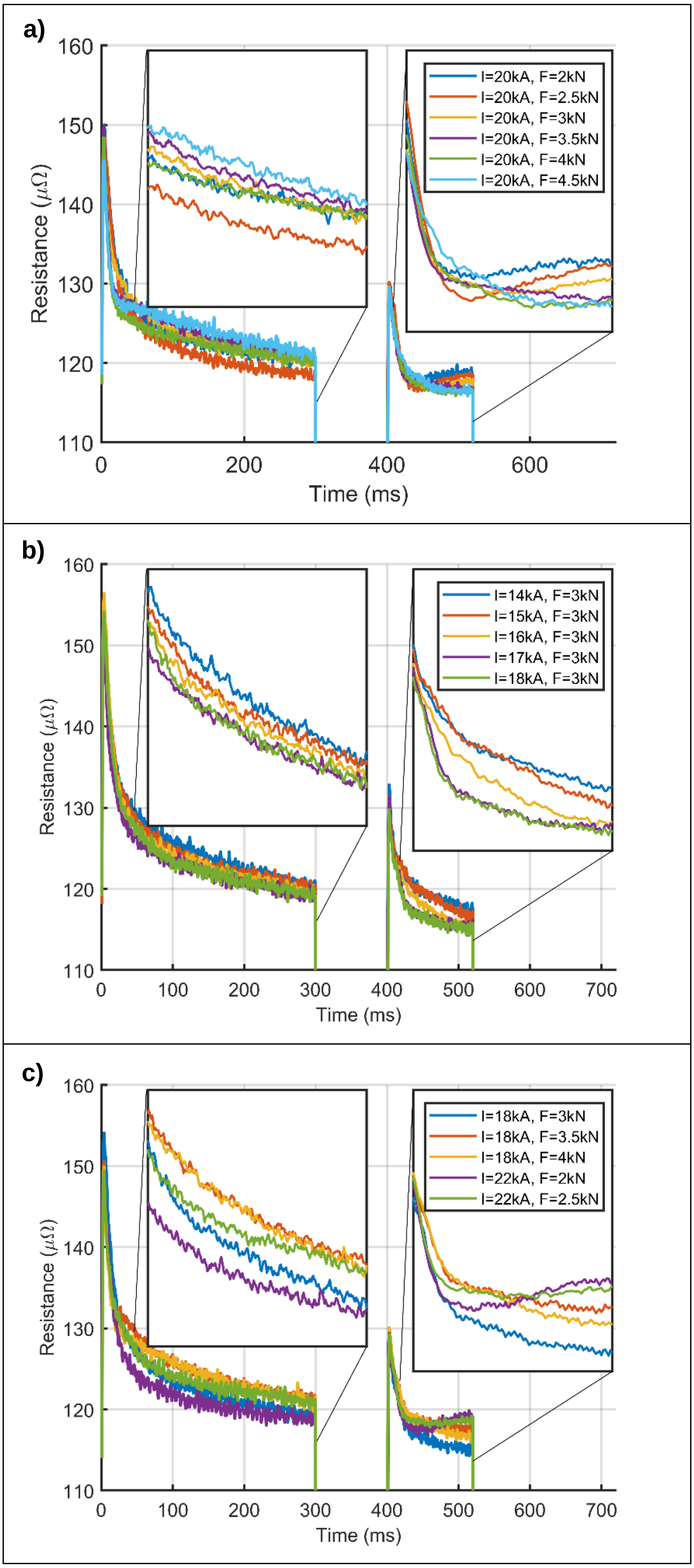

Figure 6-11: Weld lobe data resistance signals, welding current values shown in the legends

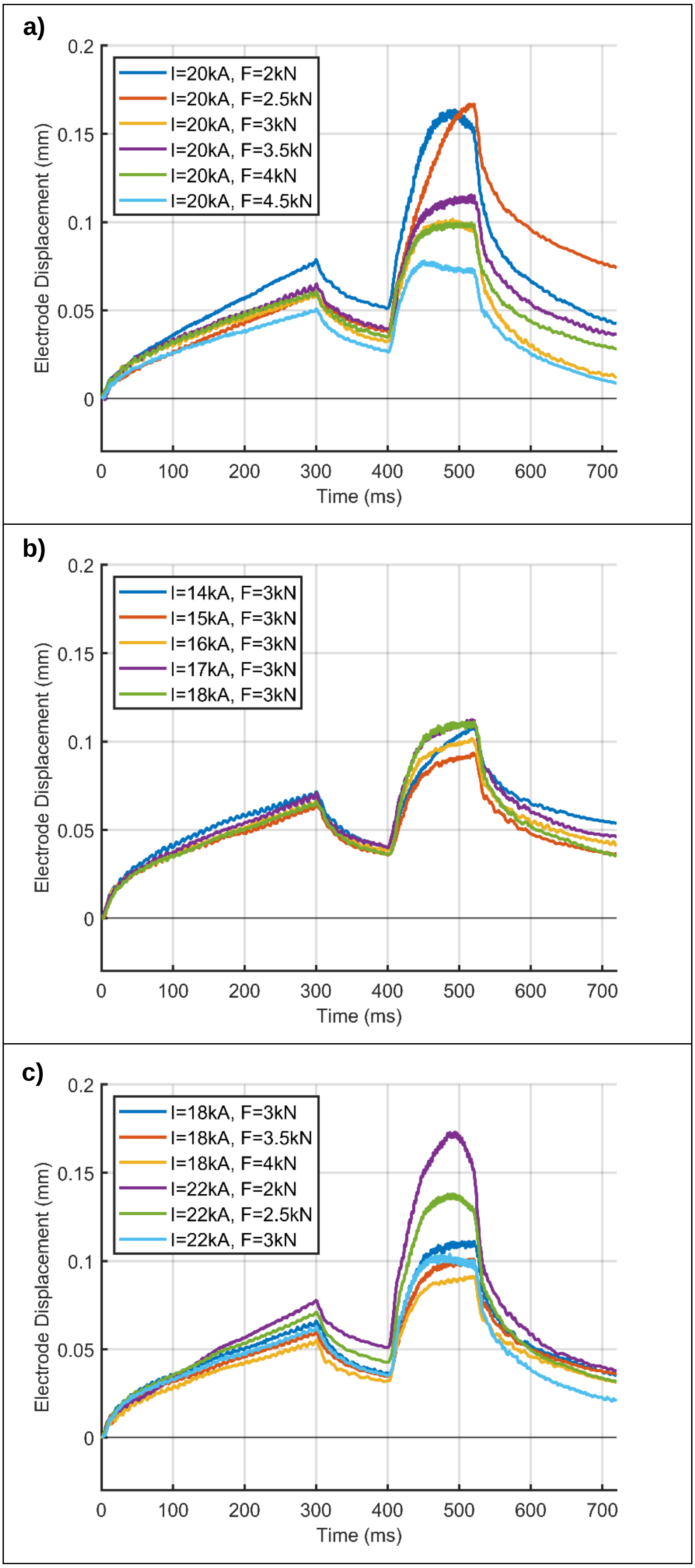

Figure 6-12: Weld lobe data displacement signals, welding current and force shown in the legends

Figure 6-13 shows mean resistance and displacement signals for the electrode wear data split into 50 weld intervals to show the progression of electrode wear. The final resistance of the welds increases with electrode wear and the thermal expansion during the pre-heating cycle reduces and the welding phase peak occurs later as the electrode wear progresses.

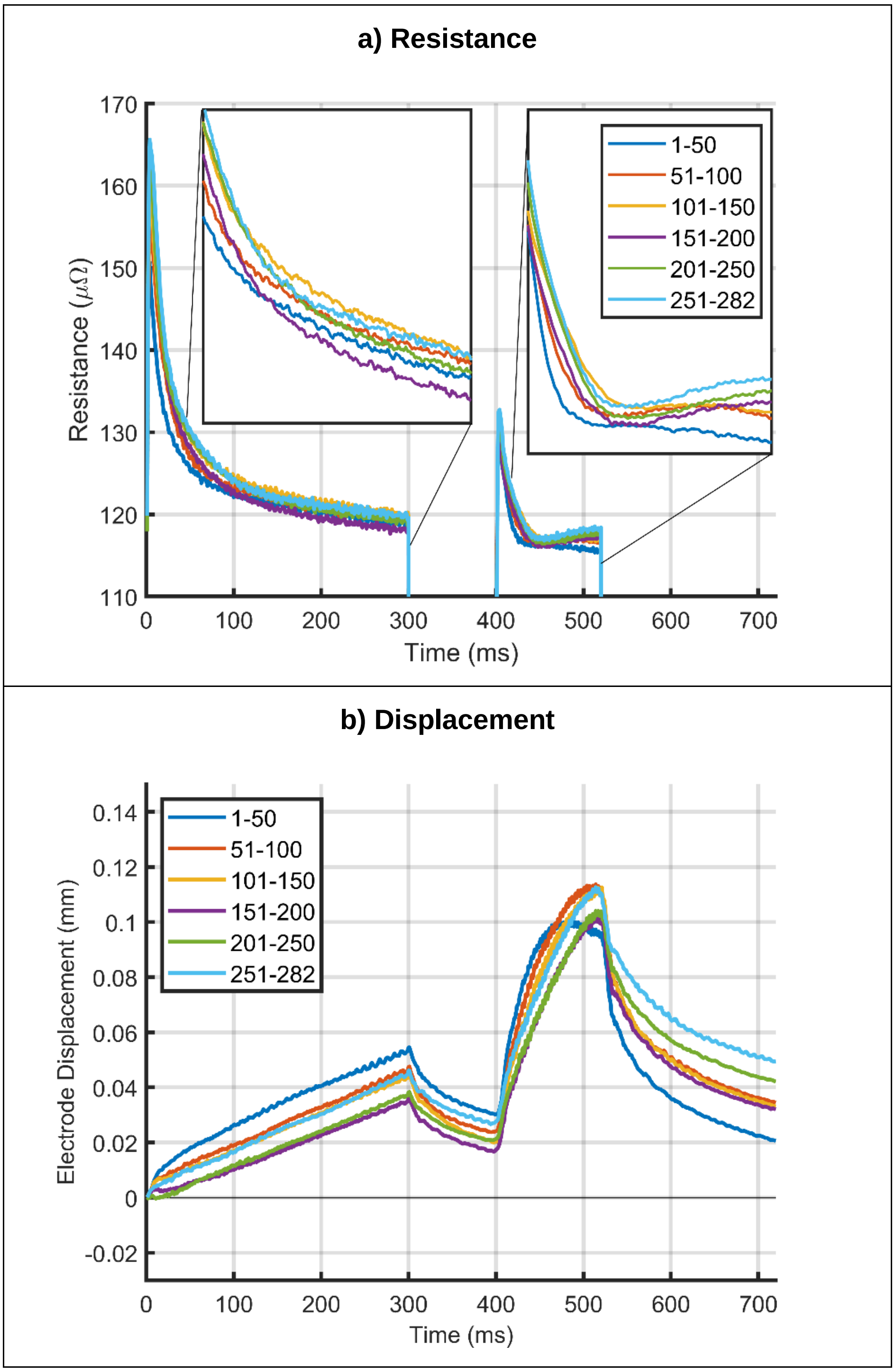

Figure 6-13: Electrode wear set mean process signals, split into 50 weld groups

Figure 6-14 shows box and whisker plots of the tensile loads to failure from a tensile shear test for the weld lobe data and electrode wear data.

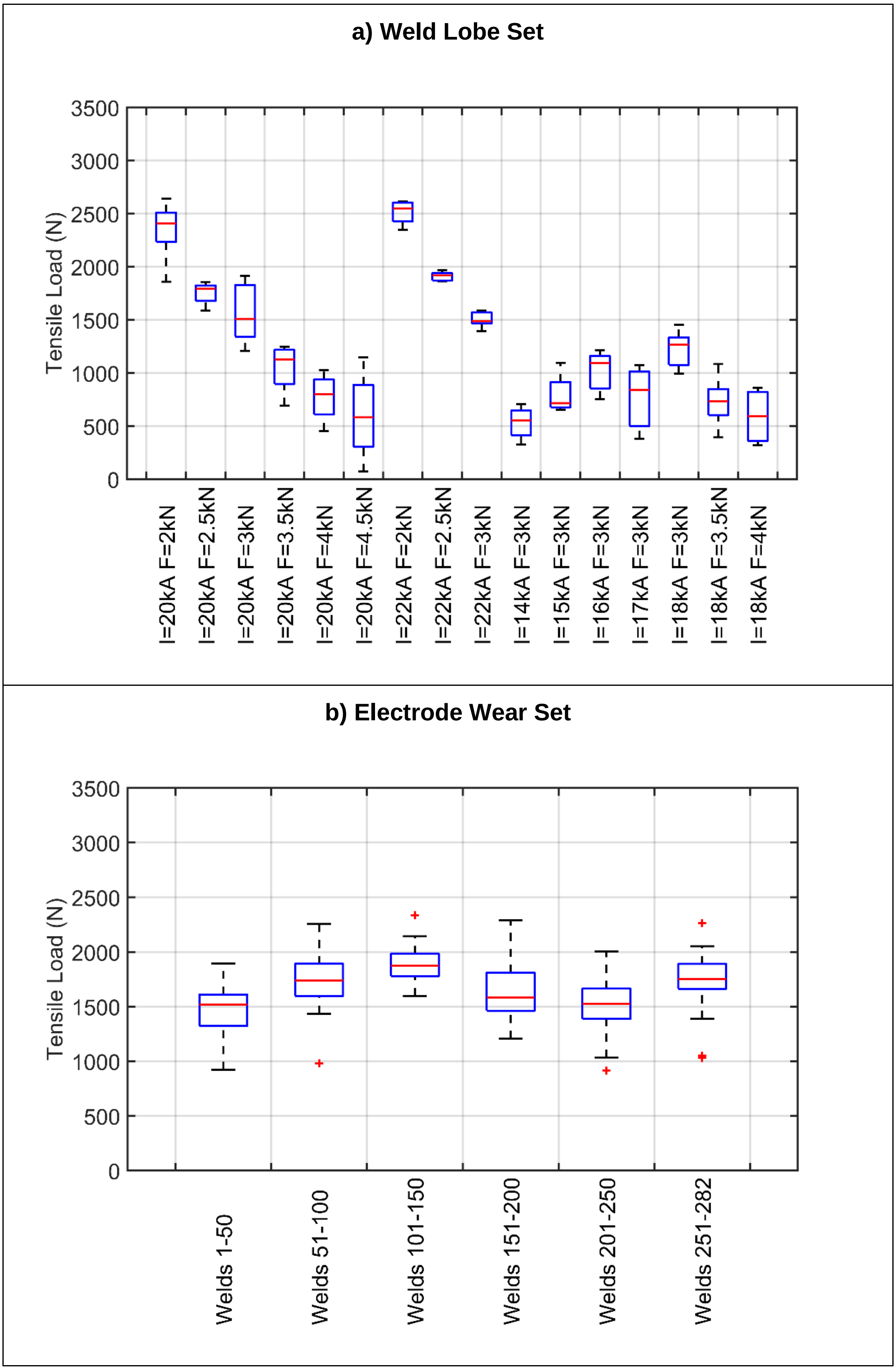

Figure 6-14: Tensile load box plots for the weld lobe set and electrode wear set

Varying the input parameters in the weld lobe dataset had a large effect on the output quality of the welds (Figure 6-14a). The data with the low clamping forces had the highest tensile shear loads caused by the higher resistance and is the result of the reduced clamping force. Unfortunately, the higher resistance leads to accelerated electrode wear.

The electrode wear over almost 300 welds (without tip dressing) had a much less pronounced effect on the tensile shear load of welds (Figure 6-14b). Initially the tensile shear loads are lower (welds 1-50) as the electrodes wear in, then the tensile loads of the welds increase, followed by a drop and slight increase in the last 50 weld window. There are various electrode wear mechanisms that can affect the condition of the electrodes in different ways as discussed in the literature review in section 2.4.2.

6.5.5 Interpreting Tensors for Weld Quality Monitoring

Interpretation of the analysis requires a few key points about weld tensors and TPCA to be understood.

- Tensors show the interaction between the two signals using the outer product (multiplication of all points in each signal arranged in a matrix as shown in Figure 6-1a).

- A high or low region on a weld tensor is the product of two sets of high or low signal values (as discussed in section 6.4.3.

- The high or low region on a weld tensor therefore shows that the two signals are positively correlated at those points in time (Table 6-7).

Table 6-7: Explanation of the correlation between signals in weld tensors

Correlation between Signal 1 and Signal 2	Signal 1 (value)		Signal 2 (value)		Tensor (value)
Positive	High	×	High	=	High
Positive	Low	×	Low	=	Low
Negative	High	×	Low	=	Medium
Negative	Low	×	High	=	Medium

- An interaction between the start of one signal and the end of another is represented on the tensor in quadrants two or three (see Figure 6-2).

- When there is large variance in the magnitude of different weld tensors it suggests there is a significant positive correlation (interaction) in the dataset between the two signals. This is because the large variance can only be caused by a high value for both signals for one weld and low values for both signals for another weld at those points in time (Table 6-8).

Table 6-8: Two welds with large variance between their tensors at the point ($\boldsymbol{i}, \boldsymbol{j}$)

	Tensor value at point (i, j)	Signal 1 (i)	Signal 2 (j)	Correlation across weld dataset at (i, j)
Weld 1	High	High	High	Positive
Weld 2	Low	Low	Low	

- TPCA shows which signal interactions are most prominent in the dataset across many welds using the concepts developed in Chapter 4 with PCA.

- When tensor principal components are strongly correlated with weld strength it shows which of the prominent signal interactions in the dataset are useful for weld quality monitoring using the same concepts that were developed in Chapter 4 with PCA.

The next section will use these key concepts to model the tensile-shear load bearing capacity of welds by representing the information from two signals as weld tensors, and decomposing them using TPCA.

6.5.6 Modelling Weld Quality with Tensors

To maximise the amount of training data available to produce a model, a 'leave-one-out' method was used. The leave-one-out process removes one weld from the dataset, trains a model on the rest of the dataset and then uses the model to predict the tensile load of the removed weld.

The tensor principal components found to be significantly correlated with the tensile load of the welds (p-value of < 0.05) in almost every iteration of the model were 2, 3, 6, 7 and 8, with tensor principal components 4 and 5 used in some of the models (approximately 9% and 30% of the iterations respectively). A selection of the tensor principal component scores are plotted against the tensile-shear load bearing capacity in Figure 6-15. The first tensor principal component components are shown in Figure 6-15a which were not found to be correlated with the tensile strength. The seventh tensor principal component scores are shown in Figure 6-15d which were most commonly found to have the strongest correlation with the tensile- shear load bearing capacity.

The total correlation between predicted and measured tensile load was $R^2 = 0.66$ with an RMSE of 247N. The first 8 tensor principal components are shown in Figure 6-17 to show the major tensor principal components of the dataset. This process was repeated for every weld (Figure 6-16).

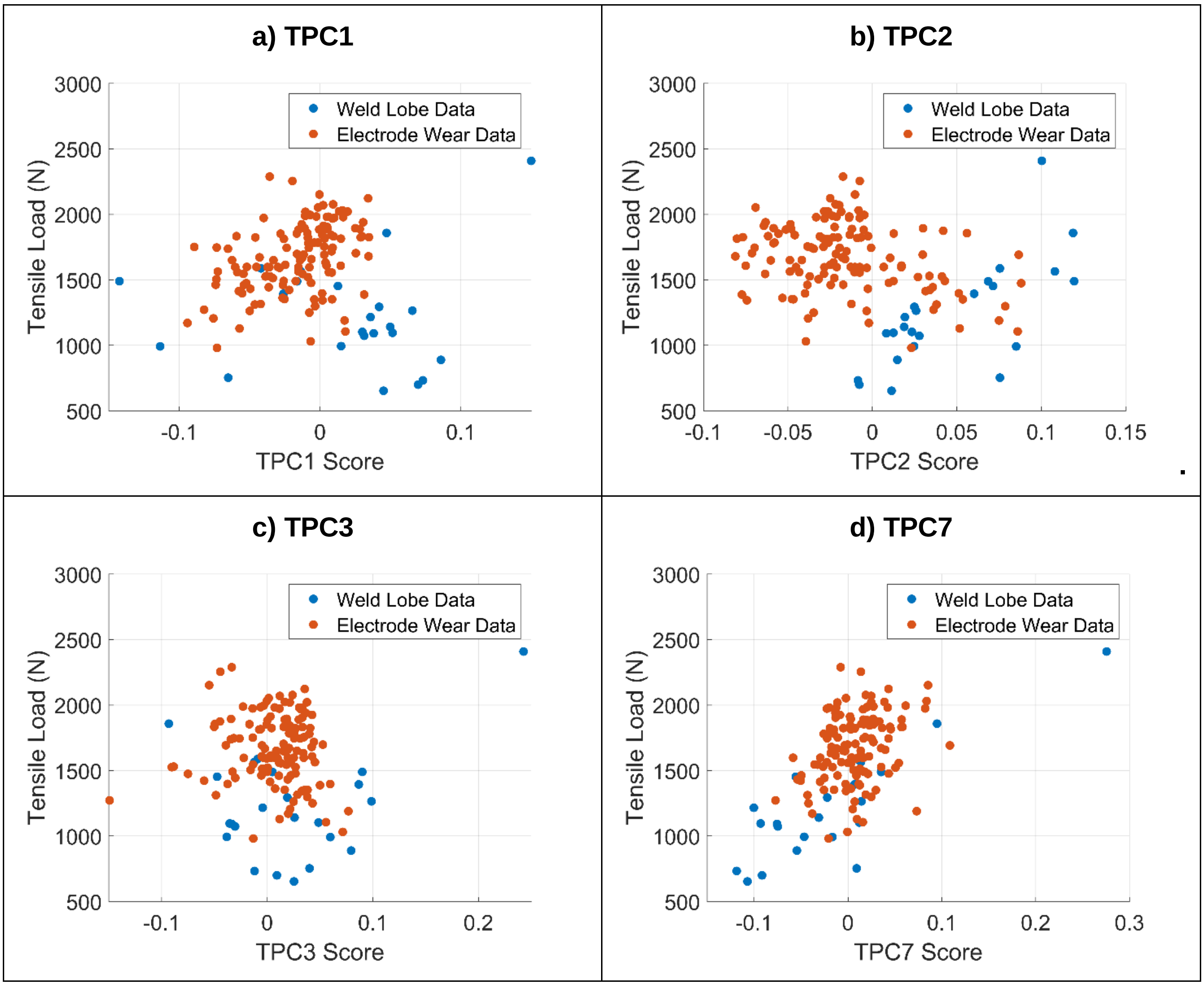

Figure 6-15: Tensor principal component scores against tensile-shear load bearing capacity

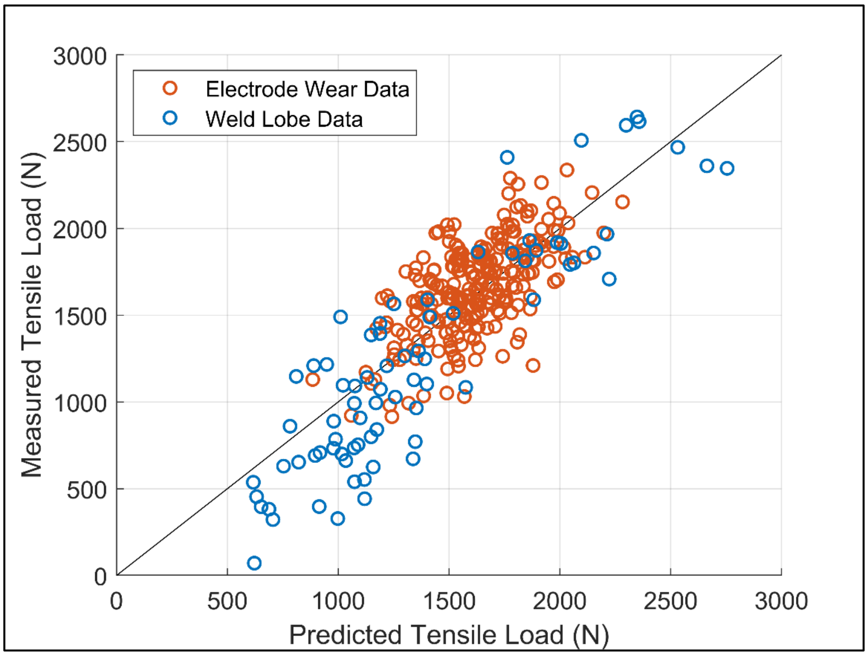

Figure 6-16: Leave-one-out predictive tensile load model

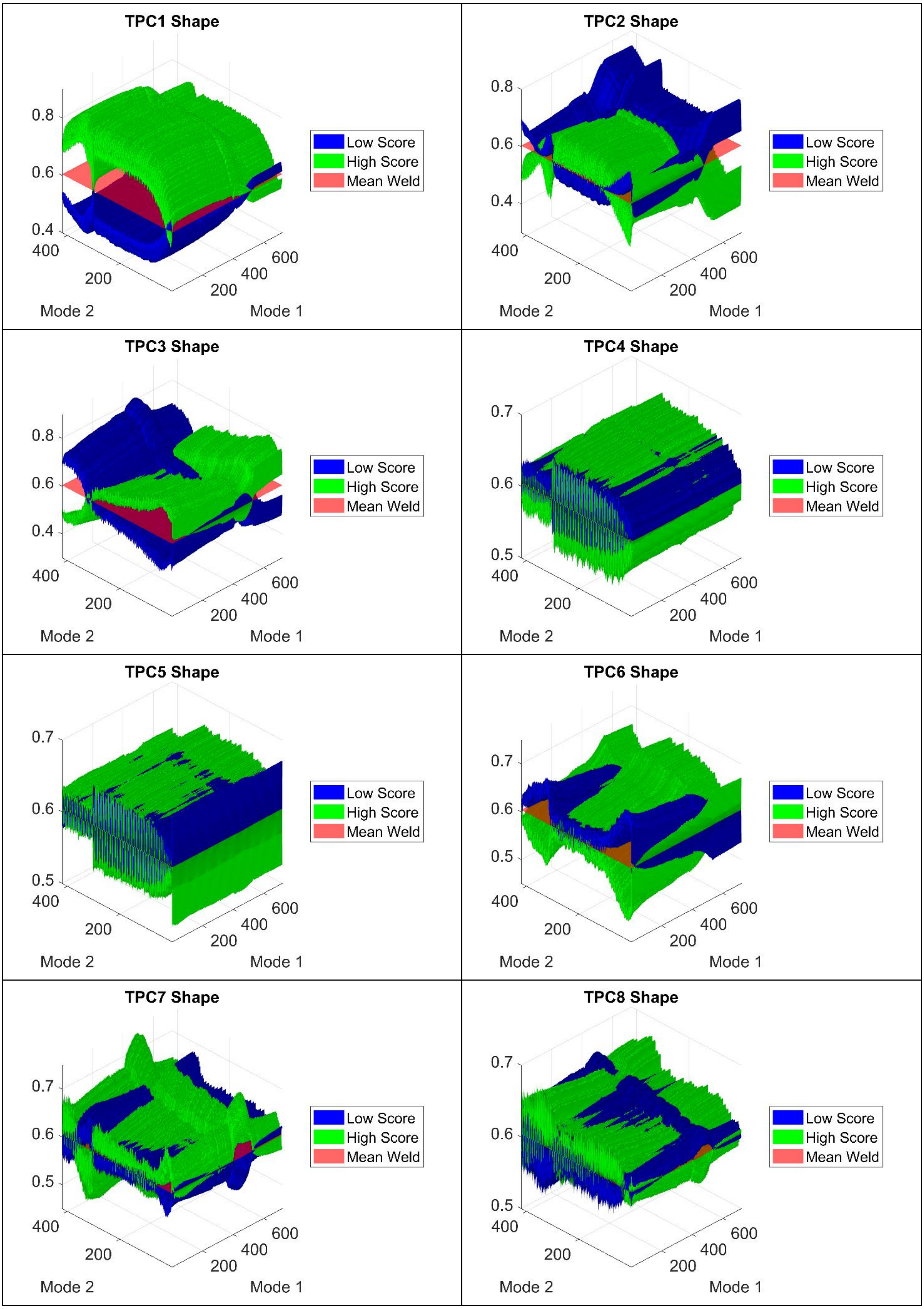

Figure 6-17: Representative tensor principal components from the leave-one-out method

The first tensor principal component shows large variation in the height of the tensor with some additional features. The features include points on the tensor where the green and blue surfaces intersect. These are early in Mode 1 (which corresponds to the displacement signal) and at 0 and 300 along Mode 2 of the tensor (which corresponds with the resistance signal). These points on the tensor all correspond to parts of the original signals that are always similar values, the resistance as the current is ramping up, and the beginning of the displacement curve which is set at zero so relative change in displacement can be measured from the start of welding.

The points at 0 and 300 on Mode 2 correspond to the start of the welding cycle and the start of the pre-heating cycle. At both of these points in time the current ramps up from zero as fast as the welder can achieve and this means that the resistance at this point in time can often be similar as it is a characteristic of the machine.

There is one other minor feature which is at the beginning of Mode 1 and the end of Mode 2 where the surfaces intersect which is not just variation in the heights of the tensors. This shows correlation between the forging part of the displacement signal (once the welding current has stopped) and the resistance at the beginning of the process.

Interestingly, the 1st tensor principal component (Figure 6-17) was not found to be correlated with the tensile strength in the models produced (Figure 6-15). This means that direct correlation between the overall heights of the two signals is not correlated with weld strength which suggests that the relationship to weld quality of the interaction is more complex than the average magnitude of the signals. The later tensor principal components which represent interactions at specific locations on the tensor are more related to weld quality than the overall height of the tensor.

The second tensor principal component scores were very weakly negatively correlated with tensile load (Figure 6-15b), meaning that a high score was weakly correlated with a low tensile load. A high score for TPC2 shows a signal interaction which is high in quadrant one and low in all other quadrants, suggesting that there was a weak interaction between the signals in which they are both initially high and then both low towards the end. The fact that this was found to be weakly correlated with tensile load may suggest that there was high heat input resulting in high thermal expansion for some welds at the start of the process and then low resistance with low electrode displacement at the end. This may be due to the material fusing too early in the process from the current in the pre-heating phase, significantly reducing the resistance and resulting in insufficient heat during the welding phase. This would cause low resistance and low thermal expansion in the second half of the process and result in a poorer quality weld. A low score for the second tensor principal component was weakly correlated with a weld of a high tensile load bearing capacity which relates to a lower than average resistance and thermal expansion during the pre-heating phase with more heat and thermal expansion in the welding phase.

Most of the variation for the third tensor principal component appears along the 2nd mode of the tensor. This would suggest there are a number of welds with resistance signals far from the mean with displacement signals that are very similar to the mean displacement signal. Because of the signal scaling necessary for the multiplication, a mean signal does not contribute to the tensor, only variation from the mean. The third tensor principal component is negatively correlated with the tensile load of the welds from the tensile shear test. This suggests that a weld with a low tensor principal component score (which is correlated with a higher tensile load) has a below average resistance signal during the pre-heating phase and a higher than average resistance during the welding phase. This is similar to the second tensor principal component but without as much contribution from the displacement signal. The higher resistance during welding equates to a higher heat input into the joint which is known to be correlated with weld quality.

Tensor principal component seven was found to be strongly positively correlated with the tensile load of the welds and shows a ridgeline in the area of the displacement curve that is during the welding phase of the process. This is known to be well correlated with weld quality as it demonstrates high thermal expansion in the welding phase. This is not the only interaction that is encapsulated in this tensor. The region of the tensor early in Mode 2 (resistance) and throughout Mode 1 (displacement) of the tensor shows a level of interaction between the two signals which may relate to the initial resistance and how this effects the rest of the process. Tensor principal components four and five appear to be dominated by the high frequency noise in the resistance signal and were not found to be useful in many of the models.

The TPCA was used to extract information from tensors calculated from two welding signals which showed interactions between the two signals. These interactions proved useful for weld quality monitoring creating a good model for the challenging task of aluminium RSW weld quality monitoring. The coefficient of determination (R^2) between the predicted and actual values of the weld lobe and electrode wear data is high with a consistent and relatively low RMSE (~16% of the mean tensile load of the welds). Notably, the first tensor principal component was not found to be correlated with the tensile load of welds which shows that the major signal correlations are not actually useful for weld quality monitoring in aluminium.

6.5.7 Modelling Button Diameter

Given the industrial context of the project, it is of interest to be able to predict the measured button diameter of a spot weld as this is the most common quality metric used in industry for RSW. The leave-one-out methodology was used to maximise the available training data for the button diameter model as only one in ten welds in the electrode wear dataset were subjected to a chisel test and half of the weld lobe data. The predicted button diameters are plotted against the measured button diameters in Figure 6-18.

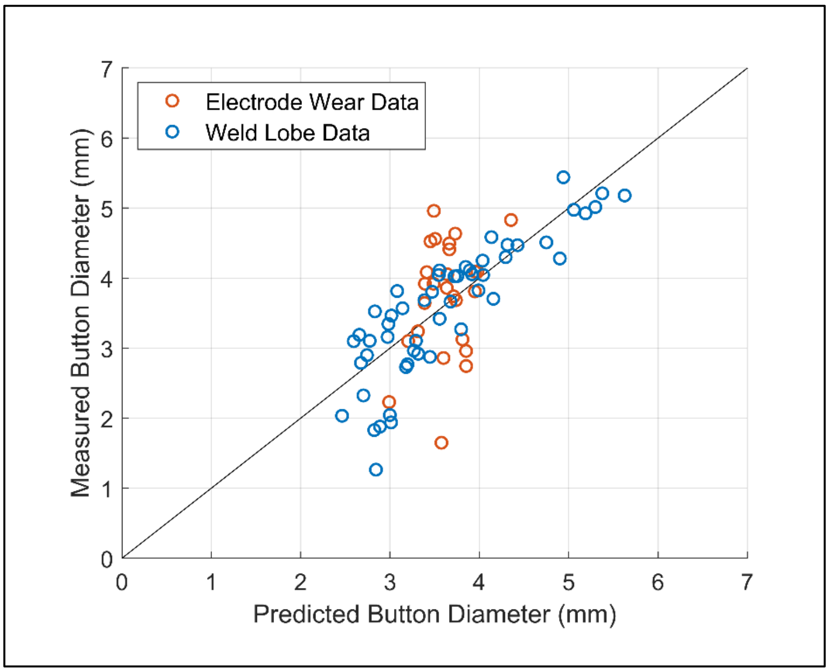

Figure 6-18: TPCA button diameter model using leave-one-out

Only 26 welds from the electrode wear dataset and 52 welds from the weld lobe dataset resulted in measureable button diameters from the chisel tests which reduced the available training data for modelling. The model for button diameter shows relatively good correlation between the predicted and measured button diameter taken from a chisel test with a correlation coefficient of $R^2 = 0.55$ and an RMSE of 0.60mm, however the model is not as good as the tensile load model. As the button diameters get smaller the error increases. This is a particular challenge associated with this particular destructive test, because as the fused zone gets smaller the result of the chisel test is more variable.

The button diameter of a weld from a destructive chisel test can sometimes be un-representative of the true spot weld quality. The result of the chisel test in aluminium RSW can often be affected by porosity and cracks in the spot weld caused by thermal contraction in aluminium. The button diameter presented in this case study is the average of two button pull-out measurements as recommended by The American Welding Society (2013). However, it does not account for partial thickness fractures, or interfacial fracture which is much more common in aluminium than in steel.

For every iteration of the leave-one-out methodology the tensor principal components significantly correlated with the button diameter were 2, 3, 7 and 8. This is interesting as it is the same tensor principal components that were most frequently found to be correlated with tensile strength in the previous section. This shows that the signal interactions shown by the tensor principal components do relate to aspects of the process that are related to quality. However further work is required to improve button diameter predictions.

6.6 Conclusion

The prediction of tensile strength under challenging experimental conditions was achieved with success using the TPCA methodology. Tensor principal component analysis was able to find aspects of the tensored welding signals that were indicative of the tensile load of the weld. Vast amounts of welding data were reduced to four tensor principal component scores for each weld which could be used in a linear regression to predict the welds tensile load before failure as well as the button diameter of welds from a chisel test. Reducing the welding data into tensor principal components revealed several interesting signal interactions that could not have been found using PCA.

The model for tensile load of the weld lobe and electrode wear data had a relatively high R^2 with a consistent level of error across the entire dataset. This shows that the features extracted from the signal data are related to the tensile strength of welds in very different conditions, varied electrode force and welding current as well as in cases with significant electrode wear.

The prediction of button diameter for the electrode wear and weld lobe data was not as successful as the prediction of the tensile load and was affected by a smaller training dataset. The prediction of button diameters in aluminium RSW quality monitoring will be investigated further in the next chapter, Chapter 7 which tests the TPCA methodology for predicting button diameter with large datasets in industrial aluminium resistance spot welding trials.

Chapter 7

Industrial Case Study: TPCA Quality Monitoring for Aluminium RSW

Publications relevant to this chapter:

- *A comparison of resistance spot weld quality assessment techniques, Summerville, C., Compston, P., Doolan, M., Procedia Manufacturing 2019.*

This Chapter presents the application of the TPCA-based weld quality monitoring technique developed in Chapter 6 to a large collection of industrial data provided by our industrial partner. This chapter will show that:

- TPCA can be used to model the button diameter of aluminium spot welds over a wide range of challenging experimental conditions that are of particular interest to the automotive industry.

- TPCA is more successful than single signal PCA based models for modelling aluminium weld quality over the broad range of faults, and that this is due to the information encapsulated by the tensors calculated from multiple welding signals.

- The interacting behaviour of the signals analysed using TPCA is useful for modelling a number of particular faults that can cause poor quality welds.

7.1 Introduction

Through our industry partner we were granted access to 51 different experimental datasets including approximately 4500 welds. The datasets included different aluminium sheet metal grades, gauges, weld schedules and process faults that could not be achieved in the laboratory at the ANU. TPCA was used to calculate models for the button diameters of the industrial data and this confirmed the performance of the TPCA weld quality monitoring technique with welds in an industrial setting.

The data was collected using a state-of-the-art servo-driven welder capable of clamping forces up to 10kN and constant welding currents of up to 50kA for welding thick gauges of aluminium. The datasets included 3 different material stacks with 10 different experimental conditions. Three sheet metal stacks were a 0.9mm – 0.9mm, 1.1mm – 1.4mm and 3.0mm – 3.0mm created with a proprietary 6xxx series aluminium alloys. For each weld two key signals were recorded (resistance and electrode force) as well as comprehensive destructive testing data.

7.2 Results

The different weld schedules used in the industrial data including which sheet metal stack and alloy they were used for is shown in Table 7-1. Four different weld schedules were applied in the 1.1mm – 1.4mm material stack (XKQ, XKR, XKT and XKU datasets) and two for the 0.9mm – 0.9mm material stack (XJE and XJF datasets).

Table 7-1: Dataset weld schedules and material stack configuration

	Schedule Time (ms)	Clamping Force (kN)	Schedule Current (kA)	Sheets (mm)	Material
XKQ	50 + 70	3.8	8 + 20	1.1 – 1.4	AA6xxx
XKR	50 + 70	4.75	8 + 21	1.1 – 1.4	AA6xxx
XKT	50 + 130	3.8	8 + 22	1.1 – 1.4	AA6xxx
XKU	50 + 130	4.75	8 + 21	1.1 – 1.4	AA6xxx
XJE	400 + 100	3.5	6 + 24	0.9 – 0.9	AA6xxx
XJF	400 + 100	3.8	6 + 22	0.9 – 0.9	AA6xxx
XJI	400 + 100	8.0	8 + 48	3.0 – 3.0	AA6xxx

Table 7-2 shows the different experimental conditions (or faults) that were investigated across the seven datasets and the number of welds in each. For every weld, resistance and force signals were collected by the weld timer and all welds were subjected to a roller peel test with a number of quality metrics recorded. Not all welds failed by complete button pull-out which is summarised in Table 7-3.

Table 7-2: XKQ, XKR, XKT, XKU, XJE, XJF and XJI dataset summary

		Number of Welds						
Letter	Condition	XKQ	XKR	XKT	XKU	XJE	XJF	XJI
-	Baseline	90	90	90	90	90	90	90
A	Adhesive	90	90	90	90	90	90	90
B	5° Tilt	90	90	90	90	90	90	90
C	1.6mm Gap	90	90	90	90	90	90	
D	Increase Force 25%					90	90	
E	Decrease Force 25%					90	90	90
F	Change one sheet to 1.0mm AA5754					90	90	90
G	Equaliser turned off	90	90	90	90	90	90	90
I	Tip dress at start of test only					90	90	90
J	2mm axial electrode misalignment					90	90	90
						Total	**4320 welds**	

The specifics of the different fault conditions are shown in Section 3.5.2 of the Methodology Chapter.

7.2.1 Destructive Testing

All welds were subjected to a roller peel test after welding (Figure 7-1). The roller peel test destroyed each weld individually so that its size and failure mechanism could be recorded.

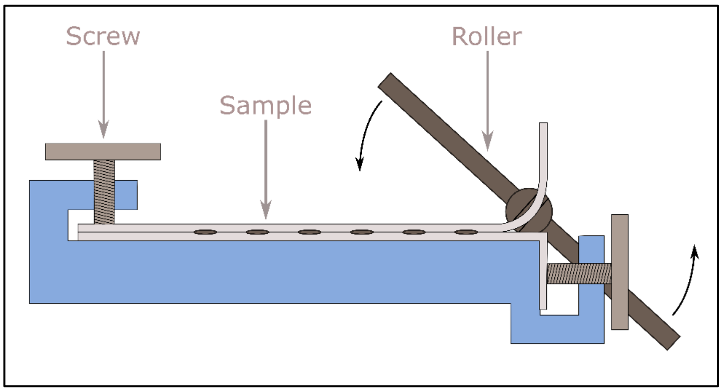

Figure 7-1: Roller peel testing setup

The roller tests were completed by an experienced technician and frequently produced a button diameter due to the peel load induced by the test. The data recorded from the destructive tests included fracture mode, major and minor button diameters, major and minor partial thickness diameters, major and minor interfacial diameters, sheet indentation and presence of expulsion on the top, bottom or faying surface.

The average of the major and minor button diameters for welds that failed by fracture mode 1 in the seven datasets are shown in Figure 7-2, Figure 7-3 and Figure 7-4. Only welds that failed by pure button pull-out were modelled due to the challenges associated with comparing welds with different fracture mechanisms. Failure mechanisms that have button pull-out as well as partial thickness fracture or partial interfacial failure are not included because the button diameter is not representative of the nugget diameter or weld quality. Modelling the 8 different possible fracture mechanisms identified by the AWS (2013) is beyond the scope of this thesis. Given enough data this should be possible, but it would be more useful to be able to identify porosity or cracking in the weld so that those welds could be identified in production as substandard welds.

From destructive testing of the 11 different fault conditions across the 7 different weld schedules and 3 unique material stacks, the number of welds that failed with complete button pull-out was 4054 and is broken down by dataset and experimental condition in Table 7-3.

Table 7-3: Welds that failed with complete button pull-out

		Number of Welds						
Letter	Condition	XKQ	XKR	XKT	XKU	XJE	XJF	XJI
-	Baseline	90	90	90	90	90	90	90
A	Adhesive	69	68	80	70	89	89	45
B	5° Tilt	90	78	90	86	90	90	68
C	1.6mm Gap	6	82	22	70	62	52	
D	Increase Force 25%					86	87	
E	Decrease Force 25%					90	77	90
F	Change one sheet to 1.0mm AA5754					90	88	90
G	Equaliser turned off	82	75	89	84	88	89	90
I	Tip dress at start of test only					77	86	90
J	2mm axial electrode misalignment					86	90	90
						Total	**4054 welds**	

There were 266 welds removed from the 4320 welds in the study. From Table 7-3 it can be seen that the gap condition for the XKQ and XKT datasets had very few welds that failed by complete button pull-out (6 and 22 respectively) making them challenging to calculate a model for.

The average button diameters of welds that failed with complete button pull-out are summarised in Figure 7-2 (1.1mm – 1.4mm data), Figure 7-3 (0.9mm – 0.9mm data) and Figure 7-4 (3.0mm – 3.0mm data). The average button diameter is calculated from the major and minor button diameters.

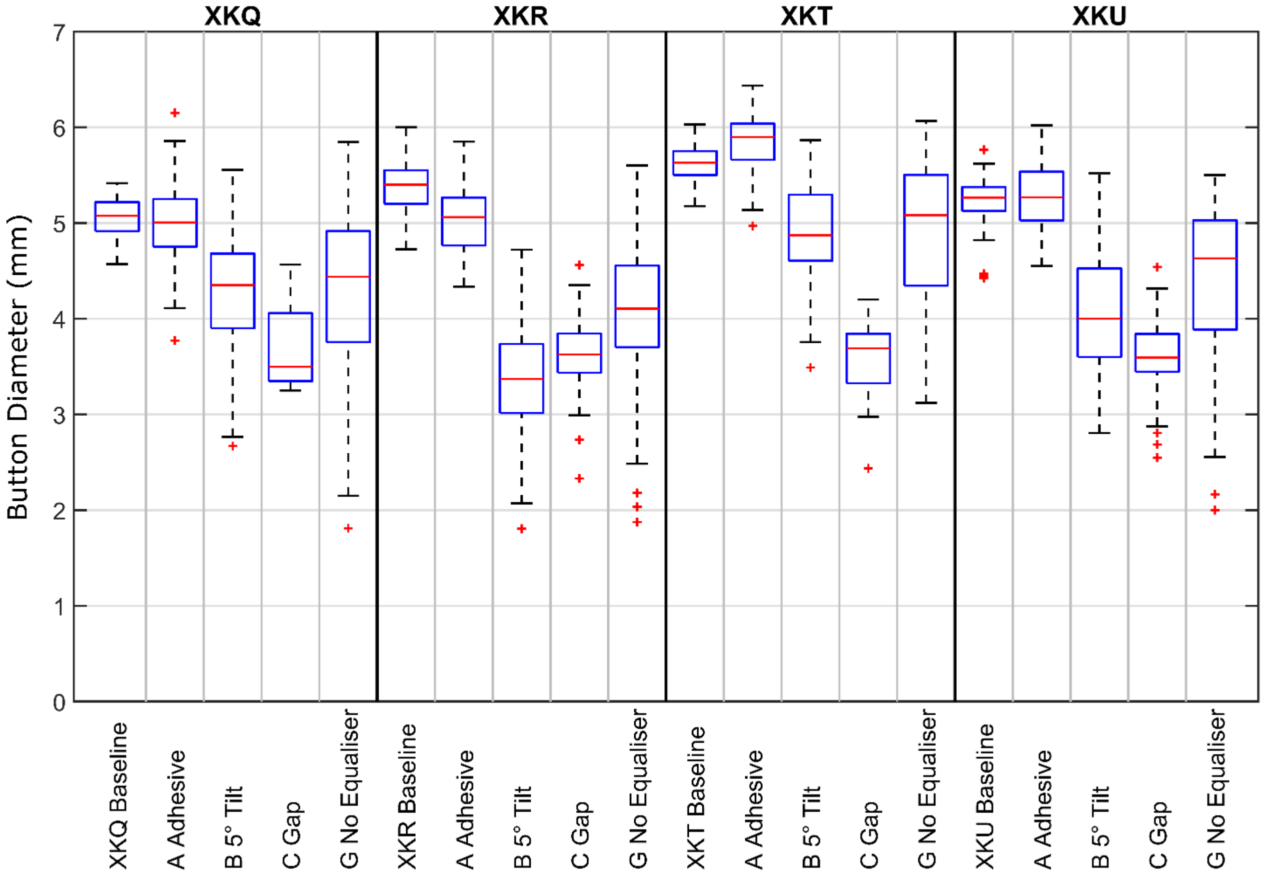

Figure 7-2: Button diameter boxplots for the 1.1mm – 1.4mm datasets and experimental conditions (fracture mode 1 only)

The adhesive, tilt and no-equaliser conditions resulted in a large spread in measured button diameters for welds that failed through pure button pull-out (Figure 7-2). The gap condition caused many welds to fail by fracture mechanisms 5 and 7 rather than pure button pull-out which reduced the number of welds available to calculate a model.

In the thinner XJE_D dataset (0.9mm – 0.9mm) the increase in clamping force significantly reduced the measured button diameters of a number of welds. The increase in force likely decreased the overall heat generated in the weld by reducing the interface resistance. The entire XJF dataset had a slightly lower average button diameter which is due to its higher clamping force and lower welding current (Table 7-1).

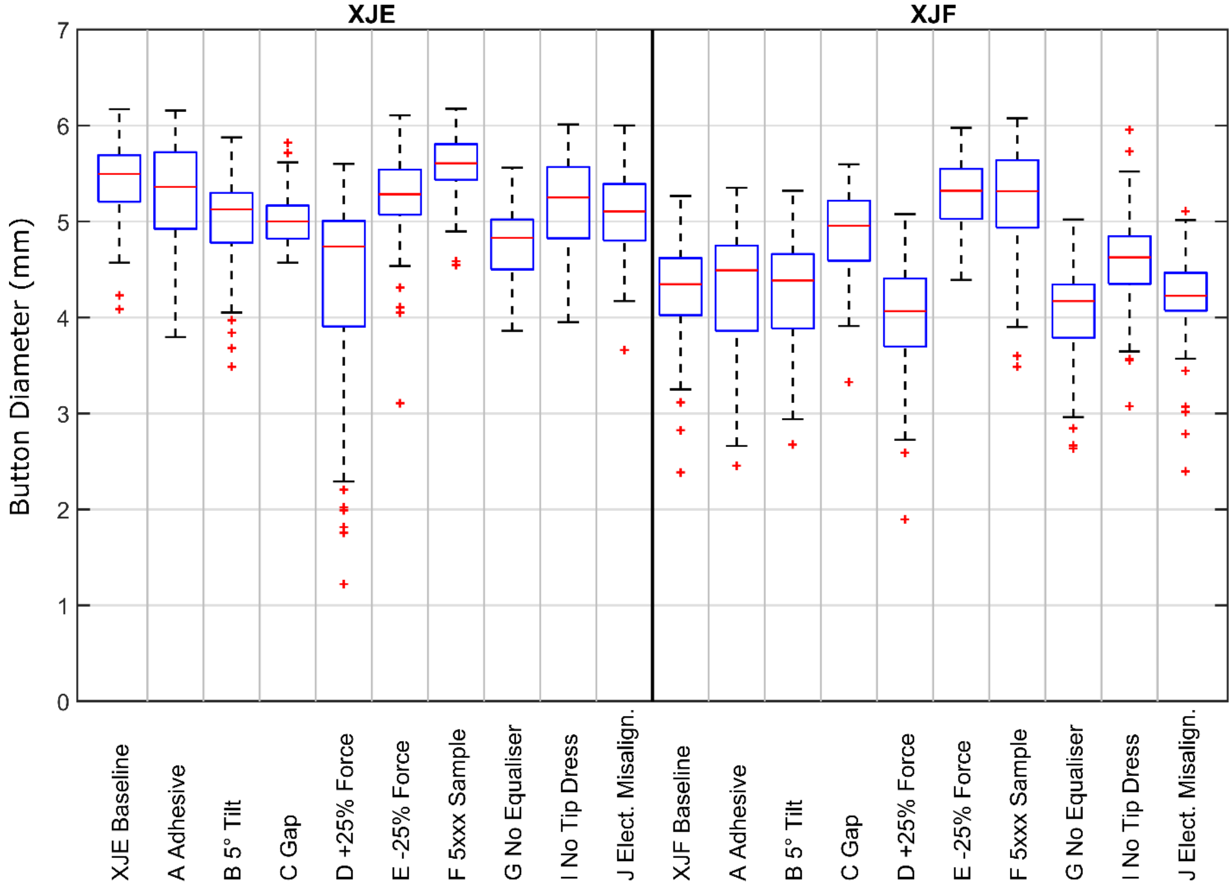

Figure 7-3: Button diameter boxplots for the 0.9mm – 0.9mm datasets and experimental conditions (fracture mode 1 only)

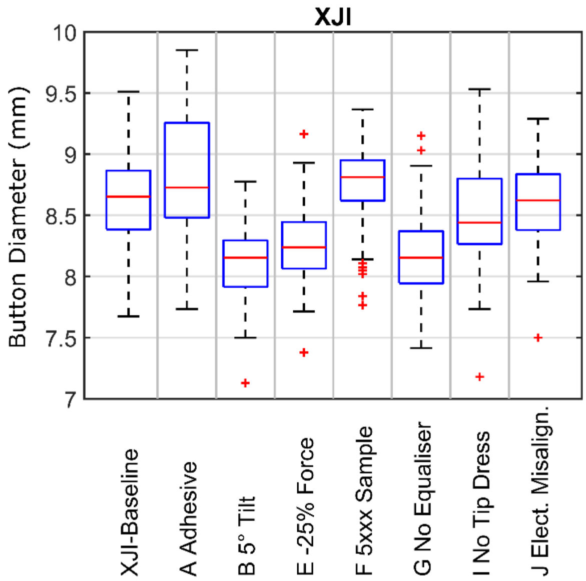

Figure 7-4: Button diameter boxplots for the 3.0mm – 3.0mm experimental conditions (fracture mode 1 only)

The baseline (control) condition for the seven material stacks resulted in 100% of the welds failing with pure button pull-out (fracture mode 1) and did not result in a wide spread of measured button diameters. This showed that the baseline weld schedules were appropriate for creating consistent, high quality spot welds.

The part gap fault did not cause a wide variation in pure button pull-out button diameters in any of the datasets, however this result was skewed by the number of welds that failed by fracture modes 5 and 7 instead of fracture mode 1.

The no-equaliser condition caused wide variation in the button diameters of the 1.1mm – 1.4mm data which was not seen in the 0.9mm – 0.9mm or 3.0mm – 3.0mm data suggesting the effects of this fault are not consistent across the different material stacks.

In the thicker 3mm – 3mm material stack (XJI) the adhesive fault caused half of the welds to fail by partial thickness fractures or interfacial failure, significantly reducing the number of welds that could be used to calculate a model.

The range of button diameters for the 3.0mm – 3.0mm data was comparable to the other datasets (approximately 2-3mm), however as a percentage of the average button diameters for each stack it was significantly smaller (Figure 7-4). Using the industry standard threshold for unacceptable button diameters ($4\sqrt{t}$) only seven welds or 1% of the 3.0mm – 3.0mm dataset were considered unacceptable (< 7mm). This shows the lack of variation present in this dataset, a factor that made it challenging to model.

7.2.2 Welding Signals

Welding signals were recorded for every weld on the weld timer. Current, voltage, resistance (calculated, secondary side) and electrode force were recorded at 1kHz. Some welds had to be removed from the fracture mode 1 data due to resistance or force signals that were very different from the expected signals. This was often due to severe expulsion or because the weld schedule selected was not able to overcome the induced process fault (such as part gap). The effects of the experimental conditions on the signals are shown by the mean signals for the 1.1mm – 1.4mm datasets in Figure 7-5. The effects of the experimental conditions on the signals of the 0.9mm – 0.9mm data are shown by the mean signals in Figure 7-6 and the same are shown for the 3.0mm – 3.0mm data in Figure 7-7.

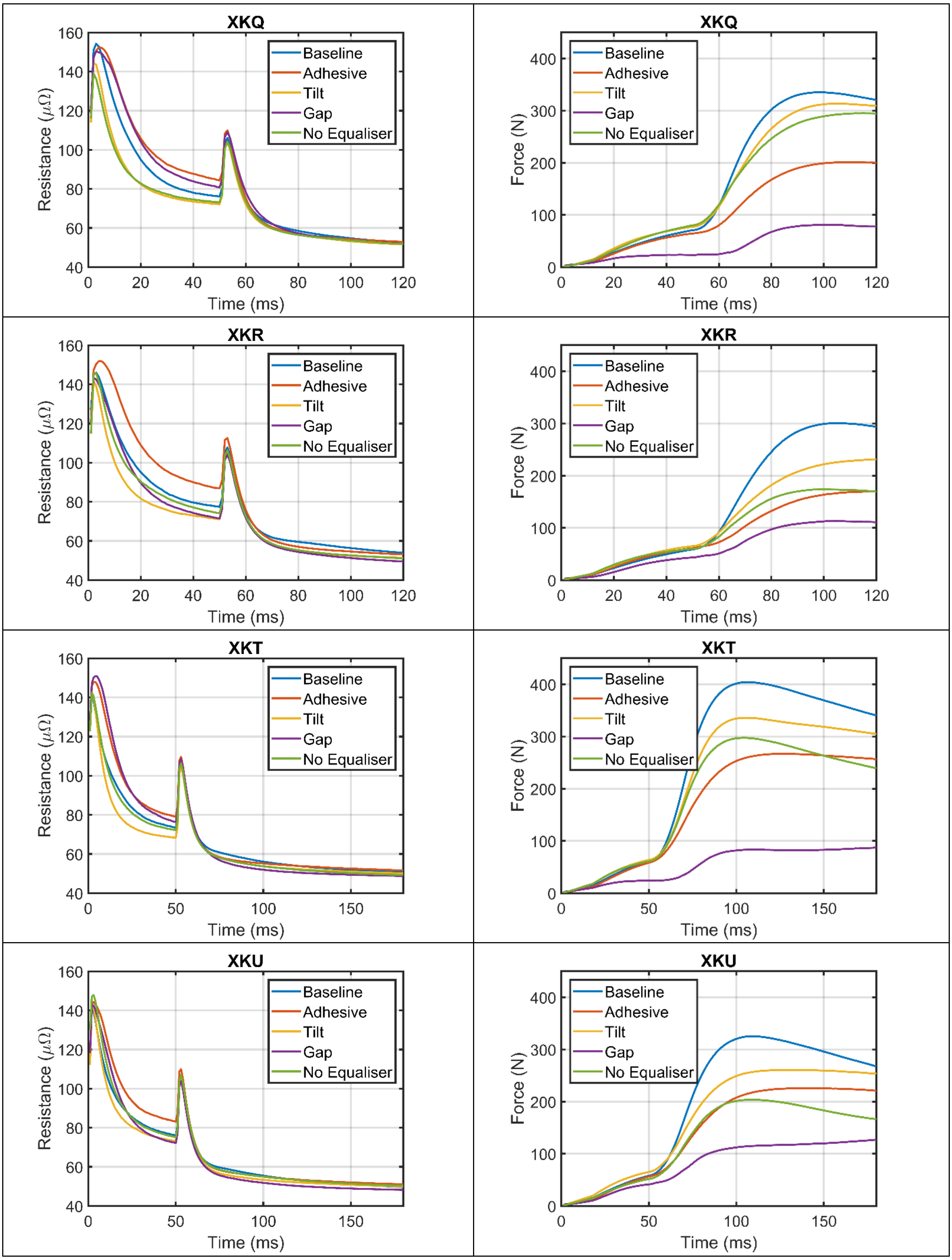

Figure 7-5: XKQ, XKR, XKT and XKU mean welding signals

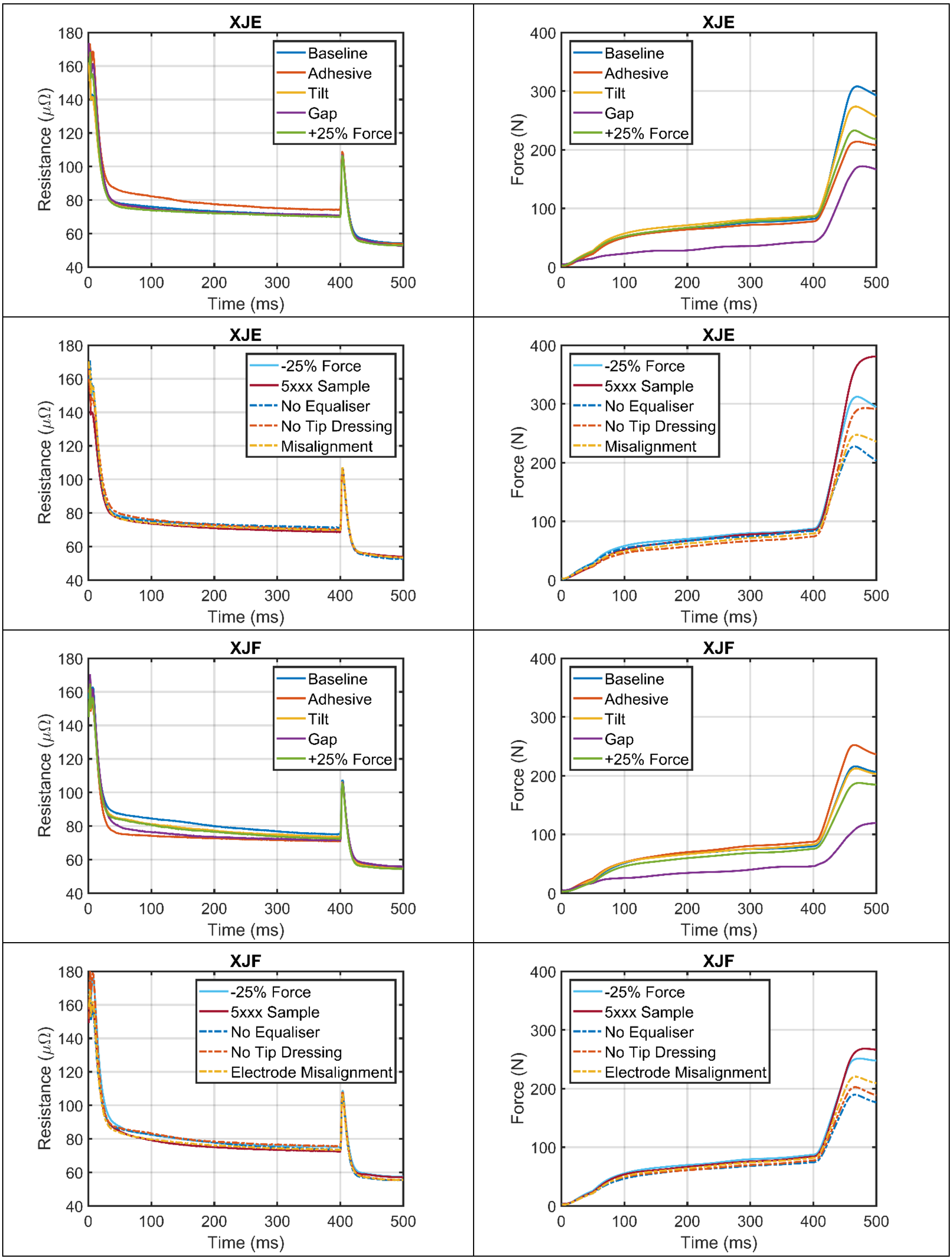

Figure 7-6: XJE and XJF mean welding signals

For the 1.1mm – 1.4mm datasets (XKQ, XKR, XKU and XKT, Figure 7-5) the fault conditions reduced the amount of thermal expansion during welding which is shown by the mean electrode force signals during welding compared to the Baseline condition. Most of the variation in the resistance signals can be seen in the pre-heating phase with only minute differences in resistance caused by the fault conditions during the welding phase. In some conditions the resistance during pre-heating phase was increased, and in some it was decreased with respect to the baseline condition.

The changes caused by the faults in the mean resistance and force signals for the 0.9mm – 0.9mm data were small (XJE and XJF, Figure 7-6). This may have been due to the lower bulk resistivity of the thinner material in the stack meaning that the changes in resistance were dominated by the oxide layer resistance. The minute variation in force signals may also be due to the thinner bulk material and the reduced force from thermal expansion.

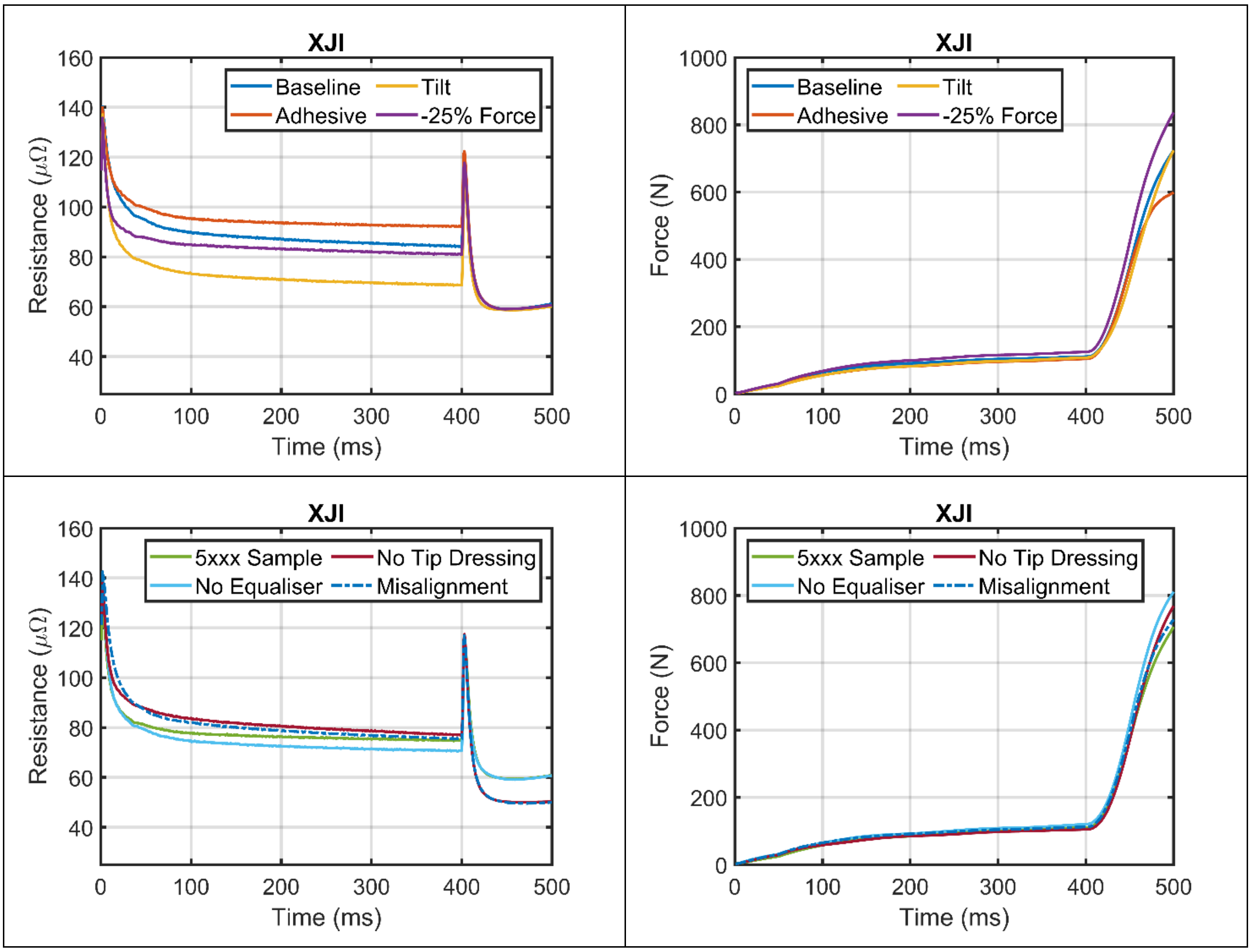

Figure 7-7: XJI mean welding signals

The variation in the force signals of the 3.0mm – 3.0mm data (XJI, Figure 7-7) was relatively similar in magnitude to the variation in the other datasets although much smaller with respect to the total increase throughout the entire welding cycle. Interestingly there was more variation in resistance during the pre-heating cycle for this material stack. There was very little variation during welding in resistance caused by the fault conditions compared to the baseline with the exception of the no tip-dressing and axial electrode misalignment faults which caused a distinct decrease in resistance during the welding cycle.

7.3 Button Diameter Modelling using Tensor Principal Components

Aluminium spot weld quality is particularly susceptible to small changes in the process and this can make it very challenging to model. As aluminium is used more and more in automotive bodies aluminium weld quality monitoring is becoming more important.

In this chapter, welds that failed by fracture mode 1 were modelled, which covered the vast majority of welds in the entire dataset. The investigation of predicting weld quality for different fracture modes was left for future work.

TPCA was introduced in Chapter 6 to investigate the interactions between 2 or more welding signals for weld quality monitoring. This included more information about the process than either signal individually and only required one set of principal components to be calculated (compared to the methodology in Chapter 5). The tensors calculated from welding signals showed the interactions of the signals at different parts of the process but also included the interaction between the two signals at the same points in time (represented on the main diagonal of the tensor). The tensors also represented aspects of both the original signals in the analysis.

This section will:

1. Model the quality of the industrial welding data using TPCA. The specifics of the datasets will be discussed later in section 7.2.

2. Compare the TPCA models to PCA models using the same signals to show the improvement that results from analysing the interactions of the two signals using TPCA.

3. Show which faults the TPCA model outperforms the PCA models of both signals, showing where signal shape interactions are important for weld quality monitoring.

4. Demonstrate the insights that can be drawn from calculating tensors from welding data for weld quality monitoring.

5. Discuss the process faults with signal shape interactions that were important for weld quality monitoring.

To incorporate the interacting signal shapes from both signals into one model, TPCA was used to model the button diameters of each of the 51 datasets (using the same method as Chapter 6). Tensors were calculated for each weld using the resistance and electrode force signals recorded by the weld timer. The comparison to the PCA models is shown in Figure 7-8 a) and is as follows:

- In 63% of the datasets TPCA was found to be as good as or better than the leading PCA model without having to choose which signal to monitor.

- One third (33%) of the datasets were unable to be modelled using the signal information collected with all 3 options (PCA of Resistance, PCA of Force and TPCA) unsuccessful at modelling weld quality.

- For two of the datasets (4%) the Force signal PCA model was slightly better than TPCA. In one case both models were good and in the other case neither was particularly successful at modelling button diameter.

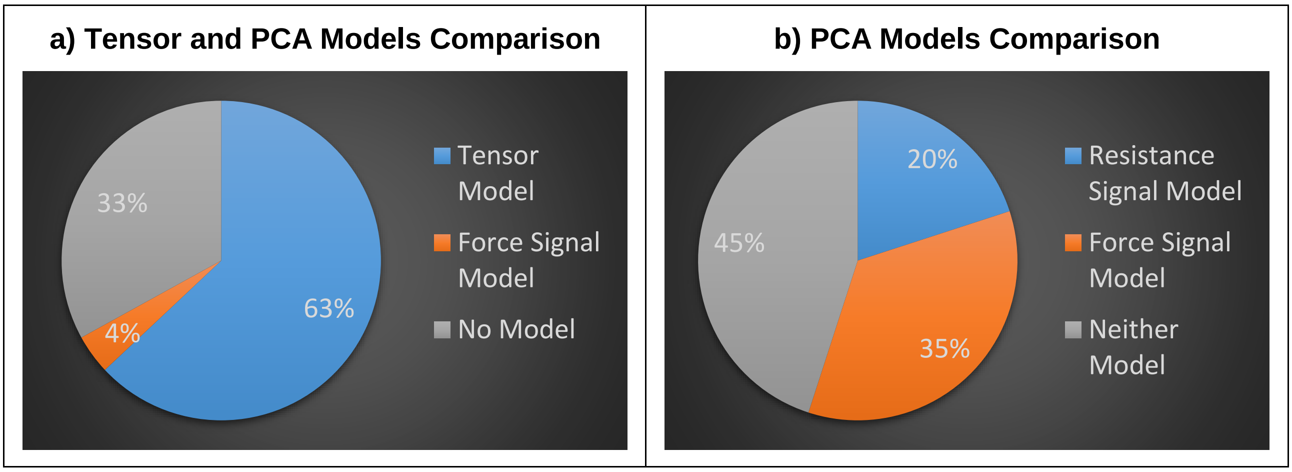

Figure 7-8: The model that performed best for each of the 51 datasets, (a) TPCA and PCA, (b) PCA models only

Figure 7-8 b) shows that using PCA of one signal for weld quality monitoring presents a difficult decision with neither signal producing a useful model for the majority of datasets.

TPCA represents a stronger technique for modelling a wide range of welding conditions in aluminium RSW than analysis of an individual signal using PCA. Table 7-4 summarises the datasets where TPCA outperformed both PCA models by a margin of $R^2 \geq 0.1$, showing the importance of the interactions between the two signals for some common fault conditions.

Table 7-4: R^2 values for the datasets where TPCA outperformed both PCA models

		R2		
Dataset	Condition	PCA Resistance	PCA Force	TPCA
XKR_A	Adhesive	0.27	0.21	0.50
XKT_A	Adhesive	0.32	0.30	0.47
XKU_A	Adhesive	0.48	0.49	0.62
XJE	Baseline	0.02	0.08	0.4
XJE_E	Decrease Force 25%	0.05	0.20	0.53
XJF_E	Decrease Force 25%	0.06	~	0.5
XJE_F	Change one sheet to 1.0 AA5754	0.07	0.38	0.54
XJF_F	Change one sheet to 1.0 AA5754	0.33	0.23	0.62
XJE_J	2mm electrode misalignment	0.27	0.21	0.43
	Colour definition (Performance)	Worst	Middle	Best

Table 7-5 summarises the datasets where TPCA performed particularly well (R^2 > 0.5 between the predicted and measured button diameters). The interactions shown by the TPCA were important for modelling adhesive, 5° tilt, no-equaliser, -25% Force and changing a single sheet for a 5xxx material conditions in a number of datasets.

Table 7-5: R^2 values of the datasets where TPCA found strong correlations to button diameter

Condition	Dataset	TPCA R^2
Adhesive	XKR_A, XKU_A, XJF_A	0.50, 0.62, 0.56
5° Tilt	XKQ_B, XKR_B, XKT_B, XKU_B	0.73, 0.51, 0.61, 0.69
No-equaliser	XKQ_G, XKR_G, XKT_G, XKU_G	0.56, 0.54, 0.64, 0.62
Decrease Force 25%	XJE_E, XJF_E	0.53, 0.50
Change one sheet to 1.0 AA5754	XJE_F, XJF_F	0.54, 0.62

The one third of datasets shown in Figure 7-8 a) that were unable to be modelled included fault conditions that resulted in challenging circumstances such as: insufficient variation in the measured signals, insufficient variation in the button diameters caused by the fault, or very erratic variation in failure mechanism due to the extreme nature of some of the faults. This made them particularly challenging to model regardless of the features that were extracted from the measured signals.

In Section 7.4 we will discuss why using the principal components of tensors calculated from the two welding signals resulted in successful model for two thirds of the datasets (Figure 7-4 a) when PCA of individual signals was not as broadly applicable.

7.4 Tensor Based Models

In Section 7.2 it was shown that TPCA based models worked for a wider range of datasets than a PCA based model. This is in part due to the tensors which capture information about the variation and signal shape of both signals as well as their interactions (through the use of the outer-product).

This section will show some examples of the experimental conditions where the signal shape interactions found using TPCA improved the modelling of weld quality compared to the PCA based model. Analysis of these cases shows which signal shape interactions were important for improving weld quality monitoring and allows us to infer the reasons why they are important.

7.4.1 Tensor Principal Component Shapes for Weld Quality Monitoring

The tensors calculated from welding data encapsulate information from both signals as well as the interaction of their signal shapes. This is exemplified in the adhesive conditions of the 1.1mm – 1.4mm datasets (XKQ, XKR, XKT and XKU) (summarised in Table 7-6).

Table 7-6: Adhesive dataset modelling summary

	Resistance Models		Force Models		Tensor Models	
Dataset	PCs	R^2	PCs	R^2	PCs	R^2
XKQ_A	1, 4	0.15, 0.33	1	0.46	1, 2	0.50, 0.06
XKR_A	1, 5, 6	0.22, 0.12, 0.09	1	0.25	1	0.54
XKT_A	3, 4, 5	0.09, 0.22, 0.10	1	0.33	1, 3, 7	0.45, 0.06, 0.06
XKU_A	3, 5	0.39, 0.12	1	0.51	1	0.63

In all four datasets, principal components of the resistance signal, force signal and signal tensor were found to be correlated with the button diameter of welds. For the adhesive condition the principal components of the force signals were more strongly correlated with button diameter than any of the principal components of the resistance signals. In all cases the first tensor principal component of the weld tensors had a stronger correlation with the button diameter of welds than any principal component of a single signal. This shows that the signal shape interactions found with TPCA are useful for modelling aluminium weld quality when adhesive is present. The first tensor principal components for these datasets have similar features (shown in Figure 7-9). The first principal components of the force signals all have similar features as well which relate to the amount of electrode displacement during the welding phase (Figure 7-10).

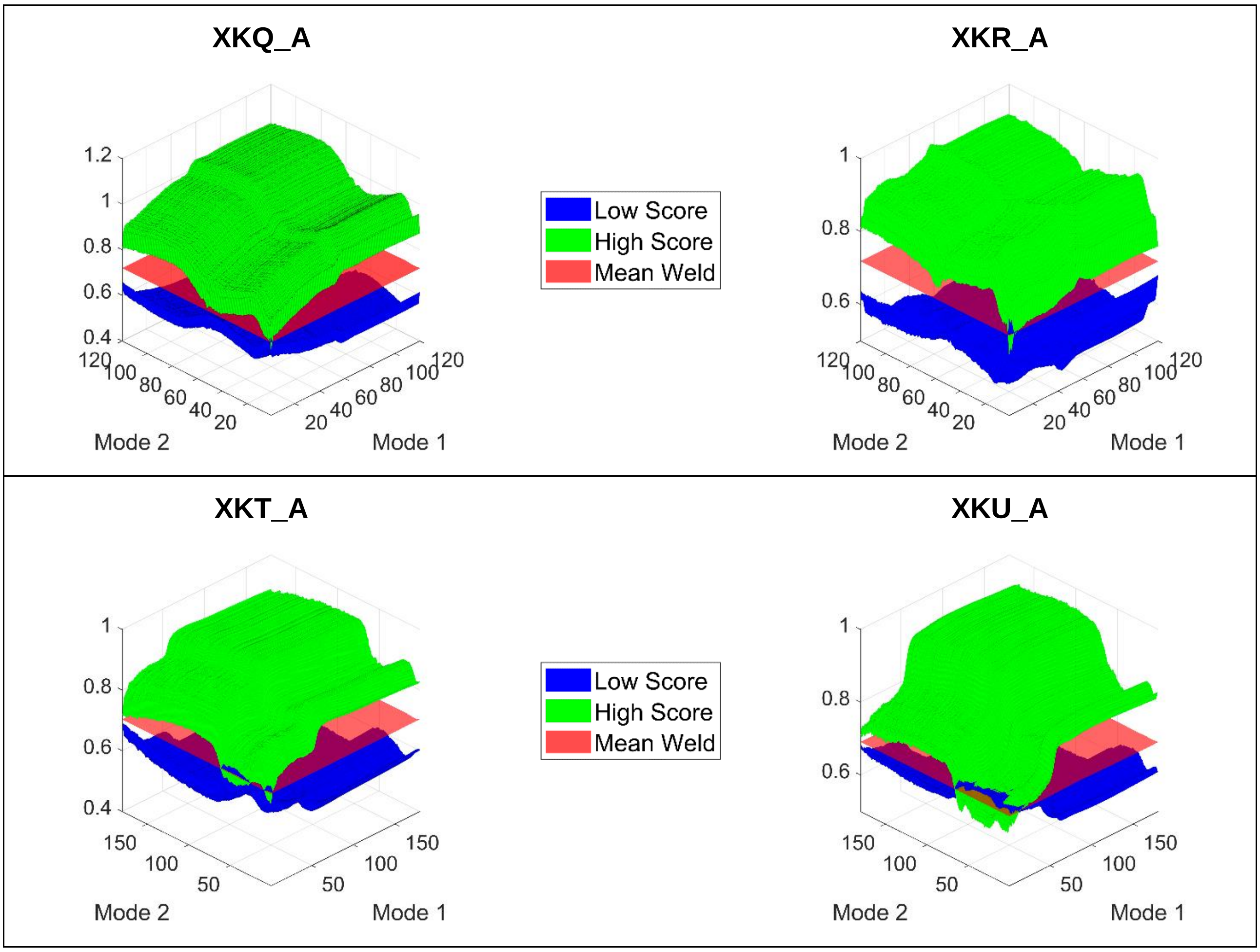

Figure 7-9: First tensor principal component shapes for the 1.1mm to 1.4mm adhesive datasets

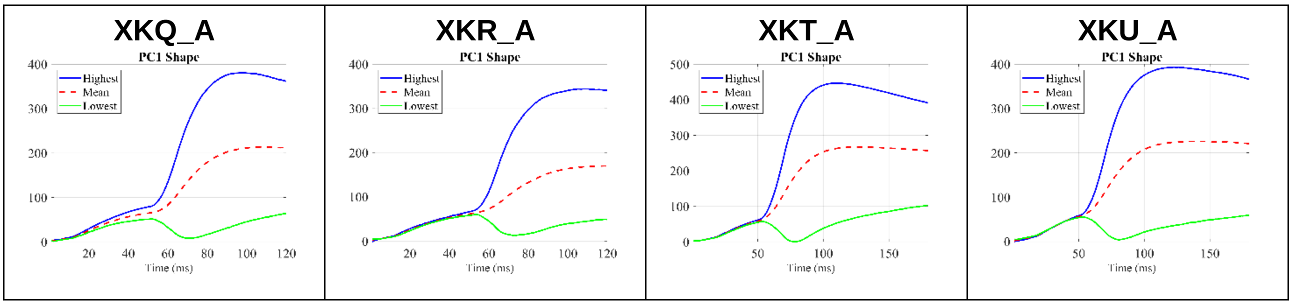

Figure 7-10: First principal component shapes of the force signals for the 1.1mm to 1.4mm adhesive datasets

The first tensor principal components for these datasets all had similar shapes broadly representing the height of the tensors with the exception of the region close to the start of both modes which is close to the mean tensor (Figure 7-9). Given that these tensor principal component shapes had the strongest correlation with button diameter of all the principal components, we can conclude that this is significant for weld quality monitoring. This shows that a tensor principal component shape which represents the height of the tensors (*both* signals above or below the mean, see Section 6.5.5 for the in depth interpretation) is important for modelling the adhesive fault for this material stack. This interaction cannot be identified by analysis of only one signal and the improvements in correlation are shown in Table 7-6.

Given the height of the tensor is correlated with larger button diameters it shows that when both the resistance and force signals are above the mean signal, a larger button diameter is more likely for the adhesive fault condition.

Direct comparison of the principal component shapes of the force signals (Figure 7-10) and the tensor principal component shapes in Figure 7-9 is challenging due to the scaling of the signals prior to calculating the tensors. However, it is clear that the first principal component of the force signals for each dataset relates to the amount of thermal expansion during the welding phase and this contributes to the height of the tensor during the welding phase even after scaling.

7.4.2 Increasing Modelling Performance using Tensors

The improvement in weld quality modelling is exemplified in the thinner 0.9mm – 0.9mm material stacks with the -25% electrode force fault. Figure 7-11 and Figure 7-12 show the models for button diameter created with PCA and TPCA respectively. It can be seen that the weld quality models calculated from the welding tensors (Figure 7-12) are more accurate than those calculated from principal components of the individual signals (Figure 7-11) and this is supported by the higher R^2 values and lower RMSE in Table 7-7.

Table 7-7: Summary of model statistics for Figure 7-11 and Figure 7-12

		PCA Resistance	PCA Force	TPCA
XJE_E	R^2	0.05	0.20	0.53
	RMSE (mm)	0.44	0.40	0.31
XJF_E	R^2	0.06	-	0.50
	RMSE (mm)	0.38	-	0.28
	Colour definition (Performance)	Worst	Middle	Best

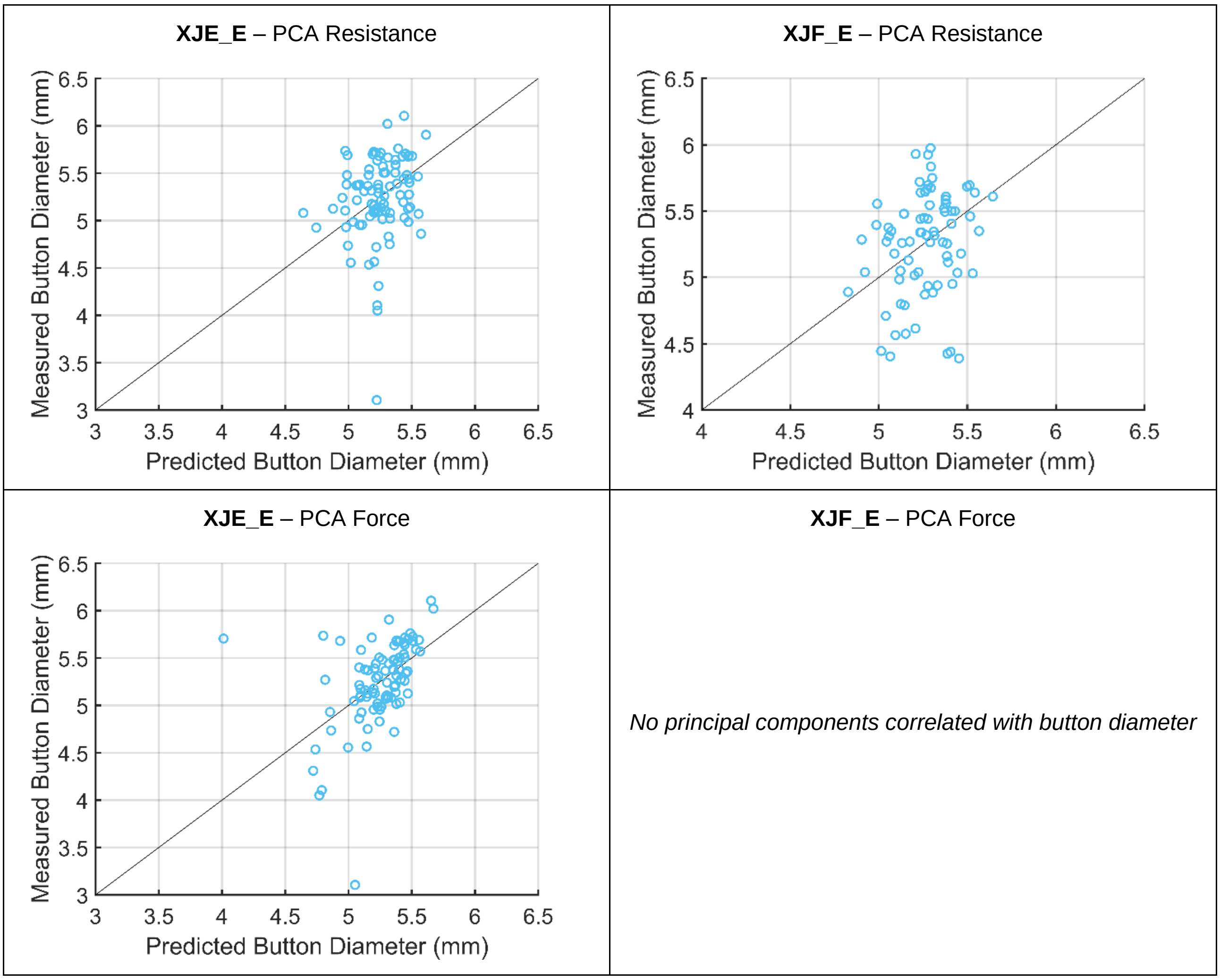

Figure 7-11: XJE_E and XJF_E datasets PCA models

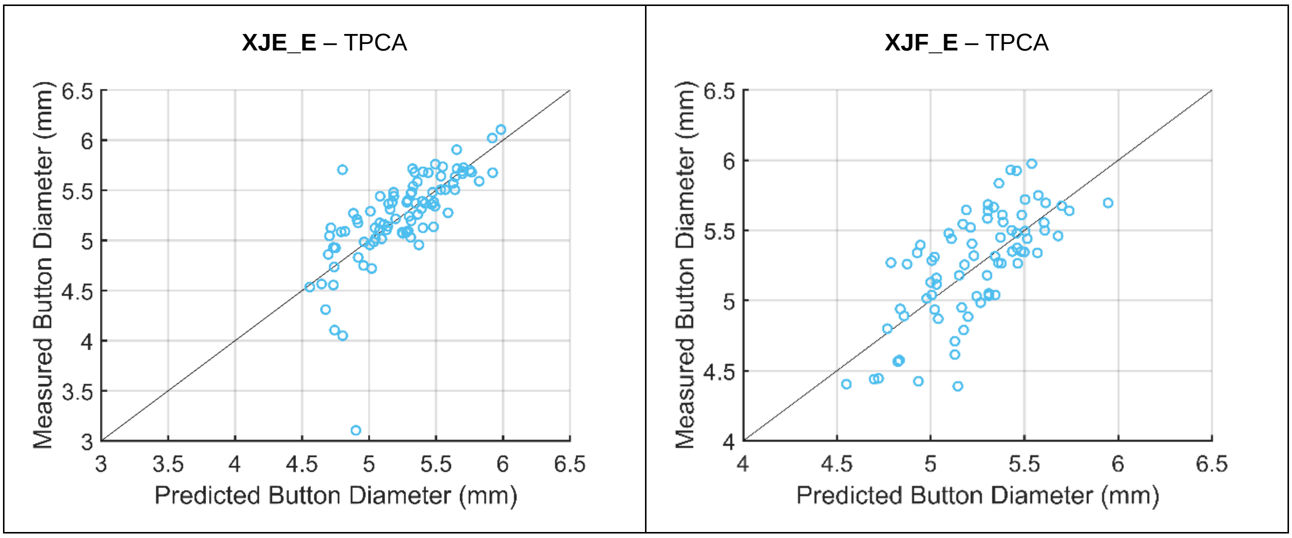

Figure 7-12: XJE_E and XJF_E datasets TPCA models

7.5 Conclusion

In this Chapter TPCA was used to model the button diameter of 51 datasets with different gauges, weld schedules and experimental conditions. The results of the TPCA models were compared to PCA based models to show the improvements that result from analysing the interactions of two signals.

The industrial data provided by our industry partner allowed for comprehensive testing of the TPCA based weld quality monitoring technique. The weld quality of more than 4000 welds was modelled under different experimental conditions and found to be successful with the signal information collected in approximately two thirds of the datasets.

For 63% of the datasets TPCA was found to be as good as or better than the PCA models calculated from the individual signals. In only 4% of the datasets PCA of the force signal was found to be slightly better than the TPCA model for button diameter. In 33% of the datasets the signal information collected from the weld timer could not produce a useful weld quality model using PCA or TPCA.

The implications of the results of this chapter are:

- TPCA can be used to analyse aluminium weld quality over a broad range of experimental conditions that are found in the automotive industry.

- TPCA allows for the analysis of multiple signals and includes the interacting behaviour of signal shapes.

- TPCA creates a more robust modelling approach than analysis of a single signal, as correlations with button diameter can be analysed for multiple signals in parallel.

Some further challenges lie in characterising welds that do not fail through pure button pull-out (fracture mode 1) which are often considered substandard welds. To achieve this, weld quality could be represented as the fusion diameter (greatest average diameter from pull-out, partial thickness fractures and interfacial failure) however, analysis of voids and cracks is likely to become very important to create a weld quality model for all aluminium welding conditions. More work is required to model the different fracture modes in aluminium RSW and this was deemed to be beyond the scope of this thesis.

Chapter 8

Discussion and Conclusion

8.1 Discussion

8.1.1 Weld Quality Monitoring Strategy

The strategy of the weld quality monitoring technique developed in this thesis was to search for underlying signal shapes in the data that were fundamentally related to the outcome of the welding process. This was achieved by inducing controlled variation in the training data and investigating how applicable these models were to more complex forms of variation. In reality, the complex nature of RSW and the number of factors that affect the outcome mean that finding the underlying signal shapes that are related to quality can be very challenging.

A different strategy was trialled to find the signal shapes related to weld quality which involved increasing the number of experimental conditions in the training data. This was done to try to capture more variation in the model in the form of faying surface modifications like gap and adhesive and changes at the electrode-sheet interface caused by turning off the welder's equaliser function (explained in Section 3.5.2) and tilting the electrodes away from the sheet. An example of this is shown in Figure 8-1 and Figure 8-2 with the XKQ-R-T-U data from Chapter 7. Each experimental condition was randomly split in half, half for training and half for validation. A TPCA model was trained on all the combined training welds and validated with the remaining welds.

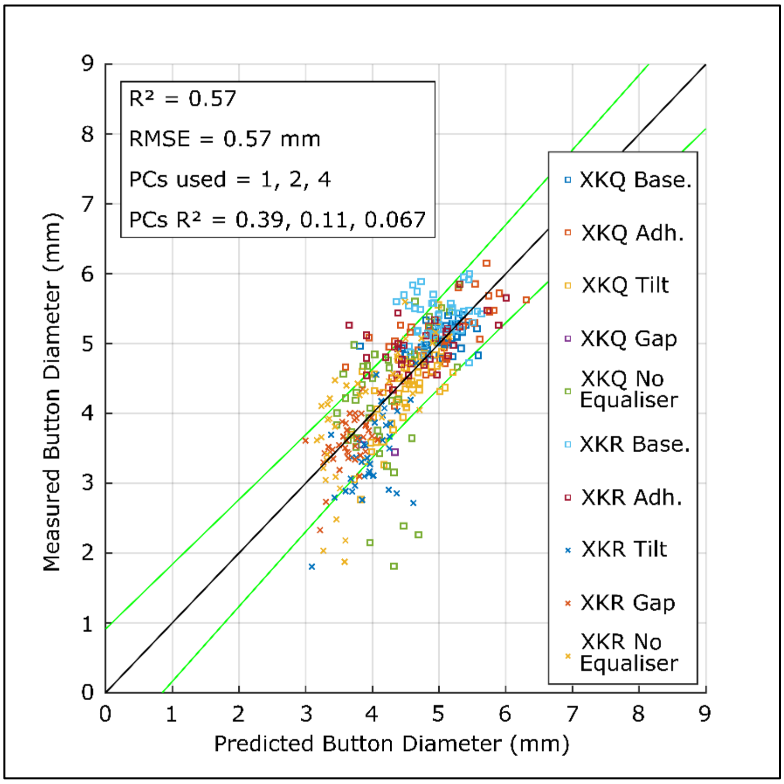

Figure 8-1: TPCA model for button diameter calculated from randomised selection of welds from the XKQ and XKR datasets from Chapter 7.

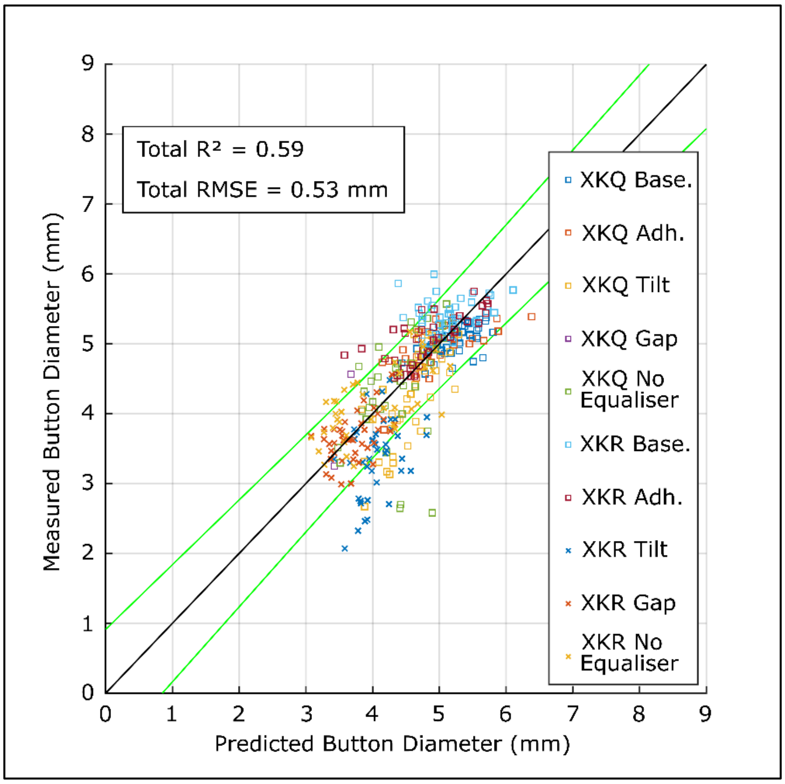

Figure 8-2: Application of the model in Figure 8-1 to the remaining welds.

It was found that the relationships between the signal shapes and weld quality became weaker as more information was added into the training data. The R^2 and RMSE values for the model and its application to the validation data were very similar suggesting the relationships in the model were equally applicable to the validation data. Some of the welds with lower measured button diameters (1.5mm – 3mm) were not very well predicted, with many falling between 3-5mm predicted button diameters. This may be in part due to the orthogonality of the principal components and that they describe unique aspects of the signals. If multiple experimental conditions had similar effects on the signal that did not affect the weld quality in the same way, this may explain the poorer performance of the model at the lower button diameters. This would be because the relationship between the signal shapes and weld quality are slightly different for the experimental conditions.

Adding many different types of variation into the training data would work well if each new experimental condition and factor that affected the process had a unique effect on the signal (which could be represented by a new principal component). However, this was not found to be the case. Similar signal shapes were found in datasets that had different effects on the weld quality under different experimental conditions.

To overcome this challenge, a different feature extraction approach could be considered such as Independent Component Analysis (ICA). ICA is similar to PCA but does not require that all components are orthogonal to one-another. The non-orthogonal nature of the components may account for the similarities in signal shapes caused by different experimental conditions while still allowing for them to be modelled independently. For signal shape analysis this could mean that new independent components could be used to describe each new experimental condition without reducing the overall model performance.

Unfortunately there are additional challenges associated with non-orthogonal approaches like ICA. Approaches such as ICA often involve an iterative process to determine the signal shapes from the training data. This means that a different result can be found each time the analysis is conducted. This makes it challenging to re-create models because the signal features can be different every time.

8.1.2 Signal Measurement Error

Throughout this thesis every effort was made to reduce the error in measurements through good wiring practices and using high-quality, highly sensitive measurement devices. However, the welding process involves high welding currents which generate magnetic fields and magnetic noise in the form of additional currents in the sensor wires which are difficult to completely alleviate. Signal measurement errors could have the potential to change the signal shapes selected in the PCA or TPCA and this would then effect their relationship to weld quality. These errors, and the effects they have on the training data and model are very hard to identify. Measurement errors are of course not related to weld quality and may in part explain some of the lower correlations with weld quality of the principal components extracted from the data.

In section 4.4 it was shown that outlier welds in a validation dataset (which were created with electrode tilt, which wasn't present in the training data) have very different welding signals (for reference Figure 4-18 is shown below). This can be considered analogous to the effects of signal measurement error for welds in production. The different welding signals, which contained signal shapes that the principal component training set was not trained on, produced very different principal component scores compared to the training data. This is because the new variation is spread across a number of the original principal components which do not efficiently describe the newly introduced variation. This is an example of validation data that is contaminated with new variation and was easily picked up in the validation stage, meaning that a technician could identify there was a problem and rectify the issue. If uncontrolled variance is present in the training data the effects are potentially harder to diagnose, which reinforces the need to collect the training data in a controlled environment.

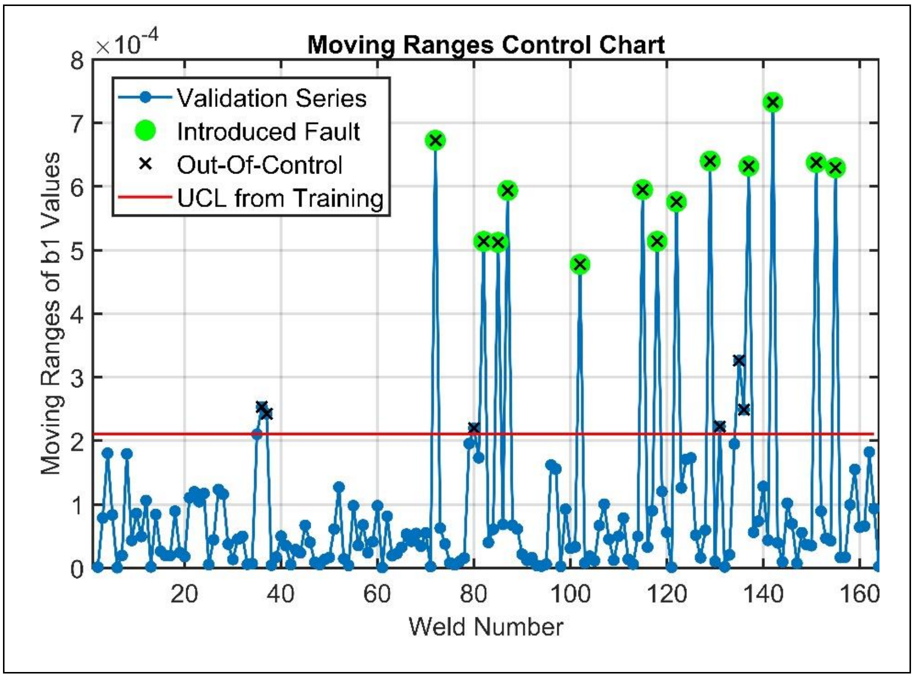

For reference Figure 4-25: Using principal components for outlier detection in steel welding process (Summerville et al., 2017)

If a training dataset is contaminated with uncontrolled variation or measurement error, this could skew the principal components, resulting in potentially meaningless correlations to weld quality. The fact that the model can *only* be as good as the training data used to train it could be considered a limitation of the approach. However, this would be the case with all modelling techniques, in that poor quality training data results in a poor model of the process. This again emphasises the importance of collecting good training data for weld quality monitoring. It should be noted that once a weld quality model is trained with good welding data, new influences to the welding process in validation are easily identified by the principal components scores as seen in section 4.4.

8.1.3 Sample Sizes and Principal Components

There are some general rules of thumb that are often applied in traditional PCA. To calculate a stable principal component matrix it is thought that the number of samples should be larger than the number of dimensions that are being investigated (Jung et al., 2009). This is because you want more points in the point cloud than the number of dimensions they are represented in. For instance you could not calculate four orthogonal principal components with only one data point. An example with many more points than dimension can be seen in Figure 6-6 which is shown below for reference.

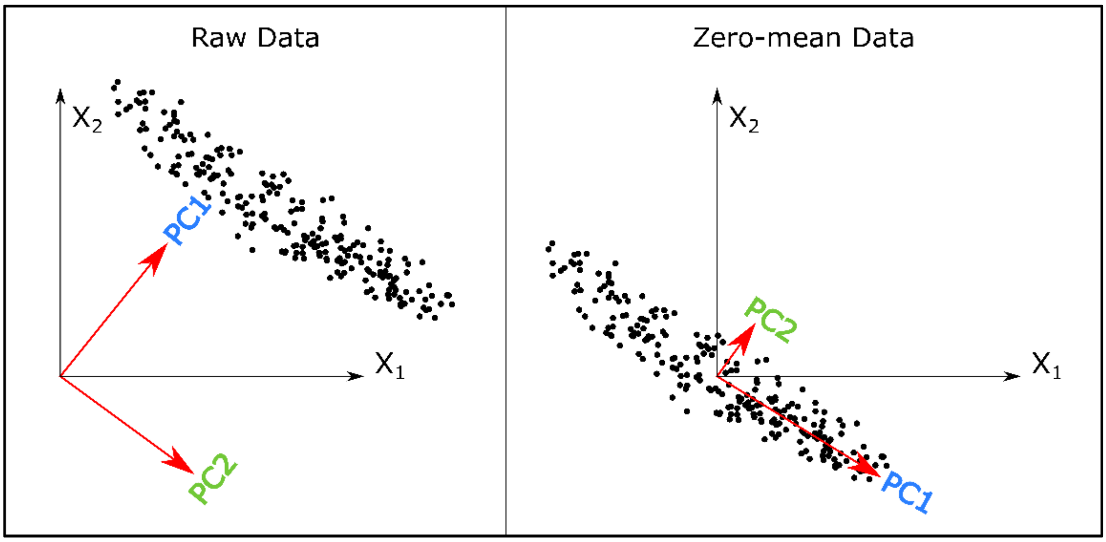

Figure 6-6 for reference: Importance of mean subtraction in PCA and TPCA. a) Raw data, the first principal component describes the distance of the cluster from the origin instead of the variance in the dataset. b) Zero-mean data, first principal component describes the major variation in the data.

If there were only two welds (two points) on the axes, only one principal component could be described and this could change dramatically with the addition of just one more weld. However, as the number of data points in the dataset increases towards the number of dimensions of the original signals, the addition of more and more welds affects the earlier principal components less and less. The effects of add more welds, is more likely to change the later principal components which end up describing nuances of a handful of signals in the dataset. With the number of points shown in Figure 6-6, the addition of one more point is unlikely to significantly change the two principal components presented and we can be fairly confident that the principal components are representative of the dataset. This is important for this work as the models are only constructed from the earlier principal components which describe (in almost all cases) more than 1% of the dataset’s variance.

For highly ordered data like welding signals it is not clear how many data points are required to calculate stable principal component matrices given the number of dimensions in the signals. Due to the constraints involved in data collection for RSW and the requirement for relatively high sampling frequencies (which increases the number of dimensions in the signals), the above convention could not always be achieved in this thesis. However, this was shown to not cause significant issues for modelling the welding process. This is because the overall shapes of welding signals tend to be very similar in a welding dataset and so the vast majority of variance can be described by typically fewer than 10 principal components.

In Chapter 4, five steel material stacks were tested with smaller or larger training datasets due to the availability of the material. The signals in the datasets had different numbers of points due to the different weld times and consistent sampling frequency that was used (1kHz). Table 8-1 summarises the number of training welds, the number of data points per signal (weld time), the model performance and the ratio of training welds to their signal length (referred to as the data ratio from hereon in).

Table 8-1: Data taken from Table 4-5, Table 4-7 and Table 4-8

	No. training welds	Welding time (ms)	Training model R^2	Training model RMSE (mm)	Ratio – training welds/dimension
Mild-Mild	20	217	0.89	0.43	0.09
Dual-Phase	25	217	0.84	0.61	0.12
DP-Mild	30	217	0.85	0.65	0.14
Usibor-Usibor	35	520	0.64	0.41	0.07
Usibor-Usibor-Mild	46	520	0.89	0.40	0.09

The models calculated for each material stack were strong shown by their high R^2 and low RMSE values. The slight differences in the model performances are most likely due to the differences in the materials and the strength of the correlation to button diameter (as discussed in Chapter 4) rather than the ratio of training welds to data dimensions (number of data points in the signal).

The Usibor-Usibor material stack had the lowest ratio (worst) and the weakest correlation to measured button diameter which was attributed to the small amount of variation that could be achieved in training with the available material. However the Mild-Mild and Usibor-Usibor-Mild models both had much higher R^2 values with similar data ratios to the Usibor-Usibor material stack, showing the variation in data ratio had little effect on this data

The trend in strong model performance even with low data ratios was shown again with industry data in section 4.3 with 46 Mild Steel welds with 350ms long signals. The model that was calculated had an RMSE of only 0.33mm (approximately 6% of the mean button diameter of the data) even though the data ratio was $46/350 = 0.13$.

In Chapter 5, 133 welds were collected on an AC welder meaning that signal data could only be sampled at every half cycle (100Hz), resulting in fewer data points per signal. Using the 133 welds, principal components were calculated for 5 different signals (each 14 data points long), resulting in a data ratio of $133/14 = 9.5$. This resulted in a similarly strong model when the information from 5 signals was amalgamated (R^2 of 0.769 and an RMSE of 114N, approximately 5% of the mean strength of the welds). In Chapter 6 and 7 when the number of dimensions for each weld tensor was far greater than the number of training welds, strong weld quality models were still produced. These cases show that the number of welds can be significantly lower than the number of dimensions in the signal and still achieve good modelling results. What was found to be much more important was the type of variation included in the training data.

The fact that principal components for welding data can be calculated from relatively few welds is thought to be due to the highly correlated nature of the adjacent points in the welding signals. Each point on the signal is reliant on the values before it because it is a physical process. For signal shape analysis, this means that the majority of welding signals in a welding dataset *look* very similar. The number of types of unique signal shapes in a RSW dataset are often relatively limited because of the highly correlated nature of the points in the welding signals. This means the number of principal components required to describe the variation in the signal dataset is significantly lower than the number of points in the typical welding signal when they are collected at the high sampling frequencies present in Medium Frequency Direct Current (MFDC) RSW.

The concept that welding signals can be represented with minimal information loss by very few principal components is shown best by the explained variance plots. The explained variance plots show the explained variance of each principal component for a signal dataset and the cumulative sum of those values. Figure 8-3 shows the explained variance for four of the signal datasets from Chapter 5: current, voltage, force and displacement (the resistance signals showed the same trend as each of the other four figures). The cumulative curve shows the amount of variance in the dataset that can described by increasing the number of principal components. The inverse of that represents the amount of information that is lost from the dataset when the later principal components are omitted. Figure 8-3 shows that welding signals in a dataset can be effectively described with very few principal components. This explained variance curve was typical of all the datasets collected in this thesis.

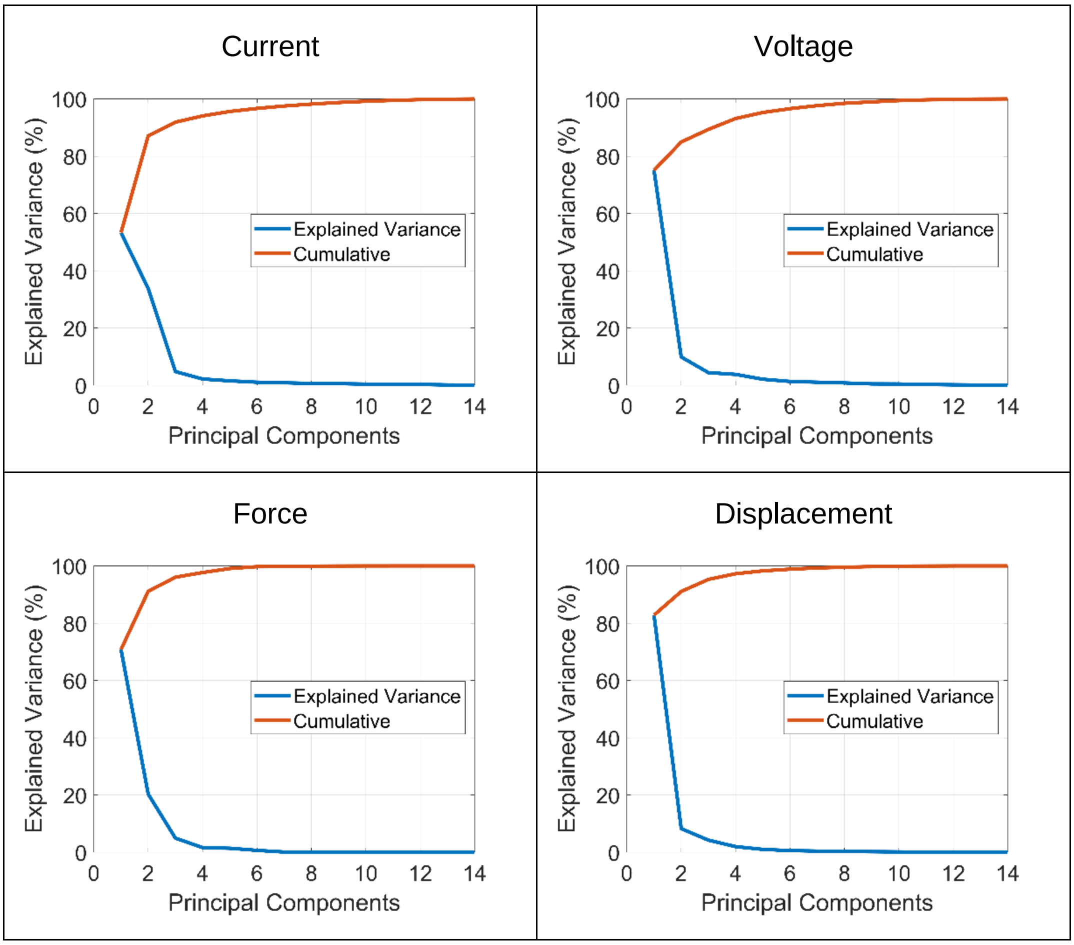

Figure 8-3: Explained Variance and Cumulative Explained Variance for four of the signal datasets from Chapter 5

The limited number of unique signal shapes in RSW signals was shown throughout this thesis by the *explained variance* of the principal components. The *explained variance* of a principal component is its eigenvalue divided by the sum of all eigenvalues and represents the percent of the total of the eigenvalues. In Table 4-8: *The explained variance of the first five principal components*, this was shown for the five different material stacks in Chapter 4. For these datasets 98% of the variation could be explained by the first five principal components. This was seen again with five signals in the aluminium welding data in Chapter 5 where 95% of the variation in each signal set could be explained by five principal components.

When more information is introduced into the analysis process with tensors, 90% of the training set variation from Chapter 6 was described with 35 tensor principal components, with more than 80% described by the first 10 principal components. The fact that more tensor principal components are required to describe the variation in a weld tensor training set is most likely because it is analysing the tensor of two unique signals which allows for more possible variation in the signal (tensor) shape. Accounting for the interacting behaviour of the signals adds additional variation that was otherwise omitted from the analysis in Chapter 4 and Chapter 5.

Even though the number of dimensions of the weld tensors is significantly larger than the number of training welds the weld quality models were still very good, showing that this factor does not result in unstable principal components in TPCA of welding data. These findings relate to the nature of the welding signals collected throughout this thesis. Each signal is a set of consecutive measurements of an aspect of the process which is strongly related to the measurements taken before it. In situations like this, it appears that the requirement for many more samples than dimensions is not as strict as suggested in the literature.

8.2 Addressing the Research Question

Throughout this thesis the methods and processes presented have provided a number of contributions to weld quality monitoring which have broader implications for the academic literature and the automotive industry. The tensor representation of welding signals and their principal components has shown that the interactions of multiple signals in aluminium RSW are useful for weld quality monitoring. The TPCA based approach outperformed the analysis of an individual signal and was able to provide useful insights into the interdependencies of the measured process signals and their relationships to weld quality. Real-time weld quality monitoring that analyses multiple process signals and their interacting behaviour represents not only a new approach to weld quality monitoring but may also assist in the monitoring of other manufacturing process that have complicated interdependencies.

The initial work in this thesis contributed to weld quality monitoring in steel RSW which was used to develop the base of the signal analysis methodology. However the aim of the thesis was to answer the research question (below) which focusses on aluminium RSW quality monitoring and the interactions of signals.

> *Can the interacting behaviour of multiple process signals measured during aluminium RSW be used to monitor weld quality? Can they provide useful insights into the process and final quality of aluminium resistance spot welds?*

Chapters 5, 6 and 7 presented the work conducted to develop and test a solution to answer the research question relating to aluminium. Chapter 4 developed the ground work for modelling a welding process using *signal shapes* which had not previously been done. Chapter 5 showed that an aluminium RSW process could be modelled using the combined information from multiple process signals but did not utilise the interacting behaviour of those signals. To incorporate the interacting behaviour of multiple signals and to address the research question, Chapter 6 developed a new weld quality monitoring technique which represented welding signal information as tensors. This allowed the interacting behaviour of multiple signals to be included in a weld quality model based of the preceding work in Chapters 4 and 5. To ensure that this work was applicable beyond the laboratory, Chapter 7 used significant amounts of industrial data to test the approach as it is designed to be used, in an industrial manufacturing facility.

From this work, useful insights were drawn from the tensor principal component shapes about the interacting behaviour of the process signals. TPCA was found to improve the weld quality models compared to models made from the analysis of individual signals (PCA). This process, spread across four results chapters, forms the answer to the research question of this thesis.

The interacting behaviour of multiple process signals in aluminium RSW can be used to monitor weld quality, and tensor principal components were found to produce better models for weld quality than comparable single-signal approaches. Useful insights about the interacting behaviour of aluminium RSW signals was drawn from the analysis of the tensor principal components (Chapters 6 & 7).

The remainder of this chapter will discuss the key outcomes for steel RSW, aluminium RSW and the implications for industry. The findings will be discussed with respect to the research question at the end of each section. Then the thesis will be concluded with the contributions to the field and future work.

8.3 The Key Outcomes for Steel RSW

The preliminary work in steel RSW generated two key contributions: the development of a signal shape analysis method for weld quality monitoring, and the process for clustering welds using their signal shapes (presented in Chapter 4).

The implications of these two contributions are as follows:

- *Steel weld quality monitoring models can be based on information from the entire signal rather than several landmark points which attempt to represent the whole signal in fewer dimensions (section 4.1).*

Using PCA to represent RSW signals means they do not have to be represented by only a few key points to maintain computational efficiency. This is a unique approach which has not been implemented in the literature or commercial weld quality monitoring systems, and represents an improvement on methods that rely on a few key points from the signal to monitor steel spot weld quality.

- *Prior knowledge of the grade or material coating of new steels is not required to develop a weld quality monitoring model as may be the case when using landmark points from a signal (section 4.2.3).*

The key points of the resistance signal for a new grade or material coating that are related to weld quality may not be known and would have to be experimentally determined. Using PCA, a training dataset that contains variability in weld quality usually results in principal components of the resistance signals that are related to weld quality. This is due to the underlying relationship between the temperature and resistivity of the material and the amount of heat required to generate a high quality spot weld.

- *Using PCA, steel welds can be clustered into different fault categories using information from the entire signal (section 4.4).*

This is an outcome from this research which is not available on any known commercial welding system, and has very limited mentions in the academic literature. This aspect represents a clear benefit for problem solving or troubleshooting issues in industry as well as identifying issues before they become significant problems for production. Additionally it provides a robust method for understanding the different effects of faults on the measured signals.

- *Signal shape analysis has the potential to advance the understanding of the types of signals that relate to weld quality as well as the effects that faults have on welding signals.*

The effects of some common faults such as expulsion are well understood in the academic literature however a multitude of additional faults were investigated in the results chapters which have not previously received attention in the literature. The types of signal shapes that occur with different faults in the RSW process were highlighted throughout the results chapters and this has increased the understanding of the effects of the faults on the signals and how they could be better identified or grouped into common underlying effects on the process.

The work in steel RSW helped to develop the methodologies for representing and analysing signal shapes in a RSW process. The methods for correlating signal shapes of welds to their quality and using them to identify faults or outliers in a set of welds is a key contribution of this work. This represents a solution to two aspects of the research question, specifically showing how *process signals collected during RSW can be used to monitor* steel *weld quality* and how they can provide *useful insights into the process*.

8.4 The Key Outcomes for Aluminium RSW

The focus of this thesis was to address the challenging problem of aluminium RSW quality monitoring. Aluminium RSW is more challenging to monitor than steel and suffers from instable weld quality due to: the aluminium oxide layer, the reduced ability to infer the heat in the process from the electrical signals, the shorter welding times, and higher currents in aluminium RSW. Prior to this thesis little work had been conducted in the academic literature on weld quality monitoring in aluminium RSW and so the contributions to this field are significant.

8.4.1 PCA-Based Weld Quality Monitoring for Aluminium RSW

The first contribution to aluminium weld quality monitoring was the application of the PCA-based approach (developed in steel) to multiple signals in aluminium RSW (Chapter 5). This work showed that the shapes of the electrical signals were more closely related to the tensile-shear load bearing capacity of welds than landmark points used in a previous study.

The implications of these contributions were:

- *Electrical signals in aluminium RSW are more useful for weld quality monitoring than previously thought (section 5.4).*

The analysis of signal shapes in aluminium RSW showed stronger correlations to weld quality than the landmark points used in a previous seminal study completed by Hao et al. (1996). The signal shapes of the electrical signals (that were not previously considered useful for weld quality monitoring) were found to be correlated with the tensile-shear load bearing capacity of aluminium spot welds.

- *The analysis of entire signals for weld quality monitoring can be applied to multiple signals in aluminium RSW (section 5.4.2).*

The PCA based analysis of welding signals represents a better approach to aluminium weld quality monitoring than selecting landmark points from the signals. The study in Chapter 5 produced a better result than the previous attempt in the academic literature by Hao et al. (1996) which used landmark points from several signals. The correlations found during this study between the signal shapes of the electrical signals and weld quality informed the subsequent work which analysed the interactions of multiple signals for quality monitoring with tensors.

The application of the PCA-based weld quality monitoring method to multiple signals in aluminium addressed a number of aspects of the research question. This work *used multiple signals to model weld quality in aluminium RSW* which *provided useful insights into the process of aluminium RSW.*

8.4.2 Tensor-Based Weld Quality Monitoring for Aluminium RSW

The major contribution of this thesis to the field of weld quality monitoring in aluminium RSW was the introduction of mathematical tensors to represent the information from multiple signals (Chapter 6). This represented a completely new approach to signal-based weld quality monitoring and aimed to analyse the shapes of signals that might have interacting behaviour during the welding process, addressing the research question of this thesis. The methodology was applied to a significant number of welds collected in industry to determine its viability in an industrial context.

The implications of these contributions are:

- *Multiple signals shapes and their interactions can be analysed simultaneously for weld quality monitoring, a concept not yet used in RSW of steel or aluminium (Chapter 6).*

- *The interdependencies of process signals in aluminium RSW can be analysed using tensor principal components, furthering the understanding of the relationships between process signals and the quality of spot welds (section 6.5.6).*

- *The interactions and interdependencies of signals can be used to model weld quality without prior knowledge of the signal features that are important for weld quality monitoring, an implication that is shared with the PCA-based approach (section 6.5.6 and section 7.4.2).*

- *The analysis of multiple signals at once represents a more robust technique for weld quality monitoring than analysing the information from an individual signal (section 7.3).*

These two studies used the *interactions of multiple process signals* to model weld quality, addressing the first half of the research question. The method was shown to *provide useful insights into the process* when the technique was applied to the industrial data case study, addressing the second half of the research question.

8.5 Implications for Industry

The contributions of this thesis include improvements to weld quality monitoring for steel and aluminium RSW which is of particular interest to the automotive industry. These contributions will be discussed in this section.

- *Real-time weld quality monitoring of steel RSW based on information from the entire signal can be implemented in production (section 4.3).*

PCA allows for entire signal shapes to be represented by their principal component scores (scalars), maintaining the computational efficiency of a landmark point based representation, while still representing information from the entire signal. This means that real-time weld quality modelling and fault clustering using information from the whole signal is viable in production.

- *Real-time weld quality monitoring of aluminium RSW based on information from multiple signals and their interactions can be implemented in production (section 7.3).*

Representing welding signals as mathematical tensors allows for the interactions and interdependencies of their signal shapes to be accounted for in signal shape analysis. TPCA allows for the information stored in the tensors to be represented efficiently using tensor principal component scores for modelling and fault separation in a RSW process. This means only the tensor principal component scores have to be calculated to achieve real-time weld quality monitoring (section 6.4.2).

- *Clustering welds into different potential fault categories using principal components of welding signals or tensors will allow technicians to identify process faults before they cause a problem, allowing for preventative maintenance and fault identification on the production line.*

Problems that stop the production line cause significant losses to an automotive manufacturer. Currently, problems on a spot welding line are mitigated by regularly re-dressing and replacing electrode caps or placing more spot welds on a part than is necessary for its function. When problems do occur, a reactionary approach is taken which could be reduced if the spot weld timer was able to identify faults early by clustering them based on signal shape information.

- *Signal based weld quality monitoring and fault clustering using signal shape analysis is likely to reduce costs in industry while increasing the confidence in the quality and safety of the vehicles that are produced.*

Implementation of the tensor representation of welding information on a weld timer allows for industry to analyse multiple signals and their interactions and interdependencies as shown in Chapter 6 and Chapter 7. This could reduce the need for off-line destructive and non-destructive testing of parts, saving time and money. Confidence in the quality of the spot welds used to make cars also helps to ensure passenger safety.

8.6 Future Work

There are several areas of research that can be highlighted for future work.

Significant challenges lie in monitoring the weld quality of high strength steels and thicker gauge aluminium. For the high-strength steels such as Usibor, the different coatings, grain structures and alloying elements appear to make the resistivity-temperature relationship ineffective for weld quality monitoring. For these applications it makes sense to investigate additional signals for use in weld quality monitoring such as the thermal expansion of the joint (through electrode displacement).

The TPCA-based technique that has been developed in this thesis for weld quality monitoring of aluminium using multiple signals may lend itself to improving weld quality monitoring in high strength steels through the analysis of additional process signals. However this was beyond the scope of the research question and was therefore not covered in this thesis.

For the thick gauge 3mm aluminium sheet that was studied in Chapter 7, none of the fault conditions could be successfully modelled. This was most likely due to the weld schedule used and the small range of weld quality that was achieved in the data. However, further work is required to determine if the technique is suitable for weld quality monitoring of the thicker gauge aluminium alloys or if additional signals need to be investigated to model the thicker gauges of aluminium.

Given that there has been very limited research into the available signals for aluminium weld quality monitoring, it would be useful to investigate additional signals such as acoustic emissions or temperature based measurements further (infrared thermography signals for example). Acoustic emissions may provide insights into cracking and porosity in aluminium welds which was highlighted as a challenge that is not well characterised by the electrical or mechanical signals. If accurate temperature measurements of the electrode-sheet interface could be achieved using infrared thermography, this may also provide useful insights into electrode wear and nugget growth in aluminium RSW.

RSW is a challenging process to create a quality monitoring technique for because it can be used to join a wide range of materials. The number of materials, potential process faults, material stack configurations, welder designs, electrode designs and different applications that are frequently used in the automotive industry create many different potential situations to be modelled in a manufacturing line.

These challenges make it difficult to determine the best approach for collecting training data and more research is required to perfect this process. Ideally, a model that has all possible types of variation in it would be created, but this is infeasible due to the data requirements of such an approach. It is thought that a tiered approach that clusters welds based on their signal shape types could be employed so that more specific models could be applied to welds in different situations.

The work in this thesis has focused on the analysis of two signals, their interactions and interdependencies, however this solution becomes significantly more computationally expensive as more and more signals are added to the analysis. More work could be conducted to understand how this method could be scaled to more than three or four signals with the current computational abilities for particularly complicated processes and how this information could be interpreted.

Finally, the TPCA-based weld quality monitoring approach could be adapted to other manufacturing processes where the analysis of the interaction of multiple signals and their interdependencies is required.

8.7 Conclusion

This thesis has shown the development of a novel approach to resistance spot weld quality monitoring for a range automotive steels as well as aluminium. The significant challenge of aluminium resistance spot weld quality monitoring, discussed in section 1.2, was addressed using the analysis of the interactions of multiple process signals to answer the research question presented in section 2.6. The analysis of the interacting behaviour of multiple process signals in aluminium RSW was found to be useful for weld quality monitoring. The TPCA-based analysis technique provided useful insights into the behaviour of different process signals and how they interact during the process. TPCA outperformed the individual signal approaches confirming that analysing the interacting behaviour of multiple signals in aluminium RSW is beneficial for weld quality monitoring and provides additional insights into the signal shapes and their relationships with weld quality.

To conclude the thesis the key contributions to the field will be summarised and recommendations and reflections from the work in this thesis will be covered.

8.7.1 Signal Shape Analysis in Resistance Spot Welding

The purpose of Chapter 4 was to develop a signal shape based approach to weld quality monitoring. To achieve this, the simplified case of steel RSW, which is well understood, was chosen to develop the methodology. Developing a signal shape based weld quality monitoring technique in steel resulted in the following contributions to the field of resistance spot weld quality monitoring as well as progressed the answer to the research question:

– The concepts of Point Distribution Models (PDM) and PCA were introduced into the field of resistance spot weld quality monitoring.

- This will allow manufacturers to move away from landmark point approaches which are not robust to changes in material, coating, welder settings or sheet metal gauge.

- The results of the signal shape based approach can be interrogated so that the reasons for poor quality welds can be rectified. A concept that is challenging to achieve with neural network based approaches.

- Through this process, insights into the signal shape behaviour can be learned for each new material, coating or joint type.

- A fault separation technique was developed which has not been thoroughly studied in the literature and is not a current known capability of any industrial spot welders.

Signal shape analysis represents a unique and novel contribution to the resistance spot welding literature and has the potential to provide more comprehensive weld quality monitoring information than the alternatives such as neural networks or the analysis of landmark points. This work formed the foundations of the analysis methodology to address the research question.

8.7.2 Signal Shape Analysis for Aluminium Weld Quality Monitoring

Chapter 5 presented a weld quality model for an aluminium RSW process, which represented a significant gap in the literature. Only one other comparable study was found, and the results of Chapter 5 showed the signal shape analysis technique produced a better model for weld quality than the previous attempt. The work in Chapter 5 introduced:

- The signal shape analysis of multiple signals for the challenging task of aluminium resistance spot weld quality monitoring.

- This allowed for the information from multiple signals to be analysed at once, which addressed the issue highlighted in the literature that no individual signal was sufficient for aluminium weld quality monitoring (Hao et al., 1996).

- From the signal shape analysis the electrical signals were found to be more correlated to weld quality than the existing literature suggested.

- This showed that the signal shape analysis could be used to increase the understanding of the variables in the process and their relationship to weld quality.

A limitation was identified from this study that the interacting behaviour between the signal shapes of different signals could not be analysed using this method. The principal components of each signal set were calculated in isolation from the other process signals which meant that any interactions between signals were not accounted for in the signal shape analysis. From this it was determined that a new approach must be developed. This showed that analysis of multiple signals in aluminium improved upon the models based on an individual signal.

8.7.3 Development of a Method that Analyses the Interactions of Multiple Signals in Aluminium RSW

The most significant and novel contribution of this thesis was the introduction of tensors to represent the information of multiple welding signals.

- Representing welding signals as tensors provided information about the interacting behaviour of two or more signals throughout the entire process.

- The concept of Point Distribution Models (PDM) from Cootes et al. (1995) was adapted to the higher order application of tensor principal components for weld signal tensor shape analysis (TPCA).

- This allowed for a better understanding of the signal features that affect other signals later in the process.

- Tensor principal component scores were used to model weld quality using the signal shape information encapsulated in the tensor principal components. This used the interactions of multiple signals to calculate a model for the tensile-shear load bearing capacity in the laboratory, addressing a major portion of the central research question.

- The technique allowed for the analysis of two or more signals simultaneously and incorporated the individual signal information as well as the interactions of those signal shapes.

- This included the interactions between the measured signals at different points in time in the process which acknowledges the importance of the interdependencies of the different signals and how they affect the final weld quality.

The work to develop a new signal shape weld quality monitoring technique that accounted for the interacting behaviour of welding signals showed that tensile-shear load bearing capacity and button diameter could be effectively modelled in the laboratory. This showed that the concept of analysis of multiple signals and their interacting behaviour could be used to model aluminium weld quality. The next step was to test that the concept worked with challenging industrial data which could not be collected in the controlled environment of a university laboratory.

8.7.4 Application of the TPCA-based Method to Industrial Data

Finally the application of the TPCA based weld quality monitoring technique to more than 4000 welds collected in an industrial automotive research facility showed that the technique was not only applicable in the laboratory, a key achievement in showing the usefulness of the research outcomes.

- This study showed which different process fault conditions could and couldn't be successfully modelled with principal components of resistance or force signals.

- It showed that the tensor based approach was better for a wider range of experimental conditions than single signal models, thus proving to be more robust to the challenges faced in industry.

- The application of the technique to the industrial data showed that TPCA based models with two process signals produced better models for weld quality than either signal's PCA-based model. This supported the hypothesis of the research question that the interacting behaviour of multiple signals is useful for aluminium weld quality monitoring.

This was a rare opportunity for a weld quality monitoring technique to be thoroughly tested with industrial data and showed the performance of the weld quality monitoring technique in the environment it was designed for.

References

1. Adams, D. W., Summerville, C. D. E., Voss, B. M., Jeswiet, J., & Doolan, M. C. (2017). Correlating Variations in the Dynamic Resistance Signature to Weld Strength in Resistance Spot Welding Using Principal Component Analysis. *Journal of Manufacturing Science and Engineering*, *139*(April), 1–4. https://doi.org/10.1115/1.4034887

2. Al Naimi, I. K., Al Saadi, M. H., Daws, K. M., & Bay, N. (2015). Influence of surface pretreatment in resistance spot welding of aluminum AA1050. *Production & Manufacturing Research*, *3*(1), 185–200. https://doi.org/10.1080/21693277.2015.1030795

3. American Welding Society. (2012). Test Methods for Evaluating the Resistance Spot Welding Behavior of Automotive Sheet Steel D8.9M:2012. In *ANSI*.

4. American Welding Society. (2013). *Specification for Automotive Weld Quality — Resistance Spot Welding of Steel* (AWS D8.1M:). American Welding Society.

5. ArcelorMittal. (2019a). ArcelorMittal - Dual phase steels. Retrieved August 9, 2019, from https://automotive.arcelormittal.com/DP

6. ArcelorMittal. (2019b). ArcelorMittal - Steels for hot stamping - Usibor® and Ductibor®. Retrieved August 9, 2019, from https://automotive.arcelormittal.com/usibor_ductibor

7. ARO. (2019). ARO iBox. Retrieved November 18, 2019, from http://www.arotechnologies.com/en-GB/1030/ibox

8. Atlas Steels. (2013). *Aluminium Alloy Data Sheet 5052* (pp. 1–3). pp. 1–3.

9. AWS. (2005). *Recommended Practices for Automotive Weld Quality - Resistance Spot Welding*.

10. Bader, B. W., & Kolda, T. G. (2015, February). *MATLAB Tensor Toolbox Version 2.6*. Retrieved from http://www.sandia.gov/~tgkolda/TensorToolbox/

11. Barnes, T. ., & Pashby, I. . (2000). Joining techniques for aluminium spaceframes used in automobiles. *Journal of Materials Processing Technology*, *99*(1–3), 62–71. https://doi.org/10.1016/S0924-0136(99)00367-2

12. Benrachou, D. E., Boulebtateche, B., & Bensaoula, S. (2013). Gabor/PCA/SVM-Based Face Detection for Driver's Monitoring. *Journal of Automation and Control Engineering*, *1*(2).

13. BlueScope Steel. (2003). *ZINCANNEAL G2S Steel - Material Data Sheet*.

14. Boomer, D. R., Hunter, J. A., & Castle, D. R. (2003). A New Approach for Robust High-Productivity Resistance Spot Welding of Aluminium. *SAE Technical Paper Series*. https://doi.org/10.4271/2003-01-0575

15. Briskham, P., Blundell, N., Han, L., Hewitt, R., Young, K., & Boomer, D. (2006). Comparison of self-pierce riveting , resistance spot welding and spot friction joining for aluminium automotive sheet. *SAE Technical Papers*, *2034*(724), 105. https://doi.org/10.4271/2006-01-0774

16. Brown, L. J., & Schwaber, J. S. (2000). Identifying Operating Conditions from Pre-weld Information for Resistance Spot Welding Lyndon J. Brown*, James S. Schwaber**. *Proceedings of the American Control Conference*, (June), 1535–1539.

17. Carle, D., & Blount, G. (1999). The suitability of aluminium as an alternative material for car bodies. *Materials & Design*, *20*, 267–272. https://doi.org/10.1016/S0261-3069(99)00003-5

18. Charde, N., Ahmad, R., & Abidin, N. I. Z. (2016). Interpreting the weld formations using acoustic emission for the carbon steels and stainless steels welds in servo-based resistance spot welding. *International Journal of Advanced Manufacturing Technology*, *86*(1–4), 1–8. https://doi.org/10.1007/s00170-015-8131-x

19. Chen, Y. (2007). *Patent No. US 7,249,482*. United States: United States Patent and Trademark Office.

20. Chien, C.-S., & Kannatey-Asibu, E. J. (2002). Investigation of Monitoring Systems for Resistance Spot Welding. *Welding Journal*, 195–199.

21. Cho, Y., & Rhee, S. (2002). Primary Circuit Dynamic Resistance Monitoring and its Application to Quality Estimation during Resistance Spot Welding. *Welding Journal*, *81*(6), 104–111.

22. Cootes, T. F., Cooper, D. H., Taylor, C. J., & Graham, J. (1992). Trainable Method of Parametric Shape Description. *Image and Vision Computing*, *10*(5), 289–294. https://doi.org/10.1016/0262-8856(92)90044-4

23. Cootes, T. F., Taylor, C. J., Cooper, D. H., & Graham, J. (1995). Active Shape Models - Their Training and Application. *Computer Vision and Image Understanding*, *61*(1), 38–59.

24. Crinon, E., & Evans, J. T. (1998). The effect of surface roughness, oxide film thickness and interfacial sliding on the electrical contact resistance of aluminium. *Materials Science & Engineering A*, *242*, 121–128.

25. Datteo, A., Lucà, F., & Busca, G. (2017). Statistical pattern recognition approach for long-time monitoring of the G.Meazza stadium by means of AR models and PCA. *Engineering Structures*, *153*(February), 317–333. https://doi.org/10.1016/j.engstruct.2017.10.022

26. Deng, L., Li, Y. B., Carlson, B. E., & Sigler, D. R. (2018). Effects of Electrode Surface Topography on Aluminum Resistance Spot Welding. *Welding Journal*, *97*, 120–132. https://doi.org/10.29391/2018.97.011

27. Desai, P. D., James, H. M., & Ho, C. Y. (1984). Electrical Resistivity of Aluminum and Manganese. *Journal of Physical and Chemical Reference Data*, Vol. 13, pp. 1131–1172. https://doi.org/10.1063/1.555725

28. Dickinson, D. W., Franklin, J. E., & Stanya, A. (1980). Characterization of Spot Welding Behavior by Dynamic Electrical Parameter Monitoring. *Welding Journal*, (June), 170–176.

29. Doolan, M. C., Kalyanasundaram, S., Cardew-Hall, M., & Hodgson, P. (2003). Use of Image Recognition Techniques in the Analysis of Sheet Metal Forming Force Signature Curves. *Journal of Manufacturing Science and Engineering*, *125*(2), 363–368.

30. Doolan, M. C., Kalyanasundaram, S., Hodgson, P., & Cardew-hall, M. (2001). *Identifying variation in sheet metal stamping*. *115*, 142–146.

31. Ferrer, A. (2007). Multivariate Statistical Process Control Based on Principal Component Analysis (MSPC-PCA): Some Reflections and a Case Study in an Autobody Assembly Process. *Quality Engineering*, *19*(4), 311–325. https://doi.org/10.1080/08982110701621304

32. Fisher, R. A. (1936). The use of multiple measurements in taxonomic problems. *Annals of Eugenics*, *7*, 179–188. https://doi.org/10.1111/j.1469-1809.1936.tb02137.x

33. Fukumoto, S., Lum, I., Biro, E., Boomer, D. R., & Zhou, Y. (2003). Effects of Electrode Degradation on Electrode Life in Resistance Spot Welding of Aluminum Alloy 5182. *Welding Journal*, (November), 307–312.

34. Fukumoto, Shinji, Fujiwara, K., Toji, S., & Yamamoto, A. (2008). Small-scale resistance spot welding of austenitic stainless steels. *Materials Science and Engineering A*, *492*(1–2), 243–249. https://doi.org/10.1016/j.msea.2008.05.002

35. Gong, L., & Liu, C. (2011). Electrode Displacement Patterns Inferred as the Optimal Control Criteria during the Resistance Spot Welding Process. *2011 IEEE International Conference on Robotics and Automation*, 148–152.

36. Haefner, K. B., Bernstein, B. M., & Overton, K. J. (1989). *Patent No. US 4,861,960*. United States: United States Patent and Trademark Office.

37. Haeufgloeckner, J. (2017). *Explanation of UIP, FQF & PSF*. Erbach, Germany: Bosch Rexroth.

38. Haeufgloeckner, J., Zeller, S., & Rathke, J. (2017). *Patent No. US 9,839,972*. Germany: United States Patent and Trademark Office.

39. Han, L., Thornton, M., Boomer, D., & Shergold, M. (2010). Effect of aluminium sheet surface conditions on feasibility and quality of resistance spot welding. *Journal of Materials Processing Technology*, *210*(8), 1076–1082. https://doi.org/10.1016/j.jmatprotec.2010.02.019

40. Han, L., Thornton, M., & Shergold, M. (2010). A comparison of the mechanical behaviour of self-piercing riveted and resistance spot welded aluminium sheets for the automotive industry. *Materials and Design*, *31*(3), 1457–1467. https://doi.org/10.1016/j.matdes.2009.08.031

41. Hao, M., Osman, K., Boomer, D., & Newton, C. (1996). Developments in Characterization of Resistance Spot Welding of Aluminum. *Welding Journal*, (January), 1–8.

42. Hao, Ming, Osman, K. A., Boomer, D. R., Newton, C. J., & Sheasby, P. G. (1996). On-Line Nugget Expulsion Detection for Aluminium Spot Welding and Weldbonding. *SAE Transactions*.

43. Hayes, D. J., & Sader, S. A. (2001). Comparison of Change-Detection Techniques for Monitoring Tropical Forest Clearing and Vegetation Regrowth in a Time Series. *Photogrammetric Engineering and Remote Sensing*, *67*(9), 1067–1075.

44. He, X., Pearson, I., & Young, K. (2008). Self-pierce riveting for sheet materials: State of the art. *Journal of Materials Processing Technology*, *199*(1), 27–36. https://doi.org/10.1016/j.jmatprotec.2007.10.071

45. James, P. S., Chandler, H. W., Evans, J. T., Wen, J., Browne, D. J., & Newton, C. J. (1997). The effect of mechanical loading on the contact resistance of coated aluminium. *Materials Science & Engineering A*, *230*, 194–201.

46. Ji, C., & Deng, L. (2010). Quality control based on electrode displacement and force in resistance spot welding. *Frontiers of Mechanical Engineering in China*, *5*(4), 412–417. https://doi.org/10.1007/s11465-010-0114-x

47. Ji, C. T., & Zhou, Y. (2004). Dynamic Electrode Force and Displacement in Resistance Spot Welding of Aluminum. *Journal of Manufacturing Science and Engineering*, *126*(August), 605–610. https://doi.org/10.1115/1.1765140

48. Jin, A., Yin, B., Morren, G., Duric, H., & Aarts, R. M. (2009). Performance evaluation of a tri-axial accelerometry-based respiration monitoring for ambient assisted living. *Proceedings of the 31st Annual International Conference of the IEEE Engineering in Medicine and Biology Society: Engineering the Future of Biomedicine, EMBC 2009*, 5677–5680. https://doi.org/10.1109/IEMBS.2009.5333116

49. Karami, A., Yazdi, M., & Mercier, G. (2012). Compression of hyperspectral images using discerete wavelet transform and tucker decomposition. *IEEE Journal of Selected Topics in Applied Earth Observations and Remote Sensing*, *5*(2), 444–450. https://doi.org/10.1109/JSTARS.2012.2189200

50. Kelkar, A., Roth, R., & Clark, J. (2001). Automobile bodies: Can aluminum be an economical alternative to steel? *The Journal of The Minerals, Metals & Materials Society*, *53*(8), 28–32. https://doi.org/10.1007/s11837-001-0131-7

51. Killian, M. L., & Orr, M. D. (1996). *Patent No. US 5,558,785*. United States: United States Patent and Trademark Office.

52. Kolda, T. G., & Bader, B. W. (2009). Tensor Decompositions and Applications. *Society for Industrial and Applied Mathematics Review*, *51*(3), 455–500.

53. Kroonenberg, P. M., & de Leeuw, J. (1980). Principal component analysis of three-mode data by means of alternating least squares algorithms. *Psychometrika*, *45*(1), 69–97. https://doi.org/10.1007/BF02293599

54. Li, W. (2007). *Manufacturing process diagnosis using functional regression*. *186*(December 2005), 323–330. https://doi.org/10.1016/j.jmatprotec.2006.12.052

55. Li, Z., Hao, C., Zhang, J., & H., Z. (2007). Effects of Sheet Surface Conditions on Electrode Life in Resistance Welding Aluminum. *Welding Journal*, (April), 81–89.

56. Livshits, A. G. (1997). Universal Quality Assurance Method for Resistance Spot Welding Based on Dynamic Resistance. *Welding Journal*, (September), 383–390.

57. Löveborn, D., Larsson, J. K., & Persson, K. A. (2017). Weldability of Aluminium Alloys for Automotive Applications. *Physics Procedia*, *89*, 89–99. https://doi.org/10.1016/j.phpro.2017.08.011

58. Lum, I., Biro, E., Zhou, Y., Fukumoto, S., & Boomer, D. R. (2004). Electrode pitting in resistance spot welding of aluminum alloy 5182. *Metallurgical and Materials Transactions A*, *35*, 217–226. https://doi.org/10.1007/s11661-004-0122-8

59. Luo, Y., Li, J. L., & Wu, W. (2013). Nugget quality prediction of resistance spot welding on aluminium alloy based on structureborne acoustic emission signals. *Science and Technology of Welding and Joining*, *18*(4), 301–306. https://doi.org/10.1179/1362171812Y.0000000102

60. Luo, Yi, Li, J., & Wu, W. (2013). Characterization of nugget nucleation quality based on the structure-borne acoustic emission signals detected during resistance spot welding process. *Measurement: Journal of the International Measurement Confederation*, *46*(3), 1053–1060. https://doi.org/10.1016/j.measurement.2012.11.016

61. Luo, Yi, Wan, R., Yang, Z., & Xie, X. (2016a). Study on the nugget growth in single-phase AC resistance spot welding on the calculation of dynamic resistance. *Journal of Materials Processing Technology*, *229*, 492–500. https://doi.org/10.1016/j.measurement.2015.09.034

62. Luo, Yi, Wan, R., Yang, Z., & Xie, X. (2016b). Study on the thermo-effect of nugget growing in single-phase AC resistance spot welding based on the calculation of dynamic resistance. *Measurement*, *78*, 18–28. https://doi.org/10.1016/j.measurement.2015.09.034

63. Luo, Z., Ao, S., Chao, Y. J., Cui, X., Li, Y., & Lin, Y. (2015). Application of Pre-heating to Improve the Consistency and Quality in AA5052 Resistance Spot Welding. *Journal of Materials Engineering and Performance*, *24*(10), 3881–3891. https://doi.org/10.1007/s11665-015-1704-x

64. Ma, Y., Wu, P., Xuan, C., Zhang, Y., & Su, H. (2013). Review on Techniques for On-Line Monitoring of Resistance Spot Welding Process. *Advances in Materials Science and Engineering*, *2013*, 1–6.

65. Maalouf, M., & Barsoum, Z. (2017). Failure strength prediction of aluminum spot-welded joints using kernel ridge regression. *International Journal of Advanced Manufacturing Technology*, *91*(9–12), 3717–3725. https://doi.org/10.1007/s00170-017-0070-2

66. Matuschek. (2018). *SPATZ + M400 / M600 / M900 Medium Frequency Inverter Power Source*.

67. Micro-Epsilon. (2017). Assembly Instructions optoNCDT 1750.

68. Miller, W. ., Zhuang, L., Bottema, J., Wittebrood, A. ., De Smet, P., Haszler, A., & Vieregge, A. (2000). Recent development in aluminium alloys for the automotive industry. *Materials Science and Engineering: A*, *280*(1), 37–49. https://doi.org/10.1016/S0921-5093(99)00653-X

69. Muhammad, N., Manurung, Y. H. P., Jaafar, R., Kiyai, S., Tham, G., & Haruman, E. (2013). *Model development for quality features of resistance spot welding using multi-objective Taguchi method and response surface methodology*. 1175–1183. https://doi.org/10.1007/s10845-012-0648-3

70. Nied, H. A. (1984). *Patent No. US 4,472,620*. United States: United States Patent and Trademark Office.

71. Pan, C., Li, D., Du, S., & Guo, S. (2008). Multiple Information Fusion of Aluminum Alloy Resistance Spot Welding Based on Principal Component Analysis. *ICSP2008 Proceedings*, (1), 1590–1594.

72. Park, Y. J., & Cho, H. (2004). Quality evaluation by classification of electrode force patterns in the resistance spot welding process using neural networks. *Proceedings of the Institution of Mechanical Engineers, Part B: Journal of Engineering Manufacture*, *218*(11), 1513–1524. https://doi.org/10.1243/0954405042418491

73. Patil, R. R., Tilak, C. J. K. A., Srivastava, V., & De, A. (2011). Minimising electrode wear in resistance spot welding of aluminium alloys. *Science and Technology of Welding and Joining*, *16*(6), 509–513. https://doi.org/10.1017/CBO9781107415324.004

74. Patrick, E. P., Auhl, J. R., & Sun, T. S. (1984). Understanding the Process Mechanisms Is Key to Reliable Resistance Spot Welding Aluminum Auto Body Components. *SAE Technical Paper Series*.

75. Pearson, K. (1900). On the Correlation of Characters not Quantitatively Measurable. *Philosophical Transactions: Mathematical Contributions to the Theory of Evolution*, *195*, 1–47.

76. Podrzaj, P., Polajnar, I., Diaci, J., & Kariz, Z. (2005). Estimating the strength of resistance spot welds based on sonic emission. *Science and Technology of Welding and Joining*, *10*(4), 399–405. https://doi.org/10.1179/174329305X44107

77. Podrzaj, P., Polajnar, I., Diaci, J., & Kariz, Z. (2008). Overview of resistance spot welding control. *Science and Technology of Welding and Joining*, *13*(3), 215–225. https://doi.org/10.1179/174329308X283893

78. Podrzaj, P., & Simoncic, S. (2014). A machine vision-based electrode displacement measurement. *Weld World*, *58*, 93–99. https://doi.org/10.1007/s40194-013-0086-7

79. Polajnar, I., Esmail, E. A., Kek, T., & Grum, J. (2009). Effect of various sensor setting up for acoustic emission detection during resistance spot welding. *10th International Conference of the Slovenian Society for Non-Destructive Testing: Application of Contemporary Non-Destructive Testing in Engineering*, 399–406.

80. Polajnar, I., Grum, J., & Esmail, E. a. (2008). Sources of Acoustic Emission in Resistance Spot Welding. *Defektoskopie 2008*, 187–194. NDT.

81. Puddle, M. W., Davies, N. C., & Bullivant-Clark, P. M. (1990). *Patent No. European 0 291 277*. European Patent Office.

82. Rashid, M. (2011). Some tribological influences on the electrode-worksheet interface during resistance spot welding of aluminum alloys. *Journal of Materials Engineering and Performance*, *20*(3), 456–462. https://doi.org/10.1007/s11665-010-9696-z

83. Rashid, M., Fukumoto, S., Medley, J. B., Villafuerte, J., & Zhou, Y. (2007). Influence of lubricants on electrode life in resistance spot welding of aluminum alloys. *Welding Journal*, *86*, 62–70.

84. Rashid, M., Medley, J. B., & Zhou, Y. (2011). Nugget formation and growth during resistance spot welding of aluminium alloy 5182. *Canadian Metallurgical Quarterly*, *50*(1), 61–71. https://doi.org/10.1179/000844311X552322

85. Resistance Welder Manufacturers' Alliance. (2009). *Resistance Welding Manual* (Revised Fo). Miami, Florida USA.

86. Rolfe, B. F., Cardew-Hall, M. J., Abdallah, S. M., & West, G. A. W. (2001). Geometric shape errors in forging: Developing a metric and an inverse model. *Proceedings of the Institution of Mechanical Engineers, Part B: Journal of Engineering Manufacture*, *215*(9), 1229–1240. https://doi.org/10.1243/0954405011519295

87. Sandeep, R., Sharma, S., Thakur, M., & Bora, P. K. (2016). Perceptual video hashing based on Tucker decomposition with application to indexing and retrieval of near-identical videos. *Multimedia Tools and Applications*, *75*(13), 7779–7797. https://doi.org/10.1007/s11042-015-2695-1

88. Sigler, D. R. (2005). *Patent No. US 6,861,609*. United States of America: United States Patent and Trademark Office.

89. Sigler, D. R., & Karagoulis, M. J. (2013). *Patent No. US 8,436,269*. United States: United States Patent and Trademark Office.

90. Simoncic, S., & Podrzaj, P. (2014). The applicability of welding force for spot weld quality assurance. *International Journal of Microstructure and Materials Properties*. https://doi.org/10.1504/IJMMP.2014.066921

91. Simončič, S., & Podržaj, P. (2014). The applicability of welding force for spot weld quality assurance. *International Journal of Microstructure and Materials Properties*, *9*(3/4/5), 422. https://doi.org/10.1504/IJMMP.2014.066921

92. Song, Q., Zhang, W., & Bay, N. (2005). An Experimental Study Determines the Electrical Contact Resistance in Resistance Welding. *Welding Journal*, *84*(May), 73–76. Retrieved from http://files.aws.org/wj/supplement/WJ_2005_05_s73.pdf

93. Summerville, C., Adams, D., Compston, P., & Doolan, M. C. (2017a). Nugget diameter in resistance spot welding: a comparison between a dynamic resistance based approach and ultrasound C-scan. *Procedia Engineering*, *183*, 257–263. https://doi.org/10.1016/j.proeng.2017.04.033

94. Summerville, C., Adams, D., Compston, P., & Doolan, M. C. (2017b). Process Monitoring of Resistance Spot Welding Using the Dynamic Resistance Signature. *Welding Journal*, *96*(November), 403–412.

95. Sun, X., Stephens, E. V., Davies, R. W., Khaleel, M. A., & Spinella, D. J. (2004). Effects of Fusion Zone Size on Failure Modes and Static Strength of Aluminum Resistance Spot Welds. *Welding Journal*, (November), 308–318.

96. Tang, H., Hou, W., & Hu, S. J. (2002). Forging force in resistance spot welding. *Proceedings of the Institution of Mechanical Engineers, Part B: Journal of Engineering Manufacture*, *216*(7), 957–968. https://doi.org/10.1243/09544050260174166

97. Thornton, P. H., Krause, A. R., & Davies, R. G. (1996). Contact Resistances in Spot Welding. *Welding Journal*, *75*(December), 402–412.

98. Thornton, P. H., Krause, A. R., & Davies, R. G. (1997). Contact Resistance of Aluminum. *Welding Journal*, *76*(8), 331–341.

99. Tucker, L. R. (1963). Implications of factor analysis of three-way matrices for measurement of change. *Problems in Measuring Change*, *15*, 122–137.

100. Turnage, S. A., Darling, K. A., Rajagopalan, M., Whittington, W. R., Tschopp, M. A., Peralta, P., & Solanki, K. N. (2018). Influence of variable processing conditions on the quasi-static and dynamic behaviors of resistance spot welded aluminum 6061-T6 sheets. *Materials Science and Engineering A*, *724*(March), 509–517. https://doi.org/10.1016/j.msea.2018.03.120

101. Urech, W. (1986). *Patent No. US 4,591,687*. Switzerland: United States Patent and Trademark Office.

102. Voss, B. M., Pereira, M. P., & Doolan, M. C. (2014). Automated identification of tool wear in sheet metal stamping. *IDDRG 2014 Conference*, 399–404. Paris, France.

103. Voss, B., Pereira, M. P., Rolfe, B. F., & Doolan, M. C. (2017). Using stamping punch force variation for the identification of changes in lubrication and wear mechanism. *Journal of Physics: Conference Series*, *896*(1). https://doi.org/10.1088/1742-6596/896/1/012028

104. Wan, X., Wang, Y., & Zhao, D. (2016a). Multi-response optimization in small scale resistance spot welding of titanium alloy by principal component analysis and genetic algorithm. *International Journal of Advanced Manufacturing Technology*, *83*(1–4), 545–559. https://doi.org/10.1007/s00170-015-7545-9

105. Wan, X., Wang, Y., & Zhao, D. (2016b). Multiple Quality Characteristics Prediction and Parameter Optimization in Small-Scale Resistance Spot Welding. *Arab Journal of Science and Engineering*, *41*, 2011–2021. https://doi.org/10.1007/s13369-016-2061-2

106. Wan, X., Wang, Y., & Zhao, D. (2016c). Quality monitoring based on dynamic resistance and principal component analysis in small scale resistance spot welding process. *The International Journal of Advanced Manufacturing Technology*, 3443–3451. https://doi.org/10.1007/s00170-016-8374-1

107. Wan, X., Wang, Y., & Zhao, D. (2018). *Quality Estimation in Small Scale Resistance Spot Welding of Titanium Alloy Based on Dynamic Electrical Signals*. *58*(4), 721–726.

108. Wang, H., Zhang, Y., & Chen, G. (2009). Resistance spot welding processing monitoring based on electrode displacement curve using moving range chart. *Measurement*, *42*(7), 1032–1038. https://doi.org/10.1016/j.measurement.2009.03.005

109. Wang, S. C., & Wei, P. S. (2001). Modeling Dynamic Electrical Resistance During Resistance Spot Welding. *Journal of Heat Transfer*, *123*(June), 576–585. https://doi.org/10.1115/1.1370502

110. Wang, X., Zhou, J., Yan, H., & Pang, C. K. (2017). *Quality monitoring of spot welding with advanced signal processing and data-driven techniques*. https://doi.org/10.1177/0142331217700703

111. Weiner, L., Chiotti, P., & Wilhelm, H. A. (1952). *Temperature dependence of electrical resistivity of metals*.

112. Welding Technology Corp. (2019). *WT6000 Servo Resistance Weld Control*. Farmington Hills, Michigan.

113. Wu, N., Chen, S., & Xiao, J. (2018). *Wavelet analysis-based expulsion identification in electrode force sensing of resistance spot welding*.

114. Xing, B., Xiao, Y., Qin, Q. H., & Cui, H. (2018). Quality assessment of resistance spot welding process based on dynamic resistance signal and random forest based. *International Journal of Advanced Manufacturing Technology*, *94*(1–4), 327–339. https://doi.org/10.1007/s00170-017-0889-6

115. Yi, L., Rui, W., Xiaojian, X., & Yang, Z. (2016). Expulsion analysis of resistance spot welding on zinc-coated steel by detection of structure-borne acoustic emission signals. *International Journal of Advanced Manufacturing Technology*, *84*(9–12), 1995–2002. https://doi.org/10.1007/s00170-015-7846-z

116. Zhang, Hongjie. (2011). *Quality Estimation of the Resistance Spot Welding Based on Genetic K-means Cluster Analysis*. 1–4.

117. Zhang, Hongjie, Hou, Y., Yang, T., Zhang, Q., & Zhao, J. (2018). Welding quality evaluation for the resistance spot welding using the time-varying inductive reactance signal. *Measurement Science and Technology*.

118. Zhang, Hongjie, Hou, Y., Zhao, J., Wang, L., Xi, T., & Li, Y. (2017). Automatic welding quality classification for the spot welding based on the Hopfield associative memory neural network and Chernoff face description of the electrode displacement signal features. *Mechanical Systems and Signal Processing*, *85*(December 2015), 1035–1043. https://doi.org/10.1016/j.ymssp.2016.06.036

119. Zhang, Hongqiang, Qiu, X., Xing, F., Bai, J., & Chen, J. (2014). Failure analysis of dissimilar thickness resistance spot welded joints in dual-phase steels during tensile shear test. *Materials and Design*, *55*, 366–372. https://doi.org/10.1016/j.matdes.2013.09.040

120. Zhang, Hongyan, & Senkara, J. (2011). *Resistance Welding - Fundamentals and Applications* (Second Ed.). CRC Press, Taylor & Francis Group.

121. Zhang, P., Zhang, H., Chen, J., & MA, Y. (2007). Quality monitoring of resistance spot welding based on electrode displacement characteristics analysis. *Frontiers of Mechanical Engineering China*, *2*(3), 330–335. https://doi.org/10.1007/s11465-007-0058-y

122. Zhang, W. J., Cross, I., Feldman, P., Rama, S., Norman, S., & Del Duca, M. (2017). Electrode life of aluminium resistance spot welding in automotive applications: a survey. *Science and Technology of Welding and Joining*, *22*(1), 22–40. https://doi.org/10.1080/13621718.2016.1180844

123. Zhang, Y. S., & Chen, G. L. (2005). A Neuro-fuzzy Approach to Part Fitup Fault Control During Resistance Spot Welding Using Servo Gun. *International Conference on Natural Computation*, 1060–1068.

124. Zhang, Y. S., Wang, H., Chen, G. L., & Zhang, X. Q. (2007). Monitoring and intelligent control of electrode wear based on a measured electrode displacement curve in resistance spot welding. *Measurement Science and Technology*, *18*(3), 867–876. https://doi.org/10.1088/0957-0233/18/3/040

125. Zhao, D., Wang, Y., Sheng, S., & Lin, Z. (2014). Multi-objective optimal design of small scale resistance spot welding process with principal component analysis and response surface methodology. *Journal of Intelligent Manufacturing*, *25*, 1335–1348. https://doi.org/10.1007/s10845-013-0733-2

126. Zhou, K., & Yao, P. (2019). Overview of recent advances of process analysis and quality control in resistance spot welding. *Mechanical Systems and Signal Processing*, *124*, 170–198. https://doi.org/10.1016/j.ymssp.2019.01.041

Appendix

Appendix Table 1: Chemical composition of the steels from Chapter 4, section 4.2

Steel	C	Si	Mn	P	S	Al	Cu	B	Ti+Nb	Cr+Mo
Mild	0.1%		0.45%	0.025%	0.03%					
DP	0.15%	0.8%	2.5%	0.05%	0.01%	0.010-1.5%	0.2%	0.005%	0.15%	1.4%
Usibor	0.25%	0.4%	1.4%	0.03%	0.01%	0.01-0.1%		0.005%	0.12%	1%

Appendix Table 2: Material properties of the steels from Chapter 4, section 4.2

Material	Coating	Tensile Strength (MPa)	Processing
Mild Steel (BlueScope Steel, 2003)	ZF100	350-400	Hot-dipped, cold-rolled
Dual Phase (ArcelorMittal, 2019a)	-	590-700	Cold-rolled
Usibor (ArcelorMittal, 2019b)	Al-Si	≥ 1400	Hot-stamped, Die-quenched

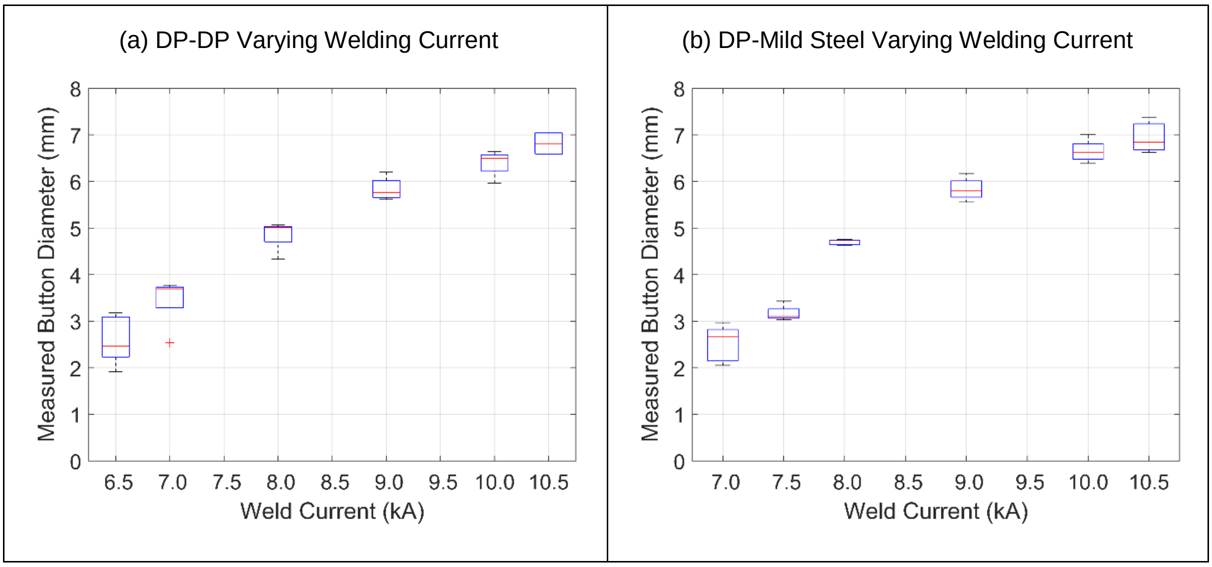

Appendix Figure 1: DP-DP and DP-Mild training set destructive testing data summaries from Chapter 4, section 4.2.2

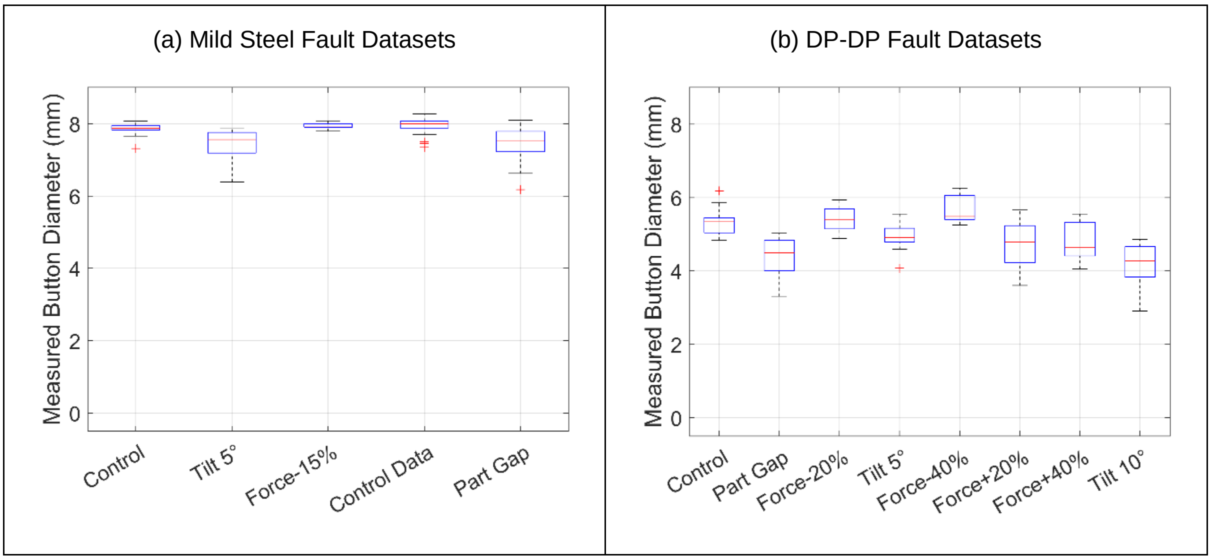

Appendix Figure 2: Mild steel and DP-DP fault dataset destructive testing summaries from Chapter 4, section 4.2.2

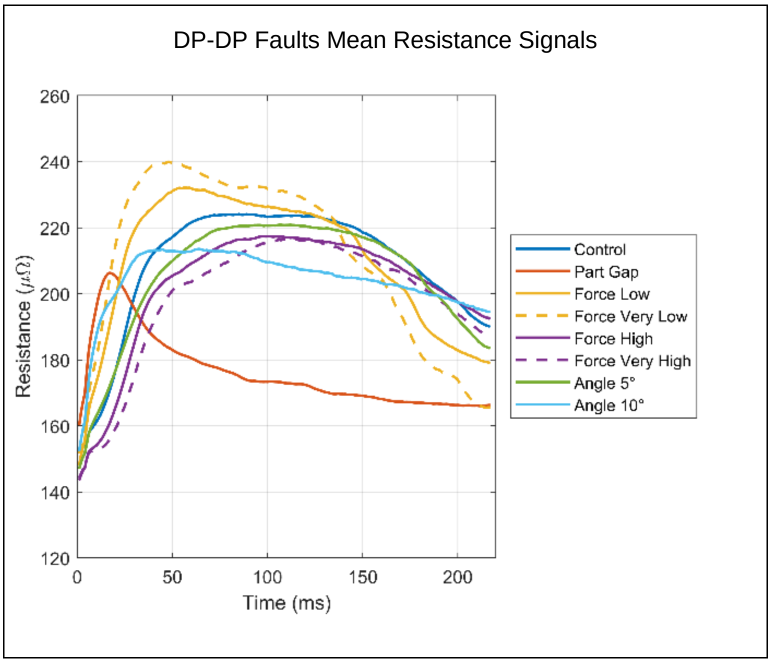

Appendix Figure 3: DP-DP fault mean resistance signals from Chapter 4, section 4.2.2

Appendix Table 3 shows the key MATLAB code from Chapter 6, section 6.4, to calculate the tensor decomposition in the first column and a more detailed process in the second column for each key function.

Appendix Table 3: Tucker decomposition process with alternating least squares

Step	Equation/Function	Process
1	B_{jq} and C_{kr}	$initialised\ with\ random\ numbers$
2	$\tilde{A}_{\mathrm{iqr}} = \mathcal{X}_{\mathrm{ijk}} B'_{jq} C'_{kr}$	
3	$A_{ip} = nvecs\left(\tilde{A}_{iqr}, 1, \mathrm{R}(1)\right)$	$Y_{ii} = \tilde{A}_{i(qr)} \tilde{A}'_{i(qr)}$ $[u, d] = eigs(Y_{ii}, 100)$ $A_{pi} = u_{pi}.$ $u\ are\ the\ eigenvectors\ of\ Y_{ii}$
4	$\tilde{B}_{\mathrm{pjr}} = \mathcal{X}_{ijk} A'_{ip} C'_{kr}$	
5	$B_{jq} = nvecs\left(\tilde{B}_{pjr}, 2, \mathrm{R}(2)\right)$	$Y_{jj} = \tilde{B}_{j(pr)} \tilde{B}'_{j(pr)}$ $[u, d] = eigs(Y, 100)$ $B_{qj} = u.$ $u\ are\ the\ eigenvectors\ of\ Y_{jj}$
6	$\tilde{C}_{\mathrm{pqk}} = \mathcal{X}_{\mathrm{ijk}} \mathrm{A}'_{\mathrm{ip}} B'_{jq}$	
7	$C_{kr} = nvecs\left(\tilde{C}_{pqk}, 3, \mathrm{R}(3)\right)$	$Y_{kk} = \tilde{C}_{k(pq)} \tilde{C}'_{k(pq)}$ $[u, d] = eigs(Y, 100)$ $C = u.$ $u\ are\ the\ eigenvectors\ of\ Y_{kk}$
8	$\mathcal{G}_{pqr} = \tilde{C}_{\mathrm{pqk}} C'_{rk} = \mathcal{X}_{\mathrm{ijk}} \mathrm{A}'_{\mathrm{ip}} B'_{jq} C'_{kr}$	
9	$\left\lvert \left(1 - \frac{\sqrt{\left(\lVert X_{ijk} \rVert^2 - \lVert \mathcal{G}_{pqr} \rVert^2\right)}}{\lVert X_{ijk} \rVert}\right)_{n-1} - \left(1 - \frac{\sqrt{\left(\lVert X_{ijk} \rVert^2 - \lVert \mathcal{G}_{pqr} \rVert^2\right)}}{\lVert X_{ijk} \rVert}\right)_{n-0} \right\rvert < 1e^{-4}$	*If the change since the last iteration in the difference in magnitude of the original data and the core tensor is less than the threshold (*$1e^{-4}$*) and it isn't the first iteration, then break. In other words, if the norm of the core and the norm of the original data are converging then stop iterating.*